

Electronic Thesis and Dissertation Repository

8-4-2021 10:00 AM

The regulation of Pannexin1 and Pannexin2 in the skin in health and disease

Rafael E. Sanchez Pupo, *The University of Western Ontario*

Supervisor: Penuela, Silvia, *The University of Western Ontario*

A thesis submitted in partial fulfillment of the requirements for the Doctor of Philosophy degree in Anatomy and Cell Biology

© Rafael E. Sanchez Pupo 2021

Follow this and additional works at: <https://ir.lib.uwo.ca/etd>



Part of the [Biochemistry Commons](#), [Cancer Biology Commons](#), [Cell Biology Commons](#), [Immunotherapy Commons](#), [Molecular Biology Commons](#), and the [Skin and Connective Tissue Diseases Commons](#)

Recommended Citation

Sanchez Pupo, Rafael E., "The regulation of Pannexin1 and Pannexin2 in the skin in health and disease" (2021). *Electronic Thesis and Dissertation Repository*. 7952.
<https://ir.lib.uwo.ca/etd/7952>

This Dissertation/Thesis is brought to you for free and open access by Scholarship@Western. It has been accepted for inclusion in Electronic Thesis and Dissertation Repository by an authorized administrator of Scholarship@Western. For more information, please contact wlsadmin@uwo.ca.

Abstract

Pannexins (PANX1, 2, 3) are a family of channel-forming glycoproteins that mediate intracellular and paracrine signaling. In contrast to PANX2, PANX1 has been extensively investigated in the skin, modulating cell differentiation, wound healing, and melanoma development. PANX1 and PANX2 can co-exist in the same cell and form mixed channels where their glycosylation seems to regulate their intermixing. N-glycosylation and caspase cleavage have been proposed as modulators of the function of PANX1, but their effects on PANX2 are unknown. We explored the PANX2 expression in mouse skin and showed that a *Panx2* splice variant (PANX2-202) is continuously expressed throughout aging skin. Furthermore, PANX2 was detected in keratinocytes and is upregulated during their *in vitro* differentiation. We showed that in UVB-induced apoptotic keratinocytes, caspase-3/7 cleaves the PANX2 C-terminus at residue D416. Notably, CRISPR-Cas9-mediated deletion of PANX2 delays but does not impair keratinocyte apoptosis, and its caspase-mediated cleavage is not required for this process. Thus, we propose that PANX2 promotes keratinocyte death after UVB, which may contribute to skin homeostasis. Moreover, we showed that N-glycosylation occurs at the N86 residue of PANX2, regulating folding and cell surface trafficking but not its interaction with PANX1. As PANX1 is known to modulate *in vitro* and *ex vivo* tumorigenicity of melanoma cells, we examined the effect of a germline deletion on *in vivo* melanoma progression by crossing *Panx1* knockout (*Panx1*^{-/-}) mice with the melanoma model: *Braf*^{CA}, *Pten*^{loxP}, *Tyr::CreER*^{T2} (BPC). We found that *Panx1*-deletion did not reduce melanoma formation or improve BPC-mice survival. However, tumors in BPC-*Panx1*^{-/-} mice exhibited increased infiltration of CD4+, CD8+ T-lymphocytes, and Granzyme B+ cells but not immunosuppressive FoxP3+ T-cells. Remarkably, splenomegaly was also found in female BPC-*Panx1*^{-/-} mice compared to males. Overall, this study revealed the location of two post-translational modifications in the PANX2 amino acid sequence modulating its localization and possibly its biological function. We provided further evidence that regulation of pannexins in the skin may influence cell death and the activity of the immune system during skin cancer conditions, which may have translational application in improving checkpoint inhibitor immunotherapy for melanoma.

Keywords

Pannexins, Pannexin 1, Pannexin 2, PANX1, PANX2, post-translational modifications, N-glycosylation, caspase cleavage, keratinocytes, cell death, mouse skin, UVB-induced apoptosis, melanoma, tumor immune infiltration, mouse model.

Summary for Lay Audience

Pannexins 1 and 2 (PANX1, PANX2) are channel-forming proteins that participate in cell growth, death, and cell-to-cell communication processes. Both proteins are present in the skin, but only PANX1 has been thoroughly investigated and shown as essential for proper skin formation and wound healing. Here, we discovered that a PANX2 variant is present in the upper layers of the mouse skin regardless of age, and its levels increase during the maturation of specific skin cells called keratinocytes. Notably, we proved that PANX2 also speeds up death in keratinocytes exposed to ultraviolet light (UV), which could be a natural mechanism for eliminating cancerous cells in the outermost layers of skin after sunburn. We also showed that specialized enzymes cut PANX2 during this cell death process, but the consequences of this cut are still unknown. Furthermore, as PANX1 and PANX2 can exist simultaneously in the same cell, they have been shown to form mixed channels depending on the presence of sugars in the PANX1 molecular structure. However, we discovered that sugars in the PANX2 molecular structure are not required to interact with PANX1 but define PANX2 location within the cell. Furthermore, abnormal levels of PANX1 have been previously shown to assist the development of melanoma, a deadly type of skin cancer. We showed that in mice genetically engineered to develop melanomas, the absence of PANX1 does not diminish tumor formation or improve survival. Nevertheless, melanoma tumors without PANX1 had increased infiltration of cells responsible for the body's natural defenses against cancer. This study contributes to understanding the effect of chemical modifications on PANX2 distribution and function within the cell. Besides, we uncovered a new role for PANX2 in promoting skin cell death that may be essential to preserve skin health after harmful insults like UV exposure. Moreover, our work lays the foundation of the translational use of targeting PANX1 to enhance current therapies that fight melanoma tumors involving specific cells used by the body's natural defense system.

Co-Authorship Statement

The work herein was carried out and written by the author, under the supervision of Dr. Silvia Penuela, who had the initial conception of the projects, funding acquisition, oversaw its implementation, and assisted with data analysis and preparation/editing of manuscripts.

Chapter 2: Brooke O'Donnell provided the skin sections and assisted with the keratinocyte differentiation and immunostaining protocols. Danielle Jonhston, MSc. provided technical assistance with mutagenesis, primary skin cell isolation, and CRISPR-Cas9 deletion. Dr. Laszlo Gyenis assisted with the design and implementation of the *in vitro* caspase-3 cleavage experiments. Dr. David Litchfield supplied the purified recombinant active caspase-3 and oversaw experimental design for caspase-cleavage and apoptosis experiments.

Chapter 3: Danielle Jonhston, MSc. provided technical assistance with mutagenesis, immunofluorescence, and confocal imaging and reviewed and edited the manuscript. I performed all the experiments, data analysis and wrote the manuscript draft.

Chapter 4: Garth Finch performed most of the real-time qPCR experiments under my supervision, assisted with initial data processing and spleen measurements. Danielle Jonhston provided technical assistance, helped with tumor monitoring, sample collection, colony breeding, and dissections. Kevin Barr assisted with mice breeding and colony establishment. Rober Abdo assisted with dissections and sample collection. Dr. Steve Kerfoot collaborated on the project, provided immunofluorescence protocols, input for experiments, and revised the early manuscript draft. Dr. Lina Dagnino collaborated with grant funding and input on the writing and data analysis.

Dedication

*In memory of my father, who always encouraged me to go beyond the horizon and follow
my dreams;*

*to my son Henry, I hope you will find this thesis an inspiration for the success I know you
will reach; with love, Dada.*

Acknowledgments

First and foremost, I would like to thank my supervisor Dr. Silvia Penuela for allowing me to join her fantastic team and offering an open door with constant support and mentorship throughout my time in the Penuela lab. It seemed like yesterday when we spoke over the phone in that first interview about six years ago, and she made me feel part of her lab even without knowing if it would become a reality to travel to this beautiful country. I also thank her husband, Dr. Laszlo Gyenis, for his constant help with my Ph.D. project and my early adaptation days in London.

I would also like to thank my advisory committee: Dr. Shawn Whitehead, Dr. Frank Beier, and Dr. David Litchfield, for their assistance in the development of this project and challenging questions. All of you made me shift into full Ph.D.-mode and improve my critical thinking during the past years. Special thanks to Dr. Beier, who offered his assistance with reading this thesis; thank you for your wise comments and suggestions. Also, thanks to the whole ACB Department, especially the faculty and administrative staff who work every day to make graduate students' lives manageable in the research and academic activities.

Big thanks to past and present lab mates: Vanessa, Taylor, Daniel, Danielle, Brooke, Brent, Garth, Rober, John, Samar, and the undergrad students in the lab. All of you have made my Canadian experience easier, helped me immensely to get the best out of my results, and made an enjoyable workspace that I will always miss. I consider you dear friends, and I will not forget the time we have spent together: "car five :)".

Last but not least, I would like to thank my beloved wife Yanetsy for always being there for me, for your love, sacrifice, and comprehension, no matter what the circumstances were. To my whole family, a huge thank you since I could not have done this without your support and encouragement over all these years. In particular, thanks to my beloved mother María, my sister Lily, and my late father, Diosmedes. Thanks to my aunt Elsie, cousin René, and his family: Judith, Ryan, and Emma. All of you made it possible for me to come to this country and reach this step in my life. Finally, thanks to my beloved son Henry for the laughter and joy you brought that helped me navigate this challenging time.

Table of Contents

Abstract	ii
Keywords	iii
Summary for Lay Audience	iv
Co-Authorship Statement.....	v
Dedication	vi
Acknowledgments.....	vii
Table of Contents	viii
List of Tables	xiv
List of Figures	xv
List of Supplemental Figures	xviii
List of Abbreviations	xix
Chapter 1	1
1 Introduction	1
1.1 Overview of the Pannexin Family of Proteins	1
1.2 Alternative splicing of Pannexin 1 and 2 genes	4
1.3 Pannexin 1	6
1.3.1 Pannexin 1 channel three-dimensional structure	6
1.4 Pannexin 2.....	8
1.5 PANX1/PANX2 heteromeric channels.....	9
1.6 Post-translational modifications and regulation of pannexins	10
1.6.1 N-glycosylation and localization of pannexins	16
1.6.2 Caspase cleavage of Pannexin 1 and 2 and their role in cell death.....	17
1.7 Pannexins in the skin	19
1.7.1 Overview of the structure and components of the skin.....	19

1.7.2	Pannexin1 and 2 in the skin	22
1.7.3	Pannexin1 roles in skin cell differentiation and wound healing	23
1.8	Pannexins 1 and 2 in cancer	24
1.8.1	Skin cancer: Melanoma.....	26
1.8.2	Pannexin1 in cutaneous melanoma	35
1.8.3	Considerations on pannexin regulation of the immune infiltration: possible implications for melanoma	36
1.9	Rationale	39
1.10	Hypothesis.....	40
1.11	Objectives	41
1.12	References.....	42
Chapter 2	56
2	Pannexin 2 is expressed in the murine skin and promotes UVB-induced apoptosis of keratinocytes	57
2.1	Introduction.....	57
2.2	Materials and Methods.....	58
2.2.1	Cell lines, transfection, and culture conditions	58
2.2.2	Isolation and culture of mouse epidermal keratinocytes and dermal fibroblasts.....	59
2.2.3	CRISPR-Cas9-mediated PANX2 deletion in REK cells	60
2.2.4	Mutagenesis of Flag-tagged PANX2 constructs.....	60
2.2.5	Protein extractions and western blots.....	61
2.2.6	Immunofluorescence and imaging	62
2.2.7	Detection of caspase cleaved PANX2 fragments	63
2.2.8	RNA isolation and real-time qPCR.....	63
2.2.9	UVB irradiation for induction of apoptosis	64

2.2.10	Live-cell imaging of UVB-induced caspase-3 activation and cytotoxicity	64
2.2.11	IncuCyte data analysis and time to apoptosis calculation.....	65
2.2.12	Statistical analysis.....	66
2.3	Results.....	66
2.3.1	Two PANX2 splice variants are expressed in the mouse dorsal skin.....	66
2.3.2	PANX2 expression is abundant in the epidermis and is likely regulated during the early stages of keratinocyte differentiation.....	70
2.3.3	<i>In vitro</i> caspase-3 cleavage of canonical PANX2 C-terminus occurs at D400 and D416	77
2.3.4	PANX2 C-terminus undergoes cleavage at D416 in UVB-induced apoptotic keratinocytes	81
2.3.5	PANX2 contributes to UVB-induced apoptosis of REK cells independently of its caspase cleavage.....	84
2.4	Discussion	100
2.4.1	PANX2 is always present in the skin and is regulated during keratinocyte differentiation	101
2.4.2	PANX2 promotes keratinocyte apoptosis independently of its caspase cleavage.....	102
2.5	Conclusions.....	103
2.6	Acknowledgments.....	103
2.7	References.....	104
Chapter 3	107
3	N-glycosylation regulates Pannexin 2 localization but is not required for interacting with Pannexin 1	108
3.1	Introduction.....	108
3.2	Materials and Methods.....	110
3.2.1	Cell lines, constructs, and transient transfections	110
3.2.2	Mutagenesis and cloning of new FLAG-tagged PANX2 constructs	110

3.2.3	Protein extractions and Western blots.....	111
3.2.4	Immunofluorescence, confocal imaging, Linescans and colocalization analysis.....	112
3.2.5	Cell surface biotinylation assays.....	113
3.2.6	Co-immunoprecipitation (Co-IP) assays.....	113
3.2.7	De-glycosylation assays.....	114
3.2.8	Densitometric analysis of Western blots.....	114
3.2.9	Statistics	115
3.3	Results.....	115
3.3.1	Characterization of the PANX2 N-glycosylation site at asparagine 86..	115
3.3.2	N86Q forms intracellular aggregates	118
3.3.3	PANX2 localization at the cell surface is reliant on N-glycosylation status and the level of PANX1	121
3.3.4	PANX2 and N86Q aggregates localize to the endoplasmic reticulum and Golgi apparatus	124
3.3.5	PANX2 N-glycosylation is not required for the interaction with PANX1	129
3.4	Discussion	133
3.5	Conclusions.....	137
3.6	Acknowledgments.....	137
3.7	References.....	137
Chapter 4	141
4	Global Pannexin 1 deletion increases tumor-infiltrating lymphocytes in the BRAF(V600E)/Pten(del) mouse melanoma model	142
4.1	Introduction.....	142
4.2	Materials and Methods.....	144
4.2.1	Mouse breeding and genotyping.....	144

4.2.2	Melanoma tumor induction, monitoring, and sample collection	144
4.2.3	Tissue Processing, RNA Extraction, real time-qPCR.....	145
4.2.4	Tissue preparation, cryo-sectioning, and immunofluorescence staining	147
4.2.5	Antibodies used for immunofluorescence.....	147
4.2.6	Image acquisition and analysis	147
4.2.7	Statistical analysis	148
4.3	Results.....	149
4.3.1	<i>Panx1</i> global-deletion does not affect primary tumor characteristics or melanoma progression of Braf(V600E)/Pten(del) mice	149
4.3.2	<i>Panx1</i> -deletion does not prevent melanoma metastasis to inguinal lymph nodes	156
4.3.3	Spleens are significantly enlarged in females of tumor-induced BPC- <i>Panx1</i> ^{-/-} mice compared to males.....	158
4.3.4	BPC-mice lacking PANX1 exhibit increased CD8 expression in the skin and melanoma tumors	161
4.3.5	Germline <i>Panx1</i> -deletion increases the tumor infiltration of CD4+, CD8+ T lymphocytes, and Granzyme B producing cells	168
4.4	Discussion	173
4.5	Conclusions.....	176
4.6	Acknowledgments.....	176
4.7	References.....	176
Chapter 5	181
5	Discussion	181
5.1	Summary of main findings.....	181
5.1.1	PANX1 and PANX2 expression and implications for regulation of skin homeostasis	182
5.1.2	Considerations on the importance of PANX2 N-glycosylation for its subcellular trafficking and interaction with PANX1	185

5.1.3	Possible pro-apoptotic roles and effects of caspase cleavage of PANX2 in skin cells	191
5.1.4	Pannexin 1: a new regulator of tumor immune infiltration in melanoma	193
5.2	Experimental Limitations.....	200
5.3	Future directions	203
5.4	Overall conclusions.....	205
5.5	References	206
	Appendix.....	213
	Curriculum Vitae	217

List of Tables

Table 1-1 List post-translational modifications reported for PANX1 and PANX2.....	11
Table 2-1 Primers used for real-time qPCR.....	64
Table 2-2 Pannexin 2 orthologs information in genomic and protein databases.....	69
Table 2-3 Predicted Caspase 3/7 cleavage sites in mouse PANX2	77
Table 4-1. List of primers used for real-time qPCR analysis.....	146

List of Figures

Figure 1-1 Representation of the mouse pannexin members and locations of residues with reported post-translational modifications.....	3
Figure 1-2. Representation of regulation of PANX1 and PANX2 by N-glycosylation and caspase cleavage	15
Figure 1-3. Schematic representation of the skin structure and layers of the epidermis. ...	21
Figure 1-4. Schematic of the two main therapy options for metastatic melanoma: targeted therapy and checkpoint inhibitors.	30
Figure 1-5. Summary of factors causing immune evasion phenotypes and immunotherapy resistance in metastatic melanoma.	33
Figure 1-6. The complexity of PANX1 expression in the tumor microenvironment.	38
Figure 2-1 Transcript and protein levels of PANX2 variants are differentially regulated in mouse dorsal skin.....	68
Figure 2-2 . Pannexin 2 is abundant in the suprabasal layers of the epidermis of mouse dorsal skin.	72
Figure 2-3 PANX2 levels are regulated in keratinocytes during <i>in vitro</i> CaCl ₂ -induced differentiation.....	76
Figure 2-4 Canonical mouse PANX2 C-terminus is cleaved by caspase-3 <i>in vitro</i> at D400 and D416.	80
Figure 2-5 PANX2 C-terminus is cleaved at D416 during UVB-induced apoptosis of REK cells.	83
Figure 2-6 PANX2 promotes UVB-induced apoptosis of REK cells independently of its caspase-3/7 cleavage.	88
Figure 3-1 PANX2 is N-glycosylated at asparagine 86.....	117

Figure 3-2 PANX2 N-glycosylation-deficient mutant (N86Q) forms intracellular aggregates in NRK cells.....	120
Figure 3-3 Localization of PANX2 and N86Q in AD293 and HEK293T cells expressing endogenous PANX1.....	123
Figure 3-4 PANX2 and N86Q colocalize with markers of the endoplasmic reticulum and Golgi.	126
Figure 3-5 PANX2 and N86Q do not localize to late endosomes/lysosomes or mitochondria.	128
Figure 3-6 PANX2 glycosylation is not required for the interaction and immunoprecipitation with PANX1.	131
Figure 3-7 N-glycosylation enhances PANX2 trafficking to the plasma membrane and colocalization with PANX1.	132
Figure 4-1 Global <i>Panx1</i> deletion does not improve survival or reduce tumor progression in the Braf(V600E)/ Pten(del) mouse melanoma model.....	152
Figure 4-2 Pigmentation or ulceration of the Braf(V600E)/Pten(del) melanoma lesions are not influenced by the global <i>Panx1</i> deletion.....	155
Figure 4-3 <i>Panx1</i> deletion does not prevent the development of Braf/Pten-driven melanoma micro-lesions or metastasis to inguinal lymph nodes in BPC mice.	157
Figure 4-4 BPC- <i>Panx1</i> ^{-/-} mice exhibit sex-dependent differences in spleen size not observed in BPC- <i>Panx1</i> ^{+/+} cohort.	160
Figure 4-5 CD8 T-lymphocyte mRNA marker is significantly increased in the non-tamoxifen treated skin and melanoma tumors of BPC-mice lacking PANX1.....	164
Figure 4-6 Global <i>Panx1</i> -deletion does not affect the mRNA expression of phenotypic markers of activation of tumor-infiltrated T-lymphocytes.	167

Figure 4-7 Tumor-infiltrating CD4+, CD8+ T-lymphocytes, and Granzyme B producing cells are significantly increased in BPC- <i>Panx1</i> ^{-/-} tumors.	170
Figure 5-1 Graphical representation of the proposed model of PANX2 regulation by N-glycosylation and caspase cleavage.	186
Figure 5-2 N-glycosylation site in mouse PANX2 is highly conserved among species.	189
Figure 5-3 Graphical representation of main findings in the <i>Panx1</i> -deficient BPC mouse melanoma model.	195
Figure 5-4 <i>PANX2</i> mRNA expression does not correlate with <i>PANX1</i> nor predict survival of patients with malignant melanoma.	197

List of Supplemental Figures

Supplemental Figure 2-1. Sequence alignments between mouse PANX2 (canonical) and Panx2-202 variants.....	90
Supplemental Figure 2-2. Immunofluorescence labeling of mouse dorsal skin with polyclonal anti-Panx2 antibodies and epitopes mapped in Panx2-202 sequence.	92
Supplemental Figure 2-3. Endogenous <i>Panx2</i> mRNA levels in primary dermal mouse fibroblasts decrease after <i>in vitro</i> myofibroblast activation with TGF- β	93
Supplemental Figure 2-4. Lane profile analysis of immunoprecipitations after <i>in vitro</i> PANX2 caspase cleavage experiments	95
Supplemental Figure 2-5. Lane profile analysis of IP after in-cell Panx2 caspase cleavage experiments in UVB-induced apoptotic REK-PANX2KO cells.	97
Supplemental Figure 2-6. Caspase cleavage site D416 in mouse PANX2 is conserved in the human but not in the rat ortholog.....	99
Supplemental Figure 4-1 <i>PANX1</i> mRNA expression is similar between patients with and without co-occurrence of BRAF(V600E) /Pten (homozygous deletion).....	172

List of Abbreviations

3D	Three dimensional
AD293	Adherent human embryonic kidney cells
ANOVA	Analysis of variance
ATP	Adenosine triphosphate nucleotide
AUC	Area under the curve
BPC	inducible melanoma model: $Braf^{CA}$, $Pten^{loxP}$, $Tyr::CreER^{T2}$
<i>BRAF/BRAF</i>	Serine/threonine-protein kinase B-Raf/ B-raf proto-oncogene
BSA	Bovine serum albumin
Ca^{2+}	Calcium
CAM	Chick chorioallantoic membrane
Cas9	Cas9 nuclease
CBX	Carbenoxolone
CCRCC	Clear cell renal carcinoma
CD	Cluster of differentiation
Chr	Chromosome
CNS	Central nervous system
Co-IP	Co-immunoprecipitation
COPII	Coat protein II
CRISPR	Clustered regularly interspaced short palindromic repeats
CT	C-terminal domain
CTLA-4	Cytotoxic T-lymphocyte-associated antigen-4
D400A	Aspartic acid to alanine substitution at amino acid position 400
D416A	Aspartic acid to alanine substitution at amino acid position 416
DCs	Dendritic presenting cells
del	deletion
DMEM	Dulbecco's Modified Eagle Medium
EL	Extracellular loop domain

EMT	Epidermal-to-mesenchymal transition
Endo H	Endoglycosidase H
ER	Endoplasmic reticulum
FBS	Fetal bovine serum
Fe ²⁺	ferrous iron
GAPDH	Glyceraldehyde 3-phosphate dehydrogenase
GFP	Green fluorescent protein
Gly0	Non-glycosylated protein species
Gly1	High-mannose N-glycosylated protein species
Gly2	Complex N-glycosylated protein species
GM130	Golgi matrix protein 130 kDa
GzmB	Granzyme B
HEK293T	Human embryonic kidney cells with SV40 T-antigen
HIV	human immunodeficiency virus
IL	Intracellular loop domain
IP	Immunoprecipitation
K ⁺	Potassium
kDa	Kilodalton
KO or -/-	knockout
LAG-3	Lymphocyte activation gene-3
LAMP2	Lysosome-associated membrane glycoprotein 2
MAPK	Mitogen-activated protein kinase
MDSC	Myeloid-derived suppressor cells
MEK	Mitogen-activated protein kinase kinases
MEM	Minimum Essential Media
Mg ²⁺	Magnesium
MHC	Major histocompatibility complex
MITF	Microphthalmia-associated transcription factor
mRNA	Messenger RNA
MW	Molecular weight

N86Q	Asparagine to glutamine substitution at amino acid position 86
NK	Natural killer cells
NLRP3	Nod-like receptor family pyrin-domain containing-3
NPC	Neural progenitor cells
NRK	Normal rat kidney cells
P	Postnatal day
P2X7R	P2X purinergic receptor 7
PANX1	Pannexin1 protein
<i>Panx1</i>	Mouse, rat gene encoding PANX1
<i>PANX1</i>	Human gene encoding PANX1
PANX2	Pannexin2 protein
<i>Panx2</i>	Mouse, rat gene encoding PANX2
<i>PANX2</i>	Human gene encoding PANX2
PBN	Probenecid
PBS	Phosphate buffer saline
PCR	Polymerase chain reaction
PD-1	programmed cell death protein 1
PDI	Protein disulfide isomerase
PD-L1	Ligand for PD-1
PI3K/AKT	Phosphoinositide 3-kinase/protein kinase B
PNGase F	Peptide-N-glycosidase F
PTEN	Phosphatase and tensin homolog
PTMs	Post-translational modifications
QC	Quality control
qPCR	Quantitative PCR
REK	rat epidermal keratinocytes cell line
REK-PANX2KO	REK <i>Panx2</i> -knockout cell line
RT	Room temperature
RNA	Ribonucleic acid
SDS	Sodium dodecyl sulfate

SDS-PAGE	SDS-polyacrylamide gel electrophoresis
STS	Staurosporine
SV40	Simian vacuolating virus 40
TGF	Transforming growth factor
TILs	Tumor-infiltrating lymphocytes
TM	Transmembrane domain
TME	Tumor microenvironment
T-reg	Regulatory T lymphocytes
UV	Ultraviolet light
V600E	Valine to glutamic substitution at amino acid position 600
WB	Western blot
WT	Wildtype

Chapter 1

1 Introduction

1.1 Overview of the Pannexin Family of Proteins

Pannexins are a family of three integral membrane glycoproteins designated Pannexin1 (PANX1), Pannexin2 (PANX2), and Pannexin3 (PANX3) discovered in the earlier 2000s [1, 2]. Pannexins share homology with innexins but not connexins, two families of proteins that physically join the cytoplasm of adjacent cells, forming gap junctions and hemichannels in invertebrates and mammals. Initially, due to their topological similarities to connexins, and limited sequence homology to innexins, it was thought that pannexins could form gap junctions. However, that theory has already been revised since their primary function is to make non-docking membrane channels [3-5]. Additionally, despite differences in sequence homology, these three protein families exhibit similar topology consisting in four α -helical transmembrane domains (TM), two extracellular loops (EL), one intracellular loop (IL), and their amino (NT) and carboxyl (CT) termini exposed to the cytoplasm [6] (Fig. 1-1). In particular, instead of six extracellular cysteines as in connexins, pannexins have four conserved extracellular cysteine residues that form disulfide bonds and are required for functional channel formation [7, 8]. Nevertheless, pannexins can form large-pore channels permeable to the diffusion of ions and macromolecules up to one kilodalton (kDa) in size and are involved in intracellular, paracrine, and autocrine signaling [9, 10]. In the following sections, a more in-depth description of the structure, function, and regulation will be focused on PANX1 and PANX2 and their contribution to health and pathological states, as these are the most relevant for my thesis.

Figure 1-1

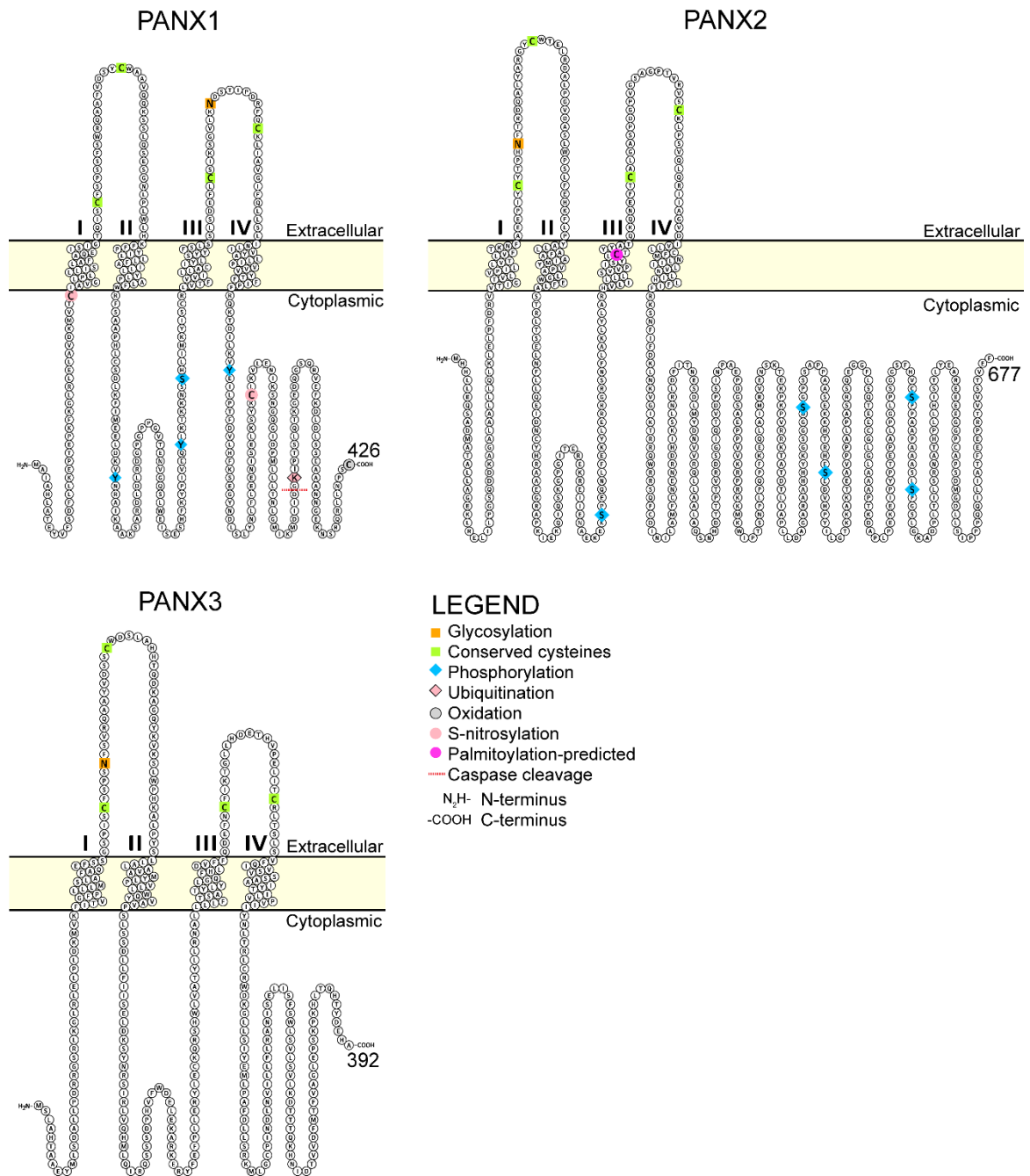


Figure 1-1 Representation of the mouse pannexin members and locations of residues with reported post-translational modifications.

The pannexin family is represented by three tetra-spanning proteins that can oligomerize to form membrane channels capable of dye uptake and conducts for nucleotides, ions, and other metabolites. All pannexins share a similar topology with two extracellular loops, one intracellular loop, and the amino and carboxyl terminus located in the cytosol. Transmembrane domains are indicated with roman numerals, and numbers indicate the last residue in the polypeptide sequence. Several post-translational modifications (colored residues) have been identified mainly for PANX1 and PANX2. Figure created with Protter [11].

1.2 Alternative splicing of Pannexin 1 and 2 genes

The Pannexin1 gene (designated *PANX1* in humans and *Panx1* in mouse and rat) comprises four introns and five exons encoding a 426 amino acids (aa) long glycosylated protein with an expected molecular weight (MW) ranging from ~41-48 kDa and exhibits broad expression in mammalian tissues and organs [6, 12]. The Pannexin 2 gene (designated *PANX2* in humans and *Panx2* in mice) comprises four exons encoding the longest pannexin protein (677 aa) with an expected molecular mass ~74.4 kDa [13]. Genes encoding PANX1 and PANX3 are located on the same chromosome (Chr) (Chr 11, in humans; Chr 9, in mouse), and their proteins share a higher homology (~41% identity) in amino acid sequence than with PANX2 (~30% identity), whose gene is located on a different Chr (human Chr22 and mouse Chr15) [2, 14]. Noticeably, the PANX2 C-terminus is longer than in the other pannexins and shares only ~8% of sequence identity with PANX1 [15, 16]. The initial gene expression profiling studies showed that *Panx2* mRNA expression seemed restricted to the central nervous system (CNS), where it was found most abundantly in the cortex, hippocampus, cerebellum, and olfactory bulb olfactory epithelium [17-19]. However, more recent reports indicated that *Panx2* is more ubiquitously expressed and is present in different cell types and other tissues such as skin, liver, retina, intestine, and kidney [20-26]. *Panx1* and *Panx2* gene expression have been found to overlap in the adult rodent brain but intriguingly are inversely regulated throughout development, with *Panx1* more abundant in neonatal and young tissues, whereas *Panx2* is increased in the adult [14, 27, 28]. Furthermore, other studies showed that *Panx2* is differentially expressed by multipotential neural progenitor cells and mature neurons, with protein expression and post-translational modifications (e.g., palmitoylation) modulating neuronal differentiation [29].

Current annotations in genomic databases predict the presence of several alternative splice variants for both pannexin genes, which some authors have confirmed in different tissues and cell types. Therefore, various pannexins protein variants (also known as isoforms) may contribute to different functions depending on their tissue of origin. To date, a more

comprehensive understanding of the potential pannexin transcripts is still lacking, but a few examples are given below.

Initially, Baranova et al. (2004) described that the exon 5 could be alternatively spliced in human *PANX1* (hPanx1a, 426 aa), generating the hPanx1b (422 aa) variant that differs in a four-amino acid insertion within the C-terminus [2]. Notably, this hPANX1b variant seems more prevalent in human tissues [30]. Ma et al. (2009) [30] uncovered another variant (hPanx1bv, 425 aa) resulting from a codon duplication for the human *PANX1* gene. Overexpression of these three human variants showed more similar localization patterns and functional properties than mouse PANX1, but the functional outcomes were species-dependent [30]. It has also been reported that alternative splicing in exons 2 and 4 generates two *Panx1* variants (Panx1b and Panx1d, 356 and 309 aa, respectively) in rat pituitary cells. However, both variants were found more intracellular than the canonical form and exerted a dominant-negative effect on the ATP-release activity when co-expressed with full-length PANX1 [31]. Another shorter PANX1 isoform (Panx1c, 356 aa) was detected in the rat male reproductive tract, likely from splicing of exon 3 of canonical rat *Panx1* (Panx1a). Remarkably, in that study, all rat *Panx1* variants were repressed by testosterone in the epididymis [32].

Regarding PANX2, despite several predicted annotations in genomic databases of NCBI and Ensembl, it appears that only one single splice variant has been discovered in the human brain. Baranova et al. (2004) reported a shorter *PANX2* splice variant (termed PANX2alt2, 509 aa), in addition to the canonical human isoform (PANX2alt1 encoding a protein of 633 aa), that is a product of the initiation in an alternative start codon and implied to have a regulatory role [2]. In zebrafish, three *Panx2* isoforms were found with differential expression among tissues: Isoform drPanx2-A exclusive of the brain, drPanx2-C, found in brain and retina, and drPanx2-B, more widely expressed in the zebrafish tissues [33]. Since PANX2 isoform expression has not been extensively examined, it is unclear whether other splice variants are differentially expressed in mammal tissues and exhibit different functional characteristics compared to the canonical.

1.3 Pannexin 1

The research interest in PANX1 has increased significantly due to its implication on several physiological and pathophysiological processes such as keratinocyte differentiation [34, 35], glucose uptake [36], myogenesis [37], apoptotic cell clearance [38], inflammation [39, 40], tumorigenesis [41-44] and metastasis [43, 45-49], hypertension [50, 51], immune response [52-56], HIV infection [57, 58] and ischemia [59-63]. Most cellular processes involving the PANX1 channel are modulated by releasing ions, nucleotides, and metabolites that vary by cell type [10, 38, 64-66]. The subcellular cycle of PANX1 starts with its synthesis in the endoplasmic reticulum (ER), from where it is trafficked towards the cell membrane regulated by COPII (coat protein II)-dependent ER-to-Golgi forward trafficking with the later channel internalization independent of clathrin/caveolin/dynamin II mechanisms [67, 68]. Interestingly, plasma membrane-localized PANX1 has a long half-life (>21-32h) [6, 69].

Some of the identified stimuli triggering PANX1 channel activation include mechanical stress, voltage, increased intracellular calcium levels, ionotropic and metabotropic receptor signaling, and C-terminus proteolytic cleavage [56, 64, 70-73]. PANX1 is mainly known for mediating adenosine triphosphate (ATP) release at the plasma membrane, but it also serves as a calcium leak channel when located at the ER [74]. Interestingly, as a negative feedback mechanism of channel regulation, it has been shown that the binding of ATP to extracellular binding sites not only blocks PANX1 currents and ATP release but can induce channel internalization [68, 75, 76]. It has also been demonstrated that PANX1 channels favor anionic over cationic permeants [10]. However, its caspase-mediated proteolytic cleavage elicits efflux of a wide variety of metabolites from apoptotic cells (e.g., spermidine) that mediate intercellular signaling processes, including inflammation and immune cell recruitment [38, 66].

1.3.1 Pannexin 1 channel three-dimensional structure

Published studies aiming at the 3D structure determination of pannexins have been limited to PANX1. At least three independent groups have determined the molecular structure of

PANX1 at near-atomic-resolution for humans (*Homo sapiens*) and frog (*Xenopus tropicalis*) by cryo-electron microscopy, revealing a unique heptameric channel architecture [77-79]. From the PANX1 structure, it was revealed that the extracellular domain of each monomer comprises one helix, three β -sheets, and two conserved disulfide bonds. Besides, the extracellular channel entrance forms a cap structure with a network of electrostatic interactions securing a neutral potential in that region. Moreover, some essential residues are placed strategically, forming the channel. For example, seven tryptophan (W74) residues line the outer region wall, restricting the maximum size of permeable molecules. An arginine (R75) residue from a neighboring helix forms a cation- π interaction with W74 and a salt bridge with an aspartic acid residue (D) at position 81, stabilizing the tryptophan ring configuration. Michalski and collaborators (2020) [79] showed that R75 residue is a significant determinant of anion selectivity of PANX1 channels in the open state that is critical for the channel inhibition by high concentrations of ATP and its analogs [79, 80]. Mou et al. reported a narrow ring structure formed by other residues (T21/E22/P23) in the N-terminus that controls channel opening [78].

The first transmembrane domain (TM) 1 appears tilted by $\sim 30^\circ$ in the membrane and places the residue isoleucine (I) 58 at the narrowest point of the pore-lining region, with a hydrated diameter of $\sim 13\text{\AA}$. Consequently, the pore is substantially widened toward the intracellular side, where TM2 makes the expanded pore with TM3 and TM4 arranged in the channel periphery. Interestingly, the 3D structure exhibits a voluminous intracellular vestibule with abundantly charged amino acids facing the pore lumen with an overall positive electrostatic potential that facilitates the recruitment of anions or negatively charged molecules [77]. Due to the dynamic nature of the intracellular segments, the C-termini regions of the oligomeric channel have not been resolved in the cryo-EM density maps. However, accumulating evidence indicates that the C-terminus blocks the channel pore permeability via a "ball-and-chain" mechanism [38, 81], a notion that is still to be proven for other family members. A previous study used a genetically engineered PANX1 containing a Tobacco Etch Virus (TEV) protease recognition sequence at the caspase cleavage site of the C-terminus [81]. These authors demonstrated that the proteolytic cleavage of PANX1 occurs at the plasma membrane and induces the channel opening. However, even the detached

PANX1 C-terminus fragment can inhibit cleavage-activated channels, implying a negative feedback mechanism to control channel activation [81]. Interestingly, a progressive $\alpha 1$ -adrenoceptor-mediated PANX1 channel activation or cleavage of the C-terminal autoinhibitory regions in each subunit produces a gradual increase in channel permeability and has been proposed as a fine-tuning activation mechanism for this multimeric channel [82].

1.4 Pannexin 2

Most studies have shown that PANX2 exhibits intracellular localization, yet in overexpression systems, it has also been found at the cell membrane and colocalizing with PANX1, forming heteromeric channels [5, 7]. However, previous colocalization studies have also indicated that overexpressed PANX2 is mostly cytoplasmic and can be found with markers of early endosomal sorting [83]. Additionally, PANX2 has been shown to colocalize with an endosomal enriched mannose-6-phosphate receptor in a neuroblastoma cell line [84]. More recently, Le Vasseur et al. (2019) have shown that ectopic and endogenously expressed PANX2 localize at ER-mitochondria contact sites in C6 glioma cells and mouse brain sections [85]. These many conflicting pieces of evidence suggest that PANX2 channel localization could be cell-type dependent or due to regulatory and sorting mechanisms such as post-translational modifications including palmitoylation and glycosylation [86, 87], as I will discuss later in this chapter.

To date, the 3D structure of PANX2 channels remains to be solved, and there has been some disagreement about whether PANX2 forms functional homomeric channels [14, 70]. Nevertheless, early studies determined that rat PANX2 forms active octameric channels in *Xenopus oocytes* and *in vitro* vesicle assays. In such studies, a voltage-dependent opening of PANX2 channels was detected at high positive membrane potentials, and unlike PANX1, PANX2 channels did not respond to extracellular K^+ and were unaffected by the PANX1 blockers, Carbenoxolone and Probenecid [7]. Furthermore, it has been suggested that PANX2 channels can be mechanically stimulated and are capable of dye uptake under physiological Ca^{2+} and Mg^{2+} conditions [5]. Remarkably, the PANX2 channel function appears to be compromised when combined with PANX1 [5, 7], suggesting that co-

expression of both pannexins in the same cells may exert mutual inhibition, which has been proposed as a mechanism of regulation. Despite this, the functional significance of PANX2 is not clear yet. Using a *Panx2*-knockout (KO) mouse model, it was proposed that PANX2 channel activation promotes neurodegeneration after ischemic brain damage [59]. In that stroke model, only when both *Panx1* and *Panx2* genes were knocked out (*Panx1*^{-/-} and *Panx2*^{-/-}), a reduction in infarct size and neurological damage was achieved after ischemia, indicating potential compensatory roles between these two proteins in the CNS [59, 88]. These authors also showed that even in the absence of PANX1, *Panx2* deletion reduced dye leakage of primary cortical neurons loaded with calcein green dye after cytotoxic-hypoxia induced with sodium cyanide (NaCN), indicating that PANX2 is also capable of forming dye-release channels in neurons.

1.5 PANX1/PANX2 heteromeric channels

Previous studies have investigated the potential interaction among pannexin family members and intermixed channel formation due to co-expression patterns in tissues and the significant sequence homology shared between pannexin family members. In *Xenopus oocytes*, coinjection of rat *Panx1* and *Panx2* RNAs resulted in channel formation with different functional properties from those formed by PANX1 alone [14]. Despite that difference, further research by the same authors found that the pharmacological sensitivity of heteromeric PANX1/PANX2 was similar to that of homomeric PANX1 channels [70]. Penuela et al. (2009) demonstrated that when HEK293T ectopically co-expressed both *Panx1* and *Panx2* murine constructs, their proteins physically interact, and there is a significant reduction in dye uptake incidence compared to cells expressing a single pannexin paralog [5]. It has been proposed that this "intermixing" attenuates the heteromeric channel function [5, 70]. Later, Ambrosi et al. (2010) focused on characterizing purified oligomeric structures of pannexins channels and confirmed these findings. However, PANX1/PANX2 heteromeric channels were unstable over time, attributed to differences in monomer size and divergences in the homomeric and heteromeric symmetry [89]. Interestingly, pannexins intermixing appears to be regulated by the glycosylation status of each monomer, as is discussed later in this chapter.

1.6 Post-translational modifications and regulation of pannexins

Various post-translational modifications (PTMs) have been reported on the pannexin family to regulate their localization, interaction, and channel activity [13, 38, 86, 90]. Although proteomic discovery by mass spectrometry has identified several PTMs in pannexins, currently PANX1 is the most characterized member, harboring at least six different types of modifications that have been experimentally validated (Fig.1-1 and Table 1-1). In contrast, most PANX2 PTMs have been predicted or identified by biochemical and high throughput studies using mass spectrometry but have not yet been studied thoroughly. Until the writing of this thesis, the four main types of PTMs identified or predicted for PANX2 were: N-glycosylation, caspase cleavage, phosphorylation, and S-palmitoylation [86, 91].

Table 1-1 List post-translational modifications reported for PANX1 and PANX2

Post-translational modification	Site	Effect on the protein or function	References
PANX1			
N-glycosylation	N254	Regulates trafficking and intermixing with PANX2	[3-5, 92] †
Phosphorylation	Y10	Influences localization and channel function	[93, 94] †
	Y150	Regulates glycosylation and trafficking	[95] †
	Y192	Unknown	[96] †
	Y198 (Y199 in human)	Possible channel activation	[96-98] †
	Y308	Activates channel	[99]
	S206	Inhibits channel	[100]
	S394* †		
	S182, S189 (S188 in human), S425	Unknown	[101-103], [104] †
S328 † (S329 in human), T302	Possible channel inhibition	[105]	
S-nitrosylation	C40, C346	Inhibits channel	[8, 90, 106]
Caspase cleavage	D167* only in human	Unknown	[38]
	D378 (D379 in human)	Irreversible channel opening	[38, 81, 86, 107]
Ubiquitination	K201, K307, K343, K355, K381 (K380 in human) †, K409*	Unknown/Putative Degradation	[96] †, [103, 108, 109] †
Oxidation	C426	Inhibits channel	[110]
Acetylation	K140; K203, K204, K212	Inhibits channel; Unknown	[96, 111] †
PANX2			

N-glycosylation	N86	Regulates subcellular localization (see Chapter 3)	[5, 92, 112] †
Palmitoylation	C246 (predicted)	Retain intracellular localization and possibly prevents N-glycosylation	[87]
Phosphorylation	S514, S204, T275* (A274 in human), S279 (S278 in human), S495* (P491 in human), S593, S604	Unknown	[113, 114] , [96]†
Ubiquitination	K183	Unknown/Putative Degradation	
Caspase cleavage	Predicted D373, D407, D416, and D479	Unknown	[86]

Table Notes: *- amino acid residue not conserved among human, mouse, and rat paralogs.

† verified/discovered by high throughput mass spectrometry reported in PhosphositePlus® database as of May-07-2021.

One of the early characterized PTM for PANX2 was S-palmitoylation and was identified by biochemical tests used to understand the reduced electrophoretic migration of neural progenitor cell (NPC)-specific PANX2 protein species. However, the specific S-palmitoylation site in the PANX2 amino acid sequence was not confirmed [87]. In that respect, Swayne et al. (2010) showed that endogenous PANX2 appeared palmitoylated with an apparent molecular weight of ~85 kDa besides the non-palmitoylated ~60 kDa immunoreactive species also found in NPC cultures. Notably, the higher MW species were absent in adult brain tissue (e.g., hippocampus) and not observed in cultured neuronal cells after differentiation. Furthermore, S-palmitoylation was implied to regulate PANX2 subcellular localization, where palmitoylated PANX2 in undifferentiated NPCs and primary neurons exhibited intracellular staining of PANX2 along with ER and Golgi markers but not in the plasma membrane. However, in mature neurons, differentiated NPCs, and N2a cells (a mouse neuroblastoma cell line), non-palmitoylated PANX2 was found at the cell membrane, indicating that this PTM may restrict the PANX2 sorting [87]. Interestingly, in that study, de-glycosylation did not markedly alter the electrophoretic band migration of endogenous PANX2, and only the higher species were sensitive to de-palmitoylation procedures.

Investigating PTMs offers a better understanding of pannexin regulation, which could differ or have implications in health and disease states. Therefore, the following subsections will focus on two mainly studied PTMs in PANX1 and PANX2: glycosylation and caspase cleavage but will not include phosphorylation as it is not within the scope of this thesis. A summary of the current model of regulation of PANX1 and PANX2 by N-glycosylation and caspase cleavage is shown in Fig. 1-2.

Figure 1-2.

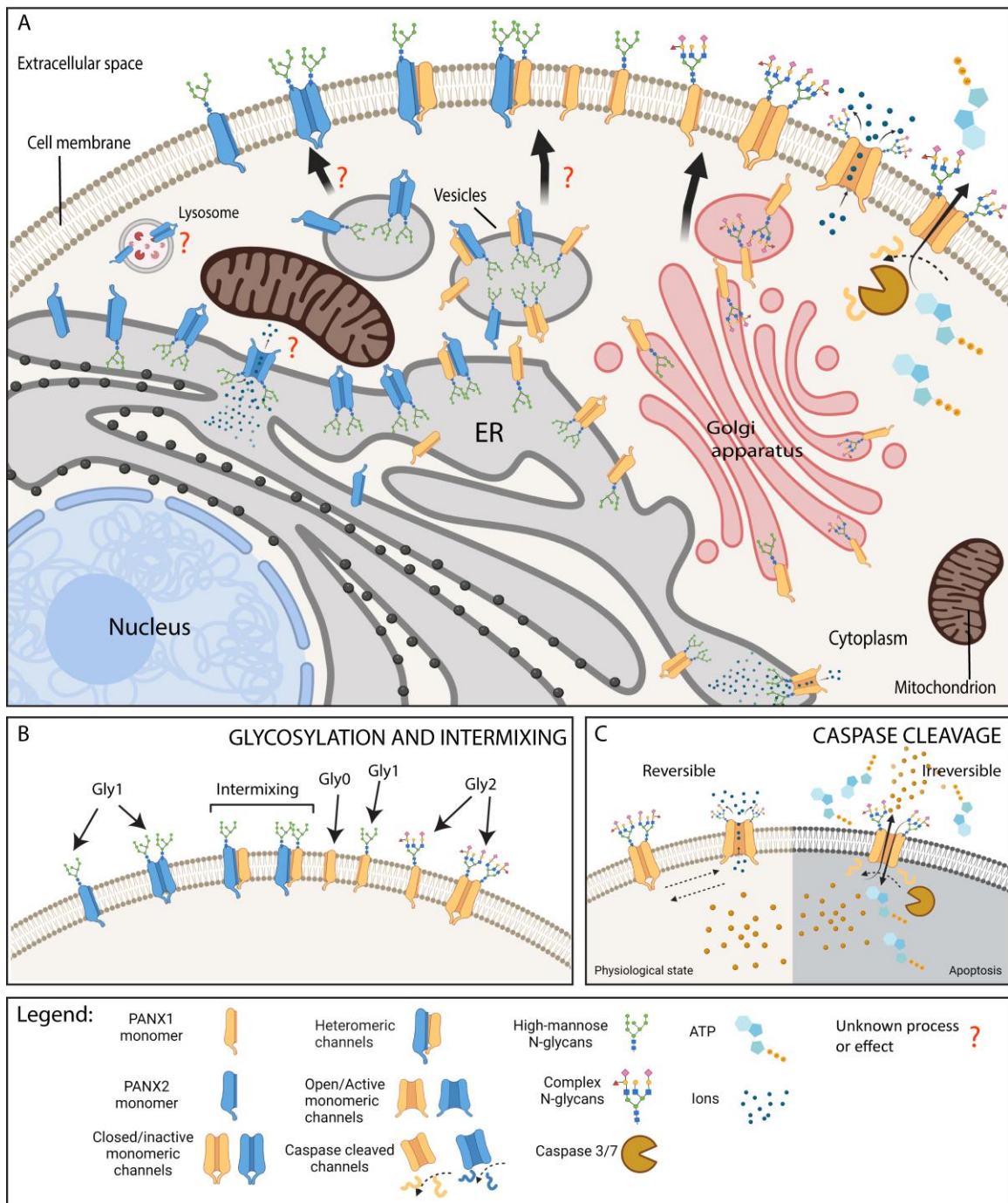


Figure 1-2. Representation of regulation of PANX1 and PANX2 by N-glycosylation and caspase cleavage

(A) Hypothesized snapshot of subcellular localization of PANX1 and PANX2. After protein synthesis, PANX1 and PANX2 are N-glycosylated and may oligomerize in the endoplasmic reticulum (ER) to function as intracellular channels, although this has not been demonstrated for PANX2. PANX1 follows anterograde trafficking through the Golgi apparatus, and high-mannose glycosylated species can be further modified to complex glycosylation and localize to the cell membrane where it works as an ATP/ion channel or can intermix with PANX2 monomers. PANX2 is N-glycosylated to high-mannose species and is predominantly intracellularly located within the ER-mitochondria contact sites and intracellular vesicles: endosomes and lysosomes. Although the details about PANX2 anterograde trafficking are yet to be elucidated, under some circumstances (overexpression or co-expression with PANX1), PANX2 can reach the cell membrane and form channels.

(B) PANX1 and PANX2 species can intermix at the ER membrane or the plasma membrane. Only PANX1 high-mannose or un-glycosylated species can intermix with PANX2 (C). In physiological conditions, the opening of PANX1 channels is a reversible process and regulated by intracellular and extracellular cues and post-translational modifications; however, during apoptosis, the C-terminus of PANX1 can be cleaved by active apoptotic caspases-3/7 causing the irreversible PANX1 channel opening and releasing ATP, ions, and other metabolites to the extracellular milieu. PANX2 can also be cleaved by caspase *in vitro*, but it is unknown if this also happens in apoptotic cells and what the consequences of the cleavage are. Figure created with BioRender.com.

1.6.1 N-glycosylation and localization of pannexins

N-linked-glycosylation (a.k.a. N-glycosylation) is a type of PTM known to modulate protein folding and trafficking of membrane-bound proteins. N-glycosylation starts in the ER lumen with the addition of high-mannose sugars to the synthesized proteins and is carried out by glycosyltransferase enzymes. Further modifications occur to the attached glycan moiety and are processed into complex-form glycans once the protein has trafficked to the Golgi apparatus [115, 116]. The sequence motif Asn-X-Ser/Thr (where X is any amino acid except Pro) constitutes a prerequisite for N-glycosylation, and prediction servers use this feature for *de novo* identification of putative N-linked glycosylation sites. Initial studies showed that PANX1 and PANX3 have consensus sites for N-linked glycosylation on asparagine (Asn, N) 254 and 71, respectively [3-5]. In such cases, enzymatic de-glycosylation and site-directed mutagenesis were used to verify the sites [14]. Later, after cloning mouse PANX2, a similar approach was used, and a bioinformatic prediction indicated its glycosylation site at N86, but the experimental confirmation of such site was still lacking [13, 117].

Depending on the degree of N-glycosylation, pannexins glycosylated species are resolved as different electrophoretic bands with increasing molecular weight. For example, unglycosylated PANX1 species (termed Gly0) are typically detected at 41 kDa, high mannose species (termed Gly1) which are produced in the ER are shown at 44 kDa, and more complex glycosylated species (termed Gly2), further modified in the Golgi compartments, confer PANX1 with an estimated molecular weight of 48 kDa [5]. However, unlike others pannexins, PANX2 is only modified to a Gly1 species and presents a primarily intracellular localization that has been previously associated with the lower level of N-glycosylation [13]. Therefore, some authors [118] have speculated that the absence of Gly2 species could indicate a differential trafficking pathway not involving the transient layover at the Golgi apparatus and subsequent trafficking to the cell membrane, as seen with PANX1 and PANX3 [67].

Previous evidence indicates that Gly2 species are evident in PANX1 and PANX3 and are readily trafficked to the cell surface [13]. In such cases, their translocation toward the cell

membrane is disrupted by glycosylation inhibitors or mutation of the respective asparagine residues [13, 69, 117, 119]. However, it remains unclear if similar outcomes take place regarding PANX2. As mentioned earlier, most of the evidence shown so far has led the scientific community to consider that PANX2 has an intracellular localization [120-123]. However, our group and others have found that, under certain circumstances, it can translocate to the plasma membrane, especially when PANX1 is co-expressed [29, 89]. In this regard, it is still unclear whether the level of glycosylation in PANX2 plays any role in such trafficking. Notably, PANX1 and PANX2 were shown to co-immunoprecipitate, but only when PANX1 remains as lower glycosylated forms (Gly0 and Gly1), which likely indicates that the glycosylation may regulate pannexins intermixing or that heteromeric interaction may occur when these proteins are glycosylated in the ER [13].

Furthermore, as the PANX1/PANX2 heteromeric channels have different properties from homomeric ones, they may be influenced by different glycosylated species between monomers. Thus, glycosylation likely plays a role in regulating the heteromeric channel function when the two pannexins are expressed in the same spatial-temporal circumstances. Herein, the confirmation of the N-glycosylation site and its role in PANX2 subcellular localization and intermixing with PANX1 will be the subject of Chapter 3.

1.6.2 Caspase cleavage of Pannexin 1 and 2 and their role in cell death

Caspases are a conserved family of cysteine-dependent aspartic-specific proteases implicated in crucial cellular processes such as programmed cell death and inflammation [124]. Caspase-3 and caspase-7 are known as executioner caspases and carry out the proteolysis of several target proteins to coordinate the terminal events of apoptosis [125]. One of the most studied gating mechanisms for PANX1 is caspase-3/7-mediated cleavage of the carboxyl-terminus inducing irreversible PANX1 channel activation [38, 81, 86, 126]. The first evidence of this caspase-mediated cleavage was demonstrated by Chekeni et al. (2010), where the cleavage of human PANX1 was found to mediate the release of find-me signals (i.e., nucleotides) from apoptotic Jurkat T-cells and consequently the recruitment of monocytes and Cluster of differentiation (CD) 45+ leukocytes towards regions infused with the supernatants of the apoptotic cells [38]. These authors showed that both caspases

cleave in the IL and CT regions using *in vitro* cleavage assays with purified active caspases 3 and 7 and immunoprecipitated PANX1 protein (See sites in Table 1.1). Notably, only the cleavage of the PANX1-CT was found responsible for the irreversible channel activation. Furthermore, it was later shown that the cleaved PANX1 C-terminal peptide could inhibit PANX1 channel function [81], but its interaction with the cytoplasmic vestibule of the PANX1 channel seems to be delocalized and with a low affinity [127].

Remarkably, work by Yang et al. (2015) also implicated the non-canonical inflammasome murine caspase-11 targeting the exact cleavage site of caspase-3/7 in PANX1-CT and promoting pyroptosis (a pro-inflammatory form of cell death) through purinergic receptor (P2X7)-dependent cytotoxicity [107]. The consequence of the caspase-mediated opening of PANX1 channels at the plasma membrane has been investigated. PANX1 cleavage is mainly recognized for inducing ATP release, impairing the cellular metabolic activity during apoptotic conditions [10, 128]. However, recent work by Medina et al. (2020) showed that this caspase-cleavage also facilitates the release of a broader subset of metabolites from apoptotic cells that modulates processes like inflammation, wound healing, and cell proliferation [66].

On the other hand, Penuela et al. (2014) confirmed caspase-cleavage in the murine paralogs PANX1 and PANX2, but not PANX3 [86]. However, although these authors demonstrated the C-terminus of PANX2 to be a target of caspase cleavage, the amino acid residue of the cleavage site was not identified, nor whether PANX2 channels can be opened by caspase cleavage *in vivo*. Interestingly, in ectopic overexpression systems, PANX2 is known to sensitize cells to apoptotic signals [85, 129] and contribute to diverse forms of cell death [25, 85, 88, 129]. Furthermore, as mentioned earlier, Bargiotas et al. (2011) showed that PANX2 (along with PANX1) is linked to neuronal cell death, as demonstrated by *in vitro* and *in vivo* models of acute neuronal damage [59]. These authors proposed that caspase cleavage of pannexins could be a mechanism for channel activation during apoptosis in ischemic stroke, a theory supported by Penuela *et al.* (2014) [86].

Accumulating evidence has shown conflicting roles of PANX2 at promoting or preventing different types of cell death. Le Vasseur et al. (2019) proposed that due to the localization

of PANX2 in the ER-mitochondria contact sites, it could promote the intrinsic apoptotic pathway, which was supported by an increased sensitivity of PANX2-overexpressing C6-glioma cells to staurosporine (STS)-induced apoptosis [85]. In contrast, Bertchold et al. (2017) indicated an anti-apoptotic role of PANX2 when expressed in the pancreatic islets where PANX2-deficiency sensitized pancreatic β -cells to cytokine-induced apoptosis and disrupted glucose tolerance *in vivo* [22]. Lastly, a study performed by Lio et al. (2020) showed a link between up-regulated PANX2 and the antioxidant response of prostate cancer cells where silencing PANX2 expression increased intracellular ferrous iron (Fe^{2+}) and the lipid peroxidation end-product malondialdehyde [25]. That study suggested that PANX2 may play a protective role against ferroptosis, a type of programmed cell death distinct from apoptosis [130]. Considering that PANX2 can be targeted by apoptotic caspases-3/7, it is unknown whether this caspase cleavage has a role in regulating cell death.

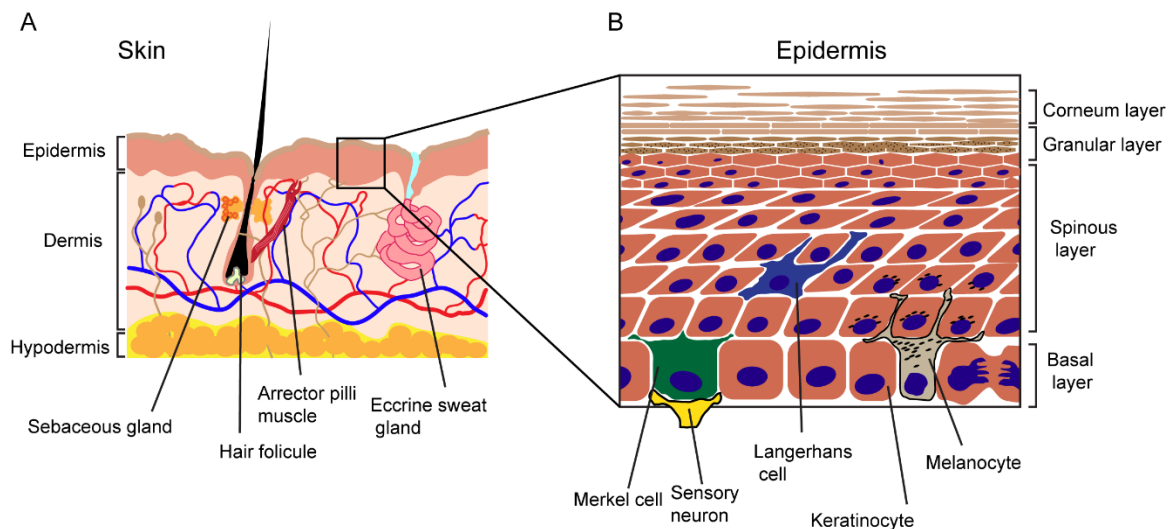
1.7 Pannexins in the skin

1.7.1 Overview of the structure and components of the skin

The skin is the outermost and most extensive organ, constituting a barrier against hazardous substances, ultraviolet radiation, and pathogens entering the body [131]. Among many protective functions, the skin provides temperature regulation, mechanical and temperature sensation through nociceptors [132] and other appendages (e.g., hair follicles, sweat glands, and pilosebaceous units) [133]. Overall, the skin comprises three main layers: epidermis, dermis, and hypodermis (Fig.1-3A).

The epidermis is the outermost layer that acts as a barrier to the external environment and insults, prevents water loss, and maintains body homeostasis. This layer is avascular and is subdivided by an inner proliferative basal keratinocyte layer, the spinous, granular, and stratum corneum upper layers. All the upper epidermal layers are mainly formed by keratinocytes that, upon a detachment from the basement membrane, undergo terminal differentiation (keratinization), forming a layer of flattened dead cells (called corneocytes) that are later shed from the skin (desquamation), where calcium plays a critical role in

regulating keratinocyte proliferation and differentiation [134]. In addition, other minor cell types can be found in the epidermis like the pigment-producing melanocytes, antigen-presenting Langerhans cells, and mechanoreceptive Merkel cells, each with a particular function in this vital layer [131] (Fig. 1-3B). For example, melanocytes are a smaller cell population in the epidermis that synthesize the UV-absorbing pigment melanin in response to the α -melanocyte-stimulating hormone that is secreted by UV-exposed keratinocytes. This pigment is stored in intracellular granules called melanosomes that are eventually transferred to keratinocytes to shield their nuclei from mutagenic effects of UV radiation [135].

Figure 1-3.**Figure 1-3. Schematic representation of the skin structure and layers of the epidermis.**

(A) Representation of the three main layers of the adult mammalian skin. The vasculature, dermal nerves, and an array of skin appendages between the epidermis and the dermis are shown. (B) In the epidermis, an inner layer (basal layer) of proliferative basal cells, known as keratinocytes, detach from the basement membrane (region delimiting dermis and epidermis) and start differentiating, forming the spinous, granular, and stratum corneum layers. Ultimately, the last layer (outer cornified envelope) constitutes a barrier made of dead cellular ghosts packing lipids and crosslinked bundles of keratin filaments. Some cell types are shown within the epidermis: the pigment-producing melanocytes (located along the basement membrane in humans and hair bulbs in mice), sensory Merkel cells, and antigen-presenting Langerhans cells. Other skin resident non-epithelial cells (e.g., dermal fibroblasts, immune, and stem cells) are not shown for simplicity. (Figure drawn in Adobe Illustrator based on descriptions from [131]).

The dermis is thicker than the epidermis and located between the basement membrane (beneath the basal layer) and the hypodermal layer. The dermis comprises two layers: the papillary layer, mainly made up of loose connective tissue, and the reticular layer containing dense elastic fibers and collagen and housing some of the skin appendages. Part of the skin vasculature (capillaries) can be found in the dermis, facilitating nutrient transport. Fibroblasts are the primary dermal cell type, and myofibroblasts (differentiated fibroblasts), mast cells, and other immune cells can also be found in this layer [136].

Underneath the dermis is the hypodermis formed by the subcutaneous fat and abundant extracellular matrix (ECM) components like proteoglycans and glycosaminoglycans. This layer comprises adipocytes, fibrocytes, and multiple immune cells and participates in numerous functions such as insulation, cushion, energy storage, and the production of growth factors, adipokines, and cytokines (reviewed at [136]).

1.7.2 Pannexin1 and 2 in the skin

Early work done by Penuela et al. (2007) showed endogenous PANX1 protein expression (and PANX3) in murine skin, which was detected in the suprabasal epidermal layers (stratum *granulosum* and *spinosum*) [3] and present in keratinocytes, fibroblasts, and hair follicles [34, 35]. Furthermore, Cowan et al. (2012) later verified that PANX1 is present in almost all layers of human skin with a profile punctate or diffused in cells of the epidermis and adnexal structures, respectively [41]. Finally, work by Celetti et al. (2010) and Penuela et al. (2014) explored the temporal regulation of PANX1 through skin aging, demonstrating that PANX1 levels are detected in newborn skin but are later downregulated in aged murine skin [34, 35]. Nevertheless, less is known about PANX2 in the skin, even though its expression was already confirmed by two independent studies [21, 118].

Notably, Abitbol et al. (2019) showed that endogenous PANX2 is expressed at similar levels in the skin of wildtype and double *Panx1/Panx3*-KO mice with a lower MW than the canonical variant, apparently due to a splice variant (called Panx2-202) not previously investigated [21]. In this case, the simultaneous germline deletion of *Panx1* and *Panx3* in mice, among other effects (e.g., litter size, body weight, and bone morphology), impacts

the dorsal skin thickness by reducing the epidermal, dermal, and hypodermal areas in neonatal mice but not at older ages [21]. Interestingly, there was no apparent compensation by the PANX2 splice variant in this double knockout mouse model as suggested with PANX3 in a *Panx1*-KO model [35]. Although there are likely unknown functional compensatory mechanisms to cope with the deficiency of these pannexins, *Panx1* and *Panx3* have been found necessary for the early development of skin and wound healing [35, 137, 138]. As PANX2 has been shown to regulate the timing of differentiation in neurons [87], it is unknown whether this functional characteristic is unique to neuronal lineage alone or present in skin cells. To the extent of our knowledge, no overt skin phenotypes have been reported for the *Panx2*-KO mice published to date [59, 88], but a closer look may reveal unnoticed significant differences.

1.7.3 Pannexin1 roles in skin cell differentiation and wound healing

The confirmation of PANX1 (and PANX3) in the epidermis increased the interest in investigating their roles in keratinocyte differentiation. Specifically, PANX1 is expressed at the cell surface in basal (undifferentiated) keratinocytes, but this localization changes to a more intracellular once keratinocytes differentiate, along with a decrease in *Panx1* expression while the levels of involucrin -a marker of keratinocyte differentiation-increases [3]. Notably, ectopic overexpression of murine PANX1 in immortalized rat epidermal keratinocytes (REK) recapitulates trafficking to the cell surface and formation of channels capable of dye-uptake [34]. However, it seems that the expression of these pannexins needs to be regulated since their overexpression reduces the *in vitro* cell proliferation of REK cells.

Moreover, in a model of REK organotypic epidermis, ectopic murine PANX1-expression causes dysregulation of REK differentiation, increasing keratin 14 (a basal/undifferentiation marker) and reducing the vital layer thickness. These results implied that PANX1 was essential for proper skin architecture, especially at the early stages of skin development. Remarkably, Penuela et al. (2014) showed that *Panx1*-KO mice had decreased dorsal skin thickness, whereas the hypothermal layer was thicker compared with that of WT mice [35]. That study also showed that PANX1 regulates the

proliferation and migration of keratinocytes and dermal fibroblasts and is needed for rapid wound healing upon injury. Significantly, *Panx1*-deletion delayed *in vivo* wound healing in mice, increased the proliferation of primary dermal fibroblasts, and made them irresponsive to differentiation upon transforming growth factor-beta 1 (TGF- β 1) stimulation compromising their *in vitro* contractile properties.

Interestingly, *in vitro* targeting PANX1-dependent ATP release in human dermal fibroblasts with PANX1 blockers (carbenoxolone (CBX), probenecid (PBN), and ¹⁰Panx1 mimetic peptide) was recently shown to accelerate their migration, increase single-cell motility, and promote F-actin redistribution [139]. In this regard, an apparent discrepancy exists between Penuela et al. (2014) and Flores-Muñoz et al. (2021) [139] studies. In the first study, the *in vitro* proliferation but not migration of murine neonatal dermal fibroblasts was enhanced by the *Panx1*-KO that showed increased fibrosis but delayed wound healing *in vivo* [35]. On the contrary, the latter study showed that PANX1-inhibition or -knockdown in human dermal fibroblasts increased *in vitro* migration, as seen in their *Panx1*-KO-derived primary dermal murine fibroblasts compared to WT-derived ones [139].

1.8 Pannexins 1 and 2 in cancer

In the previous sections, most of the research evidence was based on the characterization and regulation of pannexins during physiological conditions. However, growing research indicates their dysregulation also contributes to pathophysiological processes like cancer and inflammation [52, 97, 140]. A recent analysis by Xu et al. (2021) [141] using the Oncomine database indicated the upregulation of *PANX1* mRNA transcript levels in at least 14 different cancers and more significantly in malignancies such as sarcomas, lymphomas, breast, esophageal, and head and neck cancers. The same study showed that although *PANX2* was upregulated in breast and lung cancer, it is downregulated in other six different tumor types, including brain and CNS cancer, esophageal, lymphoma, and pancreatic cancer [141]. Notably, these data also implied that there is likely an apparent inverse relationship in the mRNA expression between both pannexins, although no significant inverse correlation has been found.

Indeed, PANX1 has been previously reported to play a tumor-promoter role and is increased in a variety of cancer cell lines and tumors (e.g., breast, melanoma, glioma, hepatocellular carcinoma, and myeloma) when compared to normal tissues (reviewed in [140]). Recently, a study examining PANX1 in hepatocellular carcinoma indicated that its upregulation is associated with poor patient prognosis and promotes invasion and metastasis [48]. Moreover, PANX1 was highly expressed in different breast cancer subtypes and linked to favoring an epidermal-to-mesenchymal transition (EMT) phenotype and poorer outcomes in breast cancer patients [47]. Another report showed that *PANX1* upregulation in testicular cancer confers sensitivity to cisplatin, a chemotherapeutic agent, but downregulation of its expression in a related cancer cell line (I-10) increases resistance to this drug [142]. However, genetic and pharmacological inhibition of PANX1 channels also reduces *in vitro* migration and invasion of the same parental cell line of testicular cancer by decreasing of ERK1/2 kinase activity, suggesting that these cancer cells may exploit PANX1 function in a selective manner to alter their tumorigenic properties [143]. Notably, our group has demonstrated that PANX1 levels are elevated in cutaneous melanoma, a melanocytic skin cancer [42-44], in contrast PANX2 has not been thoroughly investigated in this regard. Therefore, the following subsections will be limited to the current knowledge about PANX1 in cutaneous melanoma.

Conversely, PANX1 anti-tumorigenic roles have also been reported, where *PANX1* expression is downregulated (e.g., gallbladder adenocarcinoma [144]) or absent (e.g., rhabdomyosarcoma [145, 146]), and its restitution can revert the cancer progression. Notably, early studies looking at the expression of pannexins in human keratinocytic tumor biopsies showed that PANX1 was downregulated in basal and squamous cell carcinomas compared to normal skin, suggesting that its expression might offer a protective role against keratinocyte malignant transformation [41]. However, considering that PANX1 is a regulator of keratinocyte proliferation and differentiation, further work with a larger sample size and related cell lines is warranted to clarify its role in promoting or suppressing keratinocytic neoplasias.

On the other hand, less is known about PANX2 in cancer. However, some relevant information about PANX2 has been brought to light in a few studies. In that respect, PANX2 has been proposed as a potential tumor suppressor in glioma with a positive correlation between its gene expression and post-diagnosis survival time for glioma patients [147]. A recent bioinformatic analysis done by Xu et al. (2021) showed that high expression of *PANX2* is significantly associated with better overall survival but negatively correlated with tumor immune infiltration in low-grade gliomas [141], which can impact negatively the efficacy of therapies that rely on the presence and activation of anti-tumor immune cells as we will describe later for melanoma.

1.8.1 Skin cancer: Melanoma

In the pathological states of the skin, several external (i.e., sunlight, UV radiation, chemical insults) and genetic factors could give rise to cancerous lesions. Cutaneous melanoma is the most aggressive type of skin cancer that arises from uncontrolled proliferating melanocytes, the neural crest-derived and pigment-producing cells in the skin. According to the Global Cancer Observatory (<https://gco.iarc.fr/>), melanoma was responsible for ~47,2 % of skin cancer-related deaths worldwide in 2020 and is still increasing in incidence and mortality [148]. Since the development of targeted and immune checkpoint therapies, a significant reduction in mortality has been observed [149], but they are still far from perfect, and current therapies do not benefit a large number of patients.

1.8.1.1 Cutaneous Melanoma overview

According to the growth and localization pattern of the melanoma tumor, there are four major types of melanoma: Superficial spreading, nodular, lentigo malignant, and acral lentiginous melanoma, with the first one being the most common [150]. Melanoma lesions have two growth phases: radial, when malignant cells grow radially within the epidermis, and vertical when the tumor cells invade deeper in the dermis acquiring metastatic capabilities. It is suggested that these invasive malignant melanoma cells transit to a lymph node and gain physical access to both lymphatics and blood vessels to further the metastatic process. If it is not detected early, melanoma results in a highly metastatic cancer with a

fast progression and high lethality, diminishing the efficacy of therapies. Depending on the tumor location, regional melanoma metastasis occurs in the skin, near (satellite lesions), or relatively distant (in-transit) from the primary tumor site, as well as to subcutaneous tissue and lymph nodes. However, distant metastases are commonly in the skin, lung, brain, liver, and at later stages to the bone, and intestine but subclinical manifestations can appear in almost any part of the body [151, 152].

One of the significant risk factors for melanoma development and other non-melanoma skin cancers (e.g., keratinocyte-derived squamous and basal cell carcinomas) is exposure to UV radiation, which causes pyrimidine dimers and oxidation of the genomic DNA [153]. Therefore, most tumors of melanoma patients exhibit a high rate of genetic alterations (a.k.a. tumor mutational burden) due to UV exposure. However, both germline (e.g., mutations in *CDKN2A* and *CDK4*) and somatic mutations have been found to drive malignant melanocyte transformation [154, 155]. Since several driver mutations have been identified and implicated in melanoma onset and progression (reviewed at [156, 157]), the following paragraphs will succinctly describe the alterations more relevant for the context of this thesis.

The oncogenic pathway most frequently dysregulated in melanoma is the mitogen-activated protein kinase (MAPK) signaling pathway, which is crucial for the proliferation, differentiation, and survival of melanocytes and melanoma cells. Among other mutations, those in the *BRAF* gene, encoding a B-raf proto-oncogene serine/threonine-protein kinase (BRAF) critical for the MAPK pathway, are the most common (~50%), where the valine-to-glutamic acid substitution at codon 600 (V600E) and other gain-of-function somatic mutations lead to constitutive activation of downstream MAPK signaling [158]. However, rather than one, multiple mutations in other genes are usually present in melanoma cells, while alterations of BRAF alone are insufficient for driving a malignant phenotype [159]. Other relevant mutations that drive MAPK signaling are located in the neuroblastoma rat sarcoma viral oncogene homolog gene (*NRAS*), which is mutated in 20% of the cases and is associated with increased tumor aggressiveness, therapy resistance, and reduced patient survival [160]. Furthermore, the amplification of transcription factors like microphthalmia-

associated transcription factor (MITF) (especially the M-MITF isoform), which regulates differentiation and pigment production in melanocytes, has been correlated with poor patient outcomes [161].

On the other hand, melanoma also harbors mutations that inactivate important players regulating other pathways like the phosphoinositide 3-kinase/protein kinase B (PI3K/AKT) pathway regulating cell proliferation and survival of melanoma cells. As an example, the tumor-suppressor phosphatase and tensin homolog (*PTEN*) gene encoding a phosphatidylinositol-3,4,5-triphosphate 3-phosphatase (PTEN) exhibits loss-of-function mutations and focal deletion in ~20% of melanoma patients cohorts of The Cancer Genome Atlas Network (TCGA) (reviewed at [156]). PTEN constitutes a negative regulator of the PI3K/Akt signaling pathway, important for melanoma onset and therapeutic resistance [162]. Interestingly, BRAF and PTEN alterations have been found overlapping and cooperating with melanoma development [163, 164]. Moreover, the loss of PTEN has also been associated with resistance to targeted and immune checkpoint inhibition (reviewed at [156]), highlighting the significance of this genomic alteration for melanoma progression.

1.8.1.2 Overview of melanoma treatments

Overall, current treatments include the surgical removal of the localized primary tumor and surrounding healthy tissue with a sentinel lymph node biopsy depending on the thickness and ulceration of the lesion [165]. If necessary, to avoid the cancer spread, the remaining lymph nodes affected by the tumor are removed. The two main options for metastatic melanoma are targeted therapy and immunotherapy (Fig. 1-4). The former is based on inhibiting the druggable mutant proteins (BRAF^{V600E} and Mitogen-activated protein kinase kinases (MEK)) that support a dysregulated MAPK/ERK pathway (Fig. 1-4A). However, this is only pertinent for patients with BRAF-mutant metastatic melanomas. Nevertheless, the combination of BRAF and MEK inhibitors has been required to curve the continuous resistance mechanisms to single-agent therapy (like reactivation of MAPK/ERK and alternative signaling pathways [166]) and is usually accompanied by adverse side effects [167]. Although this type of therapy has improved survival for a subset of patients, there are still cases that develop resistance to treatment [165].

Figure 1-4.

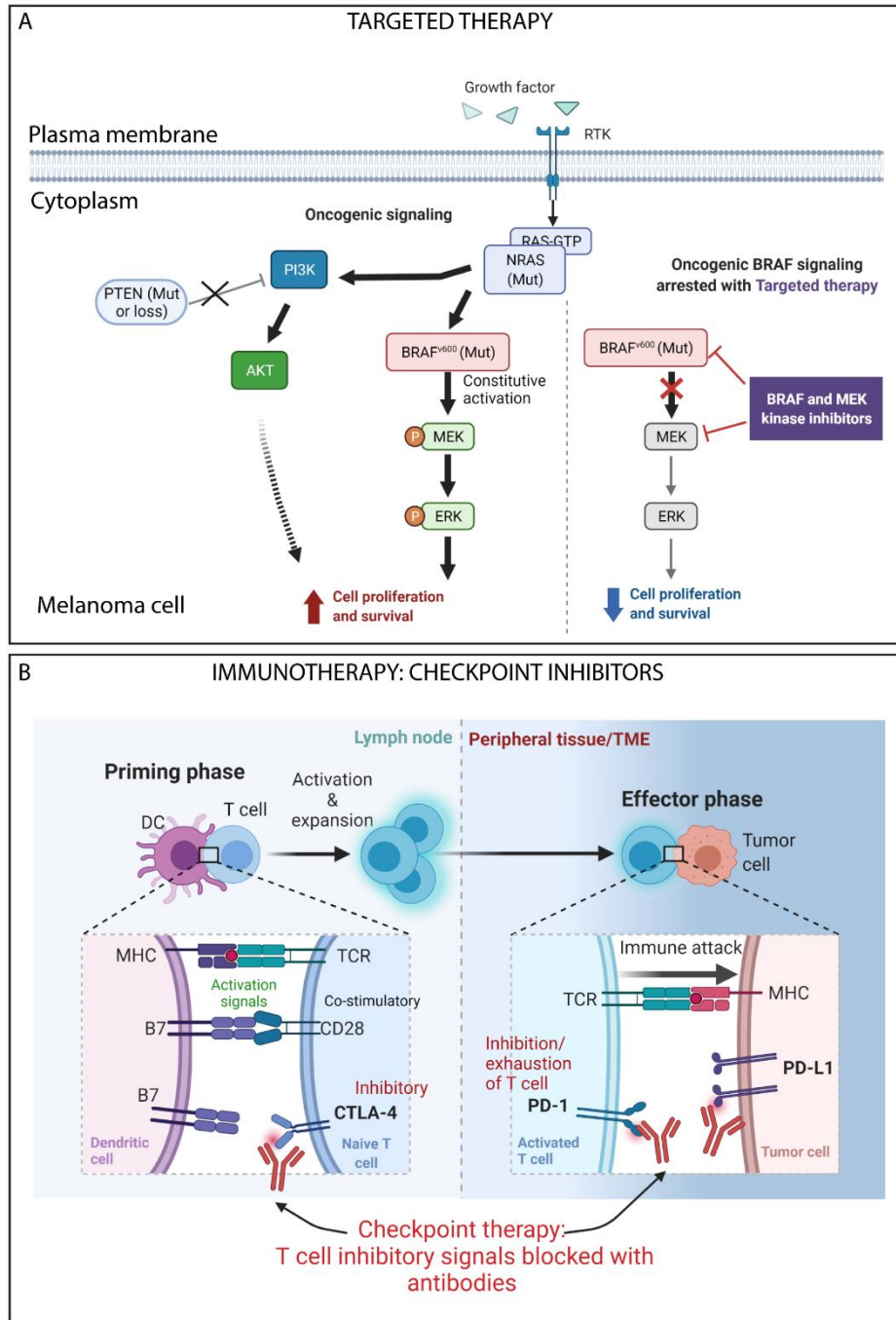


Figure 1-4. Schematic of the two main therapy options for metastatic melanoma: targeted therapy and checkpoint inhibitors.

(A) Representation of the most dysregulated pathways in melanoma. Mutations in the BRAF gene are present in ~50% of all melanoma skin cancers, causing constitutive activation of the MAPK signaling. These mutations activate BRAF kinase resulting in the gene expression that promotes cellular proliferation and survival. A combination of inhibitors targeting mutant BRAF and MEK (a downstream effector in this pathway) is currently used and has improved the patient response rate compared to single-agent treatment. The phosphatidylinositol-3-kinase/protein kinase B/mammalian target of rapamycin (PI3K/Akt/mTOR) signaling is another dysregulated pathway in melanomas where inactivating mutations or downregulation of negative PTEN tumor suppressor has been linked to alternative ways of resistance to targeted therapy. (B) Illustration recreated from [168] showing the mode of action of checkpoint inhibitors in immunotherapy. Monoclonal antibodies block PD-1, PD-L1, and CTLA-4. CTLA-4 is a negative regulator of the “activation/priming” phase in T cells by binding with high affinity to B7 ligands, needed for co-stimulation/interaction with CD28 molecules in the surface of T-cells after antigen presentation through the T cell receptor (TCR) and the MHC-antigen peptide complex (shown in red) of the antigen-presenting cells. PD-1 is on the surface of activated T cells and interacts with PD-L1 (overexpressed by tumor cells), negatively modulating the “effector” phase of the antitumoral response by inhibiting proliferation, survival, and effector functions, as well as inducing apoptosis of tumor-specific T lymphocytes. Figure created with BioRender.com.

Conversely, immunotherapies take advantage of the intrinsic immunogenicity of the melanoma tumor itself, where the high mutation burden produces recognizable tumor antigens targeted by the immune system. Within the tumor microenvironment (TME), several immune cell types can be found, for instance: tumor-infiltrating lymphocytes (TILs), Natural killer (NK) cells, macrophages, dendritic cells (DC), and polymorphonuclear neutrophils [169]. In this sense, TILs are the workhorse and the therapeutic targets of the well-known “checkpoint inhibitor therapy” to enhance tumor elimination and prolong the anti-tumoral immune response [170]. Indeed, the presence of TILs in tumors has been considered not only a predictor of melanoma prognosis but a potential biomarker of response to cancer immunotherapy [171]. Specifically, checkpoint inhibitor therapy aims to target negative immunoregulatory molecules present in the tumor cells, FoxP3⁺ T regulatory (Treg), cluster of differentiation (CD)4⁺ T helper (Th), and the effector CD8⁺ cytotoxic T lymphocytes (CTL) through an antibody-mediated blockade (Fig. 1-4B). These checkpoint molecules play a role in inhibiting the immune response and preventing autoimmunity while promoting self-tolerance and can be hijacked by the tumor to avoid immune destruction (reviewed at [172]). Some examples are the cytotoxic T-lymphocyte-associated antigen-4 (CTLA-4), present in T cells upon activation but constitutively expressed in Treg; the programmed cell-death protein 1 (PD-1) present in all T cells, NK and B cells; and PD-1 ligands (PD-L1/2) present in somatic cells but overexpressed in tumor cells. Combined MAPK inhibition and anti-PD-L1 therapy is also a newer treatment option explored to improve tumor immune infiltration and long-lasting response for patients with advanced melanoma [173]. Other immunotherapies modalities are being tested and in use for melanoma treatment but are out of the scope of this thesis and will not be addressed; however, they can be reviewed in [172, 174].

1.8.1.3 Tumor immune evasion during inflammation, implications for melanoma immunotherapy

As mentioned above, cutaneous melanoma is amenable for immunotherapy due to the high mutational load and the tumor immune cell infiltration. This crosstalk between tumor and immune cells is heavily studied and offers various intervention strategies. However, the immune component and its interaction in the TME exhibit a high degree of complexity and

involve a series of pro-tumorigenic and immune-evasive mechanisms that need to be overpowered for successful immunotherapy (Fig. 1-5). Some of these processes are briefly described in the following paragraphs, but the underlying molecular mechanisms are omitted as they are outside the scope of this thesis.

Figure 1-5.

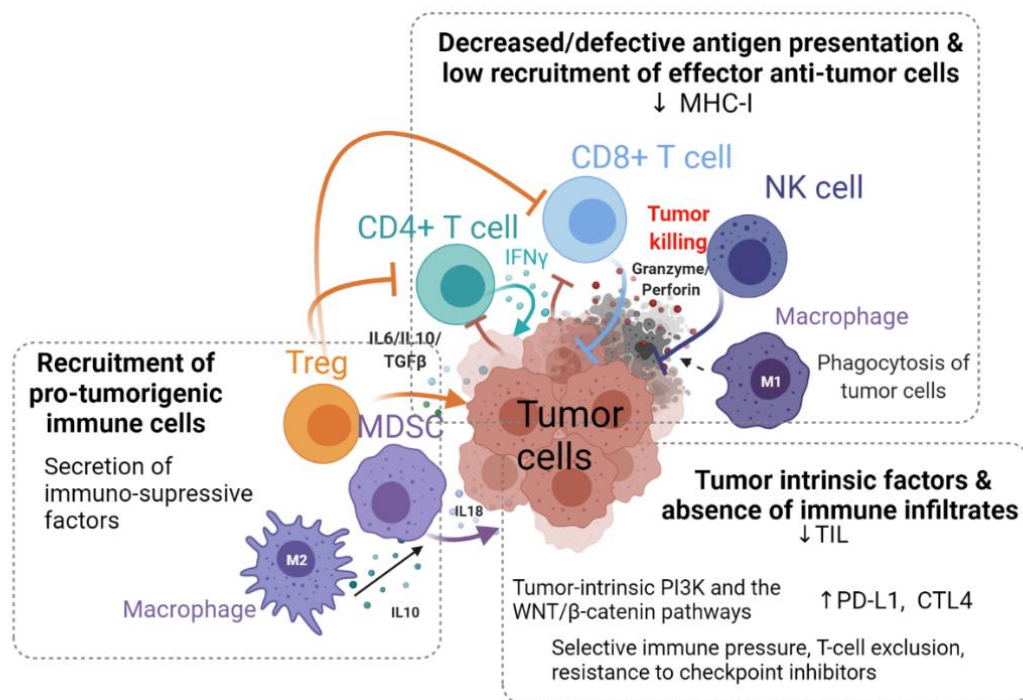


Figure 1-5. Summary of factors causing immune evasion phenotypes and immunotherapy resistance in metastatic melanoma.

Melanoma tumor cells can escape the anti-tumoral immune-mediated response by influencing the antigen presentation machinery and affecting the effector functions of anti-tumor-specific effector cells (CD8+ T lymphocytes, NK cells, and M1 macrophages). Besides, dysregulation in metabolism and associated cellular pathways can exert selective immune pressure in the TME, leading to immune exclusion and exhaustion phenotypes. Finally, the recruitment of immune-modulator cells that yield pro-tumorigenic effects (Treg, MDSC, M2 macrophages) is accompanied by the secretion of immune-suppressive factors that allow the tumors to progress despite ongoing immune response infiltration and inflammation. Figure created with BioRender.com.

Melanoma cells can suppress anti-tumor immune cells by acquiring a less immunogenic phenotype and immune escape mechanisms (reviewed in [169]). In this sense, due to genetic or epigenetic alterations, tumor cells can downregulate the expression of tumor-associated antigens, disrupting or decreasing the expression of the major histocompatibility complex (MHC) molecules. The latter reduces antigen presentation important for the first steps of activation of tumor-specific naïve T cells. This mechanism hampers the treatment with the therapies mentioned above using anti-CTLA-4 and the PD-1/PD-L1 blockade that requires peptide presentation for T cell (re)activation and clonal-proliferation of already antigen-primed T cells present in the TME [175]. In addition, other evasive mechanisms are mediated through the activation of PI3K or the WNT/ β -catenin pathways in melanoma cells [176-178]. A study in preclinical models of melanoma has shown that PTEN loss in the tumor cells inhibits T cell-mediated tumor killing and is associated with decreased T-cell infiltration into tumors, an observation confirmed in patients [177]. The consequence of this mechanism is then reducing the migration (“homing”) of T lymphocytes to tumor sites or preventing their activation due to defects in chemokine production and recruitment of DC cells to lymph nodes [178, 179].

Another mechanism involves the cargo from melanoma-derived extracellular vesicles, which affects the maturation of DC, essential for T cell activation [180]. In addition, accumulating evidence implicates the contribution of several tumor-derived soluble factors (e.g., vascular endothelial growth factor (VEGF), tumor necrosis factors (TNFs), transforming growth factor (TGF- β), interleukins (IL)-1, -6, -10, and prostaglandin E2 (PGE2)) in mediating immune cell suppression via the recruitment of tumor-associated macrophages (TAMs), Tregs, and myeloid-derived suppressor cells (MDSCs) (reviewed in [181]). Finally, even after tumoral T cell and NK cell infiltration occur, more hurdles are thrown upon those effector cell types. In this regard, apart from the melanoma-derived soluble factors and the role of immunosuppressive cells, as mentioned earlier, melanoma cells can interfere with the effector/cytolytic function of anti-tumoral T-cells by upregulating the expression of CTLA4 in T cells and expressing high levels of PD-L1, thereby causing T-cell anergy and hampering T cell activation [182]. Likewise, continuous or chronic T-cell exposure to their cognate antigens (in the TME) may give rise to

exhausted phenotypes impeding the execution of their effector function and permitting melanoma tumor progression [183].

In summary, since host immune cells are essential as the first line of defense against tumor cells, immunotherapies are desirable at the forefront of melanoma treatments. Decreased T cell infiltration and the presence of immunosuppressive cells in the TME are two factors downplaying the positive effect of immunotherapy. Even if melanoma has been branded as a “hot” tumor due to the proinflammatory TME and diverse immune cell population residing in the tumors, any increase of anti-tumoral effector immune cells would undoubtedly increase the chances of success with immunotherapy [184].

1.8.2 Pannexin1 in cutaneous melanoma

Penuela et al. (2012) showed that *Panx1* expression is low in normal mouse melanocytes and highly expressed in isogenic mouse melanoma cell lines (B16-F0, -F10, -BL6). However, no detectable protein expression was found for PANX2 or PANX3 [43]. That study demonstrated that *Panx1* knockdown in melanoma cells induces a more melanocytic phenotype with reduced *in vitro* proliferation and migration and less metastatic capacity in an *ex vivo* model [43]. In keeping with those findings, Freeman et al. (2019) demonstrated that human melanoma cell lines also exhibited a high expression of PANX1 that was confirmed in patient tumor biopsies at all stages of melanoma. Furthermore, our group showed that decreasing PANX1 levels or inhibition of its function with CBX or PBN channel blockers significantly reduced cell growth and migration of human melanoma cell lines *in vitro* and *ex vivo*. These findings confirmed that PANX1 regulates the growth and migration of melanoma cells, likely contributing to melanoma progression [42].

Some of the mechanisms involved in regulating PANX1 function in melanoma cells were recently uncovered by Sayedyahosseini et al. (2021), demonstrating a reciprocal regulation of protein expression and cell membrane localization of PANX1 and β -catenin, an important Wnt signaling transcription factor. In this case, it was found that the N-terminal region of β -catenin physically interacts with the PANX1 C-terminus, which was proposed to have a significant influence on the regulation of the stability and transcriptional activity

of β -catenin. Moreover, endogenous PANX1 also seems to interact with calmodulin, another regulator of Ca^{2+} signaling, hinting at the possibility of PANX1-modulation of both canonical and non-canonical Wnt signaling pathways and aiding melanoma malignancy. Importantly, in that study, a direct link between PANX1 and metabolic activity of melanoma cells was identified, where PANX1 knockdown suppressed mitochondrial metabolism and may also explain the PANX1-dependency of melanoma cells to sustain proliferation and migration [42-44]. Given the notorious role of the Wnt/ β -catenin pathway supporting melanoma formation, metabolism, and metastasis [185, 186] and the newly discovered links with the tumor promoter PANX1, further studies are needed to assess the effectiveness of targeting PANX1 in the preclinical setting. Nevertheless, this newly uncovered evidence establishes a dual role of PANX1 functioning as an ATP (and likely Ca^{2+}) channel and an interactome/signalome regulator within melanoma cells [187].

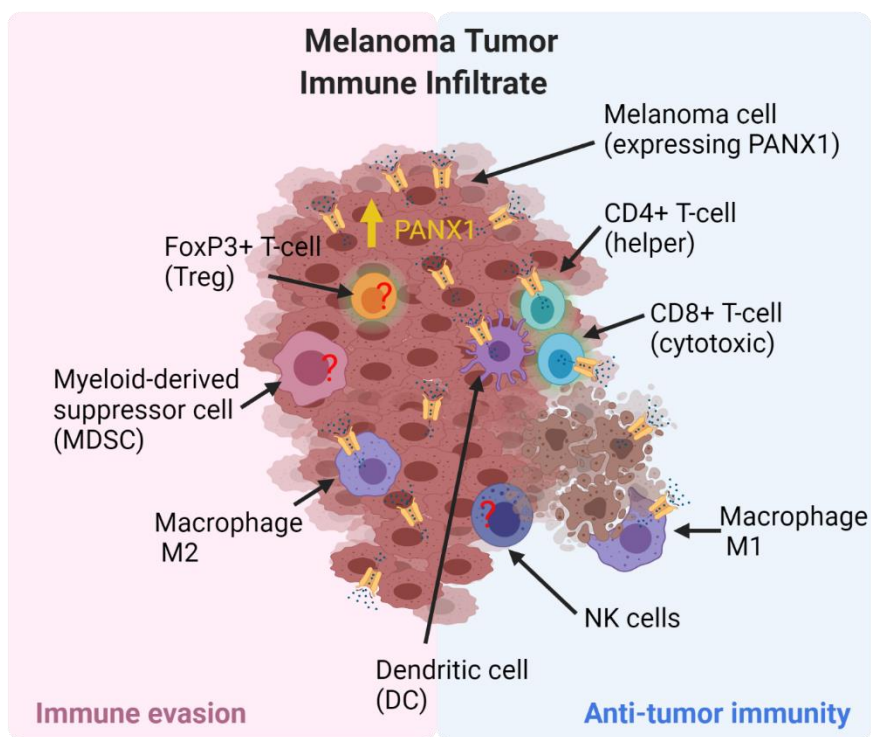
1.8.3 Considerations on pannexin regulation of the immune infiltration: possible implications for melanoma

Although the role of PANX1 in melanoma cells is becoming clear, exactly how it favors tumor progression in the TME is still a topic for future investigation. In this respect, it needs to be considered the widespread expression of PANX1 in most cell types (tumor and immune cells) constituting the TME [38, 42, 43, 97, 188]. PANX1 channels have been implicated in regulating inflammation, apoptotic cell clearance, and immune cell recruitment, which could severely influence melanoma progression [189].

Indeed, the release of ATP and other metabolites through PANX1 channels stimulates the recruitment of immune cells and modulates inflammation in the surrounding tissue [38, 66]. Given the relationship between ATP-regulated P2X7 channel/receptor (P2X7R) and PANX1 channels [39, 40, 52] and their implication in melanoma tumor growth, Schneider et al. (2014) originally proposed a model in which the increased ATP in the cellular microenvironment would influence P2X7R/PANX1 channel formation and Nod-like receptor family pyrin-domain containing-3 (NLRP3) inflammasome activation in malignant melanocytes [190]. The NLRP3-mediated activation has been previously linked to the PANX1 channel function [39, 40, 52, 191], although there is evidence that PANX1

is not essential for this to happen in macrophages [192]. On the other hand, the P2X7R is a non-selective cation channel that permits the efflux of K^+ and influx of Na^+ and Ca^{2+} , inducing plasma membrane depolarization and promotes the NLRP3 activation [193]. This subsequent activation of NLRP3 inflammasome leads to the release of pro-inflammatory cytokines interleukin- (IL-)1 β and IL-18, and increased cyclooxygenase-2 and prostaglandin-E2 by melanoma cells [194]. Notably, although it was demonstrated only in endothelial cells, a PANX1-dependent Ca^{2+} influx also supports the synthesis and release of IL-1 β independently of purinergic signaling [191].

IL-1 β has been reported to be constitutively secreted in metastases [195, 196], tumor-associated macrophages, and fibroblasts, contributing to resistance to MAPK-inhibition in melanoma [197]. Thus, it is plausible that PANX1-mediated IL-1 β release could lead to immunosuppression (reviewed in [198-200]). Interestingly, genetic or pharmacological targeting of the NLRP3 inflammasome combined with anti-PD-1 therapy has increased the treatment efficacy compared to anti-PD-1 monotherapy in a syngeneic melanoma mouse model [196]. Thus, deletion or inhibition of PANX1 channels could indirectly reduce IL-1 β -derived immunosuppression, although further research is needed to demonstrate this. On the other hand, if PANX1 is overexpressed in melanoma cells [42, 43], an excessive ATP release would also have deleterious effects on CD4 $^+$ T lymphocytes and enhance the proliferation of immunosuppressive Treg cells infiltrated in the melanoma tumor [201, 202]. Finally, another consideration is that due to the PANX1 involvement in melanoma metabolism [44], a link to the direct activation of P2X7R in cancer cells could increase the plasma membrane glucose transporter 1 (GLUT1) [203] and promote the Warburg effect, leading to lactate release and acidification of TME. This has been reported to impede both DCs differentiation and cytokine release in the TME, promoting M2 macrophage differentiation (immunosuppressive type) and MDSCs activation (reviewed at [204]), which could be advantageous for the tumor immune escape. PANX1 may influence the intratumoral immune infiltration to favor tumor progression and immunosuppression/evasion (Fig 1-6), but more research in this regard still lacks in the context of cancer.

Figure 1-6.**Figure 1-6. The complexity of PANX1 expression in the tumor microenvironment.**

PANX1 is highly expressed in melanoma cells, and its channel function modulates their proliferation, migration, and metabolism. PANX1 function also contributes to the clearance of apoptotic cells, immune cell chemotaxis and mediates the activation of dendritic cells and T cells through purinergic signaling. In other contexts than cancer, PANX1 was detected in leukocytes in the endothelium [97], dendritic cells [205], CD4+ [54], and CD8+ T cells [206], and macrophage and other myeloid cells present in the injury sites during neuroinflammation [207]. It remains to be determined the influence of PANX1 expression in other immune cell types (marked with a red question mark) and tumor-associated cells that affect the inflammatory response within the tumor site.

1.9 Rationale

Pannexins play a critical role in maintaining the skin architecture, homeostasis, and cellular properties of different skin cells. PANX2 expression was found not restricted to the CNS and has been previously reported in the skin. However, it remains elusive which skin cell type expresses PANX2 and whether it is regulated during skin aging, as shown with the other pannexin family members. Therefore, we sought to explore the PANX2 expression in the two major skin cell types (keratinocyte and dermal fibroblast) and the skin of newborn and adult wild-type C57BL/6 mice. Notably, apoptotic mechanisms balance the proliferation of the cells in the skin (e.g., keratinocytes) to maintain epidermal thickness and circumvent malignant transformation upon injury or insults like UV radiation. In the pannexin protein family, only PANX1 and PANX2 can be targeted by apoptotic effector caspases by cleaving their intracellular carboxyl-terminal domains. In this sense, the sites for caspase cleavage of PANX2 remain uncovered, and it is unclear whether this PTM occurs in cells as only *in vitro* enzymatic assays have shown its susceptibility to caspases. Given that PANX2 has been found in the ER-mitochondria contact sites, it has been suggested that it may play a role in contributing to the apoptosis process. Thus, using a combination of bioinformatic predictions and mutagenesis, we seek to uncover the role of PANX2 caspase cleavage and its consequences under UV-induced apoptosis in skin cells.

Furthermore, previous evidence pointed out that all the pannexin paralogs can be N-glycosylated, and although it is not a requirement, this influences PANX1 and PANX3 trafficking to the cell surface. However, until this thesis project, the specific glycosylation site and its role on PANX2 subcellular translocation were unknown. On the other hand, only lower glycosylated Gly0 and Gly1 PANX1 species have been shown to interact with PANX2 when co-expressed together and tentatively forming a heteromeric channel, but it was unclear whether PANX2 glycosylation status would also impact this intermixing. Hence, we sought to study the N-glycosylation role on PANX2 localization and interaction with PANX1 by generating a PANX2 glycosylation-deficient mutant at the putative site for this PTM.

Finally, during pathological states, like skin cancer, upregulation of PANX1 seems to foster the malignant cellular properties of tumor cells. In melanoma, increased PANX1 promotes proliferation and migration of malignant melanocytes. Nevertheless, the effect of high PANX1 levels in the context of melanoma has not been studied *in vivo*. Due to the ubiquitous expression of PANX1 in most cell types constituting the tumor tissues (e.g., cancer, stromal and immune cells) and its role in modulating immune cell recruitment and inflammation, there is a potential function of this channel-protein within the TME favoring pro-tumorigenic and immunosuppressive states of melanoma. To date, the PANX1 role in melanoma *in vivo* or its impact on tumor immune infiltration has not been addressed, which could have significant implications for the improvement of melanoma treatments, like immunotherapy. Therefore, we explored the effect of the global deletion of PANX1 on *in vivo* tumor progression and immune cell infiltration using a validated melanoma mouse model.

1.10 Hypothesis

The overall hypothesis of this thesis is that: *the regulation of PANX1 and PANX2 levels is necessary to maintain skin homeostasis, modulate cell death and avoid malignant transformation and cancer progression in the skin, while glycosylation and caspase cleavage control their localization and biological function.*

1.11 Objectives

The research objectives of this thesis are the following:

Objective 1 – Manuscript 1: Chapter 2

Characterize PANX2 expression in normal mouse skin and evaluate its cleavage by caspases and consequences for cell death during UV-induced apoptosis.

Objective 2 – Manuscript 2: Chapter 3

Define the site of N-glycosylation in PANX2 and its role in subcellular localization and interaction with PANX1.

Objective 3 – Manuscript 3: Chapter 4

Study the effect of the global deletion of PANX1 on tumor progression and immune infiltration in an inducible mouse model of metastatic melanoma.

1.12 References

1. Panchin, Y., et al., *A ubiquitous family of putative gap junction molecules*. *Curr Biol*, 2000. **10**(13): p. R473-4.
2. Baranova, A., et al., *The mammalian pannexin family is homologous to the invertebrate innexin gap junction proteins*. *Genomics*, 2004. **83**(4): p. 706-16.
3. Penuela, S., et al., *Pannexin 1 and pannexin 3 are glycoproteins that exhibit many distinct characteristics from the connexin family of gap junction proteins*. *J Cell Sci*, 2007. **120**(Pt 21): p. 3772-83.
4. Boassa, D., et al., *Pannexin1 channels contain a glycosylation site that targets the hexamer to the plasma membrane*. *J Biol Chem*, 2007. **282**(43): p. 31733-43.
5. Penuela, S., et al., *Glycosylation regulates pannexin intermixing and cellular localization*. *Mol Biol Cell*, 2009. **20**(20): p. 4313-23.
6. Penuela, S., R. Gehi, and D.W. Laird, *The biochemistry and function of pannexin channels*. *Biochim Biophys Acta*, 2013. **1828**(1): p. 15-22.
7. Ambrosi, C., et al., *Pannexin1 and Pannexin2 channels show quaternary similarities to connexons and different oligomerization numbers from each other*. *J Biol Chem*, 2010. **285**(32): p. 24420-31.
8. Bunse, S., et al., *Single cysteines in the extracellular and transmembrane regions modulate pannexin 1 channel function*. *J Membr Biol*, 2011. **244**(1): p. 21-33.
9. Sosinsky, G.E., et al., *Pannexin channels are not gap junction hemichannels*. *Channels (Austin)*, 2011. **5**(3): p. 193-7.
10. Narahari, A.K., et al., *ATP and large signaling metabolites flux through caspase-activated Pannexin 1 channels*. *Elife*, 2021. **10**.
11. Omasits, U., et al., *Protter: interactive protein feature visualization and integration with experimental proteomic data*. *Bioinformatics*, 2014. **30**(6): p. 884-6.
12. Tachikawa, M., et al., *Targeted Proteomics-Based Quantitative Protein Atlas of Pannexin and Connexin Subtypes in Mouse and Human Tissues and Cancer Cell Lines*. *J Pharm Sci*, 2020. **109**(2): p. 1161-1168.
13. Penuela, S., et al., *Glycosylation regulates pannexin intermixing and cellular localization*. *Molecular Biology of the Cell*, 2009. **20**: p. 4313-23.
14. Bruzzone, R., et al., *Pannexins, a family of gap junction proteins expressed in brain*. *Proc Natl Acad Sci U S A*, 2003. **100**(23): p. 13644-9.
15. Baranova, A., et al., *The mammalian pannexin family is homologous to the invertebrate innexin gap junction proteins*. *Genomics*, 2004. **83**: p. 706-716.

16. Wicki-Stordeur, L.E. and L.A. Swayne, *Panx1 regulates neural stem and progenitor cell behaviours associated with cytoskeletal dynamics and interacts with multiple cytoskeletal elements*. Cell Commun Signal, 2013. **11**: p. 62.
17. Dvorientchikova, G., et al., *Molecular characterization of pannexins in the lens*. Molecular vision, 2006. **12**: p. 1417-1426.
18. Barbe, M.T., H. Monyer, and R. Bruzzone, *Cell-cell communication beyond connexins: the pannexin channels*. Physiology (Bethesda), 2006. **21**: p. 103-14.
19. Zhang, H., Y. Chen, and C. Zhang, *Patterns of heterogeneous expression of pannexin 1 and pannexin 2 transcripts in the olfactory epithelium and olfactory bulb*. J Mol Histol, 2012. **43**(6): p. 651-60.
20. Le Vasseur, M., et al., *Pannexin 2 protein expression is not restricted to the CNS*. Frontiers in cellular neuroscience, 2014. **8**: p. 392.
21. Abitbol, J.M., et al., *Double deletion of Panx1 and Panx3 affects skin and bone but not hearing*. J Mol Med (Berl), 2019. **97**(5): p. 723-736.
22. Berchtold, L.A., et al., *Pannexin-2-deficiency sensitizes pancreatic beta-cells to cytokine-induced apoptosis in vitro and impairs glucose tolerance in vivo*. Mol Cell Endocrinol, 2017. **448**: p. 108-121.
23. Dvorientchikova, G., et al., *Expression of pannexin family of proteins in the retina*. FEBS Lett, 2006. **580**(9): p. 2178-82.
24. Hainz, N., et al., *Human stem cells express pannexins*. BMC Res Notes, 2018. **11**(1): p. 54.
25. Liao, D., et al., *Identification of Pannexin 2 as a Novel Marker Correlating with Ferroptosis and Malignant Phenotypes of Prostate Cancer Cells*. Onco Targets Ther, 2020. **13**: p. 4411-4421.
26. Diezmos, E.F., et al., *Pannexin-2 is expressed in the human colon with extensive localization in the enteric nervous system*. Neurogastroenterol Motil, 2015. **27**(5): p. 672-83.
27. Vogt, A., S.G. Hormuzdi, and H. Monyer, *Pannexin1 and Pannexin2 expression in the developing and mature rat brain*. Molecular brain research, 2005. **141**: p. 113-20.
28. Swayne, L.A. and S.A. Bennett, *Connexins and pannexins in neuronal development and adult neurogenesis*. BMC Cell Biol, 2016. **17 Suppl 1**: p. 10.
29. Swayne, L.A., C.D. Sorbara, and S.a.L. Bennett, *Pannexin 2 is expressed by postnatal hippocampal neural progenitors and modulates neuronal commitment*. Journal of Biological Chemistry, 2010. **285**: p. 24977-24986.
30. Ma, W., et al., *Pharmacological characterization of pannexin-1 currents expressed in mammalian cells*. J Pharmacol Exp Ther, 2009. **328**(2): p. 409-18.

31. Li, S., M. Tomic, and S.S. Stojilkovic, *Characterization of novel Pannexin 1 isoforms from rat pituitary cells and their association with ATP-gated P2X channels*. Gen Comp Endocrinol, 2011. **174**(2): p. 202-10.
32. Turmel, P., et al., *Characterization of pannexin1 and pannexin3 and their regulation by androgens in the male reproductive tract of the adult rat*. Mol Reprod Dev, 2011. **78**(2): p. 124-38.
33. Zoidl, G., et al., *Molecular diversity of connexin and pannexin genes in the retina of the zebrafish *Danio rerio**. Cell Commun Adhes, 2008. **15**(1): p. 169-83.
34. Celetti, S.J., et al., *Implications of pannexin 1 and pannexin 3 for keratinocyte differentiation*. J Cell Sci, 2010. **123**(Pt 8): p. 1363-72.
35. Penuela, S., et al., *Panx1 regulates cellular properties of keratinocytes and dermal fibroblasts in skin development and wound healing*. J Invest Dermatol, 2014. **134**(7): p. 2026-2035.
36. Adamson, S.E., et al., *Pannexin 1 is required for full activation of insulin-stimulated glucose uptake in adipocytes*. Mol Metab, 2015. **4**(9): p. 610-8.
37. Langlois, S. and K.N. Cowan, *Regulation of Skeletal Muscle Myoblast Differentiation and Proliferation by Pannexins*. Adv Exp Med Biol, 2017. **925**: p. 57-73.
38. Chekeni, F.B., et al., *Pannexin 1 channels mediate 'find-me' signal release and membrane permeability during apoptosis*. Nature, 2010. **467**(7317): p. 863-7.
39. Pelegrin, P., *Targeting interleukin-1 signaling in chronic inflammation: focus on P2X(7) receptor and Pannexin-1*. Drug News Perspect, 2008. **21**(8): p. 424-33.
40. Pelegrin, P. and A. Surprenant, *Pannexin-1 mediates large pore formation and interleukin-1 β release by the ATP-gated P2X7 receptor*. The EMBO journal, 2006. **25**(21): p. 5071-5082.
41. Cowan, K.N., et al., *Pannexin1 and Pannexin3 exhibit distinct localization patterns in human skin appendages and are regulated during keratinocyte differentiation and carcinogenesis*. Cell Commun Adhes, 2012. **19**(3-4): p. 45-53.
42. Freeman, T.J., et al., *Inhibition of Pannexin 1 Reduces the Tumorigenic Properties of Human Melanoma Cells*. Cancers (Basel), 2019. **11**(1).
43. Penuela, S., et al., *Loss of pannexin 1 attenuates melanoma progression by reversion to a melanocytic phenotype*. J Biol Chem, 2012. **287**(34): p. 29184-93.
44. Sayedyahosseini, S., et al., *Pannexin 1 binds beta-catenin to modulate melanoma cell growth and metabolism*. J Biol Chem, 2021: p. 100478.
45. Furlow, P.W., et al., *Mechanosensitive pannexin-1 channels mediate microvascular metastatic cell survival*. Nat Cell Biol, 2015. **17**(7): p. 943-52.

46. Gao, J., et al., *Integrative analysis of complex cancer genomics and clinical profiles using the cBioPortal*. *Sci Signal*, 2013. **6**(269): p. p11.
47. Jalaleddine, N., et al., *Pannexin1 Is Associated with Enhanced Epithelial-To-Mesenchymal Transition in Human Patient Breast Cancer Tissues and in Breast Cancer Cell Lines*. *Cancers (Basel)*, 2019. **11**(12).
48. Shi, G., et al., *Panx1 promotes invasion-metastasis cascade in hepatocellular carcinoma*. *J Cancer*, 2019. **10**(23): p. 5681-5688.
49. Wu, D., L. Li, and L. Chen, *A new perspective of mechanosensitive pannexin-1 channels in cancer metastasis: clues for the treatment of other stress-induced diseases*. *Acta Biochim Biophys Sin (Shanghai)*, 2016. **48**(5): p. 487-9.
50. Novielli-Kuntz, N.M., et al., *Ablation of both Cx40 and Panx1 results in similar cardiovascular phenotypes exhibited in Cx40 knockout mice*. *Biosci Rep*, 2019. **39**(2).
51. Nyberg, M., et al., *Probenecid Inhibits alpha-Adrenergic Receptor-Mediated Vasoconstriction in the Human Leg Vasculature*. *Hypertension*, 2018. **71**(1): p. 151-159.
52. Crespo Yanguas, S., et al., *Pannexin1 as mediator of inflammation and cell death*. *Biochim Biophys Acta Mol Cell Res*, 2017. **1864**(1): p. 51-61.
53. Douanne, T., et al., *Pannexin-1 limits the production of proinflammatory cytokines during necroptosis*. *EMBO Rep*, 2019. **20**(10): p. e47840.
54. Velasquez, S., et al., *Pannexin1 Channels Are Required for Chemokine-Mediated Migration of CD4+ T Lymphocytes: Role in Inflammation and Experimental Autoimmune Encephalomyelitis*. *J Immunol*, 2016. **196**(10): p. 4338-47.
55. Woehrle, T., et al., *Pannexin-1 hemichannel-mediated ATP release together with P2X1 and P2X4 receptors regulate T-cell activation at the immune synapse*. *Blood*, 2010. **116**(18): p. 3475-84.
56. Woehrle, T., et al., *Hypertonic stress regulates T cell function via pannexin-1 hemichannels and P2X receptors*. *J Leukoc Biol*, 2010. **88**(6): p. 1181-9.
57. Orellana, J.A., et al., *Pannexin1 hemichannels are critical for HIV infection of human primary CD4+ T lymphocytes*. *J Leukoc Biol*, 2013. **94**(3): p. 399-407.
58. Seror, C., et al., *Extracellular ATP acts on P2Y2 purinergic receptors to facilitate HIV-1 infection*. *J Exp Med*, 2011. **208**(9): p. 1823-34.
59. Bargiotas, P., et al., *Pannexins in ischemia-induced neurodegeneration*. *Proc Natl Acad Sci U S A*, 2011. **108**(51): p. 20772-7.
60. Good, M.E., et al., *Endothelial cell Pannexin1 modulates severity of ischemic stroke by regulating cerebral inflammation and myogenic tone*. *JCI Insight*, 2018. **3**(6).

61. Sharma, A.K., et al., *Pannexin-1 channels on endothelial cells mediate vascular inflammation during lung ischemia-reperfusion injury*. Am J Physiol Lung Cell Mol Physiol, 2018. **315**(2): p. L301-1312.
62. Su, L., et al., *Pannexin 1 mediates ferroptosis that contributes to renal ischemia/reperfusion injury*. J Biol Chem, 2019. **294**(50): p. 19395-19404.
63. Yin, F., et al., *Caspase-11 promotes NLRP3 inflammasome activation via the cleavage of pannexin1 in acute kidney disease*. Acta Pharmacol Sin, 2021.
64. Bao, L., S. Locovei, and G. Dahl, *Pannexin membrane channels are mechanosensitive conduits for ATP*. FEBS Lett, 2004. **572**(1-3): p. 65-8.
65. Dahl, G., *ATP release through pannexon channels*. Philos Trans R Soc Lond B Biol Sci, 2015. **370**(1672).
66. Medina, C.B., et al., *Metabolites released from apoptotic cells act as tissue messengers*. Nature, 2020. **580**(7801): p. 130-135.
67. Bhalla-Gehi, R., et al., *Pannexin1 and pannexin3 delivery, cell surface dynamics, and cytoskeletal interactions*. J Biol Chem, 2010. **285**(12): p. 9147-60.
68. Gehi, R., Q. Shao, and D.W. Laird, *Pathways regulating the trafficking and turnover of pannexin1 protein and the role of the C-terminal domain*. J Biol Chem, 2011. **286**(31): p. 27639-53.
69. Boassa, D., et al., *Trafficking dynamics of glycosylated pannexin 1 proteins*. Cell Commun Adhes, 2008. **15**(1): p. 119-32.
70. Bruzzone, R., et al., *Pharmacological properties of homomeric and heteromeric pannexin hemichannels expressed in Xenopus oocytes*. J Neurochem, 2005. **92**(5): p. 1033-43.
71. Chiu, Y.H., et al., *Revisiting multimodal activation and channel properties of Pannexin 1*. J Gen Physiol, 2018. **150**(1): p. 19-39.
72. Locovei, S., J. Wang, and G. Dahl, *Activation of pannexin 1 channels by ATP through P2Y receptors and by cytoplasmic calcium*. FEBS Lett, 2006. **580**(1): p. 239-44.
73. Wang, J., et al., *The membrane protein Pannexin1 forms two open-channel conformations depending on the mode of activation*. Sci Signal, 2014. **7**(335): p. ra69.
74. Vanden Abeele, F., et al., *Functional implications of calcium permeability of the channel formed by pannexin 1*. J Cell Biol, 2006. **174**(4): p. 535-46.
75. Boyce, A.K., et al., *ATP stimulates pannexin 1 internalization to endosomal compartments*. Biochem J, 2015. **470**(3): p. 319-30.
76. Swayne, L.A. and A.K.J. Boyce, *Regulation of Pannexin 1 Surface Expression by Extracellular ATP: Potential Implications for Nervous System Function in Health and Disease*. Front Cell Neurosci, 2017. **11**: p. 230.

77. Deng, Z., et al., *Cryo-EM structures of the ATP release channel pannexin 1*. Nat Struct Mol Biol, 2020. **27**(4): p. 373-381.
78. Mou, L., et al., *Structural basis for gating mechanism of Pannexin 1 channel*. Cell Res, 2020. **30**(5): p. 452-454.
79. Michalski, K., et al., *The Cryo-EM structure of pannexin 1 reveals unique motifs for ion selection and inhibition*. Elife, 2020. **9**.
80. Qiu, F. and G. Dahl, *A permeant regulating its permeation pore: inhibition of pannexin 1 channels by ATP*. Am J Physiol Cell Physiol, 2009. **296**(2): p. C250-5.
81. Sandilos, J.K., et al., *Pannexin 1, an ATP release channel, is activated by caspase cleavage of its pore-associated C-terminal autoinhibitory region*. J Biol Chem, 2012. **287**(14): p. 11303-11.
82. Chiu, Y.H., et al., *A quantized mechanism for activation of pannexin channels*. Nat Commun, 2017. **8**: p. 14324.
83. Boassa, D., et al., *Pannexin2 oligomers localize in the membranes of endosomal vesicles in mammalian cells while Pannexin1 channels traffic to the plasma membrane*. Front Cell Neurosci, 2014. **8**: p. 468.
84. Wicki-Stordeur, L.E., A.K. Boyce, and L.A. Swayne, *Analysis of a pannexin 2-pannexin 1 chimeric protein supports divergent roles for pannexin C-termini in cellular localization*. Cell Commun Adhes, 2013. **20**(3-4): p. 73-9.
85. Le Vasseur, M., et al., *Pannexin 2 Localizes at ER-Mitochondria Contact Sites*. Cancers (Basel), 2019. **11**(3).
86. Penuela, S., et al., *Diverse post-translational modifications of the pannexin family of channel-forming proteins*. Channels (Austin), 2014. **8**(2): p. 124-30.
87. Swayne, L.A., C.D. Sorbara, and S.A. Bennett, *Pannexin 2 is expressed by postnatal hippocampal neural progenitors and modulates neuronal commitment*. J Biol Chem, 2010. **285**(32): p. 24977-86.
88. Bargiotas, P., et al., *Functional outcome of pannexin-deficient mice after cerebral ischemia*. Channels (Austin), 2012. **6**(6): p. 453-6.
89. Ambrosi, C., et al., *Pannexin1 and pannexin2 channels show quaternary similarities to connexons and different oligomerization numbers from each other*. Journal of Biological Chemistry, 2010. **285**: p. 24420-24431.
90. Lohman, A.W., et al., *S-nitrosylation inhibits pannexin 1 channel function*. J Biol Chem, 2012. **287**(47): p. 39602-12.
91. Boyce, A.K.J., et al., *Transcriptional and post-translational regulation of pannexins*. Biochim Biophys Acta Biomembr, 2018. **1860**(1): p. 72-82.

92. Zielinska, D.F., et al., *Precision mapping of an in vivo N-glycoproteome reveals rigid topological and sequence constraints*. Cell, 2010. **141**(5): p. 897-907.
93. Palacios-Moreno, J., et al., *Neuroblastoma tyrosine kinase signaling networks involve FYN and LYN in endosomes and lipid rafts*. PLoS Comput Biol, 2015. **11**(4): p. e1004130.
94. Holland, S.H., *Regulation of Neuroblastoma Malignant Properties by Pannexin 1 Channels: Role of Post-Translational Modifications and Mutations*, in *Médecine cellulaire et moléculaire / Cellular and Molecular Medicine*. 2020, Université d'Ottawa / University of Ottawa.
95. Nouri-Nejad, D., et al., *Pannexin 1 mutation found in melanoma tumour reduces phosphorylation, glycosylation, and trafficking of the channel-forming protein*. Mol Biol Cell, 2021: p. mbcE19100585.
96. Hornbeck, P.V., et al., *PhosphoSitePlus, 2014: mutations, PTMs and recalibrations*. Nucleic Acids Res, 2015. **43**(Database issue): p. D512-20.
97. Lohman, A.W., et al., *Pannexin 1 channels regulate leukocyte emigration through the venous endothelium during acute inflammation*. Nat Commun, 2015. **6**: p. 7965.
98. DeLalio, L.J., et al., *Constitutive SRC-mediated phosphorylation of pannexin 1 at tyrosine 198 occurs at the plasma membrane*. J Biol Chem, 2019. **294**(17): p. 6940-6956.
99. Weilinger, N.L., et al., *Metabotropic NMDA receptor signaling couples Src family kinases to pannexin-1 during excitotoxicity*. Nat Neurosci, 2016. **19**(3): p. 432-42.
100. Poornima, V., et al., *Nitric oxide inhibits the pannexin 1 channel through a cGMP-PKG dependent pathway*. Nitric Oxide, 2015. **47**: p. 77-84.
101. Kettenbach, A.N., et al., *Quantitative phosphoproteomics identifies substrates and functional modules of Aurora and Polo-like kinase activities in mitotic cells*. Sci Signal, 2011. **4**(179): p. rs5.
102. Mertins, P., et al., *Proteogenomics connects somatic mutations to signalling in breast cancer*. Nature, 2016. **534**(7605): p. 55-62.
103. Mertins, P., et al., *Integrated proteomic analysis of post-translational modifications by serial enrichment*. Nat Methods, 2013. **10**(7): p. 634-7.
104. Klammer, M., et al., *Phosphosignature predicts dasatinib response in non-small cell lung cancer*. Mol Cell Proteomics, 2012. **11**(9): p. 651-68.
105. Lopez, X., et al., *Stretch-Induced Activation of Pannexin 1 Channels Can Be Prevented by PKA-Dependent Phosphorylation*. Int J Mol Sci, 2020. **21**(23).
106. Bunse, S., et al., *Intracellular cysteine 346 is essentially involved in regulating Panx1 channel activity*. J Biol Chem, 2010. **285**(49): p. 38444-52.

107. Yang, D., et al., *Caspase-11 Requires the Pannexin-1 Channel and the Purinergic P2X7 Pore to Mediate Pyroptosis and Endotoxic Shock*. *Immunity*, 2015. **43**(5): p. 923-32.
108. Akimov, V., et al., *UbiSite approach for comprehensive mapping of lysine and N-terminal ubiquitination sites*. *Nat Struct Mol Biol*, 2018. **25**(7): p. 631-640.
109. Kim, W., et al., *Systematic and quantitative assessment of the ubiquitin-modified proteome*. *Mol Cell*, 2011. **44**(2): p. 325-40.
110. Krick, S., et al., *Dual Oxidase 2 (Duox2) Regulates Pannexin 1-mediated ATP Release in Primary Human Airway Epithelial Cells via Changes in Intracellular pH and Not H₂O₂ Production*. *J Biol Chem*, 2016. **291**(12): p. 6423-32.
111. Chiu, Y.H., et al., *Deacetylation as a receptor-regulated direct activation switch for pannexin channels*. *Nat Commun*, 2021. **12**(1): p. 4482.
112. Sanchez-Pupo, R.E., D. Johnston, and S. Penuela, *N-Glycosylation Regulates Pannexin 2 Localization but Is Not Required for Interacting with Pannexin 1*. *Int J Mol Sci*, 2018. **19**(7).
113. Ultanir, S.K., et al., *Chemical genetic identification of NDR1/2 kinase substrates AAK1 and Rabin8 Uncovers their roles in dendrite arborization and spine development*. *Neuron*, 2012. **73**(6): p. 1127-42.
114. Nagai, T., et al., *Phosphoproteomics of the Dopamine Pathway Enables Discovery of Rap1 Activation as a Reward Signal In Vivo*. *Neuron*, 2016. **89**(3): p. 550-65.
115. Reily, C., et al., *Glycosylation in health and disease*. *Nat Rev Nephrol*, 2019. **15**(6): p. 346-366.
116. Aebi, M., *N-linked protein glycosylation in the ER*. *Biochim Biophys Acta*, 2013. **1833**(11): p. 2430-7.
117. Penuela, S., et al., *Pannexin 1 and pannexin 3 are glycoproteins that exhibit many distinct characteristics from the connexin family of gap junction proteins*. *Journal of Cell Science*, 2007. **120**: p. 3772-3783.
118. Le Vasseur, M., et al., *Pannexin 2 protein expression is not restricted to the CNS*. *Front Cell Neurosci*, 2014. **8**: p. 392.
119. Boassa, D., et al., *Pannexin1 channels contain a glycosylation site that targets the hexamer to the plasma membrane*. *Journal of Biological Chemistry*, 2007. **282**: p. 31733-31743.
120. Zappalà, A., et al., *Expression of pannexin2 protein in healthy and ischemized brain of adult rats*. *Neuroscience*, 2007. **148**: p. 653-67.
121. Lai, C.P.K., J.F. Bechberger, and C.C. Naus, *Pannexin2 as a novel growth regulator in C6 glioma cells*. *Oncogene*, 2009. **28**: p. 4402-4408.

122. Wicki-Stordeur, L.E., A.K.J. Boyce, and L.A. Swayne, *Analysis of a pannexin 2-pannexin 1 chimeric protein supports divergent roles for pannexin C-termini in cellular localization*. Cell Communication & Adhesion, 2013. **20**: p. 73-9.
123. Boassa, D., et al., *Pannexin2 oligomers localize in the membranes of endosomal vesicles in mammalian cells while Pannexin1 channels traffic to the plasma membrane*. Frontiers in Cellular Neuroscience, 2015. **8**: p. 15.
124. Kumar, S., et al., *Caspase cleavage sites in the human proteome: CaspDB, a database of predicted substrates*. PLoS One, 2014. **9**(10): p. e110539.
125. Slee, E.A., C. Adrain, and S.J. Martin, *Executioner caspase-3, -6, and -7 perform distinct, non-redundant roles during the demolition phase of apoptosis*. J Biol Chem, 2001. **276**(10): p. 7320-6.
126. Boyd-Tressler, A., et al., *Chemotherapeutic drugs induce ATP release via caspase-gated pannexin-1 channels and a caspase/pannexin-1-independent mechanism*. J Biol Chem, 2014. **289**(39): p. 27246-27263.
127. Dourado, M., E. Wong, and D.H. Hackos, *Pannexin-1 is blocked by its C-terminus through a delocalized non-specific interaction surface*. PLoS One, 2014. **9**(6): p. e99596.
128. Imamura, H., et al., *Single-cell dynamics of pannexin-1-facilitated programmed ATP loss during apoptosis*. Elife, 2020. **9**.
129. Lai, C.P., J.F. Bechberger, and C.C. Naus, *Pannexin2 as a novel growth regulator in C6 glioma cells*. Oncogene, 2009. **28**(49): p. 4402-8.
130. Li, J., et al., *Ferroptosis: past, present and future*. Cell Death Dis, 2020. **11**(2): p. 88.
131. Gonzales, K.A.U. and E. Fuchs, *Skin and Its Regenerative Powers: An Alliance between Stem Cells and Their Niche*. Dev Cell, 2017. **43**(4): p. 387-401.
132. Dubin, A.E. and A. Patapoutian, *Nociceptors: the sensors of the pain pathway*. J Clin Invest, 2010. **120**(11): p. 3760-72.
133. Chuong, C.M. and A. Noveen, *Phenotypic determination of epithelial appendages: genes, developmental pathways, and evolution*. J Invest Dermatol Symp Proc, 1999. **4**(3): p. 307-11.
134. Bikle, D.D., Z. Xie, and C.L. Tu, *Calcium regulation of keratinocyte differentiation*. Expert Rev Endocrinol Metab, 2012. **7**(4): p. 461-472.
135. Seiberg, M., *Keratinocyte-melanocyte interactions during melanosome transfer*. Pigment Cell Res, 2001. **14**(4): p. 236-42.
136. Nguyen, A.V. and A.M. Soulika, *The Dynamics of the Skin's Immune System*. Int J Mol Sci, 2019. **20**(8).

137. Zhang, P., et al., *Pannexin 3 regulates skin development via Epiprofin*. Sci Rep, 2021. **11**(1): p. 1779.
138. Zhang, P., et al., *Pannexin-3 Deficiency Delays Skin Wound Healing in Mice due to Defects in Channel Functionality*. J Invest Dermatol, 2019. **139**(4): p. 909-918.
139. Flores-Munoz, C., et al., *Restraint of Human Skin Fibroblast Motility, Migration, and Cell Surface Actin Dynamics, by Pannexin 1 and P2X7 Receptor Signaling*. Int J Mol Sci, 2021. **22**(3).
140. Jiang, J.X. and S. Penuela, *Connexin and pannexin channels in cancer*. BMC Cell Biol, 2016. **17 Suppl 1**: p. 12.
141. Xu, X., et al., *PANX2 and brain lower grade glioma genesis: A bioinformatic analysis*. Sci Prog, 2021. **104**(2): p. 368504211011836.
142. Wu, D., et al., *Role of Pannexin1 channels in the resistance of I-10 testicular cancer cells to cisplatin mediated by ATP/IP3 pathway*. Biomed Pharmacother, 2017. **94**: p. 514-522.
143. Liu, H., et al., *In vitro effect of Pannexin 1 channel on the invasion and migration of I-10 testicular cancer cells via ERK1/2 signaling pathway*. Biomed Pharmacother, 2019. **117**: p. 109090.
144. Schalper, K.A., D. Carvajal-Hausdorf, and M.P. Oyarzo, *Possible role of hemichannels in cancer*. Front Physiol, 2014. **5**: p. 237.
145. Xiang, X., et al., *Pannexin 1 inhibits rhabdomyosarcoma progression through a mechanism independent of its canonical channel function*. Oncogenesis, 2018. **7**(11): p. 89.
146. Xiang, X., et al., *Identification of pannexin 1-regulated genes, interactome, and pathways in rhabdomyosarcoma and its tumor inhibitory interaction with AHNAK*. Oncogene, 2021. **40**(10): p. 1868-1883.
147. Litvin, O., et al., *What is hidden in the pannexin treasure trove: the sneak peek and the guesswork*. J Cell Mol Med, 2006. **10**(3): p. 613-34.
148. Sung, H., et al., *Global Cancer Statistics 2020: GLOBOCAN Estimates of Incidence and Mortality Worldwide for 36 Cancers in 185 Countries*. CA Cancer J Clin, 2021. **71**(3): p. 209-249.
149. Berk-Krauss, J., et al., *New Systematic Therapies and Trends in Cutaneous Melanoma Deaths Among US Whites, 1986-2016*. Am J Public Health, 2020. **110**(5): p. 731-733.
150. Liu, Y. and M.S. Sheikh, *Melanoma: Molecular Pathogenesis and Therapeutic Management*. Mol Cell Pharmacol, 2014. **6**(3): p. 228.
151. Balch, C.M., et al., *Cutaneous melanoma*. 1998: Springer.

152. Tarhini, A.A., et al., *Diagnosis of Stage IV Melanoma*, in *Cutaneous Melanoma*, C. Balch, et al., Editors. 2019, Springer International Publishing: Cham. p. 1-47.
153. Ikehata, H. and T. Ono, *The mechanisms of UV mutagenesis*. J Radiat Res, 2011. **52**(2): p. 115-25.
154. Ticha, I., et al., *A comprehensive evaluation of pathogenic mutations in primary cutaneous melanomas, including the identification of novel loss-of-function variants*. Sci Rep, 2019. **9**(1): p. 17050.
155. Meyle, K.D. and P. Guldberg, *Genetic risk factors for melanoma*. Hum Genet, 2009. **126**(4): p. 499-510.
156. Reddy, B.Y., D.M. Miller, and H. Tsao, *Somatic driver mutations in melanoma*. Cancer, 2017. **123**(S11): p. 2104-2117.
157. Zhang, T., et al., *The genomic landscape of cutaneous melanoma*. Pigment Cell Melanoma Res, 2016. **29**(3): p. 266-83.
158. Davies, H., et al., *Mutations of the BRAF gene in human cancer*. Nature, 2002. **417**(6892): p. 949-54.
159. Pollock, P.M., et al., *High frequency of BRAF mutations in nevi*. Nat Genet, 2003. **33**(1): p. 19-20.
160. Manzano, J.L., et al., *Resistant mechanisms to BRAF inhibitors in melanoma*. Ann Transl Med, 2016. **4**(12): p. 237.
161. Garraway, L.A., et al., *Integrative genomic analyses identify MITF as a lineage survival oncogene amplified in malignant melanoma*. Nature, 2005. **436**(7047): p. 117-22.
162. Davies, M.A., *The role of the PI3K-AKT pathway in melanoma*. Cancer J, 2012. **18**(2): p. 142-7.
163. Tsao, H., et al., *Genetic interaction between NRAS and BRAF mutations and PTEN/MMAC1 inactivation in melanoma*. J Invest Dermatol, 2004. **122**(2): p. 337-41.
164. Dankort, D., et al., *Braf(V600E) cooperates with Pten loss to induce metastatic melanoma*. Nat Genet, 2009. **41**(5): p. 544-52.
165. Kakadia, S., et al., *Mechanisms of resistance to BRAF and MEK inhibitors and clinical update of US Food and Drug Administration-approved targeted therapy in advanced melanoma*. Onco Targets Ther, 2018. **11**: p. 7095-7107.
166. Tangella, L.P., M.E. Clark, and E.S. Gray, *Resistance mechanisms to targeted therapy in BRAF-mutant melanoma - A mini review*. Biochim Biophys Acta Gen Subj, 2021. **1865**(1): p. 129736.
167. Meirson, T., et al., *Safety of BRAF+MEK Inhibitor Combinations: Severe Adverse Event Evaluation*. Cancers (Basel), 2020. **12**(6).

168. Ribas, A., *Tumor immunotherapy directed at PD-1*. N Engl J Med, 2012. **366**(26): p. 2517-9.
169. Marzagalli, M., N.D. Ebel, and E.R. Manuel, *Unraveling the crosstalk between melanoma and immune cells in the tumor microenvironment*. Semin Cancer Biol, 2019. **59**: p. 236-250.
170. Hogan, S.A., M.P. Levesque, and P.F. Cheng, *Melanoma Immunotherapy: Next-Generation Biomarkers*. Front Oncol, 2018. **8**: p. 178.
171. Lee, N., et al., *Tumour-infiltrating lymphocytes in melanoma prognosis and cancer immunotherapy*. Pathology, 2016. **48**(2): p. 177-87.
172. Davis, L.E., S.C. Shalin, and A.J. Tackett, *Current state of melanoma diagnosis and treatment*. Cancer Biol Ther, 2019. **20**(11): p. 1366-1379.
173. Ribas, A., et al., *PD-L1 blockade in combination with inhibition of MAPK oncogenic signaling in patients with advanced melanoma*. Nat Commun, 2020. **11**(1): p. 6262.
174. Kasakovski, D., et al., *Advances in Targeting Cutaneous Melanoma*. Cancers (Basel), 2021. **13**(9).
175. O'Donnell, J.S., et al., *Resistance to PD1/PDL1 checkpoint inhibition*. Cancer Treat Rev, 2017. **52**: p. 71-81.
176. Cabrita, R., et al., *The Role of PTEN Loss in Immune Escape, Melanoma Prognosis and Therapy Response*. Cancers (Basel), 2020. **12**(3).
177. Peng, W., et al., *Loss of PTEN Promotes Resistance to T Cell-Mediated Immunotherapy*. Cancer Discov, 2016. **6**(2): p. 202-16.
178. Spranger, S., R. Bao, and T.F. Gajewski, *Melanoma-intrinsic beta-catenin signalling prevents anti-tumour immunity*. Nature, 2015. **523**(7559): p. 231-5.
179. Yaguchi, T., et al., *Immune suppression and resistance mediated by constitutive activation of Wnt/beta-catenin signaling in human melanoma cells*. J Immunol, 2012. **189**(5): p. 2110-7.
180. Maus, R.L.G., et al., *Human Melanoma-Derived Extracellular Vesicles Regulate Dendritic Cell Maturation*. Front Immunol, 2017. **8**: p. 358.
181. Tucci, M., et al., *Immune System Evasion as Hallmark of Melanoma Progression: The Role of Dendritic Cells*. Front Oncol, 2019. **9**: p. 1148.
182. Rotte, A., *Combination of CTLA-4 and PD-1 blockers for treatment of cancer*. J Exp Clin Cancer Res, 2019. **38**(1): p. 255.
183. Li, H., et al., *Dysfunctional CD8 T Cells Form a Proliferative, Dynamically Regulated Compartment within Human Melanoma*. Cell, 2019. **176**(4): p. 775-789 e18.

184. Duan, Q., et al., *Turning Cold into Hot: Firing up the Tumor Microenvironment*. Trends Cancer, 2020. **6**(7): p. 605-618.
185. Damsky, W.E., et al., *beta-catenin signaling controls metastasis in Braf-activated Pten-deficient melanomas*. Cancer Cell, 2011. **20**(6): p. 741-54.
186. Brown, K., et al., *WNT/beta-catenin signaling regulates mitochondrial activity to alter the oncogenic potential of melanoma in a PTEN-dependent manner*. Oncogene, 2017. **36**(22): p. 3119-3136.
187. Wicki-Stordeur, L.E. and L.A. Swayne, *The emerging Pannexin 1 signalome: a new nexus revealed?* Front Cell Neurosci, 2014. **7**: p. 287.
188. Chen, W., et al., *Enhanced Macrophage Pannexin 1 Expression and Hemichannel Activation Exacerbates Lethal Experimental Sepsis*. Sci Rep, 2019. **9**(1): p. 160.
189. Varela-Vazquez, A., et al., *Emerging functions and clinical prospects of connexins and pannexins in melanoma*. Biochim Biophys Acta Rev Cancer, 2020. **1874**(1): p. 188380.
190. Schneider, S.L., A.L. Ross, and J.M. Grichnik, *Do inflammatory pathways drive melanomagenesis?* Exp Dermatol, 2015. **24**(2): p. 86-90.
191. Yang, Y., et al., *Endothelial Pannexin 1 Channels Control Inflammation by Regulating Intracellular Calcium*. J Immunol, 2020. **204**(11): p. 2995-3007.
192. Qu, Y., et al., *Pannexin-1 Is Required for ATP Release during Apoptosis but Not for Inflammasome Activation*. The Journal of Immunology, 2011. **186**(11): p. 6553-6561.
193. White, N., P.E. Butler, and G. Burnstock, *Human melanomas express functional P2 X(7) receptors*. Cell Tissue Res, 2005. **321**(3): p. 411-8.
194. Ahmad, I., et al., *Thymoquinone suppresses metastasis of melanoma cells by inhibition of NLRP3 inflammasome*. Toxicol Appl Pharmacol, 2013. **270**(1): p. 70-6.
195. Okamoto, M., et al., *Constitutively active inflammasome in human melanoma cells mediating autoinflammation via caspase-1 processing and secretion of interleukin-1beta*. J Biol Chem, 2010. **285**(9): p. 6477-88.
196. Tengesdal, I.W., et al., *Targeting tumor-derived NLRP3 reduces melanoma progression by limiting MDSCs expansion*. Proc Natl Acad Sci U S A, 2021. **118**(10).
197. Young, H.L., et al., *An adaptive signaling network in melanoma inflammatory niches confers tolerance to MAPK signaling inhibition*. J Exp Med, 2017. **214**(6): p. 1691-1710.
198. Gelfo, V., et al., *Roles of IL-1 in Cancer: From Tumor Progression to Resistance to Targeted Therapies*. Int J Mol Sci, 2020. **21**(17).
199. Bent, R., et al., *Interleukin-1 Beta-A Friend or Foe in Malignancies?* Int J Mol Sci, 2018. **19**(8).

200. Baker, K.J., A. Houston, and E. Brint, *IL-1 Family Members in Cancer; Two Sides to Every Story*. Front Immunol, 2019. **10**: p. 1197.
201. Trabanelli, S., et al., *Extracellular ATP exerts opposite effects on activated and regulatory CD4+ T cells via purinergic P2 receptor activation*. J Immunol, 2012. **189**(3): p. 1303-10.
202. Jacobs, J.F., et al., *Regulatory T cells in melanoma: the final hurdle towards effective immunotherapy?* Lancet Oncol, 2012. **13**(1): p. e32-42.
203. Amoroso, F., et al., *The P2X7 receptor is a key modulator of aerobic glycolysis*. Cell Death Dis, 2012. **3**: p. e370.
204. Vaupel, P. and G. Multhoff, *Accomplices of the Hypoxic Tumor Microenvironment Compromising Antitumor Immunity: Adenosine, Lactate, Acidosis, Vascular Endothelial Growth Factor, Potassium Ions, and Phosphatidylserine*. Front Immunol, 2017. **8**: p. 1887.
205. Saez, P.J., et al., *ATP promotes the fast migration of dendritic cells through the activity of pannexin 1 channels and P2X7 receptors*. Sci Signal, 2017. **10**(506).
206. Shoji, K.F., et al., *Pannexin1 channels act downstream of P2X 7 receptors in ATP-induced murine T-cell death*. Channels (Austin), 2014. **8**(2): p. 142-56.
207. Seo, J.H., et al., *Myeloid Pannexin-1 mediates acute leukocyte infiltration and leads to worse outcomes after brain trauma*. J Neuroinflammation, 2020. **17**(1): p. 245.

Chapter 2

A mouse *Panx2* splice variant (*Panx2-202*) has been reported in the skin, but its expression has not been thoroughly investigated. Furthermore, canonical PANX2 was shown to be a substrate in vitro for apoptotic caspases, but it is unclear whether this PTM occurs in cells during apoptosis. In this chapter, we assessed the PANX2 splice variant expression in normal murine skin of different ages and identified the primary cell type where it is expressed. Moreover, we evaluated the consequences of caspase cleavage of canonical PANX2 in apoptotic keratinocytes using UVB irradiation as an apoptotic stimulus.

2 Pannexin 2 is expressed in the murine skin and promotes UVB-induced apoptosis of keratinocytes

2.1 Introduction

Pannexins (PANX1, PANX2, PANX3) are channel-forming glycoproteins that participate in paracrine signaling and are expressed in several tissues [1, 2]. Initial studies showed abundant PANX2 levels in the central nervous system leading the scientific community to consider that PANX2 expression is restricted. Recent evidence indicates a broader expression and potential functions in other tissues like the skin [3]. Only PANX1 and PANX3 orthologs have been characterized in the context of the skin, which can be found in the different skin layers and appendages with various localization profiles [4, 5]. PANX3 remains steadily expressed after skin development [4], while PANX1 has the highest expression levels at early postnatal stages but becomes downregulated in aged skin [6]. PANX2 expression has also been detected in the skin [3], but its exact distribution profile and regulation have been largely unexplored in this tissue.

Moreover, PANX1 and PANX3 channels are regulated during keratinocyte differentiation and are implicated in regulating proliferation, differentiation, and wound healing [4, 6-8]. Much less is known regarding PANX2, for which it has been established that it is expressed in brain tissue and participates in regulating neurogenesis [9] and ischemia-induced neurodegeneration [10]. Besides, PANX2 is downregulated in lower-grade glioma and was recently shown to influence multiple molecular pathways and immune infiltration in these cancer tumors [11].

Interestingly, PANX2 has been identified at the endoplasmic reticulum (ER)-mitochondria interface [12], and it has been suggested to promote cell death. However, the roles of PANX2 seem to be different depending on the type of cell death and the cell insult. For example, although PANX2 has been found downregulated in gliomas, its overexpression in rat C6 glioma cells reduces their oncogenicity and accelerates staurosporine-induced apoptosis [12, 13]. Furthermore, genetic deletion of *Panx2* (along with *Panx1*) reduces neuronal cell death through necrosis and protects mice from ischemic stroke [10]. In

contrast, it was reported that pro-inflammatory cytokines reduce PANX2 expression in pancreatic β -cells and increase cytokine-mediated apoptosis causing severe diabetes in mice [14]. More recently, PANX2 expression was shown to be enriched in prostate cancer cells, negatively regulating a form of cell death known as ferroptosis, where it was implicated in regulating lipid peroxidation and the cell uptake of ferrous iron [15]. Despite these findings, little is known about the roles that PANX2 might play in the skin and whether this pannexin influences cell death.

The skin is frequently subjected to damage by ultraviolet light (UV), where apoptosis has an important physiological function to maintain homeostasis [16]. Notably, PANX2 has been shown to undergo *in vitro* cleavage by apoptotic caspases-3/7 (Penuela et al., 2013). However, the sites for this post-translational modification have not been confirmed nor its occurrence in the cellular context. Considering PANX2 is present in the skin, it is possible that, in this context, it could undergo cleavage by apoptotic caspases and modulate the UVB-induced apoptosis of these cells.

In the current study, we sought to explore the temporal regulation of PANX2 expression in the developing and mature skin at the protein and transcript levels. Furthermore, we studied PANX2 localization, determined what cell type is primarily expressing PANX2 in the skin, and investigated whether the caspase-mediated cleavage of this pannexin can result from UVB radiation-induced apoptosis as a relevant biological model of cell death in the skin. We hypothesized that PANX2 is cleaved by executioner caspases and promotes the apoptosis of skin cells after UVB insult.

2.2 Materials and Methods

2.2.1 Cell lines, transfection, and culture conditions

Human embryonic kidney (HEK293T CRL-3216™) cells were obtained from ATCC® (Manassas, VA, USA). Rat epidermal keratinocytes (REK) immortalized cell line was a kind gift from Dr. Dale Laird and was previously characterized in [6, 17, 18]. Media and most supplements were obtained from GIBCO® (Grand Island, NY, USA) and Invitrogen™ (Carlsbad, CA, USA). Unless otherwise stated, cells were grown in DMEM

(1X) (GIBCO, REF#12430-054, Grand Island, NY, USA) supplemented with 10% fetal bovine serum (FBS) (WISENT INC Cat# 080-150, QC, Canada), 1% penicillin-streptomycin (Pen Strep) (GIBCO, REF#15140-122, Grand Island, NY, USA) and maintained at 37°C under humidified 5% CO₂–95% air. For *in vitro* differentiation studies with REK cells, the culture medium was supplemented with calcium chloride at 2.0 mM final concentration for 72 h, or stratified piles of overgrown monolayer cultures were kept for the same length of time. For transient transfections, the cells were transfected using 5 µg of plasmid DNA with Lipofectamine 3000 (Invitrogen™ REF# L3000-015, Carlsbad, CA, USA) as per manufacturer instructions. For apoptosis assays, 24 h post-transfection, cells were split in half for immunofluorescence staining, and the rest used for Incucyte® Live-cell imaging of UVB-induced apoptosis experiments.

2.2.2 Isolation and culture of mouse epidermal keratinocytes and dermal fibroblasts

The Animal Care Subcommittee of The University of Western Ontario approved all procedures with mice (Protocols 2019-069 and 2019-070). Isolation of primary keratinocytes and dermal fibroblast from neonatal dorsal skin (P4) was performed following the protocols described in [6]. Primary keratinocytes were cultured in KBM™ Gold™ Basal Medium (Lonza Cat#: 00192151, Walkersville, MD, USA) supplemented KGM-Gold™ Keratinocyte SingleQuots® (Lonza Cat#: 00192152 Walkersville, MD, USA) at 37°C, 5% CO₂. The culture medium was replaced first at 16 h post-harvesting and later every 48h. Keratinocytes were kept for up to 3 weeks until they reached 60-70% confluency without any passaging before the experiments. For primary keratinocyte *in vitro* differentiation, non-confluent cell monolayers were exposed for 72 h to culture medium supplemented with a final concentration of 1.8 mM of CaCl₂. Fibroblasts were cultured in DMEM media supplemented with 10% FBS and 1% Pen Strep and growth in plates coated with type I rat tail collagen (Corning REF#354236, Bedford, MA, USA) until cells reached 70-80% confluency. Cultures of primary dermal fibroblasts were only passaged for a maximum of three times, and visual inspection of a spindle-shaped morphology was continuously assessed before the experiments. Fibroblast stimulation with

TGF- β was performed as previously indicated in [6] with 200 pM TGF- β (PeproTech) dissolved in culture media for four days.

2.2.3 CRISPR-Cas9-mediated PANX2 deletion in REK cells

CRISPR/Cas9 technology was used to generate PANX2 knockout REK cells (REK-PANX2KO) according to Synthego's nucleofection CRISPR protocol. CRISPR Revolution single-guide RNA (sgRNA) EZ kit targeting beginning of exon 2 of rat *Panx2* gene (sequence: GCACAACUUCACCCGUGACC) and Cas 9 2NLS nuclease were obtained from Synthego (Synthego Corporation, Menlo Park, California). 10^6 cells/reaction were used for nucleofection with complexed ribonucleoprotein (9:1, sgRNA to Cas9 ratio) and Nucleofector™ solution L + supplement in a Nucleofector™ II (Amaxa biosystems, Germany) according to the manufacturer's instructions. Expansion and clonal selection were then performed post-nucleofection and genomic DNA isolated for genome sequencing and analysis by Inference of CRISPR Edits (Synthego). Platinum Taq DNA High Fidelity polymerase (Invitrogen REF#11304-011, Carlsbad, CA, USA) was used for PCR to genotype the target region as per manufacturer instructions using the following primers Px2-F (5'-GGGGGTTTCATTTGGGGAACA-3') and Px2-R (5'-CAGGAAGTTGAGCTCGGAGG-3'). The genomic deletion was confirmed by Sanger sequencing provided by the London Regional Genomics Centre (Robarts Research Institute, London, ON, Canada).

2.2.4 Mutagenesis of Flag-tagged PANX2 constructs

Mouse *Panx2* (canonical) construct from [5] was used to fuse a single FLAG epitope (DYKDDDDK) to the N-terminal region of the PANX2 using the In-Fusion HD Cloning Kit protocol (Clontech®, Mountain View, USA) as per the manufacturer's directions using the following primers: NFLAG sense (5' - ACCATGGATTACAAGGACGACGATGACAAGGGTTCTTCCCACCACCTCCTGGAGC-3') and antisense (5'-GTCGTCCTTGTAATCCATGGTGAATTCCACCACACTG-3'). Procleave web server [19] was used to predict the caspase cleavage consensus sites,

and site-directed mutagenesis was performed by NorClone Biotech Labs (London, ON, Canada).

2.2.5 Protein extractions and western blots

Cell lysates and co-immunoprecipitation assays were performed as described in [5, 20]. Total protein concentrations were quantified with Pierce™ BCA Protein assay kit (Thermo Scientific REF#23225, Rockford, IL, USA). 40 µg of total protein were resolved by 10% SDS-PAGE or TGX Stain-Free FastCast 10% Acrylamide stain-free gels (Cat#161-0183, Bio-Rad, USA) and transferred onto nitrocellulose membranes using an iBlot™ Blotting System (Invitrogen, USA). Membranes were blocked with 3% bovine fraction V heat shock serum albumin (BSA)(BioShop REF# ALB001.100, Burlington, ON, Canada) in 0.05% Tween 20-Phosphate Buffer Saline (T-PBS) for 45 min and probed overnight at 4°C with the primary antibodies. Primary antibodies used for Western blots were: anti-PANX2-CT-523 [20] (1:500 dilution); Anti-FLAG® M2 monoclonal antibody (REF#F3165, SIGMA-ALDRICH, St. Louis, MO, USA), anti-Panx2-NT (Cat#ARP42778_T100; Aviva Systems Biology, San Diego, CA) [9], mouse monoclonal anti-PANX2 (clone N121A/3175-213) antibody (UC Davis/NIH NeuroMab Facility, CA, USA) [3], and cleaved caspase-3 (D175) (REF#9661S, Cell Signaling Technology, USA) were used at 1:1000 dilution; anti-GAPDH (Cat# MAB374, RRID: AB_2107445, Millipore, USA) was used at 1:5000 as the gel loading control. For detection, secondary antibodies IRDye® -800CW and -680RD (LI-COR Biosciences, Lincoln, NE, USA) were used at 1:25000 dilution. Western blots were visualized with Odyssey® infrared imaging system (LI-COR, NE, USA) except for the skin lysates. For skin protein lysate immunoblots on nitrocellulose membranes, stain-free total protein was used for total protein determination imaged with a ChemiDoc™ MP System (Bio-RAD, USA). As an internal control to assess blot-to-blot variations, a brain lysate control was resolved on each gel and used for normalization. Normalization and densitometry measurements of bands of interest were done using Image Lab™ Software (Ver 6.0.1., Bio-Rad Laboratories, Inc). Other densitometry and lane profile analyses for molecular weight estimations of caspase-cleaved PANX2-fragments were performed using the ODYSSEY application software (ver 3.0.16, LI-COR, NE, USA).

2.2.6 Immunofluorescence and imaging

Dorsal skin tissue samples were fixed in 10% neutral buffered formalin overnight at 4°C, processed in the Molecular Pathology Core Facility at Robarts Research Institute (London, ON, Canada) and subsequently embedded in paraffin. Five µm-thick sections were deparaffinized in xylene, rehydrated in graded alcohols, and washed in PBS. Antigen retrieval was performed using 1.5% of Vector Labs Tris-based Antigen Unmasking Solution (Cat# H-3301, Vector Labs, Burlingame, CA) heating for 5 min in a 750W microwave (at 80% power) and then let cool down at room temperature (RT) for 10 min. Next, sections were rinsed once in distilled water, followed by PBS for 5 min. The sections were incubated with blocking solution (3% BSA, 0.1% Triton X-100 in 1X PBS) for 1h at room temperature in a humidity chamber. Immunofluorescence labeling of sections was performed overnight at 4°C with the primary antibodies diluted in blocking solution. Rabbit anti-PANX2 -CT, -IL, -NT polyclonal antibodies were used at ~100 µg/mL final concentration. Alexa Fluor 488 goat anti-rabbit IgG (Cat#A-11008, Thermo Fisher Scientific, USA) (2.9 µg/mL) was used as a secondary antibody. Slides were mounted using VECTASHIELD® mounting medium (Vector Laboratories). For coverslips immunostaining, cell monolayers were washed with D-PBS (Gibco) and fixed with ice-cold methanol: acetone (5:1, v/v) for 15 minutes at 4°C. Coverslips were blocked for 1h at RT with 10% Normal Goat Serum (Life Technologies REF#50062Z, Frederick, MD, USA). Primary anti-PANX2-CT or anti-FLAG antibodies were used in 1:100 and 1:500 dilutions in 1% Normal Goat Serum-2% BSA-PBS. Coverslips were incubated with primary antibodies for 1 h at RT, then washed with PBS and re-incubated with donkey anti-mouse antibody Alexa Fluor™ 488 (1:400, Cat# A-21202, Invitrogen) and Texas Red™-X goat anti-rabbit (diluted 1:500, REF#T6391, Life Technologies, Eugene, OR, USA) to label FLAG-tagged PANX2. Aqua-Mount medium (LERNER LAB, REF#13800, MI, USA) was used as mounting media. In all cases, Hoechst 33342 (REF#H3570, Life Technologies, Eugene, OR, USA) (diluted 1:1000 in double-distilled water) was incubated with the samples for 7 min at RT to stain cell nuclei. Images were obtained on a Zeiss LSM 800 AiryScan confocal microscope from the Schulich Faculty Imaging Core Facility using

the following objectives: LCI Plan-Neofluar 25x/0.8 1 mm Korr DIC for skin sections and Plan-Apochromat 63x/1.40 Oil DIC M27 for coverslips.

2.2.7 Detection of caspase cleaved PANX2 fragments

In vitro caspase-3 cleavage and IP of cleaved fragments were performed as described in [21]. For UVB-induced apoptosis assays, Protein lysates from apoptotic cells were obtained after eight hours of post-UVB-irradiation, and a similar IP (using 250 µg of total protein) was performed to capture the PANX2 cleaved fragments. 25 µg of the input protein lysates were used for assessing protein expression by Western blot. In both cases (after caspase-3 treatment or in-cell UVB-induced apoptosis), the beads used for IP were dried by aspiration and resuspended in 2X Laemmli buffer (with β-mercaptoethanol), boiled for 5 min, and ran in 10% SDS-PAGE gel for immunoblots with the anti-FLAG monoclonal antibody.

2.2.8 RNA isolation and real-time qPCR.

Total RNA was extracted from flash-frozen mouse dorsal skin samples at different ages using Ambion TRIzol™ Reagent (Life Technologies, REF#15596018, Carlsbad, CA, USA) and purified using the RNAeasy® Plus Mini kit (REF#74134, QIAGEN GmbH, Hilden, Germany). For cell cultures, RNA was extracted with the RLT lysis buffer (Qiagen), and QIAshredder spin columns (REF# 79654, QIAGEN GmbH, Hilden, Germany) were used instead of the TRIzol. All protocols were used following the manufacturer's instructions. RNA concentration was determined using an Epoch Microplate Spectrophotometer (BioTek®, Winooski, VT, USA). Reverse transcription (RT)-PCR was performed using the High Capacity cDNA Reverse Transcription Kit with RNase inhibitor (Applied biosystems REF#4374966, Thermo Fisher Scientific, Vilnius, Lithuania). A CFX96 Touch™ Real-Time PCR Detection System (Bio-Rad, Hercules, CA, USA) and Sensifast SYBR Green PCR Master Mix (Cat#1725274, Bio-RAD, USA) was used to determine the mean quantitation cycle (Cq) for each sample by triplicate and the relative transcript expression was calculated using the $\Delta\Delta C_t$ method in Bio-rad CFX

Maestro Software, ver 1.1 (Bio-rad, USA). Primer sequences used for real-time-qPCR are listed in Table 2-1.

Table 2-1 Primers used for real-time qPCR

GENES	FORWARD (5' ->3')	REVERSE (5' ->3')	AMPLICON (bp)
Mouse			
<i>Panx2</i>	ACTGTGGAGTTTTGAGGGGC	GCAGTACCGGGTGAACAGAG	118
<i>Panx2-202</i>	CAGCCCGTGTCTCCTCTCTAC	GTAGCCGCGGGCGTACA	95
<i>Krt5</i>	TGAGGAGCTGCAACAGACAG	AGGTTGGCACACTGCTTCTT	135
<i>Krt10</i>	CAGCTGGCCCTGAAACAATC	AGTTGTTGGTACTCGGCGTT	161
<i>Krt14</i>	AGTGAGAAAGTGACCATGCAGA	CTGCCAGGATCTTGCTCTTCAG	196
<i>Ivl</i>	CTCCTGTGAGTTTGTGGTCT	CACACAGTCTTGAGAGGTCCC	105
<i>Lor</i>	TCCCTGGTGCTTCAGGGTAAC	TCTTCCACAACCCACAGGA	93
<i>Gapdh</i>	TGTGTCCGTCGTGGATCTGA	TTGCTGTTGAAGTCGCAGGAG	150
<i>Rn18s (18s)</i>	GTAACCCGTTGAACCCCAT	CCATCCAATCGGTAGTAGCG	151
<i>Acta2</i>	GCTGGACTCTGGAGATGG	GCAGTAGTCACGAAGGAATAG	156
Rat			
<i>Panx2</i>	ACCAAAGATGCTCCGCTCC	GGGTGAGCACACATGGAATG	90
<i>Krt10</i>	AGCTGGCCCTGAAACAATC	ATTTGCAGGTTTCCAACATACCC	250
<i>Krt14</i>	CGTCAGTTCACCTCCTCCAGC	GAAACGAGACATGCCCCCGTA	129
<i>Ivl</i>	AGTGCCAGTGACTGTTCCAG	ATCTTTCACGGGGTTTGCT	184
<i>Lor</i>	CCCAGTGTCTCTCACATCACC	TAAGGAGAAGGGGAACCCCGA	77
<i>Gapdh</i>	GGCATTGCTCTCAATGACAA	TGTGAGGGGAGATGCTCAGTG	223

2.2.9 UVB irradiation for induction of apoptosis

48 h post-transfection REK-PANX2KO cells cultured in 60-mm plates were washed once with sterile D-PBS (without Ca²⁺ or Mg²⁺) (Gibco REF#14190-250). Cell monolayers kept in pre-warmed D-PBS were placed 16 cm below a UVM-26 EL series, 8-watts lamp (UVP, Upland, CA) and immediately subjected to lethal UVB treatment (302 nm, 1500 J/m²) or mock-irradiated. A UVB-dosimeter was used to control the irradiance intensity. Then, culture media was immediately replaced, and cells were kept in the incubator until being harvested for protein lysates or cultured in the Incucyte® Live-cell Imaging System for continuous cell death monitoring.

2.2.10 Live-cell imaging of UVB-induced caspase-3 activation and cytotoxicity

Five thousand cells/well were seeded in a flat-bottom 96-well culture plate (SARSTEDT REF#83.3924, Nümbrecht, Germany) with MEM (Gibco Cat# 11095-080, Grand Island, NY, USA) culture media supplemented with 10% FBS and 1% P/S antibiotics. Cells were

allowed to attach to the bottom of the plate for 30 min in the incubator before being monitored. After UVB treatment, pre-warmed MEM culture media was added supplemented with IncuCyte® Caspase-3/7 Green Apoptosis Reagent (Sartorius, Cat# 4440, USA) at 1/1000 dilution and Cytotox Red Reagent (Sartorius, Cat# 4632, USA) at 250 nM final concentration. Live-cell images were acquired with a 10x objective every two hours for 50h, with phase, green, and red channels using an IncuCyte® S3 Live-Cell Analysis System (Essen BioScience, Ann Arbor, MI, USA). Acquired data was analyzed using the Cell-by-cell Analysis Module in the IncuCyte® 2020A Software package (Essen BioScience Inc., USA).

2.2.11 IncuCyte data analysis and time to apoptosis calculation

The fold change (from phase or fluorescence data) over time was calculated by dividing the object counts (determined by Cell-by-cell Analysis) of any given time point by the counts acquired at the beginning of the experiment (i.e., 0 h). To account for transfection efficiency, the fold change was divided by a normalization factor (Nf) calculated as per equation 1:

$$Nf = 1 + TE \quad (1),$$

Where TE corresponds to the transfection efficiency and non-transfected cells were arbitrarily set as TE=0 (e.g., Nf=1 if cells are untransfected). TE was estimated by the percentage of cells positive for PANX2(FLAG) immunofluorescence (IF) grown in coverslips and fixed at the start of apoptosis experiments. Counts were done by automatic quantification using Cell Profiler Software (ver 4.0.7, Broad Institute, USA) [22] (Lamprecht et al., 2007) using at least fifty non-overlapping IF images per field. In this case, IF images were acquired with a Ni-E Fluorescence Microscope (Nikon, Japan) using an S Plan Fluor ELWD 20x Ph1 ADM 0.45 N/A objective. Normalized data are shown in time-course graphs after adjusting the range of values from 0 % (first measurement) to 100% (last acquired value) using GraphPad Prism software (version 8.0). For the estimation of the time to apoptosis, normalized data were fitted to an allosteric sigmoidal function (equation 2):

$$\%Cact = \frac{C_{max} \times t^a}{t_{50\%}^a + t^a} \quad (2),$$

where $\%Cact$ corresponds with the percent of caspase activation ($Cact$) at any given time (t); C_{max} is the caspase activation when $\sim 100\%$ of the cells are apoptotic and Caspase-3/7 signal is saturated, $t_{50\%}$ is the time to reach half-maximal caspase activation ($\sim 50\%$ of cells are apoptotic), and a is the slope factor in the curve. Only accurate curve fitting was used for the estimations considered when the goodness of fit (R^2) ≥ 0.95 .

2.2.12 Statistical analysis

Unless otherwise indicated, all data are presented as the mean \pm standard error mean (s.e.m) and represent at least three independent biological replicates or experiments ($N=3$) conducted with at least two technical replicates ($n=2$). Statistical analyses are indicated in the figure captions and were performed using GraphPad Prism software (version 8.0) (La Jolla, CA, USA).

2.3 Results

2.3.1 Two PANX2 splice variants are expressed in the mouse dorsal skin

Due to the previous role of PANX1 and PANX3 in regulating cellular processes in the skin (e.g., keratinocyte differentiation and wound healing) and the earlier detection of PANX2 in the skin [3], we sought to characterize PANX2 expression in mouse skin. Earlier, we reported [23] another splice variant (termed as *Panx2-202*, as mRNA transcript, PANX2-202, as protein variant) that is predicted for the mouse *Panx2* gene (Fig. 2-1A, Table 2-2) and appears in the mouse genome annotation by Ensembl (release 103). PANX2-202 differs in length from the canonical PANX2, encoding a 26 amino acid (aa) shorter protein of an estimated molecular weight (MW) of ~ 71.7 kDa.

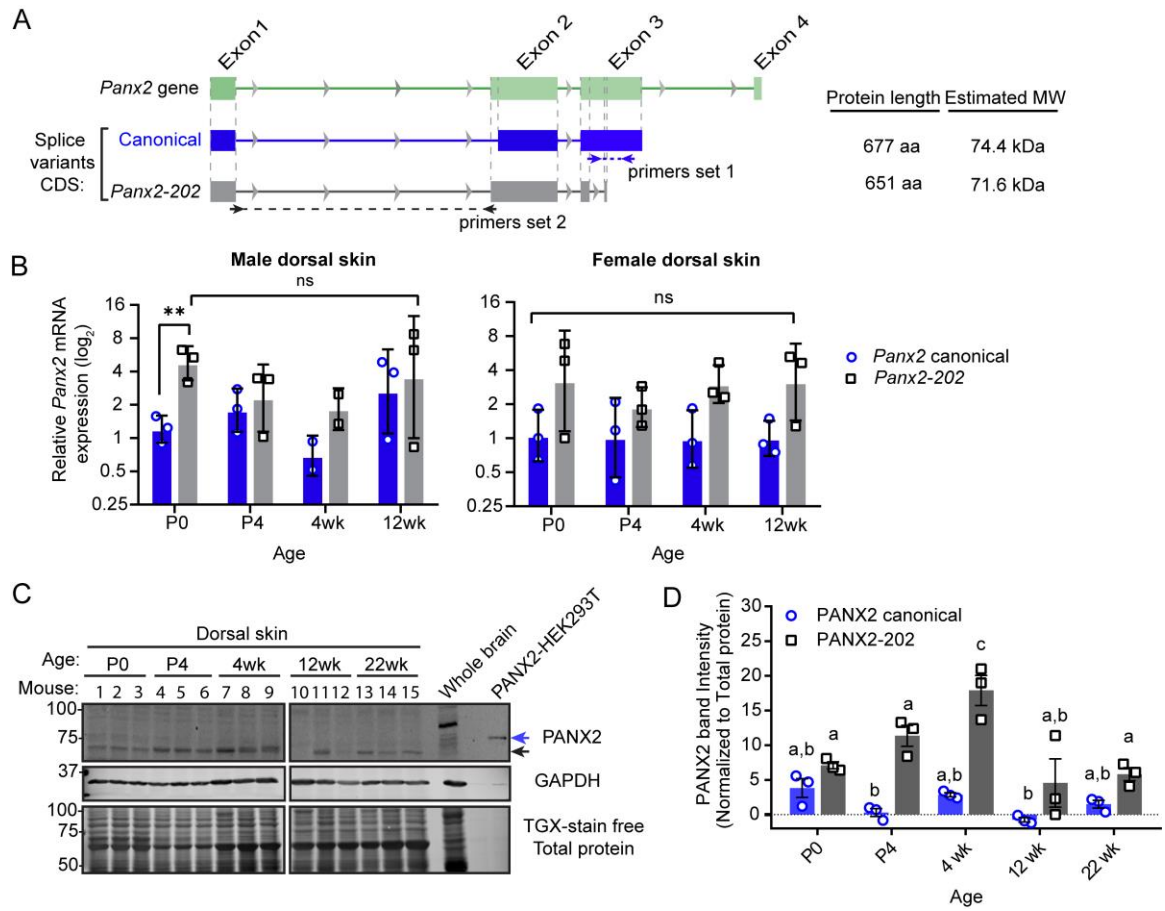
Figure 2-1.

Figure 2-1 Transcript and protein levels of PANX2 variants are differentially regulated in mouse dorsal skin.

(A) Diagram representing the *Panx2* gene coding exons in green as per Ensembl (release 103) annotation. Straight lines with grey arrowheads represent the intronic regions of the sequence. Underneath, blue and grey rectangles depict the coding sequence (CDS) of splice variants vertically aligned with the gene representation at the top. Regions amplified by qPCR primers are shown as dashed lines. Differences in protein length and molecular weight (MW) are shown on the right (B) mRNA expression of each *Panx2* splice variant in male and female dorsal skin. *Gapdh* was used as the reference gene for normalization. Bars are the geometric mean expression (geomean) \pm s.d. (C) Western blots showing the canonical PANX2 (~75 kDa, blue arrowhead) was lower in the skin than the PANX2-202 splice variant (~70 kDa, black arrowhead). Migration of skin PANX2 protein bands differed from an intense band found in mouse whole brain (4-week-old) (apparent MW of ~89 kDa). Mouse canonical PANX2 was overexpressed in HEK293T cells as control (PANX2-HEK293T lane). (D) Densitometric analysis of WB showed a more abundant PANX2-202 transiently increased in four-week-old mice skin but restored at previous levels at 12 weeks. Two-way ANOVAs and Tukey posthoc tests were used for multiple comparisons. Same letter indicates no statistical difference among groups. Significance was considered when $p < 0.05$.

Table 2-2 Pannexin 2 orthologs information in genomic and protein databases as of April 2021.

Species	Ensembl Transcript ID	NCBI RefSeq Protein ID	Uniprot ID	Isoform	Length (aa)	MW (kDa)
<i>Homo sapiens</i>	ENST00000395842.3	NP_443071.2	Q96RD6-3	Canonical	677	74.45
	ENST00000159647.9	NP_001153772.1	Q96RD6-1	Isoform-1	643	70.64
<i>Rattus norvegicus</i>	-	NP_955441.2	P60571-1	Canonical	674	74.43
	ENSRNOT0000089707.1	-	R9PXY9	Predicted Isoform	634	70.25
<i>Mus musculus</i>	ENSMUST0000162424.2	NP_001002005.2	Q6IMP4-1	Canonical	677	74.61
	ENSMUST0000161372.2	-	Q6IMP4-2	PANX2-202	651	71.69

According to computational annotations, the mouse PANX2-202 (Uniprot identifier: Q6IMP4-2) differs from the canonical PANX2 protein sequence in the insertion of eight amino acids after position 75 (insertion sequence: "ARVSSLPS") located in the first extracellular loop domain and the replacement of the distal end of the C-terminal region (from 632-677) with the "SSSPPSRSREQL" amino acid sequence (Fig. S2-1, S2-2B). Based on these differences, we designed specific qPCR primers (Fig. 2-1A) to accurately detect the expression of both isoforms in mouse dorsal skin. We used real-time qPCR to detect transcripts of both *Panx2* splice variants in the skin at all ages investigated (postnatal day (P) 0, 4 and 4-, 12-weeks-old skin). We found no significant differences in mRNA expression levels among *Panx2* transcripts at each age investigated when comparing male and female mice (Fig. 2-1B). Interestingly, *Panx2-202* mRNA was significantly increased only at P0 compared to the canonical variant in male mice, and a similar trend ($p > 0.05$) was observed in female skin, but this difference was not sustained in later ages (P4-12 weeks).

At the protein level (Fig. 2-1C), using our rabbit anti-PANX2-CT polyclonal antibody [20, 24], we detected multiple immunoreactive bands with one distinctively at the expected molecular size of the smaller PANX2-202 (~70 kDa) variant. This isoform trended more abundant than the canonical PANX2 (expected at ~75 kDa, appearing as a faint band) and was continuously detected at all ages investigated. Notably, in 4-week-old skin, PANX2-202 was transiently increased ($p < 0.05$) compared to other ages (Fig 2-1C, D). In addition, immunoblot band profile analysis in 4-week-old whole brain lysates showed that the endogenous PANX2 exhibits an immunoreactive band with a higher apparent molecular weight ($\sim 85.7 \pm 2.3$ kDa) and other multiple bands of lower intensity detected at $\sim 75.1 \pm 2.1$ kDa (Fig. 2-1C, whole-brain lane)

2.3.2 PANX2 expression is abundant in the epidermis and is likely regulated during the early stages of keratinocyte differentiation

Previously, it has been shown that PANX1 and PANX3 are expressed in the murine epidermis and other skin adnexal structures of the skin [25]. Therefore, we sought to localize PANX2 in the skin of C57BL/6N mice using immunofluorescence staining of skin

sections collected at P0, P4, and four weeks of age. We used three different rabbit polyclonal anti-PANX2 antibodies raised against the intracellular loop (IL-), carboxyl (CT-) or amino (NT) terminal domains (Fig. 2-2, Fig. S2-2) of PANX2 [20, 21]. All the antibodies exhibited abundant intracellular and diffused staining in cells from the suprabasal layers of the skin (*stratum spinosum*, *granulosum*, and the cornified layer), suggesting that PANX2 is primarily present in differentiating epidermal keratinocytes (Fig. 2-2) in the skin at P0, P4, and up to 4 weeks of age. In addition, we found staining in the cornified layer that may represent nonspecific immunostaining or remnants of PANX2 in that epidermal layer. Besides, a diffused PANX2 staining was also detected in the outer root sheaths of hair follicles and other regions of the dermis (Fig. S2-2A).

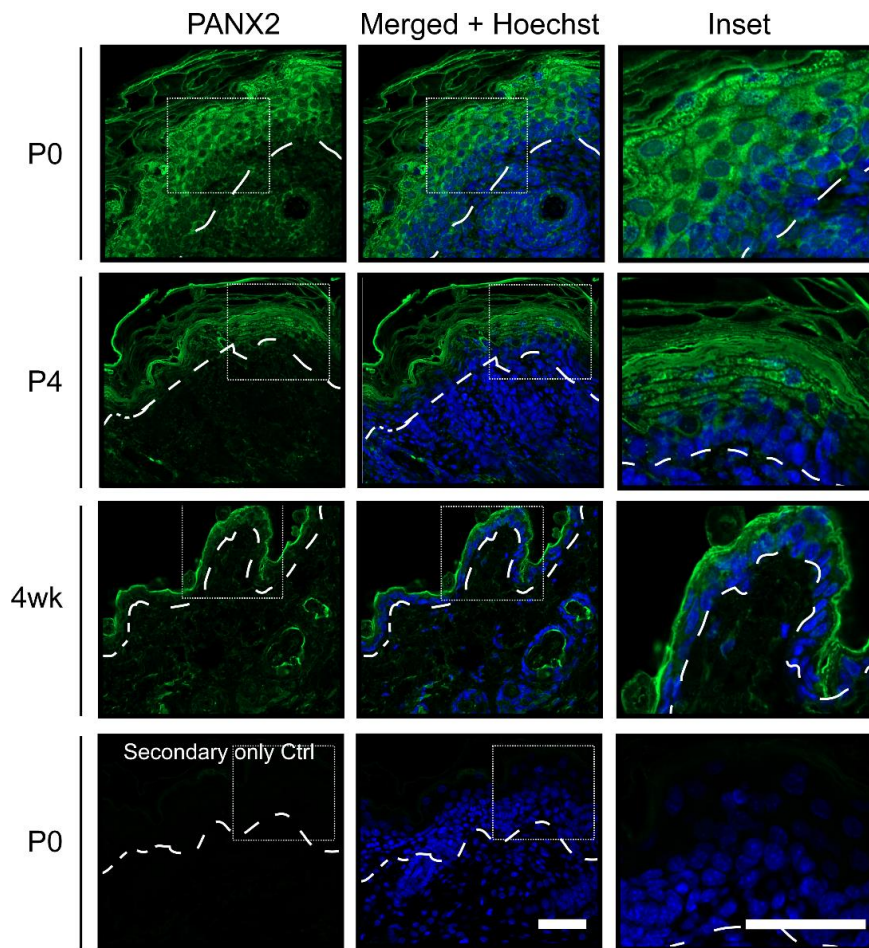
Figure 2-2.

Figure 2-2 . Pannexin 2 is abundant in the suprabasal layers of the epidermis of mouse dorsal skin.

(A) Representative immunofluorescence micrographs of endogenous PANX2 protein immunostaining (green) in formalin-fixed sections (N=3) of dorsal skin at postnatal days (P) 0, 4, and 4 weeks old. Intense intracellular PANX2 staining with anti-PANX2-CT polyclonal antibody is visualized in cells of the suprabasal layers of the skin. As a control for antibody specificity, sections were stained with the secondary antibody without the primary antibody (Secondary only Ctrl). Nuclei stained with Hoechst 33342 are shown in blue), and dashed lines denote the basal membrane dividing the epidermal and dermal layers. Scale bar = 100 μ m.

To further confirm and characterize PANX2 expression in the skin cells, we isolated primary keratinocytes and dermal mouse fibroblasts from skin at P4. Western blots with the PANX2-CT rabbit antibody confirmed the presence of the PANX2-202 protein band in both cell types corresponding with the estimated MW (~70 kDa) (Fig. 2-3A, B). This was consistent with the staining observed in the dermis and epidermis and suggested that PANX2 may not be limited to a single layer of the skin. Since we detected PANX2-202 protein in primary dermal fibroblasts, *in vitro* experiments were performed to test for changes in *Panx2* mRNA expression upon TGF- β induction of fibroblast activation into myofibroblasts. We found that mRNA levels of the canonical variant remained unchanged, but *Panx2-202* mRNA was significantly downregulated after TGF- β treatment (Fig. S2-3).

On the other hand, as the PANX2 staining was more prevalent in the suprabasal layers of the epidermis, we sought to verify whether PANX2 levels were regulated by early differentiation in keratinocytes. In the epidermis, keratinocytes detach from the basement membrane and occupy the suprabasal layers to undergo terminal differentiation ending in cornification, a specialized cell death process different from apoptosis [26]. Thus, we tested a commonly used model of *in vitro* differentiation based on the culturing of primary keratinocytes with increased levels of CaCl_2 [27]. However, the increased Ca^{2+} concentration in the culture medium did not markedly alter the protein levels of PANX2-202 (Fig. 2-3C, D) nor the expression of both *Panx2* mRNA splice variants. Nevertheless, there was a significant increase in expression of suprabasal/differentiation markers keratin 10 (*Krt10*) and loricrin (*Lor*), indicating early stages of keratinocyte differentiation (Fig. 2-3E).

As *in vitro* differentiation of primary mouse keratinocytes is limited by the finite life span of these primary cells, we also employed an immortalized rat epidermal keratinocyte (REK) cell line [17] to examine changes in the mRNA expression of the rat *Panx2* canonical ortholog during *in vitro* differentiation. These cells can be grown in traditional media and maintained in culture for long periods while spontaneously initiating differentiation upon reaching confluence when overgrown as cell monolayers [18]. Therefore, we assayed three conditions: (i) non-confluent, to resemble a basal-like state,

and 72h-cultured confluent monolayers in the presence (ii) or absence (iii) of CaCl₂ as differentiated stages. We observed that the endogenous rat *Panx2* transcript was 3.4-fold significantly upregulated (p<0.01) after confluency and with a similar effect (1.6-fold, p<0.05) after CaCl₂ supplementation compared to the non-confluent cells (Fig. 3F). While we observed drastic morphologic changes (i.e., cuboidal shape) of the cells under differentiation conditions (not shown), no changes were detected in the transcript expression of the basal marker keratin 14 (*Krt14*). Remarkably, in both confluent and +CaCl₂ conditions, we found a significant (p<0.05) increase (189.6- and 194.4-fold, respectively) in transcripts of the rat keratin 10 (*Krt10*), an early differentiation/suprabasal marker. In addition, the late differentiation marker, loricrin (*Lor*), exhibited a 5.3-fold significant (p<0.05) upregulation whereas, unexpectedly, involucrin (*Ivl*) was 3.9-fold downregulated (p<0.05) in confluent versus non-confluent REK cells. Overall, confluency and calcium supplementation stimulated REK differentiation and increased canonical *Panx2* mRNA expression in these cells.

Figure 2-3.

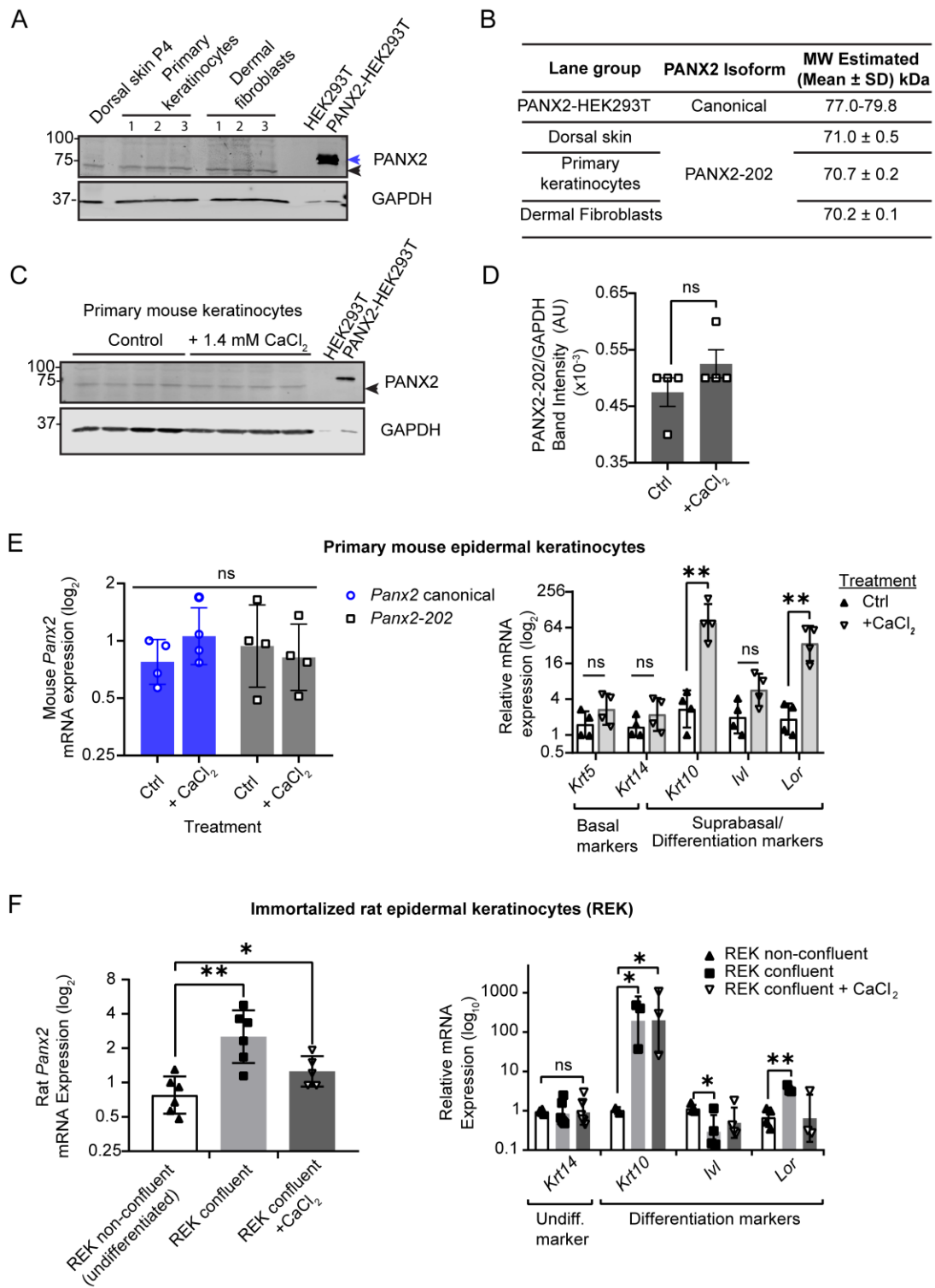


Figure 2-3 PANX2 levels are regulated in keratinocytes during *in vitro* CaCl₂-induced differentiation.

(A, B) Immunoblot used for MW estimation of PANX2 variants detected in primary mouse keratinocytes and dermal fibroblasts. Numbers indicate different mice. (C-E) Analysis of endogenous PANX2 protein and mRNA expression of *in vitro* CaCl₂- differentiation experiments with primary mouse keratinocytes. Four independent primary cell isolations (N=4) were used for the assays. Relative mRNA expression is shown as geometric mean \pm s.d. *Gapdh* was used as the reference gene. Unpaired t-test was used for statistical analysis of densitometric results in (D). ANOVA followed by a Sidak's test were used for multiple comparisons of the log₂ (mRNA expression). (F) mRNA expression analysis of *Panx2* rat paralog in rat epidermal keratinocytes (REK) cell line in different conditions. One-way ANOVA followed by a Tukey's test were used for multiple comparisons. Keratinocyte differentiation was assessed by mRNA expression of cytokeratins *Krt5*, *Krt14* for undifferentiated cells; *Krt10*, involucrin (*Ivl*), and loricrin (*Lor*) for late differentiation markers in mouse and rat cells. Unpaired t-tests were used for comparisons between treatments. Symbols represent different samples or independent experiments with at least N=3. Statistical significance was considered when *p<0.05, **: p<0.01.

2.3.3 *In vitro* caspase-3 cleavage of canonical PANX2 C-terminus occurs at D400 and D416

Considering our previous report [21] on the canonical PANX2 *in vitro* cleavage by executioner caspases-3/7, we sought to identify the specific sites for caspase-mediated cleavage. Using the webserver Procleave [19], we obtained a list of putative cleavage sites for caspase-3 (Figure 2-4A; Table 2-3). The most likely sites for cleavage were predicted to be located in the canonical PANX2 C-terminal domain and based on the size of the predicted fragment reported previously [21], we selected D400 and D416 for site-directed mutagenesis to replace the aspartic residues for alanine (D→A) and generate putative caspase-3/7 cleavage-resistant PANX2 mutants (PANX2^{D400A}, PANX2^{D416A}, and PANX2^{D400A/D416A}) for validation purposes.

Table 2-3 Predicted Caspase 3/7 cleavage sites in mouse PANX2 according to Procleave.

<i>Rank</i>	<i>Amino acid position</i>	<i>P4-P4' context</i>	<i>N-terminal fragment size (kDa)</i>	<i>C-terminal fragment size (kDa)</i>	<i>Prediction score</i>	<i>Domain</i>
1	416	AEPD†GSAE	47.1	27.5	0.965	C-terminus
2	266	ASPD†GPVG	30.1	44.5	0.925	Extracellular loop
3	650	DMGD†LLSI	71.6	3.0	0.727	C-terminus
4	400	TVRD†SGIQ	45.5	29.1	0.707	C-terminus

†, cleavage site.

Similar to the methodology used before in [21], we performed *in vitro* incubation of immunoprecipitated PANX2 with purified active caspase-3 (see Fig. 2-4B, C) to detect the remaining N-terminal PANX2 fragments after cleavage. In these experiments, caspase-3 cleavage of PANX2 resulted in the loss of immunoreactivity of the band corresponding to the full-length protein (~75 kDa) (Fig. 2-4D, E). Three major N-terminal PANX2 fragments were identified by western blot with apparent MW of 48, 46, and 30 kDa, respectively, as determined by analysis of the lane profiles (Fig. 2-4E, Fig. S2-4A). For all the caspase-3 treated groups (canonical PANX2 wildtype and mutants), a common ~30

kDa protein band was detected, corresponding with a putative cleavage product if PANX2 caspase-cleavage were to occur at D266 (Fig. 2-4A, C, E, and Fig. S2-4B-E). In contrast, caspase-3 cleaved mutants PANX2^{D400A} and PANX2^{D416A} showed the absence of the bands corresponding to each expected N-terminal cleavage product of ~46 and ~48 kDa, respectively (Fig. 2-4E, Fig. S2-4 C-D, F-H). Notably, in the caspase-3 treated (+) lane, the band corresponding to full-length protein is retained for PANX2^{D416A} although at a lower intensity, suggesting partial or reduced cleavage efficiency at the amino acid site D400 compared to the D416, which was not evident in the PANX2^{D400A} mutant. As an experimental control, the specificity of the anti-PANX2-NT antibody was verified using IgG as a control for the immunoprecipitation, which yielded no background bands in the immunoblots (Fig. 2-4F).

Figure 2-4.

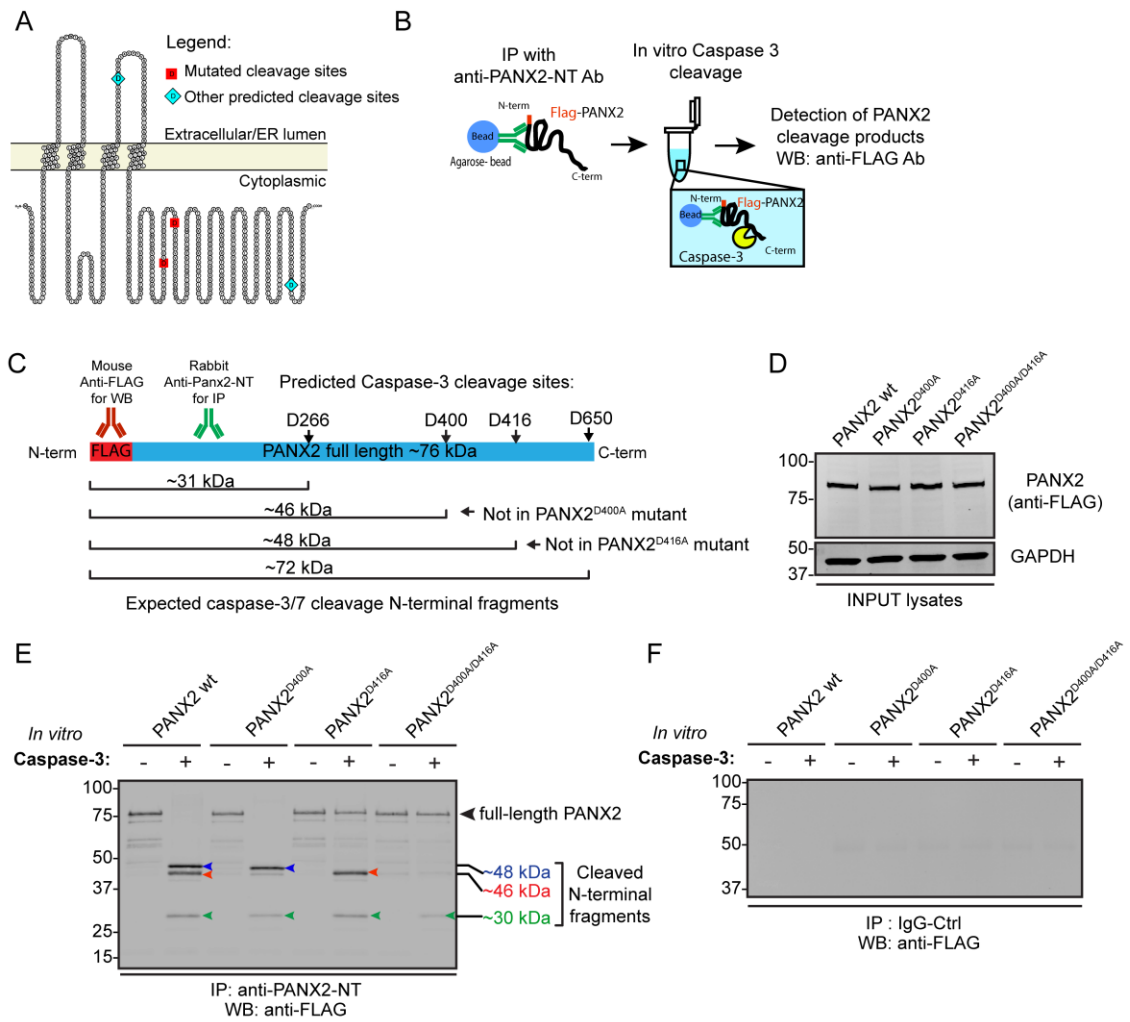


Figure 2-4 Canonical mouse PANX2 C-terminus is cleaved by caspase-3 *in vitro* at D400 and D416.

(A) Diagram of the secondary structure of mouse PANX2 showing the putative caspases cleavage sites (D266, 400, 416, and 650). D400 and D416 were selected for site-directed mutagenesis based on their CT-terminal localization and detectable cleavage products by WB. (B, C) Illustrations depicting expected N-terminal cleavage fragments and the methodology used for immunoprecipitation (IP) and detection of the fragments after incubation of PANX2 with purified caspase-3. (D) Immunoblot used as INPUT for IP of protein lysates from overexpressed N-terminal FLAG-tagged PANX2 and caspase-resistant mutants in HEK293T cells. (E) Immunoblot showing IP of full-length PANX2 incubated (+) or not (-) with purified active caspase-3. Protease digestion products were separated simultaneously in the same 10% SDS-PAGE gel and blotted with an anti-FLAG antibody to reveal the N-terminal fragments. Dim bands in the non-caspase treated lanes were considered unrelated degradation products. (F) Immunoblot of controls using IgG for IP. As expected, no background bands confirmed the specificity of anti-PANX2-NT antibody. Estimation of MW of fragments performed using densitometric analyses (see Fig. S2-4). Results are representative of four independent experiments (N=4).

2.3.4 PANX2 C-terminus undergoes cleavage at D416 in UVB-induced apoptotic keratinocytes

We explored whether caspase cleavage of PANX2 occurs in keratinocytes undergoing apoptosis after UVB exposure. For these studies, we overexpressed the mouse canonical PANX2 construct in REK cells. However, to avoid confounding factors derived from the endogenous rat *Panx2* ortholog expression in these cells, we first generated a CRISPR-Cas9-mediated *Panx2* knockout cell line (REK-PANX2KO). Genotyping and WB confirmed the success of *Panx2* knockout in one of the selected clones (clone 19), indicating a 212 bp deletion that encompasses the 1st intron and the 2nd exon of the rat *Panx2* gene verified by sanger sequencing (not shown) (Fig. 2-5A, B). In wildtype REK cells, endogenous PANX2 appeared as a faint band (~70 kDa) detected with two commercially available anti-rat PANX2 antibodies that were previously validated in [3, 9, 28] (Fig. 2-5B).

We hypothesized that the activation of effector caspases-3/7 in UVB-irradiated REK cells induces the cleavage of the PANX2 C-terminus and is likely to promote the programmed cell death process in the cells. Forty-eight hours post-transfection, REK-PANX2KO cells transiently expressing either mouse canonical PANX2 wildtype (wt), PANX2^{D400A}, PANX2^{D416A}, or PANX2^{D400A/D416A} were exposed to UVB radiation. Full-length PANX2 protein and N-terminal fragments were then IP using the anti-PANX2-NT antibody. Western blot analysis showed cleaved fragments only in PANX2 wt and PANX2^{D400A}-transfected REK-PANX2KO cells, indicating that cleavage of PANX2 in these apoptotic cells occurs only at the C-terminal D416 residue (Fig. 2-5D, Fig. S2-5). Moreover, as expected, ~30 kDa fragments were not observed with any of the constructs, indicating that executioner caspases cannot target the residue D266 in the second extracellular loop of PANX2. Moreover, cleaved-caspase-3 was detected only in the post-UVB input lysates, indicating a successful caspase activation and apoptosis after UV irradiation (Fig. 2-5E). Taken together, our results revealed that, in UVB-induced apoptotic keratinocytes, PANX2 C-terminus undergoes caspase-3/7 cleavage at residue D416.

Figure 2-5.

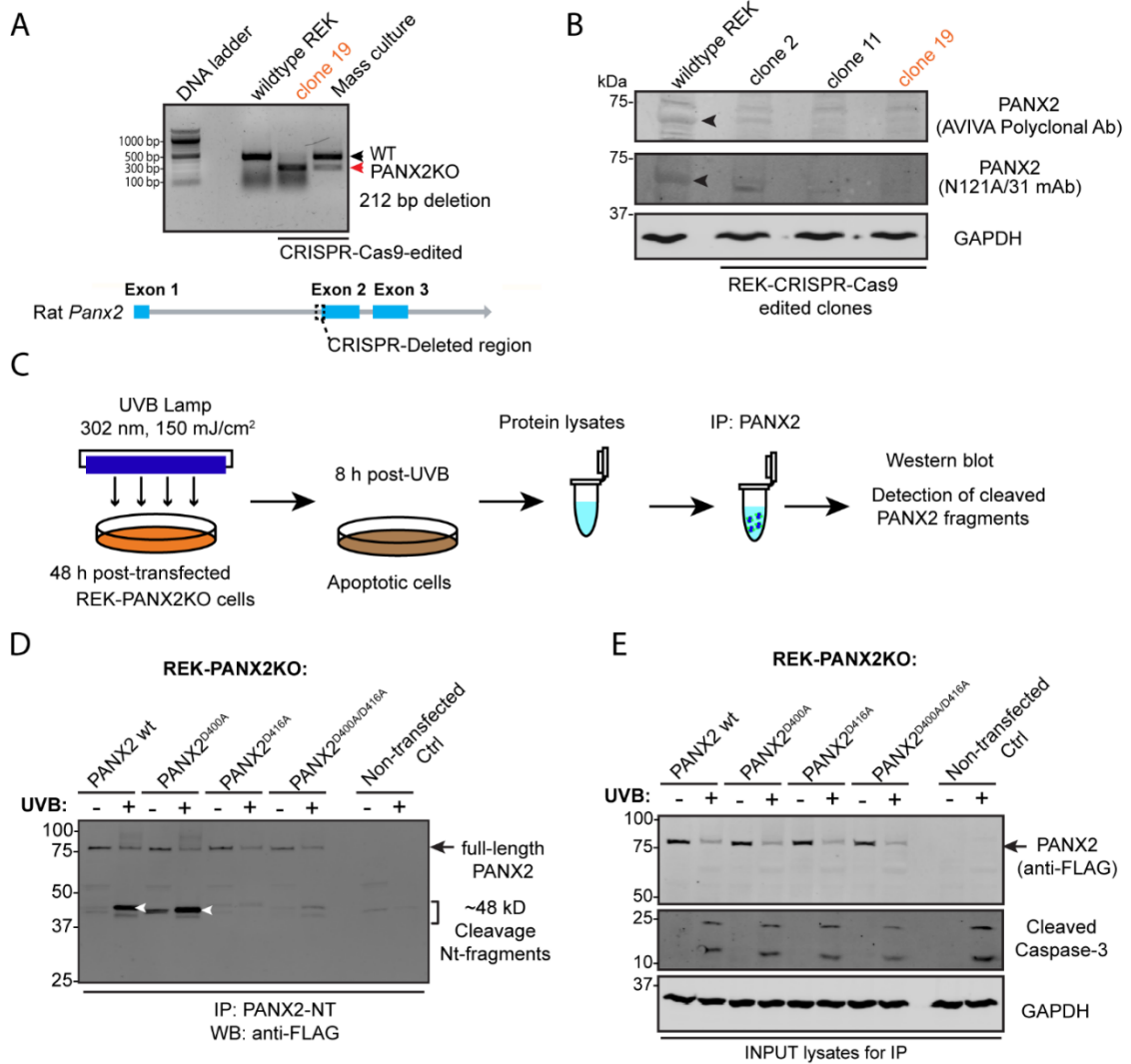


Figure 2-5 PANX2 C-terminus is cleaved at D416 during UVB-induced apoptosis of REK cells.

(A) Genotyping of rat *Panx2* CRISPR-Cas9 knockout REK cells (REK-PANX2KO). PCR of CRISPR-Cas9-targeted region amplified a band with faster migration than WT (red arrow). Sanger sequencing indicated a 212 bp deletion encompassing the 1st intron and the 2nd exon of the rat *Panx2* gene. (B) Immunoblot showing the success of PANX2 knockout in selected REK-CRISPR-Cas9-edited clones. Endogenous rat PANX2 appears as a ~70 kDa faint band (indicated by arrowhead) no longer visible in the CRISPR-edited REK-PANX2KO cells. (C) Methodology to detect PANX2 cleaved fragments. (D) Immunoblot after IP showing cleavage of canonical PANX2 wildtype (wt) and the mutant PANX2^{D400A} but no PANX2^{D416A} or PANX2^{D400A/D416A} mutant after UVB-irradiation. Non-transfected control (Ctrl) lanes indicate nonspecific bands unrelated to PANX2 cleavage. (E) Immunoblot of input lysates showing (cleaved) caspase3 activation and decreased immunodetection of full-length PANX2 post-UVB irradiation. Results are representative of three independent experiments (N=3).

2.3.5 PANX2 contributes to UVB-induced apoptosis of REK cells independently of its caspase cleavage

PANX2 has been implicated in different cell death processes [10, 12-15], from which it seems that any functions during cell death may be dependent on the cell type in question. Based on earlier studies with PANX1 in apoptotic cells [29], it has been proposed that the irreversible caspase-cleavage of PANX1 channels may be detrimental for the cells due to an increased plasma membrane permeability and the repercussion of C-terminal truncation on channel properties and cell death [30, 31]. To assess whether the PANX2 cleavage contributes to apoptosis in REK cells, we evaluated the effect of genetic deletion of endogenous *rat Panx2*, the rescue with the transient expression of the mouse canonical ortholog (PANX2 wt, 98.2 % amino acid sequence identity compared with rat PANX2) and the caspase-cleavage resistant mouse PANX2^{D416A} mutant after UVB exposure (Fig. 6). We used a green fluorescent DEVD-peptide substrate of caspase-3/7 dye multiplexed with a cell-membrane impermeable cyanine dye (Cytotox Red) to monitor UVB-induced caspase-3/7 activation and cytotoxicity concurrently in an IncuCyte live-cell imager.

Our results showed that from 20-48h post-UVB-irradiation, apoptotic caspases were activated in 100% of the cells (Inset in Fig. 2-6A). As a quantitative measure for comparing the timing for apoptotic activation between experimental groups, we estimated a parameter (defined herein as $t_{50\%}$, dashed lines in Fig. 2-6A) for the length of time post-UVB required to detect caspase-3/7 activation in ~50 % of the cell population. Thus, a delayed caspase activation would correspond with increased values of $t_{50\%}$. Notably, our analysis showed most groups had significant differences among $t_{50\%}$ ($F_{3, 32} = 38.68$, $p < 0.0001$), where REK-PANX2KO cells had a significant delay ($t_{50\%} = 8.7 \pm 0.8$ h, $p < 0.0001$) in caspase activation compared to wildtype REK cells ($t_{50\%} = 5.9 \pm 0.6$ h) (Fig. 2-6B). Compared to non-transfected REK-PANX2KO, overexpression of mouse PANX2 wt and PANX2^{D416A} caspase-resistant mutant elicited a partial rescue increasing the rate of caspase activation ($p < 0.05$) with decreased $t_{50\%}$ of 7.9 ± 0.3 h and 7.3 ± 0.3 h, respectively (not significant, ns); yet both cases had a $t_{50\%}$ significantly greater ($p < 0.0001$) than wildtype REK cells (Fig. 2-6B). These findings indicated that: (i) the genetic deletion of *Panx2* (as in REK-PANX2KO cells) delays caspase-3/7 activation and, consequently, the onset of apoptosis, and (ii)

caspase-cleavage of PANX2 (expected in mouse canonical PANX2 wt) does not affect the timing of executioner caspase activation and thus the apoptosis rate of UVB-irradiated REK cells.

Further analysis showed that at eight hours post-UVB, the % change (compared to 0h) in caspase-3/7 activation ($F_{3, 31} = 40.98$, $p < 0.0001$) was significantly greater ($p < 0.0001$) for wildtype REK ($89.25 \pm 4.76\%$) compared to the rest of REK-PANX2KO groups and regardless of their transfection or not with the mouse *Panx2* orthologs (wt or D416A). Interestingly, after eight hours post-UVB, REK-PANX2KO cells overexpressing the non-cleavable PANX2^{D416A} mutant ($66.52 \pm 4.94\%$) had a significantly higher ($p < 0.05$ and $p < 0.0001$) caspase-3/7 activation than the overexpressing PANX2 wt ($54.99 \pm 8.43\%$) and non-transfected (nt) ($42.08 \pm 14.91\%$) cells, respectively (Fig. 2-6C). To assess the outcome of the caspase-3/7 activation and apoptotic process across all the time points, we compared the differences ($F_{3, 32} = 12.42$, $p < 0.0001$) in the area under the curve (AUC) from the kinetic caspase activation plots and noticed that regardless of PANX2 wt (or PANX2^{D416A}) transfection, REK WT remained significantly higher ($p < 0.05$) compared to REK-PANX2KO cells (Fig. 2-6D). However, no differences in the overall caspase-3/7 activation were found between PANX2^{D416A} and PANX2KO wt-transfected cells, while, remarkably, the non-transfected REK-PANX2KO group exhibited the lowest ($p < 0.05$) caspase activation. In agreement with the above, these results suggested that in UVB-irradiated REK cells, PANX2 promotes the apoptosis rate (based on the caspase-3/7 activation) regardless of its proteolytic cleavage at D416.

As another measure of cell death, we also assessed changes in the membrane integrity that occurred upon UVB exposure indicating cytotoxicity. After UVB-irradiation, a delay in the time of detection in the loss of membrane integrity was found in non-transfected REK-PANX2KO (at ~22-24h) that was approximately three-fold compared to the other groups expressing any PANX2 (~6-8h) (Fig. 2-6E). Overall, the AUC ($F_{3, 29} = 13.91$, $p < 0.0001$) in the plots of % of change in cytotoxicity was markedly lower ($p < 0.05$) in non-transfected REK-PANX2KO compared to the other groups, while the ectopic expression of mouse PANX2 wt (or PANX2^{D416A} mutant) ultimately rescued the pattern observed in the REK

wildtype cells (Fig. 2-6E, F). This finding indicates that PANX2 may play a role in influencing membrane disruption or alteration at the later stages of apoptosis in the UVB-irradiated REK cells. Finally, we conducted immunofluorescence staining and confocal microscopy imaging analysis to rule out any possible effects of the D416A mutation on the subcellular localization of PANX2. The PANX2 wt and PANX2^{D416A} mutant showed a similar intracellular distribution within REK-PANX2KO cells (Fig. 2-6G) along with the occasional cell membrane and perinuclear localization described in our work presented in Chapter 3 [24]. In summary, our results suggest that PANX2 promotes UVB-induced apoptotic cell death of keratinocytes, independent of its caspase cleavage.

Figure 2-6.

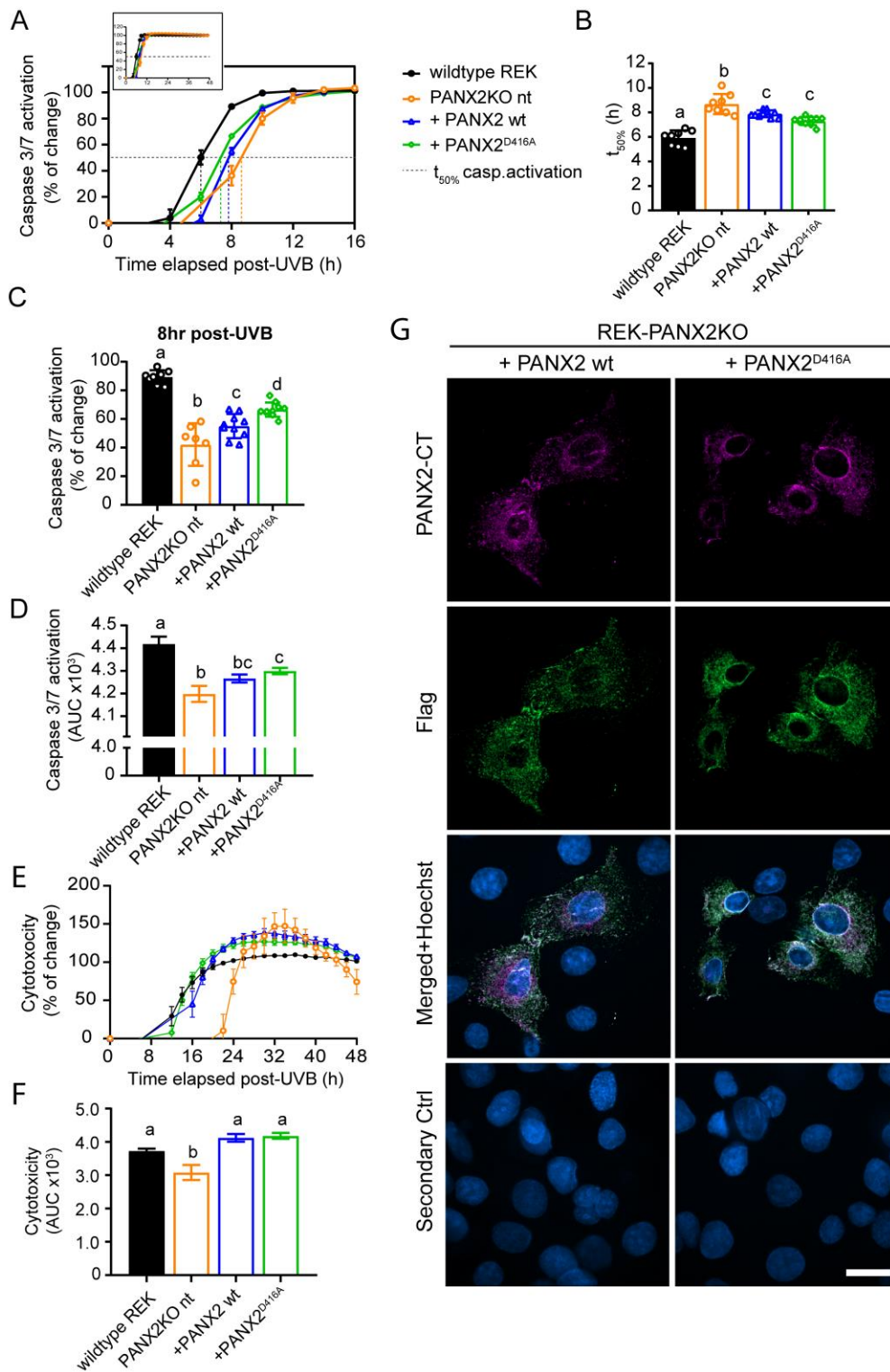


Figure 2-6 PANX2 promotes UVB-induced apoptosis of REK cells independently of its caspase-3/7 cleavage.

(A-C) Time-course, half-maximal caspase activity ($t_{50\%}$), and timepoint analysis of the caspase-3/7 activation. A significant delay in caspase-3/7 activity (increased $t_{50\%}$) was found in REK-PANX2KO compared to wildtype REK cells. Transient expression of canonical PANX2 wt partially (~50%) rescues caspase activation in REK-PANX2KO cells with a modest increase when PANX2^{D416A} mutant is expressed. (D) Overall caspase-3 activation (area under the curve (AUC)) was no different between PANX2^{D416A} and PANX2 wt overexpressed in REK-PANX2KO cells (E). Cytotoxicity time-course revealed a delayed and significantly decreased uptake of Cytotox Red Dye by the REK-PANX2KO cells. Similar cytotoxicity onset was found between wildtype REK and PANX2 wt- and PANX2^{D416A}-expressing REK-PANX2KO cells. (F) Overall cytotoxicity (AUC) in PANX2 wt and the PANX2^{D416A} mutant was similar to that observed in REK wildtype. (G) Representative immunofluorescence confocal micrographs of REK-PANX2KO cells 48h post-transfected with PANX2 wt or PANX2^{D416A} mutant. Similar PANX2 intracellular localization was observed using either the polyclonal PANX2-CT or monoclonal anti-Flag antibodies. Scale bar=20 μm . IncuCyte live-imaging caspase-3/7 activation and cytotoxicity data result from ten technical replicates per group (n=10). One-way ANOVA followed by Tukey's post hoc test was used to compare the means. Same letters denote groups with no difference in statistical significance considered when $p < 0.05$.

Figure S2-1

A

CLUSTAL O(1.2.4) multiple sequence alignment

```

PANX2      MHHLLEQSADMATALLAGEKRELILPGSQDDKAGALAALLLQLKLELPDRVVTIGTVL      60
PANX2-202  MHHLLEQSADMATALLAGEKRELILPGSQDDKAGALAALLLQLKLELPDRVVTIGTVL      60
*****

PANX2      VPILLVTLVFTKNFA-----EPIYCYTPHNFTRDQALYARGYCWTELRDALPGVDA      112
PANX2-202  VPILLVTLVFTKNFAARVSSLPSEPIYCYTPHNFTRDQALYARGYCWTELRDALPGVDA      120
*****

PANX2      SLWPSLFEHKFLPYALLAFAAIMYVPALGWFLASTRLTSELNLLQEIDNCYHRAAEGR      172
PANX2-202  SLWPSLFEHKFLPYALLAFAAIMYVPALGWFLASTRLTSELNLLQEIDNCYHRAAEGR      180
*****

PANX2      APKIEKQIQSKGPGITEREKREIIEAEKEKSPEQNLFEKYLERRGRSNFLAKLYLARHV      232
PANX2-202  APKIEKQIQSKGPGITEREKREIIEAEKEKSPEQNLFEKYLERRGRSNFLAKLYLARHV      240
*****

PANX2      LILLSVVPISYLCTYYATQKQNEFTCALGASPDGPVGSAGPTVRVSCKLPSVQLQRIIA      292
PANX2-202  LILLSVVPISYLCTYYATQKQNEFTCALGASPDGPVGSAGPTVRVSCKLPSVQLQRIIA      300
*****

PANX2      GVDIVLLCFMNL IILVNL IHLFIFRKS NFI FDKLNKVG IKT RRQWRRSQ FCDINILAMFC      352
PANX2-202  GVDIVLLCFMNL IILVNL IHLFIFRKS NFI FDKLNKVG IKT RRQWRRSQ FCDINILAMFC      360
*****

PANX2      NENRDHIKSLNRLDFITNESDLMYDNVVRQLLAALAQSNHDTTPTVRDSGIQTVDP SINP      412
PANX2-202  NENRDHIKSLNRLDFITNESDLMYDNVVRQLLAALAQSNHDTTPTVRDSGIQTVDP SINP      420
*****

PANX2      AEPDGS AEPVVKRPRKMKWIPTS NPLQP PFKEQLAIMRVENSKTEKPKVRRKTATDT      472
PANX2-202  AEPDGS AEPVVKRPRKMKWIPTS NPLQP PFKEQLAIMRVENSKTEKPKVRRKTATDT      480
*****

PANX2      LIAPLLDAGARA AHYKGGSGDSSAPPAASEKKHTRHFLDVHPYILGTKKAKTEAV      532
PANX2-202  LIAPLLDAGARA AHYKGGSGDSSAPPAASEKKHTRHFLDVHPYILGTKKAKTEAV      540
*****

PANX2      PPALPASRSQEGGFLSQTEECGLGLAAAPT KDAPLPEKEIPYPT EPALPGLPSGGSFHVC      592
PANX2-202  PPALPASRSQEGGFLSQTEECGLGLAAAPT KDAPLPEKEIPYPT EPALPGLPSGGSFHVC      600
*****

PANX2      SPPAAPAAASLSPGSLGKADPLTILSRNATHPL LHISTLYEAREEEEEGGPCAPSDMGDLL      652
PANX2-202  SPPAAPAAASLSPGSLGKADPLTILSRNATHPL LHISTLSSSPPSRSREQL-----      651
*****
                .:  ...

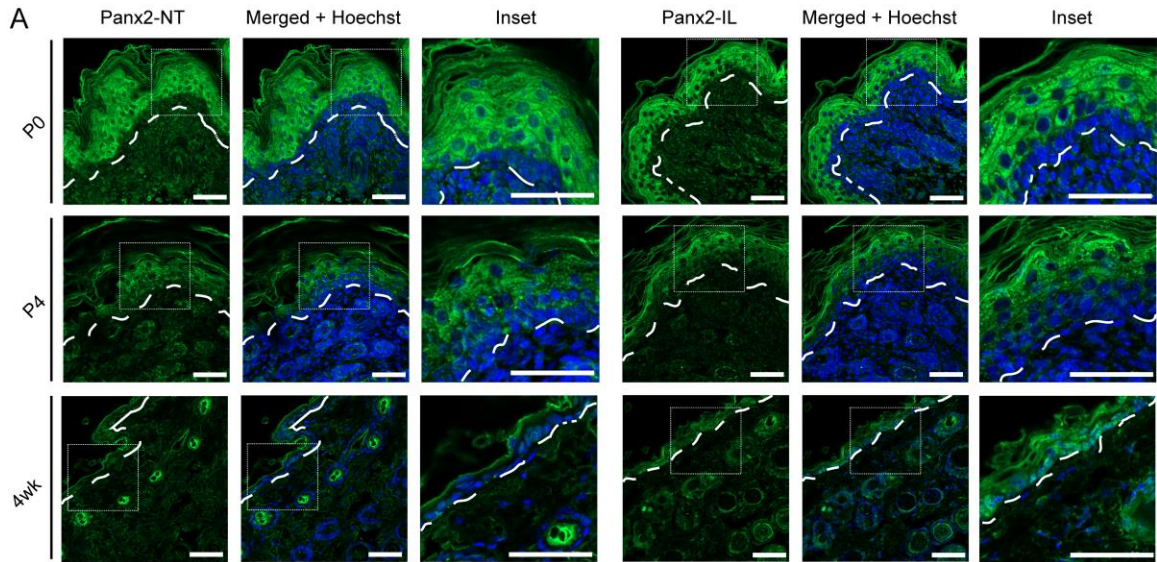
PANX2      SIPPPQQIL IATFEEPRTVVSTVEF      677
PANX2-202  -----      651

```

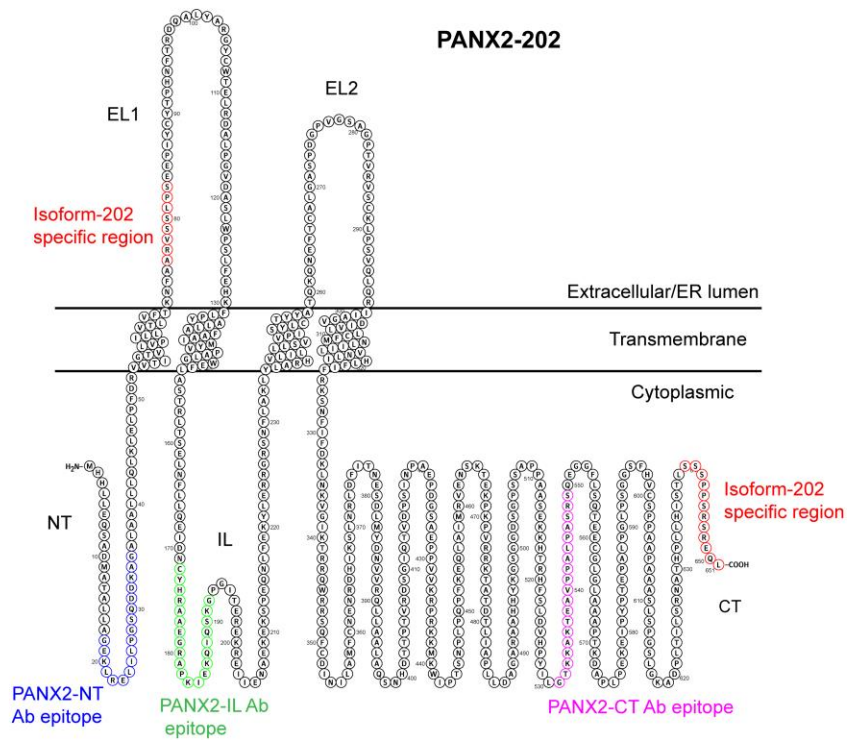
Supplemental Figure 2-1. Sequence alignments between mouse PANX2 (canonical) and PANX2-202 variants.

CLUSTAL O (1.2.4) was used to compare the amino acid sequences of mouse Panx2 variants. An asterisk denotes amino acid conservation; a colon denotes strong conservative substitution; a period denotes a weakly conservative substitution; a space denotes non-conservative substitution with a different amino acid; while a dash represents an insertion or deletion. Sequence regions characteristic of the PANX2-202 are highlighted with red font.

Figure S2-2



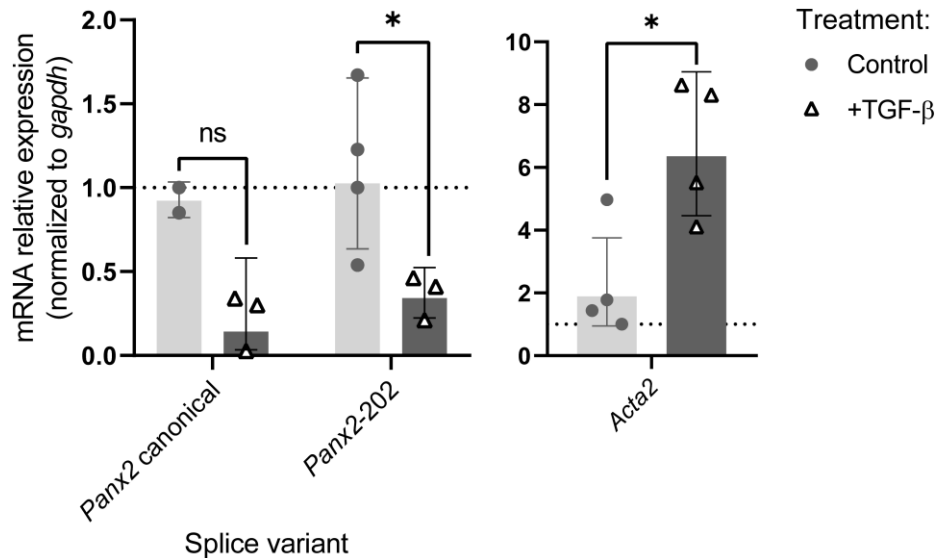
B



Supplemental Figure 2-2. Immunofluorescence labeling of mouse dorsal skin with polyclonal anti-PANX2 antibodies and epitopes mapped in PANX2-202 sequence.

(A) Representative immunofluorescence micrographs of endogenous PANX2 immunostaining (green) in formalin-fixed sections (N=3) of dorsal skin at postnatal days 0, 4, and 4 weeks old. Immunofluorescence using polyclonal antibodies against N-terminal domain (NT) and the intracellular loop (IL) of mouse PANX2. Nuclei were stained with Hoechst 33342 (shown in blue), and dashed lines denote the basal membrane dividing the epidermal and dermal layers. Scale bar = 100 μ m. (B) Topological representation of the PANX2-202 splice variant. In red, residues corresponding to the unique regions of this *Panx2* splice variant. In blue, light green and purple, epitopes recognized by the three rabbit anti-mouse polyclonal antibodies used in this study.

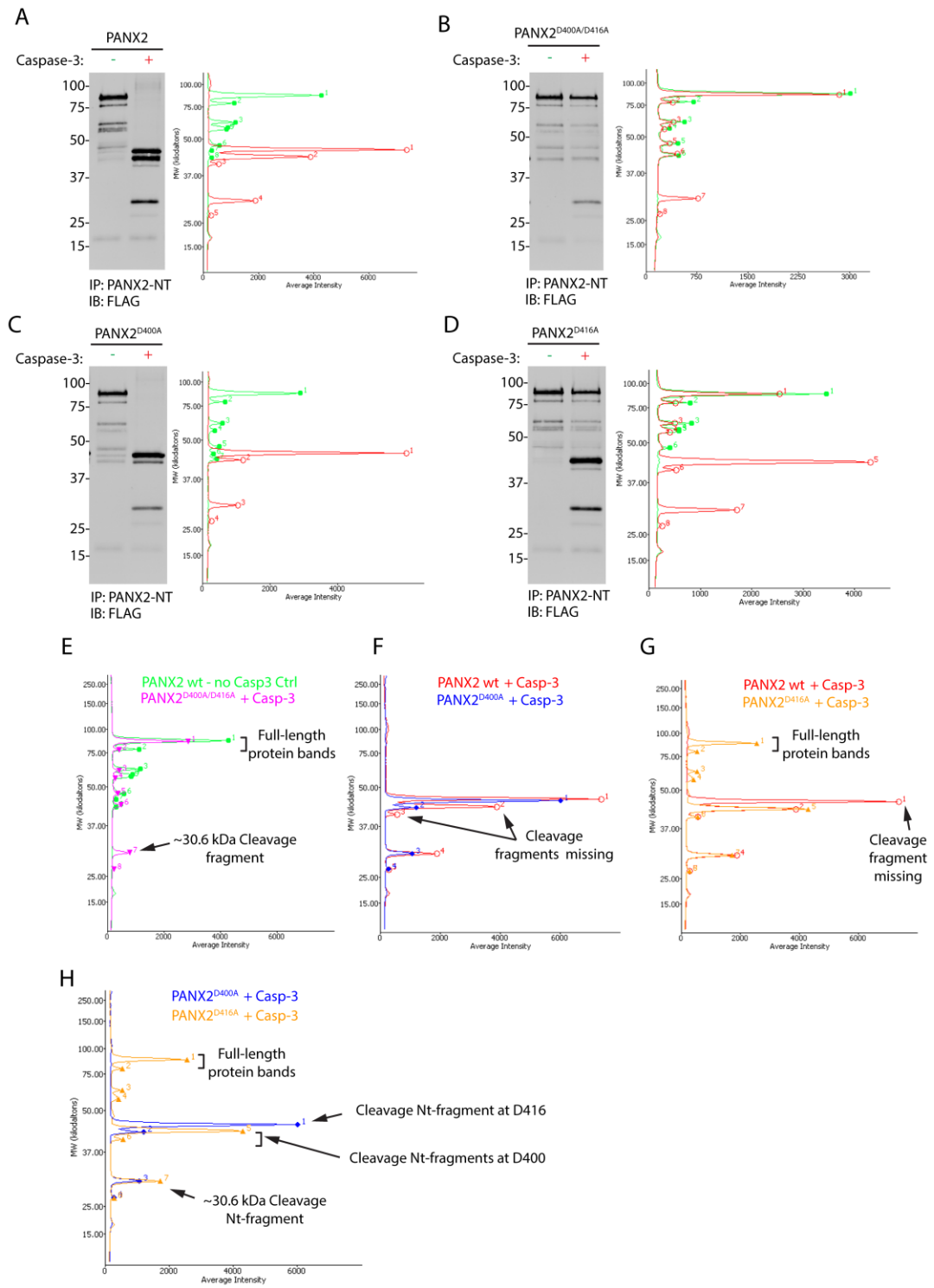
Figure S2-3



Supplemental Figure 2-3. Endogenous *Panx2* mRNA levels in primary dermal mouse fibroblasts decrease after *in vitro* myofibroblast activation with TGF- β .

TGF- β differentiation protocol was performed as reported in [99]. Alpha-smooth muscle actin (α -SMA) (*Acta2* mouse gene) was used as a myofibroblast activation marker. At least N=3 biological replicates were assayed by duplicate. A paired t-test was used to compare the means $\log_2(\text{relative expression})$ among treatments. Statistical significance is shown as $p < 0.05$ (*).

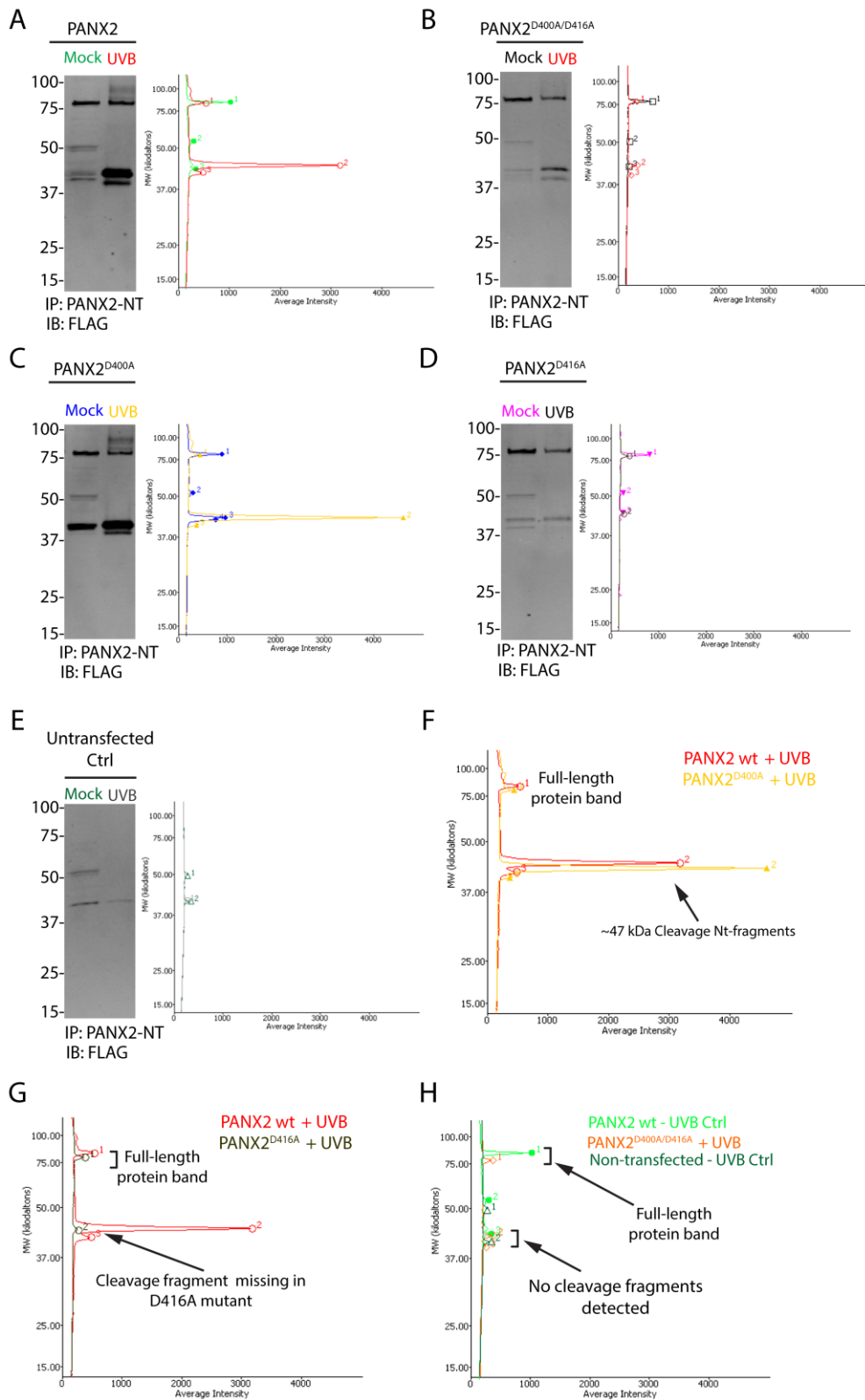
Figure S2-4



Supplemental Figure 2-4. Lane profile analysis of immunoprecipitations after *in vitro* PANX2 caspase cleavage experiments

(A-D) Molecular weight estimation of bands detected after IP of PANX2 in protein lysates treated (+) or not (-) with active caspase-3. Protein lysates were obtained from HEK293T cells overexpressing PANX2 and caspase-resistant mutants D400, D416, and D400/D416. Graphs on the right show the lane profiles with the peaks' vertical position indicating the relative migration of bands in WB as per MW markers (y-axis, in kDa). The high of the peak (in the x-axis) corresponds with the band's integrated intensity (densitometry) normalized over the whole WB. (E-H) Superposition of peaks between different lanes (indicated by colored text) to compare the appearance of cleavage fragments by evaluating their migration and band intensity. (see Fig. 2-4 for other details and whole WB).

Figure S2-5



Supplemental Figure 2-5. Lane profile analysis of IP after in-cell PANX2 caspase cleavage experiments in UVB-induced apoptotic REK-PANX2KO cells.

(A-E) Molecular weight estimation of bands detected after IP of PANX2 from protein lysates of cells treated (UVB) or not (Mock) with UVB radiation. REK-PANX2KO cells overexpressed PANX2 and caspase-resistant mutants D400, D416, and D400/D416. Graphs on the right show the lane profiles with the peaks' vertical position indicating the relative migration of bands in WB as per MW markers (y-axis, in kDa). The high of the peak (in the x-axis) corresponds with the band integrated intensity (densitometry) normalized over the whole WB. (F-H) Superposition of peaks between different lanes (indicated by colored text) to compare the appearance of cleavage fragments by evaluating their migration and band intensity. (see Fig. 2-5 for other details and whole WB).

Figure S2-6

CLUSTAL O(1.2.4) multiple sequence alignment

```

SP|Q6IMP4|PANX2_MOUSE MHLLLEQSDMATALLAGEKLRLEILPGSQDDKAGALAALLLQKLELFPDRVVTIGTVL 60
SP|P60571|PANX2_RAT MHLLLEQSDMATALLAGEKLRLEILPGSQDDKAGALAALLLQKLELFPDRVVTIGTVL 60
SP|Q96RD6|PANX2_HUMAN MHLLLEQSDMATALLAGEKLRLEILPGSQDDKAGALAALLLQKLELFPDRVVTIGTVL 60
*****

SP|Q6IMP4|PANX2_MOUSE VPILLVTLVFTKNFAEEPICYTPHNFRDQALYARGYCWTEL RDALPGVDASLWPSLFE 120
SP|P60571|PANX2_RAT VPILLVTLVFTKNFAEEPICYTPHNFRDQALYARGYCWTEL RDALPGVDASLWPSLFE 120
SP|Q96RD6|PANX2_HUMAN VPILLVTLVFTKNFAEEPICYTPHNFRDQALYARGYCWTEL RDALPGVDASLWPSLFE 120
*****

SP|Q6IMP4|PANX2_MOUSE HKFLPYALLAFAAIMYVPALGWFLASTRLTSELNFLQEI DNCYHRAAEGRAPKIEKQI 180
SP|P60571|PANX2_RAT HKFLPYALLAFAAIMYVPALGWFLASTRLTSELNFLQEI DNCYHRAAEGRAPKIEKQI 180
SP|Q96RD6|PANX2_HUMAN HKFLPYALLAFAAIMYVPALGWFLASTRLTSELNFLQEI DNCYHRAAEGRAPKIEKQI 180
*****

SP|Q6IMP4|PANX2_MOUSE QSKGPGITEREKREIENAEKEKSPEQNLFEKYLERRGRSNFLAKLYLARHVLILLSSV 240
SP|P60571|PANX2_RAT QSKGPGITEREKREIENAEKEKSPEQNLFEKYLERRGRSNFLAKLYLARHVLILLSSV 240
SP|Q96RD6|PANX2_HUMAN QSKGPGITEREKREIENAEKEKSPEQNLFEKYLERRGRSNFLAKLYLARHVLILLSSV 240
*****

SP|Q6IMP4|PANX2_MOUSE PISYLCTYYATQKQNEFTCALGASPDGVPVGSAGPTVRVSC LPSVQLQRIIAGVDIVLLC 300
SP|P60571|PANX2_RAT PISYLCTYYATQKQNEFTCALGASPDGVPVGSAGPTVRVSC LPSVQLQRIIAGVDIVLLC 300
SP|Q96RD6|PANX2_HUMAN PISYLCTYYATQKQNEFTCALGASPDGAAG-AGPAVRVSC LPSVQLQRIIAGVDIVLLC 299
*****

SP|Q6IMP4|PANX2_MOUSE FMNLIILVNL IHLFIFRKS NFI DKL NKGVIKTRRQWRRSQFC DINI LAMFCNENRDHIK 360
SP|P60571|PANX2_RAT FMNLIILVNL IHLFIFRKS NFI DKL NKGVIKTRRQWRRSQFC DINI LAMFCNENRDHIK 360
SP|Q96RD6|PANX2_HUMAN VMNLIILVNL IHLFIFRKS NFI DKL NKGVIKTRRQWRRSQFC DINI LAMFCNENRDHIK 359
*****

SP|Q6IMP4|PANX2_MOUSE SLNRLDFITNESDLMYDNVVRQLLAALAQSNHDTTPTVRD SGIQTVDPSINPAEPDSSAE 420
SP|P60571|PANX2_RAT SLNRLDFITNESDLMYDNVVRQLLAALAQSNHDTTPTVRD SGIQTVDPSINPAEPDSSAE 420
SP|Q96RD6|PANX2_HUMAN SLNRLDFITNESDLMYDNVVRQLLAALAQSNHDATPTVRD SGVQTVDP SANPAEPDSSAE 419
*****

SP|Q6IMP4|PANX2_MOUSE PPVVKRPRKMKMKIPTS NPLQP FKEQLAIMRVENSKTEKPKVRRKTATDTLIAPLLDA 480
SP|P60571|PANX2_RAT PPVVKRPRKMKMKIPTS NPLQP FKEQLAIMRVENSKTEKPKVRRKTATDTLIAPLLDA 480
SP|Q96RD6|PANX2_HUMAN PPVVKRPRKMKMKIPTS NPLQP FKEQLAIMRVENSKAEKPKARRKTATDTLIAPLLDR 479
*****

SP|Q6IMP4|PANX2_MOUSE GARAHHYKGGSGDGPSS---APPAASEKKHTRHFSLDVHPYILGT KKAKEAVPPAL 536
SP|P60571|PANX2_RAT GARAHHYKGGSGDGPSS---APPAASEKKHTRHFSLDVHPYILGT KKAKEAVPPAL 536
SP|Q96RD6|PANX2_HUMAN ---SAHHYKGGGDPGPGPAPAPAPPPAPDKKHARHFSLDVHPYILGT KKAKEAVPAAL 536
*****

SP|Q6IMP4|PANX2_MOUSE PASRSQEGGFLSQTEECGLGAAAPTKDAPLPEKEIPYPTEPALPGLPSGGSFHVCSPPA 596
SP|P60571|PANX2_RAT PASRSQEGGFLSQTEECGLGAAAPTKDAPLPEKEIPYPTESA---LP SGGPFHVCSPPT 593
SP|Q96RD6|PANX2_HUMAN PASRSQEGGFLSQAEDCGLGAPAPTKDAPLPEKEIPYPTEPARAGLPSGGPFHVRSPPA 596
*****

SP|Q6IMP4|PANX2_MOUSE APAAASLSPGSLGKADPLTILSRNATHPL LHISTLYEAREEEEGGPCAPSDMGLLSIPP 656
SP|P60571|PANX2_RAT ASAAA LSPSSLGKADPLTILSRNATHPL LHISTLYEAREEEEGGPCAPSDMGLLSIPP 653
SP|Q96RD6|PANX2_HUMAN APAVAPLTPASLGKAEPLTILSRNATHPL LHINTLYEAREEEEGGPRLPQDVGLIAIPA 656
*****

SP|Q6IMP4|PANX2_MOUSE PQQIL IATFE EPRTVVSTVEF 677
SP|P60571|PANX2_RAT PQQIL IATFE EPRTVVSTVEF 674
SP|Q96RD6|PANX2_HUMAN PQQIL IATFE EPRTVVSTVEF 677
*****

```

Color Legend: Transmembrane regions Predicted cleavage sites Caspase-3 cleavage site (mouse)

Supplemental Figure 2-6. Caspase cleavage site D416 in mouse PANX2 is conserved in the human but not in the rat ortholog.

Clustal-O tool in the Uniprot database was used for multiple sequence alignment of canonical PANX2 isoforms of the mouse, rat, and human orthologs. An asterisk denotes amino acid conservation; a colon denotes strong conservative substitution; a period denotes a weakly conservative substitution; space denotes non-conservative substitution with a different amino acid; while a dash represents an insertion or deletion.

2.4 Discussion

Alternative splicing has been reported for pannexin genes, but in most cases, the biological relevance of these splicing events remains unknown. Initial work by Baranova et al. (2004) analyzed the human *PANX2* sequence identifying two PANX2 human splice variants, PANX2alt1 and PANX2alt2, with the latter encoding a shorter protein isoform that was speculated to play an unknown regulatory role. In that study, a single mouse *Panx2* ortholog was identified by BLAST search, and comparative analysis of the genomic sequence and the transcript expression was validated by *in situ* hybridizations, but it was limited to the adult murine brain. Here, we have characterized the expression of a novel PANX2 isoform (*Panx2-202*) previously unveiled in [23] that bears a different molecular weight and partial sequence than canonical PANX2 found initially in the brain [1, 32]. Furthermore, Abitbol *et al.* (2019) showed that in *Panx1/Panx3* double knockout mice, PANX2-202 was expressed in the skin at similar levels to wildtype mice. Although we observed that canonical *Panx2* mRNA transcripts were also present in the skin at all ages investigated, our results confirmed such findings.

In the literature, discrepancies in the length and sequence of annotated PANX2 variants exist and are attributed to differences in cloning/sequencing procedures and predictions based on the available genomic sequences [33]. Interestingly, the mouse PANX2-202 isoform is reported exclusively in the Ensembl database (release 103 – as of February 2021) (Table 2-2) and not in NCBI. It is important to note that the transcript annotation may vary per Genomic database. Ensembl transcripts are automatically annotated based on experimental evidence and are, in most cases, manually curated by the HAVANA group [34]. However, the NCBI annotations may not match those in Ensembl and include predictions done by a different automated computational analysis (Gnomon method), combining homology searching with *ab initio* modeling supported by expressed sequence tag (EST) evidence from the current genomic sequences. Most of the studies analyzing mouse PANX2 have worked with the canonical sequence, but it should be noted that the expression of different splice variants may be tissue-specific. Based on the length and sequence, PANX2-202 may have different properties (e.g., subcellular localization,

channel function, and interaction with binding partners) than canonical PANX2. However, the functional implications of these differences and the consequences of their differential expression remain to be evaluated.

2.4.1 PANX2 is always present in the skin and is regulated during keratinocyte differentiation

We found that PANX2 is present in the suprabasal layers of the skin epidermis and, in contrast to the other pannexins paralogs [4, 6, 25], its expression is not drastically affected by age or the sex of the mice. Notably, the PANX2-202 variant trended to be more abundant than the canonical isoform at all ages and sex assayed. However, transient differences at P0 (at mRNA level in male mice) and four weeks old (at the protein level) could indicate an age-specific temporal regulation of PANX2 levels in the skin, yet with unknown biological significance. Nevertheless, the apparent disparity in mRNA and protein expression levels agrees with previous findings that mouse *Panx2* transcripts do not correlate with their protein levels [3].

PANX2 seems to have a similar localization pattern as PANX1 and PANX3 in the stratum granulosum and spinosum of thin murine skin [4, 5, 25]. In this work, three different anti-PANX2 polyclonal antibodies were employed for immunofluorescence, showing an intracellular localization, which correlates with previous observations made by us and others in other cell types and ectopic overexpression systems [3, 12, 20, 24, 35]. However, given that this endogenous labeling was not compared with a true negative control (e.g., *Panx2* knockout tissue), the diffuse staining pattern may arise from other proteins due to the polyclonal nature of the antibodies, and further confirmation is still warranted.

The level of PANX1 and PANX3 is regulated during keratinocyte differentiation [4, 6, 25]; therefore, we asked whether PANX2 could be influenced by differentiation in keratinocytes. PANX2-202 was more abundant than the canonical isoform in primary mouse keratinocytes, suggesting that this splice variant is more prominent than the canonical variant in this cell type. Our *in vitro* differentiation experiments with primary keratinocytes and REK cells showed similar trends with increased mRNA and protein

expression of endogenous PANX2 orthologs in differentiated keratinocytes. Considering the high staining intensity of PANX2 in the *stratum spinosum and granulosum* of the mouse epidermis, the putative detection of both variants of our antibodies, and the trends of increasing protein levels after Ca^{2+} -induced keratinocyte *in vitro* differentiation, we concluded that PANX2 is most likely to be upregulated during keratinocyte differentiation. Nevertheless, further work should address whether PANX2 modulates keratinocyte differentiation directly and forms functional channels in keratinocytes.

2.4.2 PANX2 promotes keratinocyte apoptosis independently of its caspase cleavage

Accumulating evidence implicates PANX2 in different cell death processes such as necrosis in neurons, apoptosis in glioma cells, cytokine-induced apoptosis in β -cells, and ferroptosis in prostate cancer cells [10, 12-15]. The skin is often challenged by UV radiation (particularly UVB), causing several skin pathological conditions [36]; therefore, apoptosis constitutes a protective mechanism essential to remove UV-damaged skin cells (e.g., keratinocytes) and avoid the risk of malignant transformation. Keeping in mind that PANX2 could be implicated in cell death, we sought to study the contribution of PANX2 during UVB-induced cell death of keratinocytes. Here, we uncovered for the first time that PANX2 undergoes caspase-mediated cleavage in apoptotic keratinocytes. In continuation with our previous studies [21], we have identified two sites (D400 and D416) in the PANX2 C-terminus that are targeted *in vitro* by executioner caspase-3 and demonstrated that in REK cells, at least only one of the predicted sites (D416) undergoes cleavage upon UV irradiation. Notably, genetic deletion of endogenous PANX2 delayed but did not prevent REK UVB-induced apoptosis, indicating that PANX2 is not essential but contributes to the apoptotic machinery in these cells. Furthermore, overexpression of canonical mouse PANX2, especially the caspase-resistant mutant PANX2^{D416A}, accelerated the caspase-3 activation rate and membrane permeability in UVB-irradiated REK-PANX2KO cells. Therefore, we concluded that caspase-mediated cleavage is not needed for the role of PANX2 in the apoptosis of UVB-damaged cells. Nevertheless, these results are in keeping with the pro-apoptotic function of PANX2 [12].

It is essential to note that despite the high conservation of PANX2 proteins between both mouse and rat species (98.2 % identity), the amino acid sequence of endogenous rat PANX2 has a natural conservative substitution of aspartic acid with glutamate at the position 416 (D→E), that is not present in human PANX2 (Fig. S2-6). Based on this difference, endogenous rat PANX2 (as in wildtype REK) is not expected to be cleaved by caspases 3/7. In this respect, our results support our hypothesis that PANX2, but not its caspase-mediated cleavage, functions as a promoter of UVB-induced apoptosis, as shown with both PANX2 orthologs. Moreover, regarding the murine PANX2-202 isoform, both cleavage sites at D400 and D416 are still conserved in the amino acid sequence; therefore, we speculate a similar caspase cleavage is likely to occur. However, future work should address whether the PANX2-202 function is affected by caspase cleavage under apoptotic conditions. To our knowledge, there are no reports of abnormal skin phenotypes in the *Panx2* knockout (KO) mouse model [10, 14, 37, 38]. Nevertheless, considering that PANX2 assists with the death of UV-damaged keratinocytes, skin homeostasis in *Panx2*-KO mice might be compromised after UV exposure or other apoptotic insults. Thus, it will be interesting to determine whether *Panx2*-KO mice have skin repair or renewal defects.

2.5 Conclusions

In conclusion, this work sheds light on PANX2 regulation in the skin and specifically during two critical processes related to skin homeostasis: keratinocyte differentiation and apoptosis. We demonstrated that the expression of splice variants is a factor to be considered when studying PANX2 in the skin and perhaps in other tissues. This is the first study to identify the caspase-3 cleavage sites in PANX2 and its pro-apoptotic role in keratinocytes. These novel findings provide a better understanding of the tissue-specific regulation and function of PANX2.

2.6 Acknowledgments

We thank Dr. Lina Dagnino for supplementing the UV setup and guidance with the keratinocyte differentiation experiments. We thank Kevin Barr for helping with the mice

breeding and sample collection. We would like to thank Dr. John Di Guglielmo for supplementing the TGF- β for dermal fibroblast stimulation experiments.

2.7 References

1. Panchin, Y., et al., *A ubiquitous family of putative gap junction molecules*. *Curr Biol*, 2000. **10**(13): p. R473-4.
2. Penuela, S., R. Gehi, and D.W. Laird, *The biochemistry and function of pannexin channels*. *Biochim Biophys Acta*, 2013. **1828**(1): p. 15-22.
3. Le Vasseur, M., et al., *Pannexin 2 protein expression is not restricted to the CNS*. *Front Cell Neurosci*, 2014. **8**: p. 392.
4. Celetti, S.J., et al., *Implications of pannexin 1 and pannexin 3 for keratinocyte differentiation*. *J Cell Sci*, 2010. **123**(Pt 8): p. 1363-72.
5. Penuela, S., et al., *Pannexin 1 and pannexin 3 are glycoproteins that exhibit many distinct characteristics from the connexin family of gap junction proteins*. *J Cell Sci*, 2007. **120**(Pt 21): p. 3772-83.
6. Penuela, S., et al., *Panx1 regulates cellular properties of keratinocytes and dermal fibroblasts in skin development and wound healing*. *J Invest Dermatol*, 2014. **134**(7): p. 2026-2035.
7. Zhang, P., et al., *Pannexin 3 regulates skin development via Epiprofin*. *Sci Rep*, 2021. **11**(1): p. 1779.
8. Zhang, P., et al., *Pannexin-3 Deficiency Delays Skin Wound Healing in Mice due to Defects in Channel Functionality*. *J Invest Dermatol*, 2019. **139**(4): p. 909-918.
9. Swayne, L.A., C.D. Sorbara, and S.A. Bennett, *Pannexin 2 is expressed by postnatal hippocampal neural progenitors and modulates neuronal commitment*. *J Biol Chem*, 2010. **285**(32): p. 24977-86.
10. Bargiotas, P., et al., *Pannexins in ischemia-induced neurodegeneration*. *Proc Natl Acad Sci U S A*, 2011. **108**(51): p. 20772-7.
11. Xu, X., et al., *PANX2 and brain lower grade glioma genesis: A bioinformatic analysis*. *Sci Prog*, 2021. **104**(2): p. 368504211011836.
12. Le Vasseur, M., et al., *Pannexin 2 Localizes at ER-Mitochondria Contact Sites*. *Cancers (Basel)*, 2019. **11**(3).
13. Lai, C.P., J.F. Bechberger, and C.C. Naus, *Pannexin2 as a novel growth regulator in C6 glioma cells*. *Oncogene*, 2009. **28**(49): p. 4402-8.

14. Berchtold, L.A., et al., *Pannexin-2-deficiency sensitizes pancreatic beta-cells to cytokine-induced apoptosis in vitro and impairs glucose tolerance in vivo*. Mol Cell Endocrinol, 2017. **448**: p. 108-121.
15. Liao, D., et al., *Identification of Pannexin 2 as a Novel Marker Correlating with Ferroptosis and Malignant Phenotypes of Prostate Cancer Cells*. Onco Targets Ther, 2020. **13**: p. 4411-4421.
16. Lippens, S., et al., *Death penalty for keratinocytes: apoptosis versus cornification*. Cell Death Differ, 2005. **12 Suppl 2**: p. 1497-508.
17. Baden, H.P. and J. Kubilus, *The growth and differentiation of cultured newborn rat keratinocytes*. J Invest Dermatol, 1983. **80**(2): p. 124-30.
18. Maher, A.C., et al., *Rat epidermal keratinocytes as an organotypic model for examining the role of Cx43 and Cx26 in skin differentiation*. Cell Commun Adhes, 2005. **12**(5-6): p. 219-30.
19. Li, F., et al., *Procleave: Predicting Protease-specific Substrate Cleavage Sites by Combining Sequence and Structural Information*. Genomics Proteomics Bioinformatics, 2020. **18**(1): p. 52-64.
20. Penuela, S., et al., *Glycosylation regulates pannexin intermixing and cellular localization*. Mol Biol Cell, 2009. **20**(20): p. 4313-23.
21. Penuela, S., et al., *Diverse post-translational modifications of the pannexin family of channel-forming proteins*. Channels (Austin), 2014. **8**(2): p. 124-30.
22. Lamprecht, M.R., D.M. Sabatini, and A.E. Carpenter, *CellProfiler: free, versatile software for automated biological image analysis*. Biotechniques, 2007. **42**(1): p. 71-5.
23. Abitbol, J.M., et al., *Double deletion of Panx1 and Panx3 affects skin and bone but not hearing*. J Mol Med (Berl), 2019. **97**(5): p. 723-736.
24. Sanchez-Pupo, R.E., D. Johnston, and S. Penuela, *N-Glycosylation Regulates Pannexin 2 Localization but Is Not Required for Interacting with Pannexin 1*. Int J Mol Sci, 2018. **19**(7).
25. Cowan, K.N., et al., *Pannexin1 and Pannexin3 exhibit distinct localization patterns in human skin appendages and are regulated during keratinocyte differentiation and carcinogenesis*. Cell Commun Adhes, 2012. **19**(3-4): p. 45-53.
26. Candi, E., et al., *Cornification of the Skin: A Non-apoptotic Cell Death Mechanism*. eLS, 2016: p. 1-10.
27. Borowiec, A.S., et al., *Optimal differentiation of in vitro keratinocytes requires multifactorial external control*. PLoS One, 2013. **8**(10): p. e77507.
28. Wang, X.H., et al., *Identification and characterization of pannexin expression in the mammalian cochlea*. J Comp Neurol, 2009. **512**(3): p. 336-46.

29. Chekeni, F.B., et al., *Pannexin 1 channels mediate 'find-me' signal release and membrane permeability during apoptosis*. Nature, 2010. **467**(7317): p. 863-7.
30. Engelhardt, K., et al., *Effects on channel properties and induction of cell death induced by c-terminal truncations of pannexin1 depend on domain length*. J Membr Biol, 2015. **248**(2): p. 285-94.
31. Sandilos, J.K., et al., *Pannexin 1, an ATP release channel, is activated by caspase cleavage of its pore-associated C-terminal autoinhibitory region*. J Biol Chem, 2012. **287**(14): p. 11303-11.
32. Bruzzone, R., et al., *Pannexins, a family of gap junction proteins expressed in brain*. Proc Natl Acad Sci U S A, 2003. **100**(23): p. 13644-9.
33. Scemes, E. and J. Veliskova, *Exciting and not so exciting roles of pannexins*. Neurosci Lett, 2019. **695**: p. 25-31.
34. Aken, B.L., et al., *The Ensembl gene annotation system*. Database (Oxford), 2016. **2016**.
35. Wicki-Stordeur, L.E., A.K. Boyce, and L.A. Swayne, *Analysis of a pannexin 2-pannexin 1 chimeric protein supports divergent roles for pannexin C-termini in cellular localization*. Cell Commun Adhes, 2013. **20**(3-4): p. 73-9.
36. Li, D., et al., *Rays and arrays: the transcriptional program in the response of human epidermal keratinocytes to UVB illumination*. FASEB J, 2001. **15**(13): p. 2533-5.
37. Bargiotas, P., et al., *Functional outcome of pannexin-deficient mice after cerebral ischemia*. Channels (Austin), 2012. **6**(6): p. 453-6.
38. Dickinson, M.E., et al., *High-throughput discovery of novel developmental phenotypes*. Nature, 2016. **537**(7621): p. 508-514.

Chapter 3

N-glycosylation is a post-translational modification that acts as a regulator of the localization and intermixing of PANX1 and PANX3, but its effects on PANX2 are currently unknown. Since PANX1 and PANX2 have been reported to interact, the objectives in this chapter were to validate the predicted N-glycosylation site of PANX2 and study the effects of glycosylation on PANX2 localization and interaction with PANX1.

A version of this paper is published:

Sanchez-Pupo RE, Johnston D, Penuela S. N-Glycosylation Regulates Pannexin 2 Localization but Is Not Required for Interacting with Pannexin 1. *Int J Mol Sci.* 2018 Jun 22;**19**(7):1837. doi: 10.3390/ijms19071837. PMID: 29932112; PMCID: PMC6073767.

3 N-glycosylation regulates Pannexin 2 localization but is not required for interacting with Pannexin 1

3.1 Introduction

Pannexins (PANX1, PANX2, and PANX3) are membrane-spanning glycoproteins capable of forming large-pore channels that allow the passage of ions and macromolecules involved in paracrine and autocrine signaling [1, 2]. PANX1 is the most widely expressed pannexin family member and the most studied, with evidence supporting that its channels act as ATP and Ca^{2+} conduits [3-6] and are implicated in critical cellular processes such as cell death after brain ischemia [7] and inflammation [8]. On the other hand, PANX2 is the largest family member, and its expression was thought to be restricted to the central nervous system (CNS). Recently, it has been reported that PANX2 can also be expressed in other tissues such as skin, kidney, and liver [9, 10], while PANX3 is predominantly expressed in skin, cartilage, and bone [4, 5, 11-13]. In contrast to the heptameric type of channels formed by PANX1, it has been suggested that PANX2 can form octameric or heptameric channels [14], and it is still unclear whether its channel function would be similar to the other family members.

Interestingly, PANX1 and PANX2 expression have been found to overlap in adult rodent brains, although they are inversely regulated throughout development, with PANX1 being more abundant in neonatal and young tissues, whereas PANX2 is more abundant in the adult [15-18]. Under ischemic conditions, both PANX1 and PANX2 are expressed in the brain, and their overlapping channel functions contribute to neurodegeneration. The deletion of PANX1 and PANX2 in a double knockout mouse model was necessary to observe a reduction in cell death after ischemia, perhaps due to their redundant or complementary functions [19].

N-glycosylation is a post-translational modification in the endoplasmic reticulum (ER) and is recognized to profoundly affect protein folding and trafficking of membrane-bound proteins [20]. The prediction of putative N-linked glycosylation sites for pannexins has been made in the past, and it has been demonstrated that PANX1 and PANX3 can be N-

glycosylated at Asn (N) 254 and N71, respectively. These studies comprised further characterization using enzymatic digestion with endoglycosidases that confirmed that all three members of the pannexin family are differentially N-glycosylated but not O-glycosylated [11, 21]. However, for PANX2, the predicted site of N-glycosylation at residue N86 remains to be validated [22].

Unlike other pannexins, PANX2 is only modified to a high-mannose glycosylation species (termed as Gly1) and presents a predominantly intracellular localization that has been associated with this lower level of N-glycosylation [22-26]. Previous evidence supports the concept that complex glycoprotein species (Gly2) (further processed at Golgi) present in PANX1 and PANX3 traffic readily to the cell surface [22]. However, our group and others have stated that PANX2 can also translocate to the plasma membrane [17, 22] [14], but it is still unclear whether glycosylation plays a role in regulating PANX2 trafficking.

PANX2 has been shown to interact with PANX1, and when co-expressed together, they can form heteromeric channels with reduced channel properties compared to homomeric ones [22, 27]. Although this has only been tested in ectopic expression systems, it has been suggested that it might function as a mode of regulation in cells that endogenously express both proteins. Interestingly, the PANX1/PANX2 interaction only occurs with the Gly0 and Gly1 species of PANX1 [22], and it is unknown whether PANX2 glycosylation has any impact on the formation of these intermixed channels. Previous studies have shown that PANX1 and PANX2 are often co-expressed in the same cells under normal conditions [15, 16, 27-30], which may later modulate pathological processes such as ischemia-induced neurodegeneration and brain damage *in vivo* [31]. Understanding how these channels are regulated by post-translational modifications (PTM)s, such as N-glycosylation, may provide further insight into their role in homeostasis and disease and be used for therapeutic purposes.

The present study aimed to validate the predicted N-linked-glycosylation site of PANX2 and determine its role in regulating the subcellular localization and intermixing of PANX2 with PANX1. Herein, we generated a PANX2 mutant protein completely devoid of N-glycosylation that, when overexpressed, exhibits a high level of intracellular aggregation

with decreased traffic to the plasma membrane compared with wildtype PANX2. We found that N-glycosylation of PANX2 is not required for PANX1/PANX2 intermixing but facilitates PANX2 trafficking and localization at the plasma membrane when co-expressed with PANX1. Nevertheless, the intracellular localization of un-glycosylated PANX2 reduces its interaction with PANX1 at the cell surface and may impact their channel function in cells that co-express both glycoproteins, such as neurons. Collectively, we propose that N-glycosylation may be necessary for the proper processing of PANX2 at the endoplasmic reticulum, regulating its intracellular distribution, but it is not required for interacting with PANX1.

3.2 Materials and Methods

3.2.1 Cell lines, constructs, and transient transfections

Media, supplements, and reagents were obtained from GIBCO® and Invitrogen™ (Carlsbad, CA, USA). Normal rat kidney (NRK) (ATCC® CRL-6509™), human embryonic kidney cells (HEK293T) (ATCC® CRL-3216™) were obtained from ATCC (Manassas, VA, USA). Adherent HEK293 cells (AD293, Cat# 240085) were obtained from Agilent Technologies, Inc. (Santa Clara, CA, USA). Cell cultures were grown in high-glucose DMEM supplemented with 10% fetal bovine serum (FBS), 100 U/ml penicillin, 100 µg/ml streptomycin, and 2 mM L-Glutamine. At ~50% of confluency, cells were transfected adding Lipofectamine 3000 (Invitrogen™) following manufacturer directions. 2 µg of pcDNA3.1 (Invitrogen™) plasmids encoding mouse PANX2 [22] or PANX2^{N86Q} or their respective FLAG-tagged versions were used for transfections in 35 mm culture plates. After 48h for single transfections and 72h for co-transfections, proteins were extracted, and expression levels were determined by Western blot. For co-transfections experiments with mouse Panx1 construct [11], the DNA levels were reduced to 0.5 µg.

3.2.2 Mutagenesis and cloning of new FLAG-tagged PANX2 constructs

As described by [11], PANX2 has a predicted N-glycosylation consensus site located at asparagine (N) 86 on the first extracellular loop. Site-directed mutagenesis service (NorClone Biotech Labs, London, ON, Canada) was used to generate a new expression

PANX2 construct encoding a replacement of asparagine by glutamine at position 86, referred as PANX2 N86Q. FLAG-tagged PANX2 was obtained by inserting a single FLAG sequence with In-Fusion HD Cloning Kit (Takara Bio, Inc.) at the end of the coding region of the PANX2 C-termini. Primers used for FLAG insertion were Forward: 5'-GTTTAAACTTAAGCTTCATGCACCACCTCCTGGAG-3' and Reverse: 5'-GCCCTCTAGACTCGAGCTCACTTGTCATCGTCGTCCTTGTAATCAAACCTCCACAGTACT-3'. All the constructs were verified by sequencing.

3.2.3 Protein extractions and Western blots

For co-immunoprecipitation (Co-IP) assays, cell lysates were obtained using Triton-based extraction buffer (IP buffer) (1% Triton X-100, 150 mM NaCl, 10 mM Tris, 1 mM EDTA, 1 mM EGTA, 0.5% NP-40). The rest of the protein extractions were performed with SDS-based buffer (RIPA buffer) (0.1% SDS, 50 mM Tris-HCl, pH 8.0, 150 mM NaCl, 1% NP-40 and 0.5% Sodium Deoxycholate). In each case, lysis buffers were complemented with a final concentration of 1 mM NaF, 1 mM Na₃VO₄, and one tablet of cOmplete™-mini, EDTA-free Protease Inhibitor Cocktail (Roche). Total protein concentrations were quantitated by bicinchoninic acid (BCA) assay (Thermo Scientific Pierce). For Western Blots, 50 µg of total protein were resolved in 8% SDS-PAGE and transferred onto nitrocellulose membranes using an iBlot™ Blotting System (Invitrogen). Membranes were blocked with 3% bovine serum albumin (BSA) and 0.05% Tween 20-Phosphate Buffer Saline (T-PBS) for 45 min at room temperature and probed overnight with a 1:1000 dilution of the rabbit affinity-purified antibodies anti-PANX2 -CT-523 [22]. Mouse monoclonal anti-FLAG® M2 (Sigma, Cat. # F3165), monoclonal mouse anti-GAPDH (Millipore Cat# MAB374, RRID: AB_2107445), and anti-α-Tubulin (Millipore-Sigma Cat# 05-829, clone DM1A) antibodies were used at 1:2000, 1:1000 and 1:5000 dilutions, respectively. For detection IRDye -800 and -680RD (Life Technologies™) were used as secondary antibodies at 1:10000 dilution, and the membranes were scanned on a Li-Cor Odyssey infrared system (Li-Cor, USA). Unless otherwise indicated, GAPDH was used as a loading control.

3.2.4 Immunofluorescence, confocal imaging, Linescans and colocalization analysis

Cells were grown on coverslips at ~70% of confluency and were transfected as described previously in subsection 4.1. After 48h of transfection, coverslips were washed with D-PBS (Gibco®) and fixed with ice-cold 80% methanol and 20% acetone for 15 minutes at 4°C. Coverslips were blocked with 2% BSA-PBS for 1h and primary antibodies were used diluted in blocking buffer as follows: polyclonal anti-PANX2-CT (2 mg/mL, 1:100 dilution), polyclonal anti-PANX1-CT (1 mg/mL, 1:100 dilution), anti-PDI monoclonal antibody (1 mg/mL, 1:400 dilution) (1D3, Enzo® Life Sciences, ADI-SPA-891-D), cis-Golgi marker anti-GM130 (1 mg/mL, 1:300) (Abcam, Prod#: ab169276), anti-FLAG® M2 (1mg/mL, 1:500) (Sigma, F3165), mouse monoclonal anti-Lamp-2 (1 mg/mL, 1:300) (DHSB, clone H4B4). Coverslips were incubated with primary antibodies 1 hour at room temperature, then washed with PBS and incubated with the secondary antibodies: Alexa Fluor 488 goat anti-rabbit IgG (2 mg/mL, 1:700) or goat anti-mouse antibody Alexa Fluor 647 (2 mg/mL, 1:400) (LifeTechnologies), that were selected to avoid bleed-through between dyes. Mitochondrial labeling was performed using MitoTracker™ Red CMXRos (M7512, Thermofisher) as per manufacturer directions, and cells were fixed with freshly prepared paraformaldehyde (4%) and then permeabilized with 0.1% Triton X-100 before blocking step. Coverslips were rinsed with PBS followed by water once and counterstained with Hoechst 33342 (Life Technologies™, USA) (1:1000, in water) for 5 min to stain nuclei and then mounted with the custom-made Airvol mounting medium. Imaging was performed with an LSM 800 Confocal Microscope (Carl Zeiss) using a Plan-Apochromat 63x/1.40 Oil DIC objective (Zeiss). Image acquisition for colocalization was performed sequential laser scanning and with the multitracking feature of the Zeiss software with settings to avoid wrong excitation-crosstalk and bleed-through of the channels. Colocalization was quantitated with the colocalization plug-in of the Zeiss software. Regions of interest (ROI) were drawn in dual-labeled cells selecting individual cells expressing PANX2 or the mutant and co-stained with organelle markers. Controls of single-labeled cells were used to determine thresholds of intensities for every single channel and manual thresholding was used to determine the region of pixels colocalized in

the intensity scatterplots. Pearson correlation coefficient was determined for each cell as a colocalization measure and was expressed as means \pm S.E.M., representative of at least three independent transfections. Linescans using the Zeiss software tool were used to detect overlapping fluorescence peaks in cells co-transfected with PANX1.

3.2.5 Cell surface biotinylation assays

Cell surface biotinylation assays were performed as described in [22]. Briefly, cells were grown in 60 mm plates and used for biotinylation 72h following transfection with PANX2 or N86Q constructs. After culture media was aspirated, the cell monolayer was rinsed twice with ice-cold D-PBS supplemented with Ca^{2+} and Mg^{2+} (Gibco®). Then, cells were incubated only with D-PBS (non-labeling as a negative control) or with a solution of 1,5 mg/mL EZ-Link™ Sulfo-NHS-SS-Biotin (Thermo Scientific) in D-PBS for 30 min on ice and covered from light. Plates were washed once again with D-PBS and then incubated with 100 mM glycine dissolved in D-PBS for 30 min to quench the remaining labeling biotin washed once more with D-PBS. Lysates were prepared using RIPA buffer as described before. For pull-down of cell surface biotinylated proteins, 250 μg of total protein was incubated overnight with 50% slurry of 50 μL NeutrAvidin agarose beads (Thermo Scientific). Samples from lysates and initial flow-through wash were collected, the beads were spun down (at $\times 500$ g, 4°C), and then washed three times with RIPA buffer. The samples and the beads were mixed with 2x Laemmli buffer plus 10% β -mercaptoethanol and placed at 95°C in a heat block for 5 min. 50 μg of total protein from lysates and the beads supernatant were resolved in parallel with 8% SDS-PAGE gel and then transferred to nitrocellulose membranes as previously described. PDI or GAPDH were used as controls of non-specific biotinylation of intracellular/cytoplasmic proteins, and E-cadherin was used as a positive control of cell surface protein.

3.2.6 Co-immunoprecipitation (Co-IP) assays

Co-immunoprecipitation (Co-IP) of protein complexes was performed at 4°C by incubating overnight 1 mg of total protein from pre-cleared (with Protein A/G beads alone) lysates with 5 $\mu\text{g}/\text{ml}$ of rabbit polyclonal anti-PANX2-CT or anti-PANX1-CT affinity-purified

antibody crosslinked to Pierce Protein A/G-Agarose beads (Thermo Scientific), and the same amount of beads (~30 μ L) was used for IP in each case. Control experiments to evaluate unspecific binding to the beads were performed in parallel using beads with no antibody. To remove unbound proteins, four washes with 500 μ l of ice-cold IP buffer were performed. Then, beads were dried by aspiration and resuspended in 2X Laemmli buffer (10% (v:v) β -mercaptoethanol), boiled for 5 min, spun down, and the supernatants (IP samples) were used for WB. For WB analysis, 50 μ g of protein of each lysate was loaded into the INPUT lanes and ran along with the IP samples. The intensities of the bands in each lane were obtained by densitometry and were used for quantitation.

3.2.7 De-glycosylation assays

Lysates from HEK293T ectopically expressing mouse PANX2 and the N86Q were used to validate the N-glycosylation site of the mouse PANX2 construct. Enzymatic de-glycosylation with Peptide-N-glycosidase F (PNGase F) and Endoglycosidase H (EndoH) were used to detect the presence of all complex forms of N-glycosylation and high-mannose modification, respectively. PNGase F (Sigma-Aldrich) and EndoH (New England Biolabs) digestions were performed according to their manufacturer's instructions. Briefly, at least 35 μ g of total protein was denatured at 100 $^{\circ}$ C for 5 minutes in denaturing buffer (0.1% (v/v) SDS, 0.05 M 2-mercaptoethanol, 50 mM phosphate buffer, pH 7.5) and subsequently incubated for 1h at 37 $^{\circ}$ C with 10 units of the PNGase F, 0.7 % (v/v) of Triton X-100 or 2500 U of Endo H in supplier's digestion buffer. In parallel, control samples were assayed without endoglycosidases. Protein samples were separated on an 8% SDS-polyacrylamide gel electrophoresis gel (PAGE) and transferred to nitrocellulose membranes for WB.

3.2.8 Densitometric analysis of Western blots

Densitometry analysis was performed in the Odyssey Application Software Version 3.0.16 (LI-COR Biosciences, USA). For cell surface biotinylation experiments, the fraction of biotinylated protein detected at the cell surface was calculated using the integrated intensity (I.I.) of protein bands detected in the Neutravidin lanes divided by the I.I. of protein bands detected in their corresponding input-lysate lanes. For Co-IP experiments, quantitative

analysis was performed by calculating the I.I. ratio (Co-IP protein / IP-target protein). Quantitation results were expressed as means \pm SEM representative of at least three independent experiments.

3.2.9 Statistics

Statistical analysis was performed using the statistical package of GraphPad Prism® Ver. 5.03 (GraphPad Software, Inc.). Cell surface biotinylation data were analyzed with a non-parametric Mann-Whitney U test for unpaired data. Data derived from quantitation of Co-IP assays and colocalization were analyzed with a two-tailed unpaired t-test with Welch's correction. A probability of $p < 0.05$ was considered statistically significant.

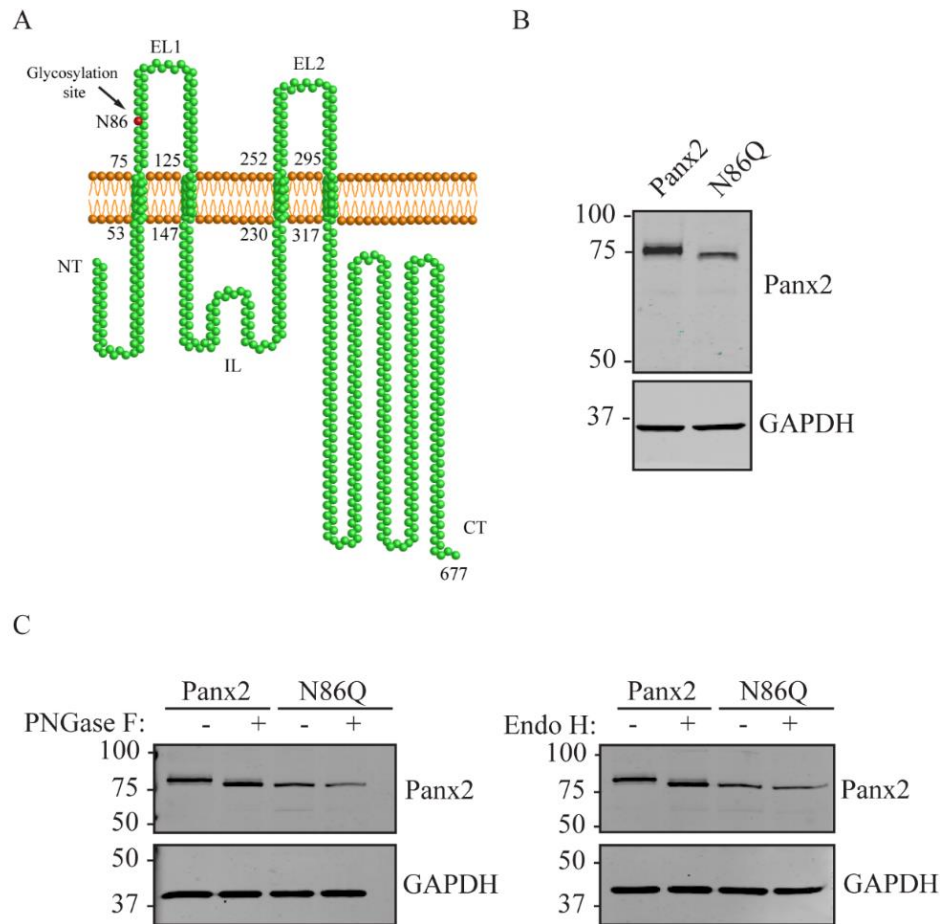
3.3 Results

3.3.1 Characterization of the PANX2 N-glycosylation site at asparagine 86

Previous research has shown that ectopic expression of full-length mouse PANX2 presented N-glycosylated species with high-mannose modification [22]. Based on the analysis of the canonical sequence of PANX2 (UniProt ID: Q6IMP4-1), this modification might occur at N86 that is located in the first extracellular loop of PANX2 [20] (Fig. 3-1A). To validate this prediction, we generated a full-length PANX2 mutant (*PANX2^{N86Q}*, referred to herein as N86Q) with the substitution of the N86 with glutamine (Gln, Q) that prevents the attachment of N-linked glycans to this specific site. As shown in Fig. 3-1B, Western blotting (WB) of overexpressed constructs of N86Q and wildtype PANX2 (as glycosylated control) indicated that the electrophoretic band corresponding to N86Q mutant migrated faster than its wildtype counterpart, characteristic of a reduction in molecular weight.

To analyze whether N-glycosylation was prevented in the N86Q mutant, enzymatic deglycosylation with endoglycosidase H (Endo H) and Peptide -N-Glycosidase F (PNGase F) were applied to the protein lysates and analyzed by WB (Fig. 3-1C). Both deglycosylation treatments did not cause any shift in migration of the N86Q band. However, wildtype PANX2 exhibited a small shift after treatment which relocated the migration of

this band to the same position as that of the faster migrating N86Q mutant. Thereby, the differences in electrophoretic migration can be explained by differences in molecular weight due to the elimination or absence of N-glycosylation. These findings validate N86 as the only N-glycosylation site in PANX2, as Penuela *et al.* and others predicted [22].

Figure 3-1.**Figure 3-1 PANX2 is N-glycosylated at asparagine 86.**

(A) Based on sequence analysis, PANX2 (Uniprot ID: Q6IMP4-1) is predicted to contain four transmembrane domains, one intracellular (IL) and two extracellular loops (EL). The predicted N-glycosylation site is located at Asn86 in the first extracellular loop (EL1) (red residue) (B) Western blot (WB) comparing wildtype PANX2 and mutant N86Q, the latter shows a faster-migrating band than the wildtype counterpart indicative of decreased molecular weight. (C) Cell lysates of HEK293T transiently expressing PANX2 and N86Q mutant were subjected to enzymatic digestions with PNGase F and EndoH N-glycosidases. WB analysis confirmed that N86 is the only glycosylation site for PANX2 since only the wildtype protein exhibited a band shift after treatment with both glycosidases and the deglycosylated PANX2 band ran to the same position as the N86Q mutant. GAPDH was used as the loading control. Molecular weights are noted in kDa.

3.3.2 N86Q forms intracellular aggregates

To determine whether glycosylation influences PANX2 subcellular localization, we ectopically expressed PANX2 WT and N86Q in different reference cell lines and evaluated whether the subcellular distribution changes due to the cell type as reported for PANX1 and PANX3 [32]. Because our group had demonstrated before [33] that PANX1 influences PANX2 trafficking, we selected Normal Rat Kidney cells (NRK), that in our experience have a minimal expression of endogenous PANX1 (Fig. 3-2D), and "adherent" human embryonic kidney cells (AD293) that endogenously express the human ortholog *PANX1* (Fig. 3-3D). Likewise, these cell lines were selected as they are suitable transfection hosts with a relatively large cytoplasm which facilitates the visualization of the subcellular localization of proteins.

Confocal immunofluorescence imaging revealed an intracellular localization of ectopic PANX2 (Figures 3-2A and 3-3A, top panel), with perinuclear distribution and spread in intracellular compartments. Interestingly, in both cell types assayed, the mutant N86Q localized intracellularly with a large subpopulation forming punctate aggregates (Figures 3-2A and 3-3A, bottom panel).

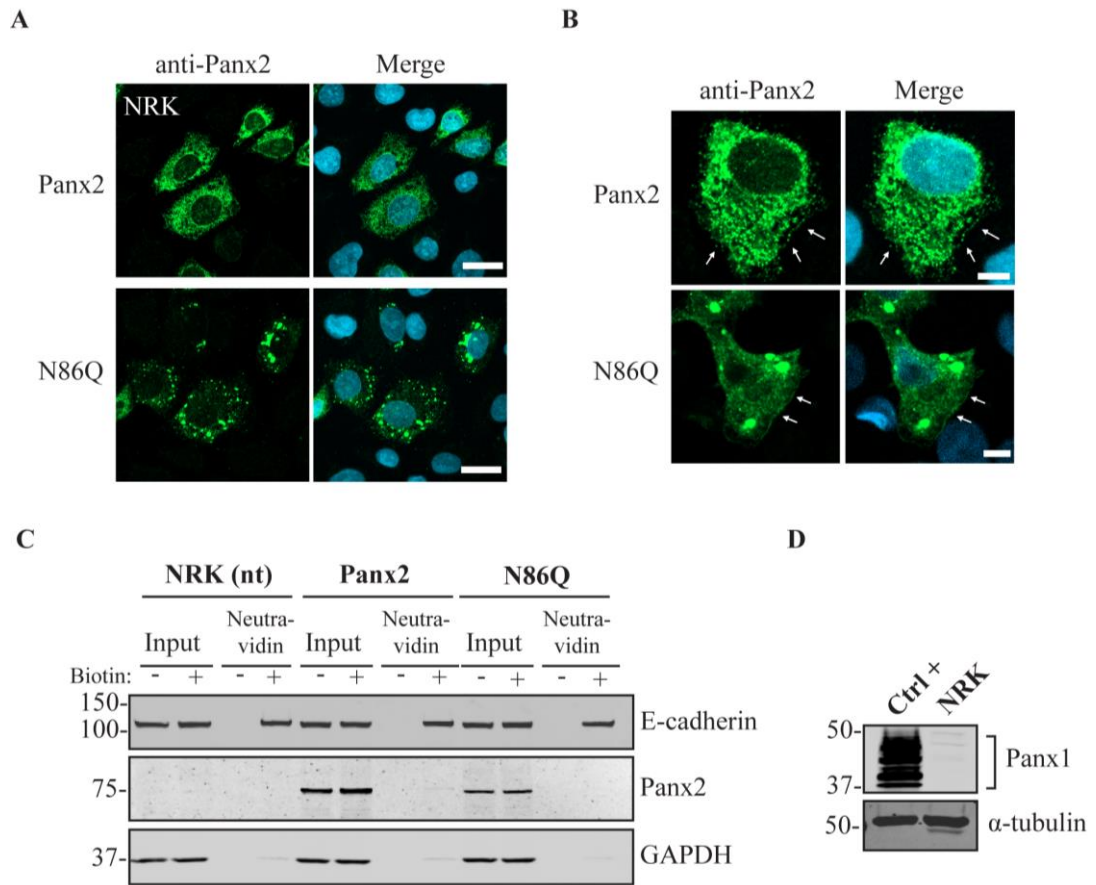
Figure 3-2

Figure 3-2 PANX2 N-glycosylation-deficient mutant (N86Q) forms intracellular aggregates in NRK cells.

(A) Confocal micrographs of PANX2 and N86Q ectopically expressed in NRK cells, immunolabeled with anti-PANX2 antibody (green), revealed that PANX2 is predominantly localized intracellularly. The mutant N86Q is also localized intracellularly but appeared mostly as punctate aggregates. Nuclei (blue) were counterstained with Hoechst 33342. Scale bars = 20 μm . (B) Representative images of a small subpopulation of NRK cells expressing PANX2 or N86Q showed minimal apparent localization at the cell surface (indicated with white arrows). Scale bars = 5 μm . (C) Western blot analysis of cell-surface-biotinylated proteins with EZ-Link™ Sulfo-NHS-SS-Biotin pulled down with NeutrAvidin® beads showed very low detection of PANX2 but not the N86Q mutant at the cell surface of NRK cells. E-cadherin was used as a positive control of cell surface protein labeling and GAPDH was used as a negative control of intracellular proteins (no biotin internalization). Non-transfected NRKs (nt) were used as a negative control (D) Western blot of protein lysate from NRK cells indicated that endogenous PANX1 protein is barely detectable in these cells. Overexpressed PANX1 was used as a positive control (Ctrl +), and endogenous α -tubulin was used as the protein loading control. Molecular weights noted in kDa.

3.3.3 PANX2 localization at the cell surface is reliant on N-glycosylation status and the level of PANX1

Despite the predominant intracellular localization, in a subpopulation of cells, PANX2 and the N86Q mutant (to a lesser extent) were apparent in limited regions of the cell surface (Figures 3-2B and 3-3B, arrows). To corroborate these results, cell surface biotinylation assays followed by immunoblotting were conducted using a cell-impermeable biotinylation reagent (Sulfo-NHS-SS-Biotin). NRKs (low endogenous PANX1, Fig. 3-2D) showed a faint band of PANX2 and no detection of N86Q at the cell surface in the neutravidin pull-downs (Fig. 3-2C). Also, AD293 cells (with a higher level of endogenous PANX1, Fig. 3-3D) exhibited low PANX2 and no detectable N86Q mutant protein at the cell surface (Fig. 3-3C). However, in subsequent experiments, we also used human embryonic kidney (HEK293T) cells (Fig. 3-3D) that have been used in previous studies [11, 22] because of their increased transfection efficiency and enhanced protein expression due to the SV40 T-antigen [34]. After ectopic expression in HEK293T cells, we performed the same cell-surface biotinylation assays and noticed that PANX2 WT protein was detected (~4% of the total PANX2 expression) at the cell surface (Fig. 3-3E). Under these overexpression conditions, the N86Q mutant was also detected in the biotinylated-protein fractions (Fig. 3E), with a significant ($p=0.0286$, $N=4$) reduction (to ~1% of its total amount) in the cell surface protein pool compared to PANX2 WT (Fig. 3-3F). Therefore, although the PANX2 cell membrane trafficking is reduced when it is not N-glycosylated, its cell surface localization is not entirely abrogated when overexpressed in HEK293T cells.

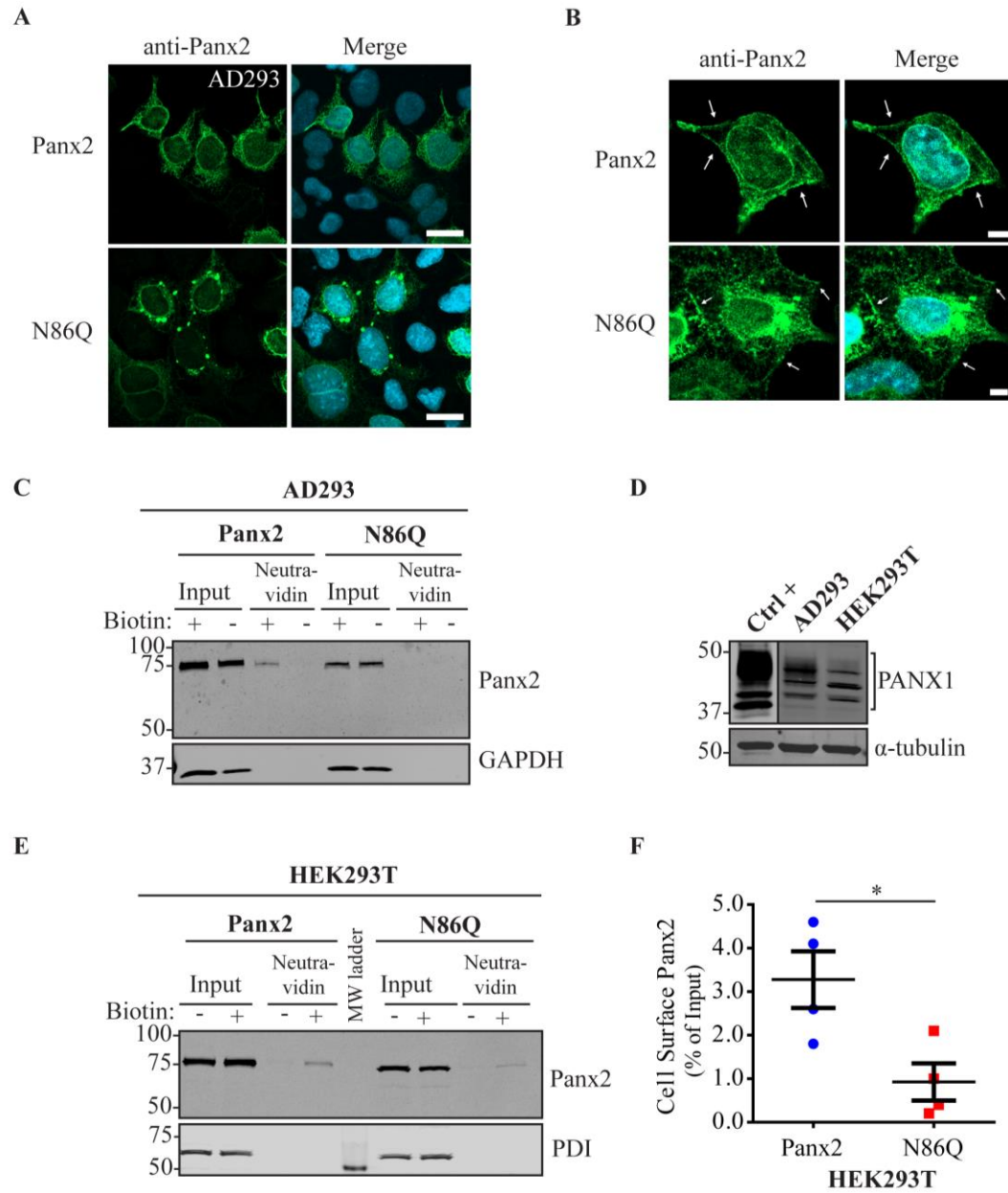
Figure 3-3.

Figure 3-3 Localization of PANX2 and N86Q in AD293 and HEK293T cells expressing endogenous PANX1.

(A) Immunolabeling of PANX2 and N86Q mutant (green) showed that both localize mostly intracellularly, but the N86Q mutant aggregates intracellularly in AD293 cells. Scale bars = 20 μm . (B) A subpopulation of AD293 cells displayed PANX2 localization at the cell surface, less evident with the N86Q mutant (indicated with white arrows) Scale bars = 5 μm . Nuclei (blue). (C) Cell Surface Biotinylation Assays on AD293 cells showed a weak detection of the PANX2 wildtype but not N86Q mutant in surface-labeled fractions. GAPDH was used as a control for biotin internalization. (D) Immunoblots of AD293 and HEK293T cells confirmed that both cell lines express endogenous PANX1. Overexpressed human PANX1 served as a positive control (Ctrl +), and endogenous α -tubulin was used as the loading control. Line dividing upper panel of PANX1 WB indicates differences in exposure of the same blot to better detect endogenous PANX1 compared to the overexpressed positive control. (E) Cell surface biotinylation experiments performed on HEK293T cells showed that overexpressed PANX2 and the mutant N86Q are detectable at the cell surface. Protein disulfide-isomerase (PDI) was used as a control for biotin internalization. (F) Densitometric analysis and quantification of cell surface biotinylation experiments performed in HEK293T cells revealed a significant reduction of N86Q cell surface detection compared to PANX2. Cell surface detection was calculated relative to the total protein in input lanes. Statistical significance was considered when $p < 0.05$ (* $p = 0.0286$, $N = 4$ independent experiments), Mann Whitney U test. Error bars denote mean \pm SEM Molecular weights are noted in kDa.

3.3.4 PANX2 and N86Q aggregates localize to the endoplasmic reticulum and Golgi apparatus

Because of the prominent intracellular localization of PANX2 and the mutant N86Q, we were interested in determining the subcellular compartments to which these proteins could be trafficking. We transiently overexpressed these proteins in AD293 cells and used immunolabeling with different organelle markers to assess their intracellular location by confocal microscopy (Figures 3-4 and 3-5).

As shown in Fig. 3-4A, PANX2 immunolabeling exhibits a broad cytoplasmic distribution highly overlapping (Pearson's Colocalization Coefficient (PCC)_{PANX2-PDI}= 0.49 ± 0.02 ; n=41, N=3) with the chaperone protein disulfide-isomerase (PDI), a known marker of the endoplasmic reticulum (ER). The mutant N86Q had significantly ($p < 0.0001$) less overlap (PCC_{N86Q-PDI}= 0.34 ± 0.03 , n=57, N=3) with PDI, although there was also a more punctate distribution of PDI that colocalized with N86Q. These observations suggest that N86Q is confined to some punctate regions enriched in PDI and other subcellular organelles. We also observed an apparent alteration of the ER morphology when N86Q was expressed.

Figure 3-4.

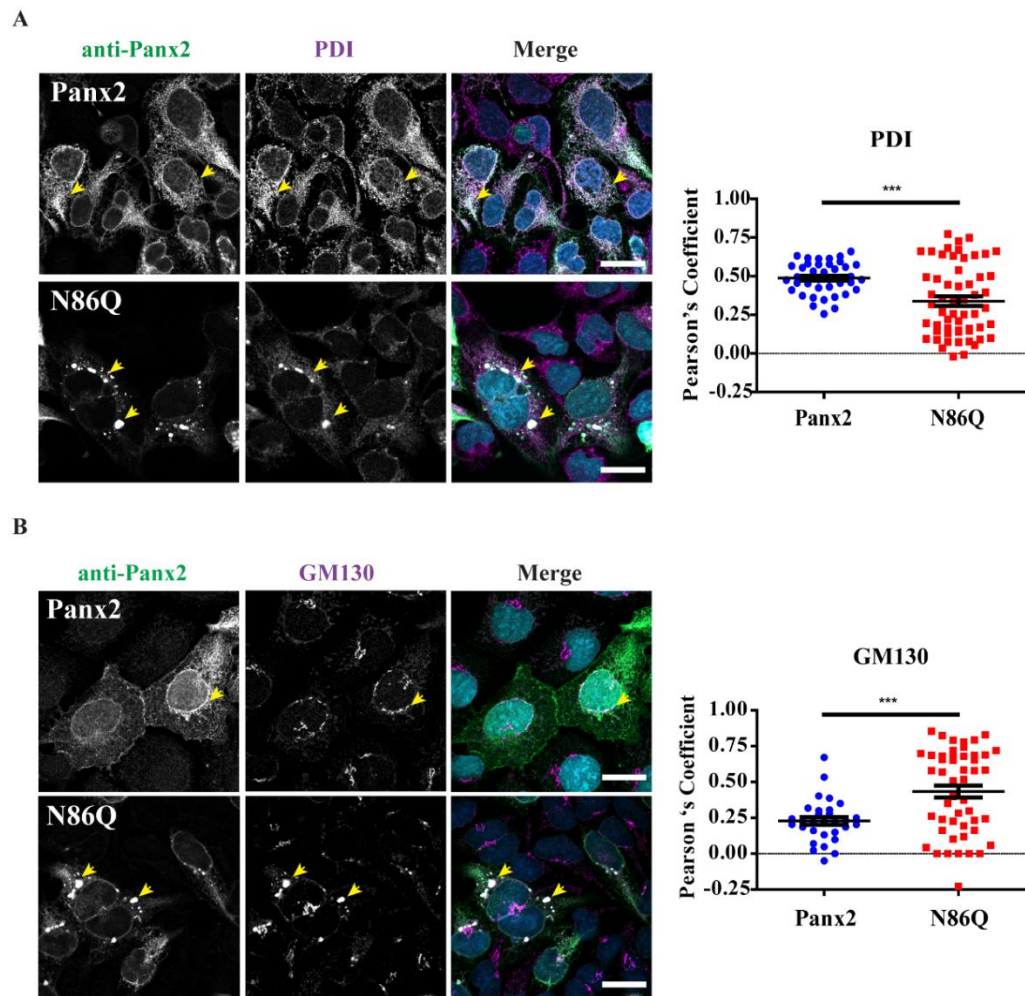
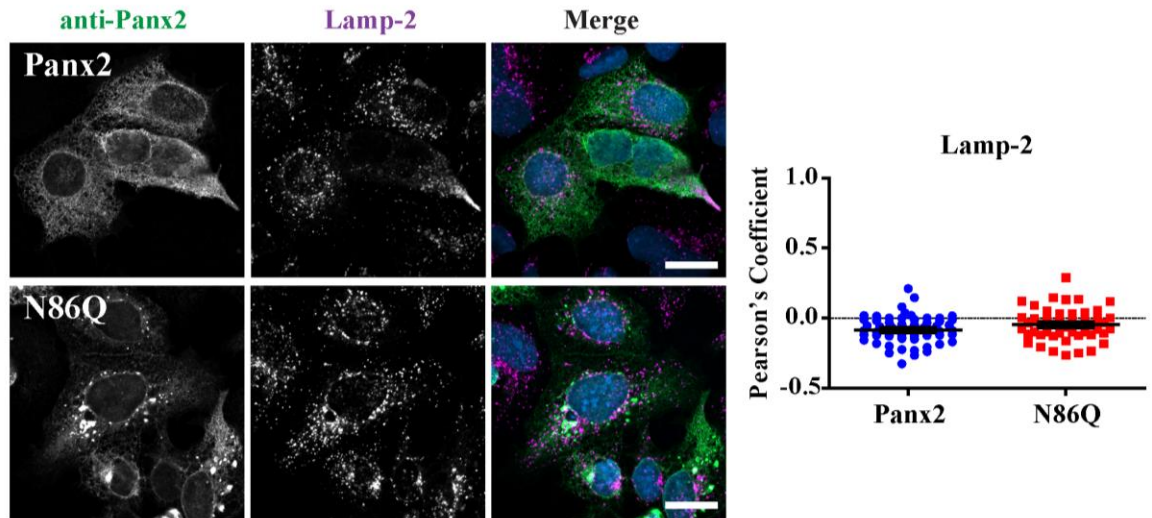


Figure 3-4 PANX2 and N86Q colocalize with markers of the endoplasmic reticulum and Golgi.

Representative confocal micrographs of PANX2 and N86Q ectopically expressed in AD293 cells. Co-immunolabeling with anti-PANX2 antibody (green) and organelle markers (magenta): (A) PDI, endoplasmic reticulum (ER); (B) GM-130, cis-Golgi matrix. PANX2 has a perinuclear localization and is spread intracellularly in the cytoplasm, partially colocalizing with endoplasmic reticulum and Golgi markers. N86Q aggregates also overlap with ER and Golgi markers and disrupt their distribution. Yellow arrowheads indicate representative regions of colocalization. Nuclei (blue) were counterstained with Hoechst 33342. Scale bars = 20 μm . Pearson Correlation Coefficients (right) were calculated for multiple regions of interest (ROI)s corresponding to double-labeled cells. Statistical significance was considered when $p < 0.05$ (***) $p < 0.0001$, $N = 3$ independent experiments), Unpaired two-tailed t-test with Welch's correction. Error bars denote mean \pm SEM.

Figure 3-5.

A



B

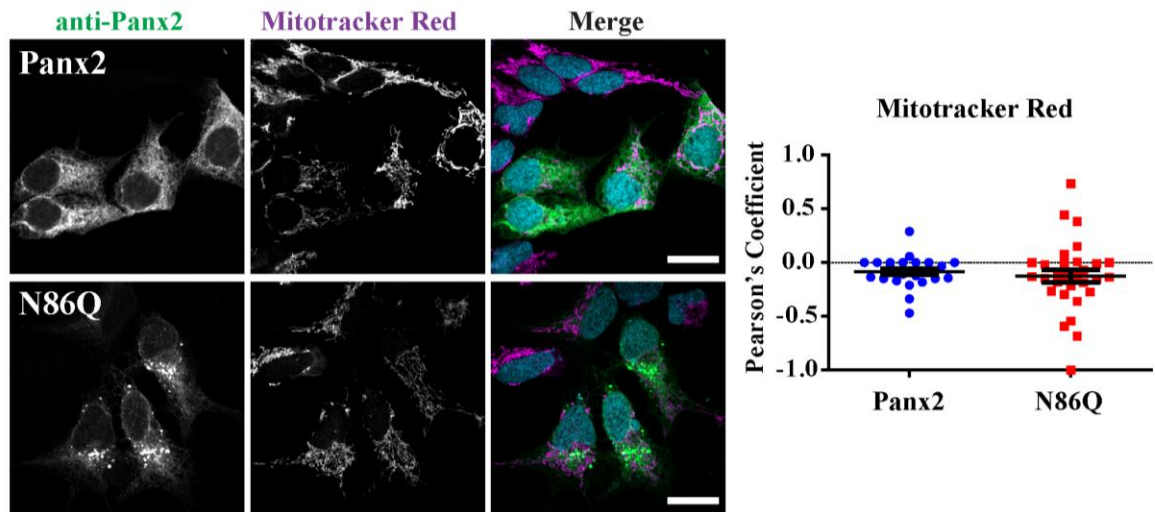


Figure 3-5 PANX2 and N86Q do not localize to late endosomes/lysosomes or mitochondria.

Confocal micrographs of PANX2 and N86Q ectopically expressed in AD293 cells. Co-immunolabeling with anti-PANX2 antibody (green) and organelle markers (magenta): (A) Lamp-2, lysosomes and late endosomes, and (B) Mitotracker® Red, mitochondria showed that neither PANX2 nor N86Q mutant exhibited significant overlap with the markers. Nuclei (blue) were counterstained with Hoechst 33342. Scale bars = 20 μm . Pearson Correlation Coefficients (right) were calculated for multiples ROIs corresponding to double-labeled cells. There was no statistical significance ($p > 0.05$, $N=3$, unpaired two-tailed t-test with Welch's correction) in the degree of colocalization between PANX2 and N86Q with the markers. Error bars denote mean \pm SEM.

Quantitation of colocalization with cis-Golgi marker, Golgi matrix protein 130 (GM130) (Fig. 3-4B) showed a significantly ($p=0.0001$) higher colocalization with N86Q mutant ($PCC_{N86Q-GM130}= 0.43 \pm 0.04$; $n=41$, $N=3$) than with PANX2 WT ($PCC_{PANX2-GM130}= 0.23 \pm 0.03$; $n=30$, $N=3$). In this case, cells that overexpressed PANX2 WT exhibited changes in the distribution of GM130 compared to un-transfected ones (seen in the same field of view, Fig. 3-4B). These changes were more pronounced in cells overexpressing the mutant N86Q, in which not only the cis-Golgi morphology changed, but GM130 also appeared to accumulate within N86Q aggregates.

On the other hand, lysosome-associated membrane protein 2 (LAMP-2) and the fixable and cell-permeant Mitotracker™ Red CMXRos were assayed to label lysosomes/late endosomes and active mitochondria, respectively (Fig. 3-5). We did not observe colocalization with LAMP-2 ($PCC_{PANX2-Lamp-2}= -0.08 \pm 0.01$; $n=59$, $N=3$; $PCC_{N86Q-Lamp-2}= -0.05 \pm 0.02$; $n=49$, $N=3$) or Mitotracker ($PCC_{PANX2-Mitotracker}= -0.08 \pm 0.03$; $n=25$, $N=3$; $PCC_{N86Q-Mitotracker}= -0.13 \pm 0.06$; $n=31$, $N=3$), and there was no difference in the distribution of both markers upon overexpression of PANX2 WT or N86Q.

3.3.5 PANX2 N-glycosylation is not required for the interaction with PANX1

Since PANX2 interacts only with the core non-glycosylated Gly0 and Gly1 species of PANX1 [22], we were interested in determining the outcome with the un-glycosylated species of PANX2. For these experiments, PANX1 was ectopically co-expressed with either PANX2 or non-glycosylated N86Q mutant in HEK293T cells. Using co-immunoprecipitation assays (co-IP, Fig. 3-6A), we observed that both PANX2 and N86Q could co-IP in a complex with PANX1 and occasionally, although not statistically significant ($p>0.05$, $N=4$) (Fig. 3-6B and C), N86Q pulled down more PANX1 than the WT PANX2. In addition, consistent with what was reported before by Penuela *et al.* (2009) [22], we noticed that only Gly0 and Gly1 PANX1 species interacted with both variants of PANX2.

Due to the lack of available antibodies from different species to perform double immunolabeling of both pannexins, we used C-terminal FLAG-tagged PANX2 and N86Q co-expressed with PANX1 in HEK293T cells. Confocal imaging of PANX2-FLAG or N86Q-FLAG coexpressed with PANX1 (Fig. 3-7A) showed that PANX2-FLAG exhibits intracellular and cell surface localization overlapping with PANX1 (see Linescan analysis on the right upper panel, Fig. 3-7A). N86Q-FLAG formed predominantly intracellular aggregates like its untagged counterpart (Fig. 3-3A); however, a small subpopulation of N86Q-FLAG could still be detected at the cell surface colocalizing with PANX1 (see Linescan analysis on the right bottom panel, Fig. 3-7B), but to a lesser degree than PANX2-FLAG. Taken together, these findings suggest that the glycosylation of PANX2 is not required for the interaction of PANX1/PANX2 but can determine the differential subcellular localization of glycosylated and un-glycosylated species, especially in the presence of PANX1.

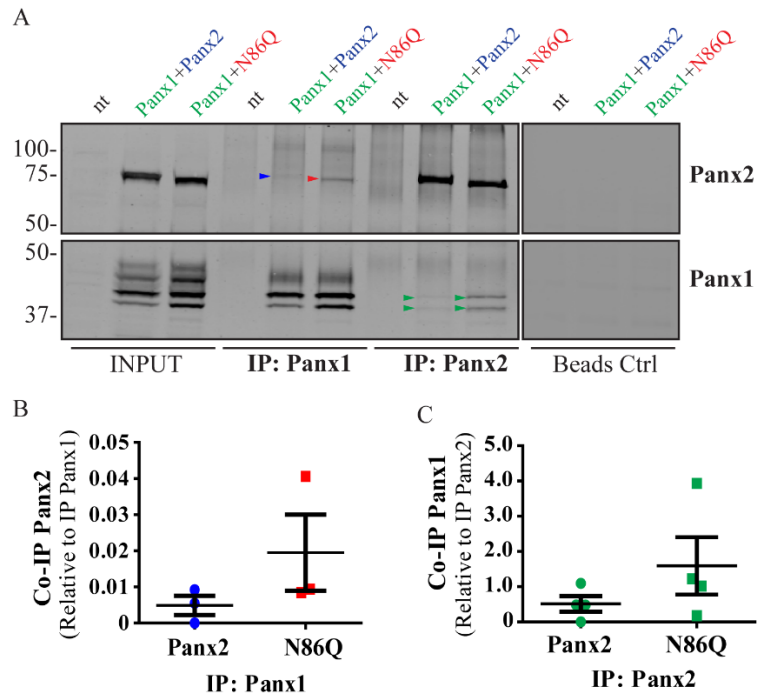
Figure 3-6.

Figure 3-6 PANX2 glycosylation is not required for the interaction and immunoprecipitation with PANX1.

(A) Reciprocal co-immunoprecipitation (co-IP) experiments showed that PANX2 and N86Q co-IP in a complex with overexpressed PANX1 in HEK293T cells. Colored arrowheads denote bands of co-IP proteins detected in WB. (B and C). Quantitative analysis (see Materials and Methods section 3.4.8) of co-IP shows that the interaction of N86Q with PANX1 is not significantly different ($p > 0.05$, $N=4$) than with PANX2, and in both cases, the complexes only involved the non- and lower- glycosylated species of PANX1 (Gly0 and Gly1). Beads Ctrl denote control IPs done in parallel without antibodies. Protein sizes in kDa.

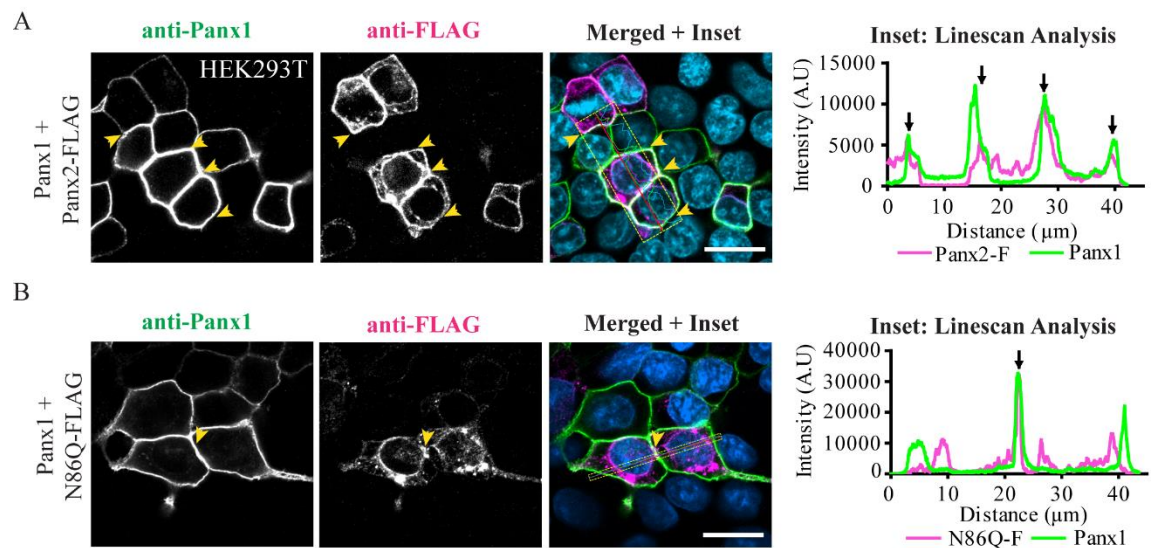
Figure 3-7.

Figure 3-7 N-glycosylation enhances PANX2 trafficking to the plasma membrane and colocalization with PANX1.

Confocal micrographs of PANX2-FLAG (A) and N86Q-FLAG (B) (both shown in magenta) ectopically co-expressed with mouse PANX1 (shown in green) in HEK293T cells. Seventy-two hours post-transfection, PANX2-FLAG partially colocalized with PANX1 at the cell membrane (black arrows in Linescan, panel A) with a subpopulation still in intracellular compartments. N86Q-FLAG formed intracellular aggregates and showed limited colocalization with PANX1 at the plasma membrane (Linescan, panel B). Yellow arrowheads denote regions of colocalization of PANX1 and FLAG labeling, also depicted with black arrows in the corresponding linescans. Insets: Linescans profiles showing regions of maximal colocalization of overlapping fluorescence peaks (black arrows). Nuclei (blue, Hoechst 33342). Scale bars = 20 μm.

3.4 Discussion

Pannexins are a family of channel proteins implicated in significant physiological and pathological functions, and most of the current research has been conducted to analyze their level of expression and distribution within mammalian tissues and their role in diverse diseases [35]. However, there is still a need to understand the biophysical properties of these channels and the different ways of regulation that prevent or promote detrimental effects of their exacerbated channel activity. Pannexins are N-glycosylated, and as integral membrane proteins, this modification seems essential in regulating their trafficking, as was demonstrated formerly for PANX1 and PANX3 [11, 22]. Unlike the other pannexins, PANX2 is modified only to Gly1 species, an early post-translational modification occurring in the ER lumen. This step is generally followed by further oligosaccharide editing in the Golgi apparatus to yield complex glycosylation. To date, there is no evidence showing further processing of PANX2 in Golgi, and only studies in PANX1 and PANX3 showed that trafficking of these two pannexins to the plasma membrane is mediated by Sar1-dependent COPII vesicles [36] with N-glycosylation affecting their final destination [11, 37, 38]. Thus, it is not surprising that N-glycosylation would regulate the route of PANX2 trafficking and localization and possibly its channel formation.

This study sought to determine the N-glycosylation site by generating a glycosylation-deficient mutant (N86Q) based on the predicted N-linked glycosylation site reported by Penuela *et al.* [22]. Our results showed that N86Q substitution generated a PANX2 mutant with a faster-migrating electrophoretic band than PANX2 WT, which does not shift after N-glycosidase digestion, confirming that N86 is the only N-glycosylation site for PANX2. In all the cell lines assayed (NRK, HEK293T, and AD293), we observed that overexpression of the PANX2 WT and N86Q constructs exhibited the same electrophoretic properties (Figures 3-2C and 3-3C).

Independently of the cell type used for ectopic expression, the N86Q mutant appeared to form punctate aggregates localized to intracellular compartments along with the ER-chaperone PDI and the cis-Golgi matrix marker GM130. Compared to the N-glycosylation-deficient mutants of PANX1 and PANX3 [11], un-glycosylated PANX2 exhibited an

exacerbated abnormal intracellular aggregation. This raises the possibility that the lack of N-glycosylation may have affected the proper protein folding of PANX2. We cannot rule out that the intracellular accumulation of N86Q could be an artifact of overexpression, which, concomitant with the lack of glycosylation, might have induced misfolding and ER-stress [39].

As mentioned earlier, PANX2 has been reported to be mostly intracellularly localized, but in some instances, it can also translocate to the plasma membrane [14, 17]. Interestingly, a previous report by Swayne *et al.* (2010) showed endogenous PANX2 expressed in postnatal murine hippocampal neural stem and progenitor cells (NPCs) and the mouse neuroblastoma (N2a) cell line, with immunoreactive species likely N-glycosylated and other of higher molecular weight, sensitive to de-palmitoylation. In that study, the authors showed that S-palmitoylated PANX2 species are likely not N-glycosylated and are predominantly distributed to the Golgi apparatus and ER in undifferentiated neurons [17]. However, hippocampal granule neurons and differentiated N2a cells expressed "un-palmitoylated" PANX2 species localized to the cell membrane with a shift to the expected electrophoretic migration of N-glycosylated and un-glycosylated species [17]. Although that study could not determine which glycosylated (or not) species were at the cell membrane, our results showed that it is possible for un- and N-glycosylated species to traffic to the cell membrane, especially when it is co-expressed with PANX1 (also known to be present in neurons). Therefore, N-glycosylation may be dispensable for PANX2 cell membrane trafficking but is certainly a regulator of the PANX2 intracellular sorting and its cell membrane expression.

Moreover, Swayne *et al.* (2010) showed that treatment with glycosidases had no significant effect on endogenous PANX2 electrophoretic mobility suggesting that they were un-glycosylated [17]. That study relied on antibody detection of endogenous PANX2, and the protein bands identified were of lower molecular weight than the predicted full-length PANX2 used in this study (677 aa, [40]). Further studies are needed to determine if the expression of certain un-glycosylated endogenous isoforms of PANX2 is cell-type specific and whether glycosylation has measurable effects on the PANX2 cellular function. To date,

there are no reports of mutations in the *PANX2* gene site encoding N86, but our results predict significant changes in *PANX2* behavior if its glycosylation is affected. It is also possible that the un-glycosylated form of *PANX2* may be preferentially expressed in some cells and tissues determining the primary function of the *PANX2* channel and its subcellular localization.

Our study showed significant intracellular subpopulations of *PANX2* likely localized in the ER and partially colocalized with the cis-Golgi marker. Interestingly, the overexpression of the N86Q mutant changed the distribution of PDI and GM130 compared to *PANX2* WT, suggesting that the formation of aggregates may disrupt the morphology of ER and cis-Golgi. GM-130 is a peripheral membrane protein in the *cis*-Golgi matrix that is important for maintaining Golgi structure [41] and regulating ER-to-Golgi transport of proteins and glycosylation [42]. Thus, the aggregation of N86Q may interfere with the protein transport from the ER, causing the accumulation of GM130.

Boyce *et al.* (2014) indicated that pannexins contain putative recognition sequences for endocytic and endo-lysosomal targeting, which could account for the control of pannexin trafficking. Interestingly, recently published work by Boassa *et al.* described the localization of a recombinant *PANX2* fused to mini-SOG tag that was transiently expressed in HeLa cells [26]. These authors used correlated light and electron microscopy imaging to detect *PANX2* localization at cytoplasmic protrusions. Also, immuno-colocalization in HEK293T cells using assorted vesicular markers displayed *PANX2* WT (untagged) localized to early or recycling endosomes rather than ER. However, they mentioned that when the ER marker calnexin was used, they detected colocalization with overexpressed *PANX2* in HEK293T cells. Our findings are consistent with these reports [24] since we found *PANX2* primarily in the ER (Fig. 3-4A). However, as others have reported, we did not find conclusive evidence of *PANX2* in endo-lysosome compartments (Fig. 3-5A) [25, 26]. Based on our results, *PANX2* may have an intracellular channel function in the ER, similar to the proposed calcium-leak channels formed by *PANX1* and *PANX3* [6].

In some instances, *PANX2* distribution exhibited limited cell surface localization that was more apparent when higher endogenous or ectopic *PANX1* protein was expressed in the

studied cell lines. This is consistent with our previous observation of increased PANX2 at the cell surface when co-expressed with PANX1 under overexpression conditions [22]. Herein, we used three different cell lines with varying endogenous PANX1 levels and different protein production capacities. We noticed that in cells with low endogenous PANX1 (e.g., NRKs), there was barely any PANX2 at the cell surface based on immunolabeling and cell surface biotinylation pull-downs. In AD293 and HEK293T cells, it was possible to detect low levels of overexpressed PANX2 at the cell surface, while the mutant PANX2 (N86Q) had a detectable but significantly decreased presence only at the cell membrane of HEK293T cells. This result could be attributed to the increased protein expression in HEK293T cells that contains the SV40 T-antigen and have high transfection efficiency. This feature might have allowed the overexpressed PANX2 to bypass protein quality control mechanisms resulting in more PANX2 trafficking to the plasma membrane [43].

Further research is needed to evaluate N-glycosylation of endogenous PANX2 and examine if PANX2 can form channels at the plasma membrane under physiological conditions. To date, limited studies have attempted to evaluate PANX2 channel function [14, 15], and several factors make it challenging to test PANX2 channel activity, such as its intracellular localization, the lack of evidence of *in vivo* functional channel formation [27], and the unknown mechanisms of activation [14].

Work done by Bruzzone *et al.* [15] showed that PANX1 and PANX2 were abundantly expressed in the CNS, and co-injection of both pannexin RNAs in paired *Xenopus* oocytes resulted in the formation of heteromeric channels with functional characteristics different from those formed by PANX1 monomers but with similar pharmacological sensitivity [27]. Ambrosi *et al.* [14] suggested that PANX1/PANX2 heteromeric channels tend to be unstable, and they attributed that to differences in monomer size and oligomeric symmetry between these two pannexins. We have previously shown that PANX1 and PANX2 do form a complex as determined by co-IP experiments. Interestingly, when both pannexins are co-expressed, the level of interaction between PANX2 and glycosylated species of PANX1 depends on the latter's glycosylation [22]. Here, we showed *in vitro* that the

PANX2 glycosylation-deficient mutant could readily form complexes with PANX1; thus, PANX2 glycosylation is not required to intermix the two pannexins. Although it was not statistically significant, N86Q seemed to pull down PANX1 more efficiently than WT PANX2. However, in confocal images, the N86Q aggregates did not show higher overlap with PANX1-immunolabeling than PANX2 WT. Consistent with our previous report [22], complex N-glycosylation of PANX1 hinders their interaction since PANX2 and N86Q interacted only with the Gly0 and Gly1 forms of PANX1.

3.5 Conclusions

Finally, we conclude that PANX2 glycosylation is not required for PANX1/PANX2 intermixing but assists the cell surface localization of PANX2, which is also increased by the presence of PANX1. In cells where both pannexins are co-expressed, glycosylation may act as a mechanism of regulation defining whether these channels will serve as intracellular or plasma membrane channels with different physiological and pathological functions.

3.6 Acknowledgments

This work and the cost of publication were funded by the Natural Sciences and Engineering Research Council of Canada with an NSERC Discovery Grant to Dr. Silvia Penuela.

3.7 References

1. Sosinsky, G.E., et al., *Pannexin channels are not gap junction hemichannels*. Channels (Austin), 2011. **5**(3): p. 193-7.
2. Panchin, Y., et al., *A ubiquitous family of putative gap junction molecules*. Curr Biol, 2000. **10**(13): p. R473-4.
3. Bao, L., S. Locovei, and G. Dahl, *Pannexin membrane channels are mechanosensitive conduits for ATP*. FEBS Letters, 2004. **572**: p. 65-68.
4. Iwamoto, T., et al., *Pannexin 3 regulates intracellular ATP/cAMP levels and promotes chondrocyte differentiation*. J Biol Chem, 2010. **285**(24): p. 18948-58.
5. Ishikawa, M., et al., *Pannexin 3 functions as an ER Ca(2+) channel, hemichannel, and gap junction to promote osteoblast differentiation*. J Cell Biol, 2011. **193**(7): p. 1257-74.

6. Vanden Abeele, F., et al., *Functional implications of calcium permeability of the channel formed by pannexin 1*. Journal of Cell Biology, 2006. **174**: p. 535-546.
7. Thompson, R.J., *Pannexin channels and ischaemia*. J Physiol, 2015. **593**(16): p. 3463-70.
8. Pelegrin, P. and A. Surprenant, *Pannexin-1 couples to maitotoxin- and nigericin-induced interleukin-1beta release through a dye uptake-independent pathway*. J Biol Chem, 2007. **282**(4): p. 2386-94.
9. Baranova, A., et al., *The mammalian pannexin family is homologous to the invertebrate innexin gap junction proteins*. Genomics, 2004. **83**: p. 706-716.
10. Le Vasseur, M., et al., *Pannexin 2 protein expression is not restricted to the CNS*. Front Cell Neurosci, 2014. **8**: p. 392.
11. Penuela, S., et al., *Pannexin 1 and pannexin 3 are glycoproteins that exhibit many distinct characteristics from the connexin family of gap junction proteins*. Journal of Cell Science, 2007. **120**: p. 3772-3783.
12. Celetti, S.J., et al., *Implications of pannexin 1 and pannexin 3 for keratinocyte differentiation*. J Cell Sci, 2010. **123**(Pt 8): p. 1363-72.
13. Bond, S.R., et al., *Pannexin 3 is a novel target for Runx2, expressed by osteoblasts and mature growth plate chondrocytes*. J Bone Miner Res, 2011. **26**(12): p. 2911-22.
14. Ambrosi, C., et al., *Pannexin1 and Pannexin2 channels show quaternary similarities to connexons and different oligomerization numbers from each other*. J Biol Chem, 2010. **285**(32): p. 24420-31.
15. Bruzzone, R., et al., *Pannexins, a family of gap junction proteins expressed in brain*. Proc Natl Acad Sci U S A, 2003. **100**(23): p. 13644-9.
16. Vogt, A., S.G. Hormuzdi, and H. Monyer, *Pannexin1 and Pannexin2 expression in the developing and mature rat brain*. Brain Res Mol Brain Res, 2005. **141**(1): p. 113-20.
17. Swayne, L.A., C.D. Sorbara, and S.A. Bennett, *Pannexin 2 is expressed by postnatal hippocampal neural progenitors and modulates neuronal commitment*. J Biol Chem, 2010. **285**(32): p. 24977-86.
18. Swayne, L.A. and S.A. Bennett, *Connexins and pannexins in neuronal development and adult neurogenesis*. BMC Cell Biol, 2016. **17 Suppl 1**: p. 10.
19. Bargiotas, P., et al., *Functional outcome of pannexin-deficient mice after cerebral ischemia*. Channels (Austin), 2012. **6**(6): p. 453-6.
20. Blom, N., et al., *Prediction of post-translational glycosylation and phosphorylation of proteins from the amino acid sequence*. Proteomics, 2004. **4**(6): p. 1633-49.
21. Penuela, S., et al., *Diverse post-translational modifications of the pannexin family of channel-forming proteins*. Channels (Austin, Tex.), 2014. **8**: p. 124-30.

22. Penuela, S., et al., *Glycosylation regulates pannexin intermixing and cellular localization*. Molecular Biology of the Cell, 2009. **20**: p. 4313-23.
23. Zappalà, A., et al., *Expression of pannexin2 protein in healthy and ischemized brain of adult rats*. Neuroscience, 2007. **148**: p. 653-67.
24. Lai, C.P.K., J.F. Bechberger, and C.C. Naus, *Pannexin2 as a novel growth regulator in C6 glioma cells*. Oncogene, 2009. **28**: p. 4402-4408.
25. Wicki-Stordeur, L.E., A.K.J. Boyce, and L.A. Swayne, *Analysis of a pannexin 2-pannexin 1 chimeric protein supports divergent roles for pannexin C-termini in cellular localization*. Cell Communication & Adhesion, 2013. **20**: p. 73-9.
26. Boassa, D., et al., *Pannexin2 oligomers localize in the membranes of endosomal vesicles in mammalian cells while Pannexin1 channels traffic to the plasma membrane*. Frontiers in Cellular Neuroscience, 2015. **8**: p. 15.
27. Bruzzone, R., et al., *Pharmacological properties of homomeric and heteromeric pannexin hemichannels expressed in Xenopus oocytes*. J Neurochem, 2005. **92**(5): p. 1033-43.
28. Bruzzone, R. and R. Dermietzel, *Structure and function of gap junctions in the developing brain*. Cell Tissue Res, 2006. **326**(2): p. 239-48.
29. Dvorientchikova, G., et al., *Expression of pannexin family of proteins in the retina*. FEBS Lett, 2006. **580**(9): p. 2178-82.
30. Tang, W., et al., *Pannexins are new molecular candidates for assembling gap junctions in the cochlea*. Neuroreport, 2008. **19**(13): p. 1253-7.
31. Bargiotas, P., et al., *Pannexins in ischemia-induced neurodegeneration*. Proceedings of the National Academy of Sciences of the United States of America, 2011. **108**: p. 20772-7.
32. Penuela, S., et al., *Diverse subcellular distribution profiles of pannexin 1 and pannexin 3*. Cell Commun Adhes, 2008. **15**(1): p. 133-42.
33. Penuela, S., et al., *Diverse post-translational modifications of the pannexin family of channel-forming proteins*. Channels (Austin), 2014. **8**(2): p. 124-30.
34. DuBridg, R.B., et al., *Analysis of mutation in human cells by using an Epstein-Barr virus shuttle system*. Mol Cell Biol, 1987. **7**(1): p. 379-87.
35. Penuela, S., et al., *Pannexin channels and their links to human disease*. Biochem J, 2014. **461**(3): p. 371-81.
36. Bhalla-Gehi, R., et al., *Pannexin1 and pannexin3 delivery, cell surface dynamics, and cytoskeletal interactions*. J Biol Chem, 2010. **285**(12): p. 9147-60.
37. Boassa, D., et al., *Pannexin1 channels contain a glycosylation site that targets the hexamer to the plasma membrane*. Journal of Biological Chemistry, 2007. **282**: p. 31733-31743.

38. Boassa, D., et al., *Trafficking dynamics of glycosylated pannexin 1 proteins*. Cell Commun Adhes, 2008. **15**(1): p. 119-32.
39. Hiramatsu, N., V.T. Joseph, and J.H. Lin, *Monitoring and manipulating mammalian unfolded protein response*. Methods in enzymology, 2011. **491**: p. 183-98.
40. Penuela, S. and D.W. Laird, *The cellular life of pannexins*. Wiley Interdisciplinary Reviews: Membrane Transport and Signaling, 2012. **1**(5): p. 621-632.
41. Nakamura, N., et al., *Characterization of a cis-Golgi matrix protein, GM130*. J Cell Biol, 1995. **131**(6 Pt 2): p. 1715-26.
42. Nakamura, N., *Emerging new roles of GM130, a cis-Golgi matrix protein, in higher order cell functions*. J Pharmacol Sci, 2010. **112**(3): p. 255-64.
43. Chen, B., et al., *Cellular strategies of protein quality control*. Cold Spring Harb Perspect Biol, 2011. **3**(8): p. a004374.

Chapter 4

PANX1 regulates immune cell recruitment, is implicated in tissue inflammation and plays pro-tumorigenic roles in melanoma cells. Although genetic or pharmacological inhibition of PANX1 decreases tumorigenic properties of mouse and human melanoma cells *in vitro* and *ex vivo*, studies assessing its function on *in vivo* melanoma tumor formation and immune cell infiltration are lacking. In this chapter, we used an inducible mouse model of melanoma with a *Panx1* global deletion to evaluate tumor progression and immune cell infiltration compared to the corresponding wildtype controls.

4 Global Pannexin 1 deletion increases tumor-infiltrating lymphocytes in the BRAF(V600E)/Pten(del) mouse melanoma model

4.1 Introduction

Malignant melanoma is a type of skin cancer that develops from melanocytes and becomes a life-threatening disease when it spreads to various organs [1]. Depending on the diagnosis and the mutational landscape of the tumor biopsies (e.g., *BRAF* mutation status), targeted therapy with mutant kinase inhibitors or immunotherapies with monoclonal antibodies against immune checkpoint inhibitors are currently being used for melanoma treatment. The use of immune checkpoint inhibitors enhances anti-tumoral T cell-mediated immune responses, but unfortunately, about ~60% of melanoma patients do not respond to this type of therapy [2-4]. Regardless of the treatment options, their effectiveness is usually dampened due to the insufficient effector activity of tumor-infiltrating lymphocytes (TILs) [5], recurrence, and development of multiple resistance mechanisms [6, 7]; therefore, innovative therapy concepts are still warranted.

Pannexin1 (PANX1) is a channel-forming membrane glycoprotein that mediates the passage of nucleotides, ions, and other metabolites involved in intercellular communication [8]. We have previously demonstrated that PANX1 expression correlates with tumor cell aggressiveness in isogenic mouse melanoma cell lines, and its knockdown reduces melanoma tumor size and metastasis to the liver in chick chorioallantoic membrane (CAM) xenografts [9]. More recently, we showed that PANX1 is highly expressed in human melanomas, and genetic or pharmacological PANX1-targeting decreases the tumorigenic properties of melanoma cells [10]. Mechanistically, we have recently demonstrated that PANX1 regulates melanoma cell growth and metabolism through direct interaction with β -catenin and modulation of the Wnt signaling pathway [11]. Considering all these findings, PANX1 has become an attractive target for preclinical melanoma research, but it is still unclear whether genetic silencing of the *Panx1* mouse gene would impact melanoma development *in vivo*.

In addition, PANX1 influences the inflammatory response [12-17] and is expressed in different subtypes of immune cells like macrophages and lymphocytes [12, 18, 19]. Previous evidence shows that PANX1-mediated adenosine-5'-triphosphate (ATP) permeability enables activation and functional enhancement of T cells [16, 17]. On the other hand, the release of ATP through caspase cleaved PANX1 channels in apoptotic leukemic lymphocytes has been shown to induce the recruitment of inflammatory cells (e.g., monocytes)[12]. Paradoxically, the caspase-dependent PANX1 channel opening in dying macrophages and lymphocytes releases other metabolites that suppress, *in vivo*, proinflammatory signals of myeloid cells in the surrounding tissue [8]. Considering the broad PANX1 expression in different cell types present in the tumor microenvironment (TME), no studies have specifically addressed yet whether PANX1 modulates tumoral recruitment of immune cells that are critical players in the TME and targets of the current immunotherapies [13].

Previous characterization of a constitutive global *Panx1* knockout mouse (*Panx1*^{-/-}, *Panx1*KO)(developed by Genentech) [15] demonstrated that mice are viable, and no overt phenotypes were detected on *Panx1*^{-/-} mice by histological and pathological examinations. However, due to *Panx1* expression in the skin [9, 20], our group used the same *Panx1*^{-/-} mouse strain to characterize skin in normal and pathological conditions (e.g., wound healing) and demonstrated differences in dorsal skin thickness and delayed wound healing [9, 20]. These observations indicated an essential role of PANX1 in keratinocyte and dermal fibroblast differentiation and wound repair in the skin. However, melanocytes are also known to express low levels of PANX1 that become upregulated in mouse melanoma cells [9]. The combination of this *Panx1*^{-/-} mouse line with a cancer model had not been tested yet, and in the case of cutaneous melanoma, this approach may offer new insights into the roles of PANX1 in the context of this cancer and its immune infiltration, which could be useful for testing future therapeutic interventions.

In this work, we crossed a global *Panx1*^{-/-} mouse strain with the inducible melanoma model *BRaf*^{CA/+}, *Pten*^{LoxP/LoxP}, *Tyr::CreER*^{T2} (abbreviated as BPC) mice that harbors two oncogenic driver mutations found in human melanomas [21-23]. Furthermore, due to the

role of PANX1 in regulating tumor growth and in various aspects of the immune response [12-17], we sought to evaluate the effects of the *Panx1* germline deletion on *in vivo* melanoma progression and the tumor immune infiltration of a hybrid mouse model.

Our results showed that *Panx1* global deletion did not reduce *in vivo* BRAF/Pten-driven melanoma progression but increased the tumor infiltration of effector immune T cell populations and Granzyme B⁺ cells. Besides, the expression of early T cell activation marker CD69, the LAG-3 checkpoint receptor or PD-L1 in the tumors was similar among genotypes, indicating that *Panx1* germline deletion may not influence the T cell immune activation or immunosuppressive mechanisms through T cell exhaustion and immune checkpoint regulators. This study also showed that female PANX1-deficient BPC mice might have significant changes in their immune phenotype with increased spleen size compared to their male counterparts. Future preclinical work targeting PANX1 in melanoma may increase the incidence of effector T-lymphocytes in the tumors and improve the response to immunotherapies using immune checkpoint inhibitors.

4.2 Materials and Methods

4.2.1 Mouse breeding and genotyping

C57BL/6, Tyr::CreER^{T2}; Brat^{CA/+}; Pten^{LoxP/LoxP} (BPC) mice were obtained from Jackson Laboratory, (Stock # 013590). Mice were kept on a 12:12 h light:dark cycle with normal chow and water available *ab libitum*. For deletion of *Panx1*, BPC mice were crossed with the previously characterized global *Panx1*^{-/-} mice in a C57BL/6N background strain [15, 20] (Genentech Inc., San Francisco, CA). Genotyping was performed on genomic DNA derived from the toes using PCR as described in [21].

4.2.2 Melanoma tumor induction, monitoring, and sample collection

All experiments performed on the mice were approved by the Animal Care Committee of the University Council on Animal Care at the University of Western Ontario, London ON, Canada (UWO AUP# 2019-070). 3–4-weeks-old BPC mice were used for tumor induction experiments: *Panx1*^{+/+} (7 females and 8 males) and *Panx1*^{-/-} (9 females and 4 males). Cutaneous melanomas were induced with topical application of 4-hydroxytamoxifen (4-

HT) (Sigma) on the skin of the lower back as per protocol in [21]. Mouse body weight and tumor dimensions were monitored every 3–4 days as soon as the tumors were visible for up to 4 months. Measurements were done with a digital caliper, and tumor volume was calculated using the modified ellipsoid formula $V = (W(\times 2) \times L)/2$, where V is tumor volume, L and W are the longest (length) and shortest (width) tumor diameters, respectively. The endpoint was considered when the tumor volume (or total combined tumor volume, in case of multiple tumors per animal) reached 2.0 cm^3 , or tumors showed signs of heavy ulceration, or the animals had poor body condition. Euthanasia was carried out using carbon dioxide asphyxiation followed by cervical dislocation. The spleens were weighed and measured using a ruler. Draining inguinal lymph nodes compromised with pigmented lesions were classified as metastatic sites and counted per mouse. All the collected tissue samples were fixed overnight with Periodate-Lysine-Paraformaldehyde (PLP) fixative or flash-frozen in liquid nitrogen and stored at $-80 \text{ }^\circ\text{C}$ until processing for RNA extraction.

4.2.3 Tissue Processing, RNA Extraction, real time-qPCR

Frozen tissues/tumor samples were ground in liquid nitrogen with a mortar and pestle and then used for RNA extraction. Total RNA was extracted using TRIzol™ Reagent (Invitrogen) according to the manufacturer's protocol and purified using the RNAeasy® Plus Mini kit (Qiagen). RNA concentration was determined using an Epoch Microplate Spectrophotometer (BioTek®). cDNA was generated using the High Capacity cDNA Synthesis Kit (Thermo Fisher Scientific; REF 4368814) in a T100™ Thermal Cycler (Bio-Rad). SYBR®Green Real-Time PCR Master Mix (Bio-Rad) was used along with the primers listed in Table 4-1, where mouse *gapdh* and *18S* were the housekeeping gene controls. Real-time qPCR was performed in a CFX96 Touch™ Real-Time PCR Detection System (Bio-Rad). All the assays involved at least three technical replicates ($n=3$), and the relative mRNA expression analysis was determined using the $\Delta\Delta\text{Ct}$ method calculated in the Bio-rad CFX Maestro Software, ver 1.1 (Bio-rad). Between assays, a non-tamoxifen treated skin BPC-*Panx1*^{+/+} sample was used as the control for interplate variation.

Table 4-1. List of primers used for real-time qPCR analysis

Target gene	Forward primer (5'-3')	Reverse primer (5'-3')
<i>Panx1</i>	ACAGGCTGCCTTTGTGGATTCA	GGGCAGGTACAGGAGTATG
<i>S100a1</i>	CCATGGAGACCCTCATCAAT	TTCTGGACATCCAGGAAGC
<i>CD3ε</i>	ATGCGGTGGAACACTTTCTGG	GCACGTCAACTCTACACTGGT
<i>CD4</i>	GCGAGAGTTCCCAGAAGAAG	AAACGATCAAACCTGCGAAGG
<i>CD8β1</i>	AAGAAGCAATGCCCGTTCC	TGAGGGTGGTAAGGCTGCA
<i>Ptpnc1(CD45)</i>	ATGGTCCTCTGAATAAAGCCCA	TCAGCACTATTGGTAGGCTCC
<i>FoxP3</i>	TTGCCAAGCTGGAAGACTGC	CAGACGGTGCCACCATGACT
<i>ncr1</i>	TGTTGAGAACAGCAGCCTTG	AGGATTATGCATGCCAGACC
<i>Adgre1(F4/80)</i>	CTTTGGCTATGGGCTTCCAGTC	GCAAGGAGGACAGAGTTTATCGTG
<i>CD69*</i>	GGGCTGTGTTAATAGTGGTCCTC	CTTGCAGGTAGCAACATGGTGG
<i>LAG-3*</i>	CTCCATCACGTACAACCTCAAGG	GGAGTCCACTTGGCAATGAGCA
<i>PD-L1*</i>	TGCGGACTACAAGCGAATCACG	CTCAGCTTCTGGATAACCCTCG
<i>IL-1β*</i>	TGGACCTTCCAGGATGAGGACA	GTTCATCTCGGAGCCTGTAGTG
<i>gapdh</i>	TGTGTCCGTCGTGGATCTGA	TTGCTGTTGAAGTCGCAGGAG
<i>18s</i>	CGGACAGGATTGACAGATTG	CAAATCGCTCCACCAACTAA

* qSTAR qPCR mouse primer pairs from OriGene Technologies Inc., Rockville, MD, USA, CD69 (Cat.# MP201944); Lag-3 (Cat.# MP207670); PD-L1 (Cat.# MP201906); IL-1b (Cat.# MP206724)

4.2.4 Tissue preparation, cryo-sectioning, and immunofluorescence staining

Tumor tissues samples that were fixed in PLP (1% PFA, 0.1 M L-Lysine, 0.01 M sodium periodate) overnight at 4°C were washed three times for 5 mins in phosphate buffer (0.075 M sodium phosphate dibasic and 0.025 M sodium phosphate monobasic) and incubated sequentially in 10%, 20% and 30% sucrose phosphate solutions, each overnight at 4°C. Tumors were then embedded and frozen in Fisher Healthcare™ Tissue-Plus™ O.C.T. Compound (Fisher Scientific Cat.# 23-730-571) and stored at -80 °C until sectioning. Eight-micron-thick serial cryostat sections were immuno-stained with the fluorescent-conjugated antibodies diluted in 1% BSA, 0.1% Tween-20 and 5% rat blocking buffer. Counterstaining was done with 10 µg/mL of Hoechst 33342 (Life Technologies Ref.# H3570) for 7 min, at room temperature. Sections were mounted with ProLong™ Gold Antifade Mountant (ThermoFisher Cat. # P10144).

4.2.5 Antibodies used for immunofluorescence

Alexa Fluor® 647 anti-mouse CD4 (clone RM4-5) and Alexa Fluor® 647 anti-mouse CD8a (clone 53-6.7) (BioLegend, USA, Cat.#: 100530 and 100727, respectively) were used for immunofluorescence at a final concentration of 2.5 µg/mL, and eFluor 660 anti-mouse FOXP3 (clone FJK-16s) eBioscience™ (ThermoFisher Scientific, Cat.# 50-5773-80) was used at 1 µg/mL. As controls for staining specificity, the eFluor 660 rat IgG2a kappa Isotype Control (eBR2a) (eBioscience™, ThermoFisher Sci., Cat. # 50-4321-80) and Alexa Fluor® 647 Rat IgG2a, κ Isotype Ctrl (BioLegend, USA, Cat. #: 400526) were used at the same dilution of their corresponding conjugated antibodies. Granzyme B (clone D2H2F) rabbit mAb (Cell Signaling Cat. # 17215S), and rabbit Anti-Ki67 antibody (ab833) were used at 1:200 dilution. Secondary antibodies goat anti-rabbit AF488 (Life technologies) and Texas Red (ThermoFisher Cat. # T6391) were used at 1:500 dilution in blocking buffer.

4.2.6 Image acquisition and analysis

Tile-scan imaging of whole tumor sections (20×) was acquired using an ORCA-flash4.0 LT plus (Model C11440) Hamamatsu digital camera with DAPI and Cy5 filters in an

Eclipse Ni-E Fluorescence Microscope (Nikon) using an S Plan Fluor ELWD 20x Ph1 ADM objective N/A 0.45 and refractive index of 1. Granzyme B imaging was performed in an LSM 800 Confocal Microscope (Carl Zeiss) using a Plan-Apochromat LCI Plan-Neofluar 25x/0.8 Imm Korr Water DIC objective for tiles or 63x/1.40 Oil DIC objective (Zeiss). For the images acquired with Nikon Fluorescence microscope, the noise component was removed with Denoise. AI utility, and the fluorescence background was subtracted in NIS-Elements Advanced Research Analysis software (ver. 5.21.02, Nikon). Separated tile images per channel were converted to binary images, and automated image analysis was performed using Cell Profiler Software (ver. 4.0.7, Broad Institute MIT)[24], using a custom pipeline to determine the percent of nuclei (cells) with positive immunostaining for the marker over the total number of cells normalized to the area of the field of view. At least two serial cryosections per tumor were used for quantification.

4.2.7 Statistical analysis

All the statistical analyses were performed using GraphPad Prism® ver. 8 (San Diego, CA, USA). Unless otherwise indicated, the results are expressed as the mean \pm standard deviation (SD), and the biological (N) and technical replicates (n) for a given experiment are indicated in each figure. Animal numbers were estimated by *a priori* power analysis (G*Power ver.3.1 [25]) based on a pilot study using spontaneous tumor incidence data comparing BPC-*Panx1*^{+/-} (heterozygous) vs. BPC-*Panx1*^{-/-}, with an effect size of 1.0 and a power of 0.8. For multiple comparisons involving the genotype and sex of mice, two-way ANOVA was performed, followed by a Tukey-Kramer *post hoc* test for unequal sample sizes. For real-time qPCR data, log₂ (Relative Normalized expression) was used for statistical comparisons. One-way ANOVAs followed by a Sidak's *post hoc* test were done to analyze relevant preplanned multiple mean comparisons in the mRNA expression between tissues (skin vs. tumor) within the same genotype and among mouse genotypes (BPC-*Panx1*^{+/+} vs. BPC-*Panx1*^{-/-}) within the same tissue type. Outliers were removed using the ROUT method with a False Discovery Rate of less than 1%, and normality was verified with the D'Agostino-Pearson test. Immunofluorescence (IF) quantification data were obtained from individual tumors of four different mice (at least N=3) per genotype and

analyzed with a two-tailed non-parametric Mann-Whitney test. Statistical significance was considered when $p < 0.05$.

4.3 Results

4.3.1 *Panx1* global-deletion does not affect primary tumor characteristics or melanoma progression of *Braf*(V600E)/*Pten*(del) mice

To explore the *in vivo* effects of the *Panx1* global deletion on melanoma progression, we crossed *BRaf*^{CA/+}, *Pten*^{LoxP/Loxp}, *Tyr::CreER*^{T2} (BPC) mice with the global *Panx1* knockout (*Panx1*^{-/-}, *Panx1*KO) mouse line, reported on [15, 21]. In the BPC model, a 4-hydroxytamoxifen (4-HT)-inducible Cre recombinase is used for the melanocyte-specific expression of mutant *BRAF*^{V600E}—a constitutively active protein serine kinase—and inactivation of the *Pten* phosphatase to produce primary cutaneous malignant melanomas (11). However, as in (23), we observed that spontaneous melanomas occurred in approximately 70% of the BPC colony in the absence of tamoxifen exposure. Thus, we started the 4-HT induction experiments in mice between 3–4 weeks of age that looked healthy and had no spontaneous melanoma formation.

Our results showed that regardless of the *Panx1* genotype, melanocytic pigmented lesions arose from the skin and quickly grew to form cutaneous melanomas as early as three weeks after topical application of 4-HT. Furthermore, although we applied 4-HT to a small zone in the dorsal skin of the lower back, we found that, in both animal groups, multiple tumor lesions grew not only in the application region but also in distant sites (Fig. 4-1A). As a result, all the visible melanoma lesions found in the dorsal and ventral/lateral skin of the animals were considered to determine tumor burden (Fig. 4-1B) and endpoint conditions. Overall, we observed that BPC-*Panx1*^{-/-} mice had similar tumor incidence (Fig. 4-1B), survival (Fig. 4-1C), and mouse weight among sexes (Fig.4-1D) compared to *Panx1*-wildtype counterparts. However, although the total combined tumor growth over time (Fig.4-1E) was similar between genotypes, two-way ANOVA statistical analysis in estimated tumor growth parameters (Fig.4-1F and G) showed that the sex of the mouse might influence melanoma tumor growth in BPC-*Panx1*^{+/+} mice. BPC-*Panx1*-wildtype male mice had a slightly lower (though not significant) tumor growth rate (Fig.4-1G, two-

way ANOVA, Sex factor: $F_{1,23} = 4.64$, $p < .05$) and a significant increase ($p = 0.188$) in tumor doubling time (Fig. 1F, two-way ANOVA, Sex factor: $F_{1,23} = 7.86$, $p < .05$) compared to female BPC-*Panx1*-wildtype counterparts. However, this sex-driven difference was not statistically significant in BPC-*Panx1*-deficient mice, and overall tumor growth did not differ between genotypes. These results indicated that *Panx1* global deletion in this mouse model did not impact BRAF^{V600E}/Pten-driven melanoma development.

Figure 4-1.

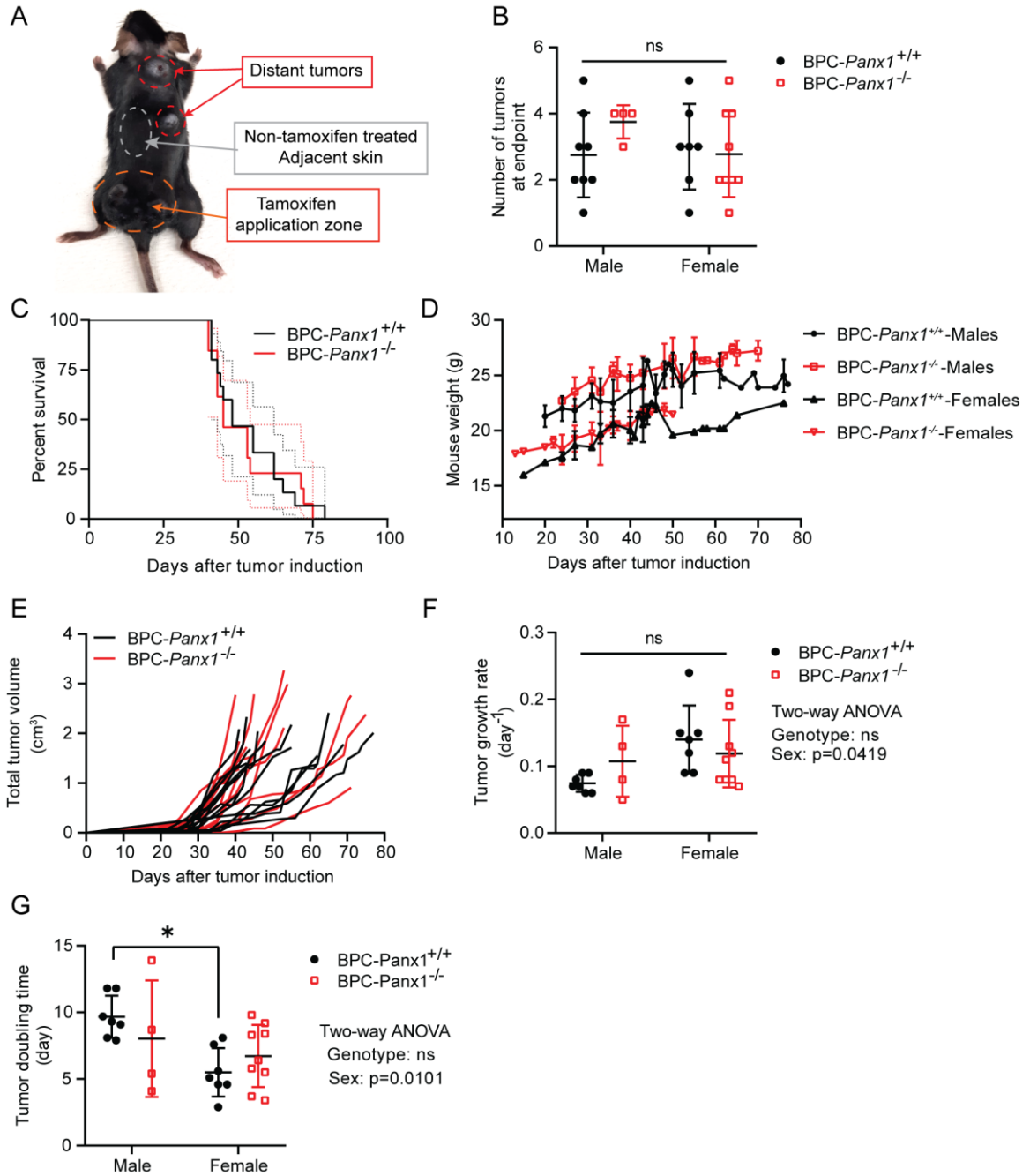


Figure 4-1 Global *Panx1* deletion does not improve survival or reduce tumor progression in the *Braf(V600E)/ Pten(del)* mouse melanoma model.

(A) Representative picture of *Tyr::CreER; BRAF^{CA/+}; Pten^{-/-}* (BPC) mice knockout (-/-) for *Panx1* with multiples tumors at endpoint. Region of the tamoxifen application is indicated in the picture. (B) Tumor incidence, recorded as the number of visible cutaneous melanoma lesions at endpoint, was similar between both mouse sexes and genotypes. (C) Kaplan-Meier survival curves were similar among BPC-*Panx1* wildtype (^{+/+}) or BPC-*Panx1*^{-/-} mice (Log-rank test, $p = 0.7803$). Dotted lines denote 95% confidence intervals. (D) Comparison of mice body weight after tumor induction showed no differences among genotypes within the same sex group. Statistical significance was determined by multiple t-tests per timepoint using the Holm-Sidak method without assuming a consistent *SD*. (E) Tumor growth curves showed overlap between genotypes, with a group of mice exhibiting slightly delayed tumor growth. Individual lines depict measurements per mouse. (F, G) Tumor growth rate and doubling time were similar among genotypes but significantly different between males and females within the BPC-*Panx1*^{+/+} group. Two-way ANOVA showed no interaction between genotype and sex, but significant *p*-values for the sex factor in tumor doubling time ($F_{1,23} = 7.855$, $p < .05$) and growth rate ($F_{1,23} = 4.642$, $p < .05$), respectively. Symbols stand for individual data per mouse (BPC-*Panx1*^{+/+}, $n=15$, and BPC-*Panx1*^{-/-}, $n=13$) except for the graph in D, where mean \pm *SD* are shown. Due to unequal sample sizes per sex, the Tukey-Kramer test was used as *posthoc* test for pairwise comparisons shown in F and G. Statistical significance was considered when $p < 0.05$.

In general, most melanoma lesions were presented with a combination of melanotic (black) and amelanotic (white) regions (Fig. 4-2A). However, a few exceptions (less than 30% of animals per genotype) also had completely amelanotic tumors primarily distant from the tamoxifen application site. A classification of the tumors with the presence or complete absence of black pigmentation rendered no significant differences in their number among genotypes (Fig. 4-2A). All mice, regardless of the genotype, developed fast-growing tumors that, in most cases, were ulcerated by the time of endpoint (Fig. 4-2B). Since our previous reports indicated that PANX1 is highly expressed in human melanoma tumors compared to normal skin, we performed real-time-qPCR in matched samples of non-tamoxifen treated (adjacent) skin and tumor. *Panx1* mRNA expression was found to be 3.2-fold increased (Fig. 4-2C) in tumors of BPC-*Panx1*^{+/+} mice compared to non-tamoxifen induced skin, while undetectable in any tissue sample from BPC-*Panx1*^{-/-} mice, as expected. Moreover, mRNA expression of *S100a1* melanoma marker [26, 27] had a 5.1-fold increase ($p < 0.05$) in tumors of BPC-*Panx1*^{-/-} compared to non-tamoxifen treated skin (Fig. 4-2D), indicating that the development of primary tumors occurred independently of *Panx1* expression.

Figure 4-2

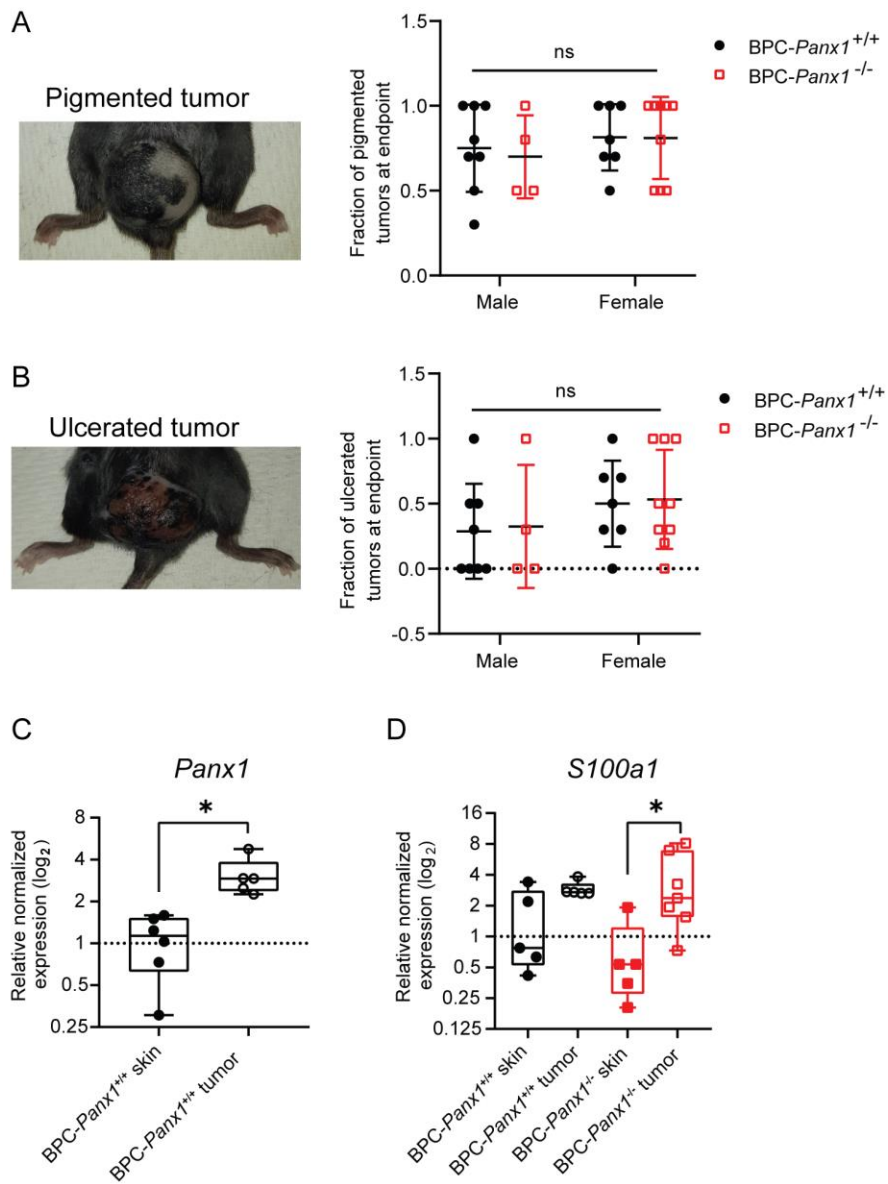


Figure 4-2 Pigmentation or ulceration of the Braf(V600E)/Pten(del) melanoma lesions are not influenced by the global *Panx1* deletion.

(A, B) Representative pictures of pigmented and ulcerated tumors. Fractions (out of the total tumors per mice) of pigmented or ulcerated tumors were similar among the genotype and sex groups. Symbols show individual data per mouse and horizontal lines, and error bars represent mean \pm SD. Data were analyzed with two-way ANOVA. (C, D) mRNA expression of *Panx1* and melanoma marker *s100a1* in tumors compared to matched samples of non-tamoxifen treated skin per mouse. *Gapdh* and *18s* were used as reference genes, and the normalized expression is shown relative to one of the BPC-*Panx1*^{+/+} skin samples. Box plots represent the 95% confidence interval (CI) and the median (inner line), with whiskers representing the maximum and minimum values of the gene expression. Symbols display the individual expression data per mouse. Paired t-test was used to compare the log₂ (normalized expression) of *Panx1* and one-way ANOVA followed by a Tukey test used to compare the expression of *S100a1*. At least N=5 paired samples were assayed by triplicate (n=3) for real-time-qPCR analysis. Statistical significance is shown as p<0.05(*).

4.3.2 *Panx1*-deletion does not prevent melanoma metastasis to inguinal lymph nodes

In all cases, we observed localized and distant clusters of small black pigmented spots spread in the underside of dorsal skin that was not treated with tamoxifen, suggesting the presence of melanoma microlesions or that in-transit metastasis may have occurred (Fig. 4-3A). Upon visual inspection after euthanasia, we did not find any evident presence of black metastatic lesions in major organs (e.g., lungs, liver, or brain). However, melanoma tumor cells are known for passing through the lymphatic system and entering the bloodstream to metastasize to other organs [28]. As is characteristic of this mouse model, we found regional melanoma metastases located in both right and left inguinal lymph nodes in both BPC-*Panx1* genotypes regardless of the sex of the animals (Fig. 4-3B, C, and D).

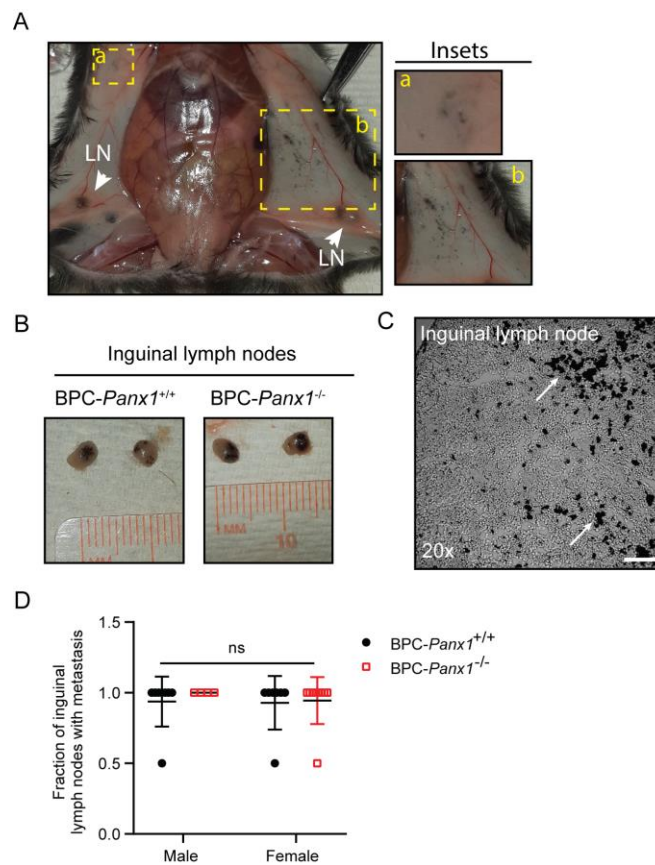
Figure 4-3.

Figure 4-3 *Panx1* deletion does not prevent the development of Braf/Pten-driven melanoma micro-lesions or metastasis to inguinal lymph nodes in BPC mice.

(A) Representative pictures of melanoma micro-lesions found underside the dorsal and ventral/lateral skin and located distant (inset a) and nearby (inset b) to the application sites of tamoxifen (e.g., lower back dorsal skin). LN: Inguinal draining lymph nodes. (B) Representative pictures of right and left inguinal lymph nodes showing black pigmentation indicative of melanoma metastasis. (C) Phase-contrast micrograph of an inguinal draining lymph node cryosection exhibiting melanin deposits and pigmented cells (white arrows). (D) Fraction (out of two inguinal LN per mice) of draining lymph nodes classified with melanoma metastasis based on the presence or absence of visible pigmented lesions. Symbols correspond to the individual data per mouse where mean \pm SD are shown. Data were analyzed with a two-way ANOVA. Statistical significance was considered when $p < 0.05$.

4.3.3 Spleens are significantly enlarged in females of tumor-induced BPC-*Panx1*^{-/-} mice compared to males

Initial visual inspection of the spleens in BPC-*Panx1*^{-/-} mice showed an apparent increase in spleen size compared with the BPC-*Panx1*^{+/+} cohort (Fig. 4-4A). Therefore, we measured spleen length and weight (normalized to body mass and referred to here as weight index) (Fig. 4-4B, C) and observed statistically significant sex-dependent differences in BPC-*Panx1*^{-/-} mice (two-way ANOVA, $F_{1,20} = 10.91$, $p < 0.01$). In that case, a statistically significant increased spleen weight index was found in females compared to males of the BPC-*Panx1*^{-/-} cohort but not in the BPC-*Panx1*^{+/+} mice or among genotypes. Moreover, spleen weight and length measurements showed a positive correlation (Fig. 4-4D) with statistically significant ($p=0.0247$ and $p=0.0087$) Pearson's coefficients ($r \geq 0.7$) in both BPC-*Panx1*^{+/+} and BPC-*Panx1*^{-/-} mice, respectively, which confirmed the similar trend observed with both parameters. We also assessed the cellular proliferation in spleen cryosections from randomly selected animals of both genotypes (Fig. 4-4E). Interestingly, quantification of the immunofluorescence staining with the proliferation marker ki67 (Fig. 4-4F) showed significantly fewer proliferative splenic cells in tumor-bearing BPC-*Panx1*^{-/-} mice than the BPC-*Panx1*^{+/+} cohort suggesting that this morphological difference in spleen size is not due to an increased *in situ* proliferation of cells (resident or in transit) in the spleens of tumor-bearing BPC mice.

Figure 4-4.

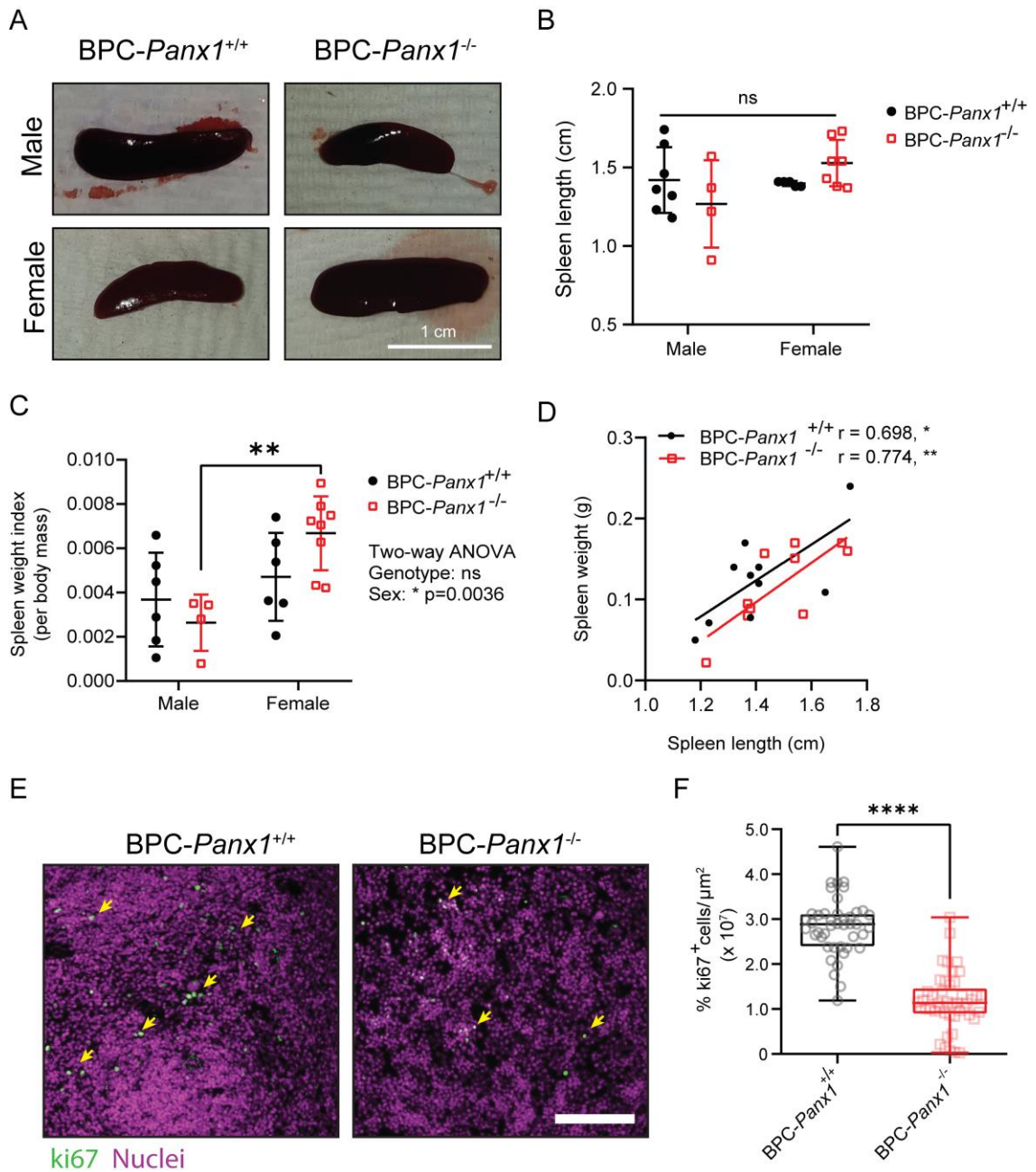


Figure 4-4 BPC-*Panx1*^{-/-} mice exhibit sex-dependent differences in spleen size not observed in BPC-*Panx1*^{+/+} cohort.

(A) Representative pictures of BPC mice spleens. (B) Morphological comparison of the spleen measured by length and (C) weight index (spleen weight normalized to body mass) Two-way ANOVA, $F_{1, 20} = 10.91$, $p < 0.01$. A Tukey-Kramer test used as *posthoc* test for pairwise comparisons showed a significantly ($p < 0.01$) higher spleen weight index in BPC-*Panx1*^{-/-} females than males, but not in the BPC-*Panx1*^{+/+} cohort. Symbols correspond to data from individual mice where mean \pm SD are shown. (D) A positive correlation was found between the spleen weight and length, confirming the trends of increased spleen size in female BPC-*Panx1*^{-/-} mice observed by both measurements. (E) Representative immunofluorescence micrographs (20x magnification) of cross-sectional views of the spleen sections stained with the proliferation marker ki67. Yellow arrows indicate the location of proliferating cells (green). Nuclei (magenta) were counterstained with Hoechst 33342. Scale bar = 200 μ m (F) Quantification of ki67 staining in the spleens showing significant reduction in the % of proliferative cells in spleens of BPC-*Panx1*^{-/-} mice; symbols represent individual measurements of at least 12 non-overlapping fields of view from randomly selected animals: BPC-*Panx1*^{+/+} (N=3; n=1 female and n=2 males) and BPC-*Panx1*^{-/-} (N=4 females) mice. Box plots represent the 95% confidence interval (CI), and the mean (inner line), whiskers represent the maximum and minimum counts per image. Data were analyzed with two-tailed unpaired t-tests. Statistical significance is shown as $p < 0.05$ (*), $p < 0.01$ (**) and $p < 0.0001$ (****).

4.3.4 BPC-mice lacking PANX1 exhibit increased CD8 expression in the skin and melanoma tumors

Due to PANX1's role in the inflammatory response [12-17], we sought to examine changes in the infiltration of immune cells within the tumor microenvironment. We performed a real-time qPCR analysis of gene expression for markers of a selected immune cell population known to modulate the immune response against melanoma. Therefore, we included protein tyrosine phosphatase, receptor type, C (*Ptprc*) (also known as cluster of differentiation (CD) 45) for leukocytes; CD3 antigen, epsilon polypeptide (*CD3ε*) for T-lymphocytes; CD4 antigen (*CD4*) for T-helper lymphocytes; CD8 antigen, beta polypeptide (*CD8b*) for cytotoxic T cells; forkhead box P3 (*Foxp3*) for regulatory T cells (T-reg); natural cytotoxicity triggering receptor-1 or NCTR1 (*Ncr1*) for Natural killer (NK) cells and the cell surface glycoprotein F4/80 (*Agre1*) for monocytes/macrophages. Of note, marker expression was evaluated in melanoma tumors as well as matched samples of dorsal skin not treated with tamoxifen and devoid of any visible melanoma lesions (referred to as "adjacent skin"). These adjacent skin samples were used to account for basal immune infiltration levels or skin-resident immune cells [29, 30] at the time of sample collection.

When analyzing tumors compared with their matched skin samples, we observed a statistically significant ~4.3 fold-increase in the expression of CD45 ($F_{3, 20} = 6.24$, $p < 0.01$) in the BPC-*Panx1*^{+/+} mice group (Fig. 4-5A) but no differences between genotypes. The mRNA expression of F4/80 ($F_{3, 18} = 19.38$, $p < 0.0001$) was 14.0 ($p < 0.0001$) and 7.7-fold ($p < 0.01$) higher in tumors than the skin of BPC-*Panx1*^{+/+} and BPC-*Panx1*^{-/-}, respectively (Fig. 4-5B). On the other hand, transcripts of NCTR1 ($F_{3, 11} = 8.24$, $p < 0.01$) (Fig. 4-5C) were 9.3-fold upregulated ($p < 0.01$) in BPC-*Panx1*^{-/-} tumors versus adjacent skin. Overall, T-lymphocyte infiltration measured by *CD3ε* (Fig. 4-5D) showed a similar expression regardless of the sample type or *Panx1* genotype. However, *CD4* mRNA expression ($F_{3, 11} = 27.46$, $p < 0.0001$) was significantly augmented in the tumors compared to the skin (Fig. 4-5E) with a 10.5 ($p < 0.01$) and 18.9-fold ($p < 0.001$) increase in the BPC-*Panx1*^{-/-} and BPC-*Panx1*^{+/+}, respectively; and 5-fold upregulated ($p < 0.05$) in the adjacent skin of BPC-*Panx1*^{-/-} vs. that of BPC-*Panx1*^{+/+}. Moreover, *Foxp3* ($F_{3, 16} = 9.80$, $p < 0.001$) was upregulated in

tumors of BPC-*Panx1*^{+/+} and BPC-*Panx1*^{-/-} mice compared to the skin (5.9-fold, $p < 0.05$, and 15.2-fold, $p < 0.01$, respectively) (Fig 4-5G). Lastly, cytotoxic T cell marker *CD8* ($F_{3,16} = 15.39$, $p < 0.0001$) was the only marker with a significant increase (9-fold, $p < 0.01$) in the skin and (9.5-fold, $p < 0.01$) in tumors of the BPC-*Panx1*^{-/-} mice compared to BPC-*Panx1*^{+/+} animals (Fig. 4-5F). Overall, these results indicated that *Panx1* deficiency did not impair the recruitment of immune cells to the primary tumors. Interestingly, a higher *CD8* mRNA expression in the tissues of BPC-*Panx1*^{-/-} mice suggested that PANX1 may modulate migration of CD8⁺ T cells to target tissues.

Figure 4-5.

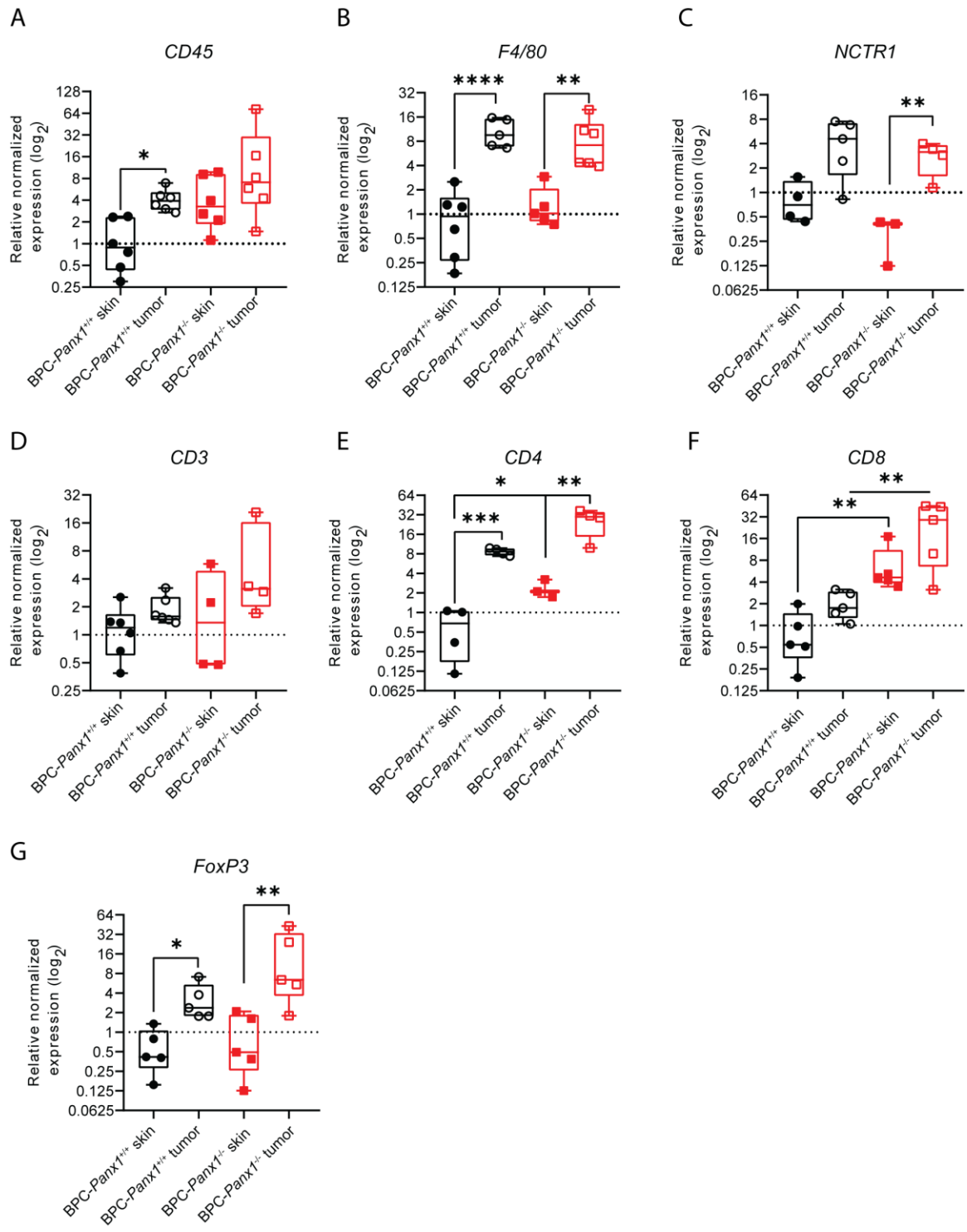


Figure 4-5 CD8 T-lymphocyte mRNA marker is significantly increased in the non-tamoxifen treated skin and melanoma tumors of BPC-mice lacking PANX1.

(A-G) Real-time qPCR analysis of immune cell markers expression in tamoxifen-induced tumors and matched non-tamoxifen treated skin. *Gapdh* and *18s* were used as reference genes, and the normalized expression was calculated relative to one of the BPC-*Panx1*^{+/+} skin samples. Box plots represent the 95% confidence interval (CI) and the median (inner line), with whiskers showing the maximum and minimum values of the gene expression. Each sample was assayed by triplicate (n=3). The symbols represent the expression data of each mouse (at least N=3 per genotype). The log₂ of the expression per group was analyzed by one-way ANOVA followed by a Sidak *post hoc* test. Only significant *p* values of relevant comparisons between groups are shown as *p*<0.05 (*), <0.01(**), <0.001(***)).

Given the lack of differences in tumor burden among genotypes and the increased *CD8* transcript expression indicative of infiltration of cytotoxic T-lymphocytes in the BPC-*Panx1*^{-/-} tumors, we questioned whether tumor-infiltrated T cells lacking *Panx1* had differences in the anti-tumoral response compared to those of the BPC-*Panx1*^{+/+} cohort. Thus, we assessed the expression of early activation T cell antigen *CD69*, a membrane-bound, type II C-lectin receptor known as an early classical marker of lymphocyte activation [31]. *CD69* mRNA trended lower (but not significant) in BPC-*Panx1*^{-/-} tumors (Fig. 4-6A). On the other hand, we also investigated the mRNA expression of a marker for T cell exhaustion, the negative regulatory immune checkpoint receptor lymphocyte activation gene-3 (*LAG-3*) [32], but no significant differences in *LAG-3* expression were found between genotypes (Fig. 4-6B). These findings suggested that PANX1 may not influence tumor-infiltrating T cell activation or exhaustion phenotypes in this BPC model.

We also investigated the mRNA expression of another central player in regulating the immune responses in melanoma, programmed cell death protein-ligand 1 (PD-L1) [33]. PD-L1 can be expressed by tumor cells and exert a negative regulation on cytotoxic T cell activation. However, PD-L1 mRNA expression in tumors was not significantly different between the *Panx1*-genotypes (Fig. 4-6C). Therefore, we concluded that the *Panx1* deletion does not influence PD-L1-derived immunosuppression of T cells in the tumor microenvironment. Finally, due to the association of PANX1 channel function and the proinflammatory and tumor promoter cytokine: interleukin-1 β (IL-1 β), we asked whether the *IL-1 β* expression was affected within the tumor microenvironment of BPC *Panx1*-deficient mice. However, IL-1 β mRNA levels (Fig. 4-6D) were highly variable in the BPC-*Panx1*^{-/-} tumors but were not significantly different compared to tumors of the BPC-*Panx1*^{+/+} mice.

Figure 4-6.

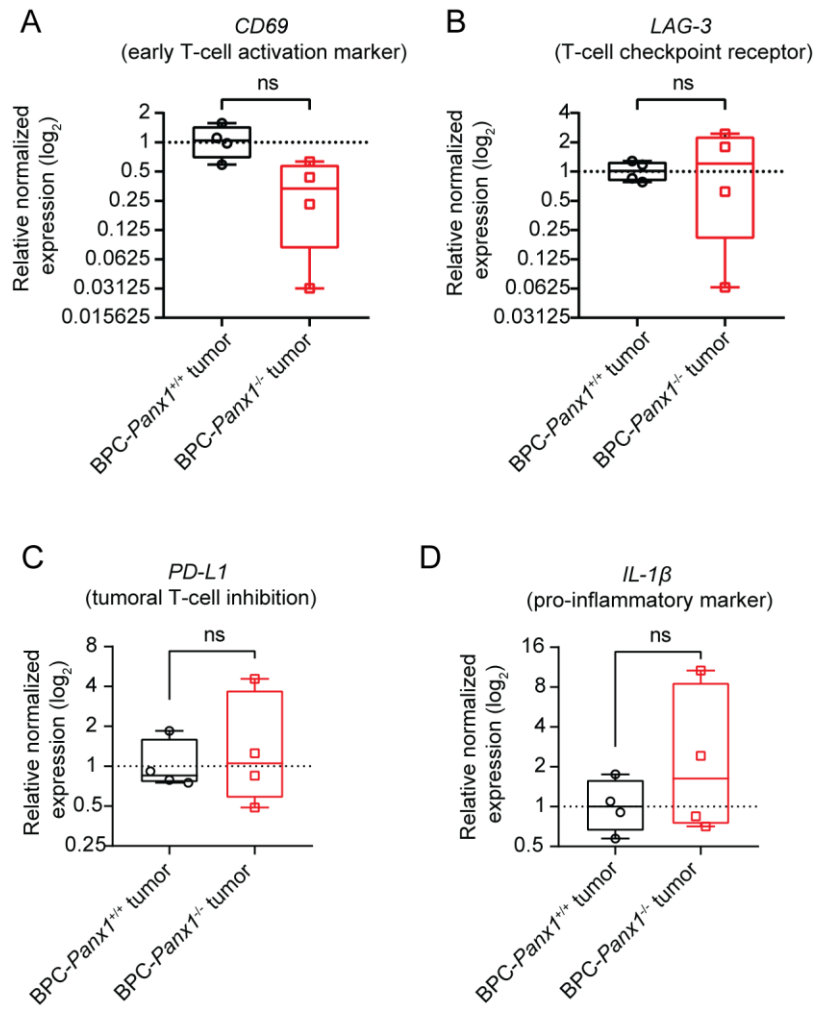


Figure 4-6 Global *Panx1*-deletion does not affect the mRNA expression of phenotypic markers of activation of tumor-infiltrated T-lymphocytes.

Real-time qPCR analysis of (A) the early T cell immune activation marker *CD69*, (B) checkpoint receptor lymphocyte activation gene-3 (*LAG-3*), (C) immune checkpoint molecule programmed cell death 1-ligand (*PD-L1*), and (D) *IL-1 β* in tumor samples. *Gapdh* was used as a reference gene, and the normalized expression is relative to one of the BPC-*Panx1*^{+/+} skin samples. Box plots represent the 95% confidence interval (CI) and the median (inner line), with whiskers showing the maximum and minimum values of the gene expression. Each sample was assayed by triplicate (n=3), and the symbols represent the expression data of each mouse (at least N=4 per genotype). A t-test compared the mean of the log₂ of the relative expression per group; statistical significance was considered when $p < 0.05$ (*).

4.3.5 Germline *Panx1*-deletion increases the tumor infiltration of CD4⁺, CD8⁺ T lymphocytes, and Granzyme B producing cells

We wanted to confirm the differences in tumor T cell infiltration between *Panx1* genotypes using an orthogonal approach. Therefore, we performed immunofluorescence staining on PLP-fixed tumor cryosections for CD4, CD8, and Foxp3 lymphocytic markers (Fig. 4-7A). Overall, CD4⁺ and CD8⁺ T cells were seen in small but sparsely distributed clusters closer to the skin epidermis of the primary melanoma tumors, and Foxp3⁺ T cells showed a more homogeneous distribution within the tumor core irrespective of genotype (Fig. 4-7A). Overall, the trends in immune cell infiltration of these markers agreed with our real-time qPCR results, and in tumors, BPC-*Panx1*^{-/-} mice had 4 and 2.4 times increased staining for positive CD4⁺ and CD8⁺ T cells, respectively (Fig. 4-7B). On the other hand, the percent of Foxp3⁺ T cells in tumors was similar between genotypes. Collectively, these results confirmed that the deletion of *Panx1* favored the infiltration of CD4⁺ and CD8⁺ T cells in the tumors.

We then used staining of the cytotoxic cell protease Granzyme B (GzmB) to assess whether differences in T- or NK cells' immune effector capacity (cytotoxicity) could be identified within the TME. As shown in Fig.4-7 E-F, we observed a significant increase (8.4-fold, p<0.0001) in the percentage of GzmB⁺ cells in tumors of BPC-*Panx1*^{-/-} compared to BPC-*Panx1*^{+/+} mice. Notably, GzmB protein was localized in intracellular granules, and very rarely, any extracellular GzmB staining was discernible. These results agree with the higher infiltration of CD8⁺ T cells and, likely, NK cells since GzmB can be abundant as cytosolic granules in both cytolytic immune cell types. Furthermore, these findings suggest that global *Panx1*-deletion did not affect the activation and migration of such cell types and may favor the increased presence of anti-tumoral effector cells within BPC-melanoma tumors.

Figure 4-7.

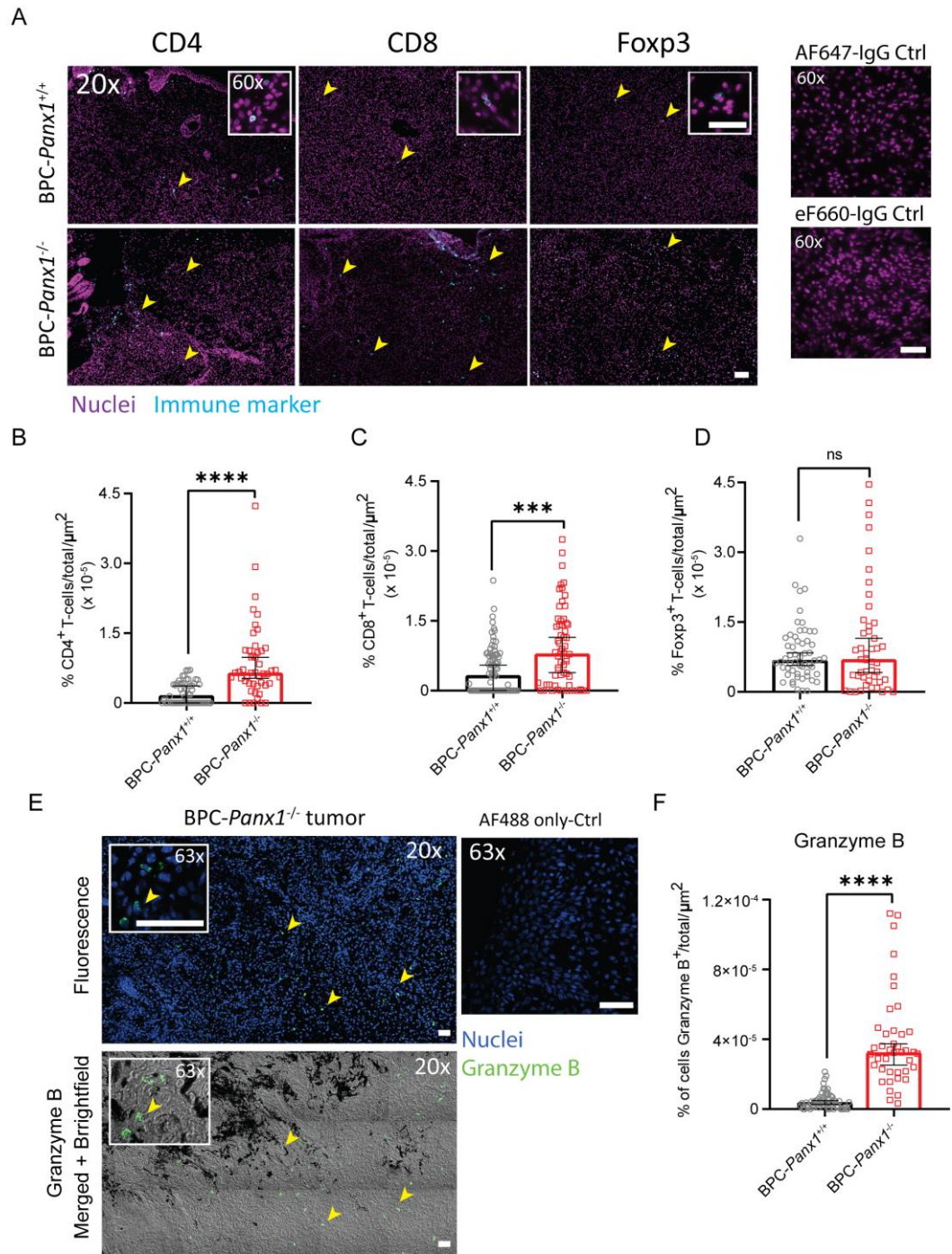
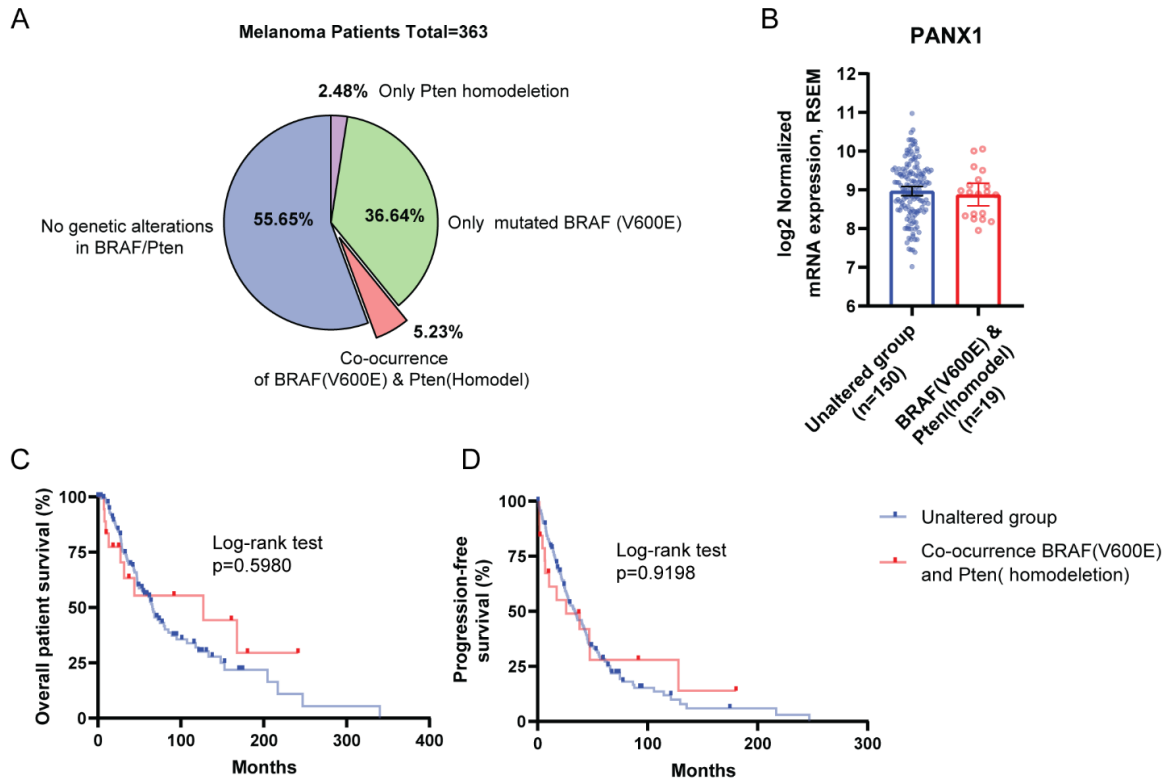


Figure 4-7 Tumor-infiltrating CD4+, CD8+ T-lymphocytes, and Granzyme B producing cells are significantly increased in BPC-*Panx1*^{-/-} tumors.

(A) Representative micrographs (20x, insets at 60x magnification) showing immunofluorescence staining of primary melanoma tumor cryosections with immune cell infiltration markers for CD4+, CD8+, and FoxP3+ T-lymphocytes (shown in cyan). Nuclei (in magenta) was counterstained with Hoechst 33324. (B-D) Immunofluorescence quantification of CD4, CD8, and FoxP3 positive cells for the whole tumor section. (E) Representative granzyme B (GzmB) immunofluorescence staining of a BPC-*Panx1*^{-/-} tumor (fluorescence channels on top and brightfield channel at the bottom) with the intra-tumoral distribution of GzmB+ cells and black pigmented regions in the tumor. Nuclei are shown in blue, and GzmB is shown in green. Yellow arrowheads indicate stained immune cells. Scale bars = 40 μ m. (F) Quantification of GzmB immunostaining. The percent of nuclei with positive immune marker staining was normalized per area of the field of view (FOV). At least three mice (N=3) per genotype were examined with at least 12 non-overlapping FOV per tumor. Bar graphs stand for the median with 95% CI, and individual measurements are depicted with symbols. Data were compared using a two-tailed Mann-Whitney test. Statistical significance is shown as $p < 0.001$ (***) and $p < 0.0001$ (****).

Figure S4-1.



Supplemental Figure 4-1 *PANX1* mRNA expression is similar between patients with and without co-occurrence of BRAF(V600E) /Pten (homozygous deletion).

(A) Analysis of Skin Cutaneous Melanoma TCGA PanCancer data shows a low proportion (~5.0 %) of patients have co-occurrence of the BRAF(V600E) and homozygous deletion of PTEN. (B) Both cohorts of patients exhibit similar levels ($p=0.4970$) of PANX1 mRNA expression. Overall (C) and progression-free survival (D) are similar between patients with (red line; $n=144$) or without (blue line; $n=19$) co-occurrence of BRAF(V600E) mutation/Pten (deep deletion). Data in graphs were exported from cBioPortal (as of Jan/12/2021)[34, 35]. RNASeqV2 data (Batch normalized from Illumina HiSeq) is derived from TCGA PanCancer Atlas datasets, processed, and normalized using RSEM. Bar and error graphs stand for the geometric mean with 95% CI, and individual patient expression data is depicted with symbols. A two-tailed unpaired t-test with Welch's correction was used to compare the means of $\log_2(\text{mRNA PANX1 expression})$, and a log-rank test was used to determine statistical significance ($p<0.05$) in the Kaplan-Meier curves.

4.4 Discussion

PANX1 channels have attracted considerable attention due to their multiple roles in inflammation, cell death, and cancer [13, 36]. Recently, we have demonstrated that PANX1 influences the regulation of effector molecules that control melanocyte differentiation (e.g., MITF and β -catenin) and the metabolism of melanoma cells [9-11]. Furthermore, we have shown promising results after silencing *Panx1* expression and reducing the growth and tumorigenicity of melanoma cell lines *in vitro*. In contrast, using the immunocompetent BPC mouse melanoma model, we did not observe a reduction in Braf(V600E)/Pten(del)-driven melanomas or improve mice survival upon global *Panx1* deletion. Interestingly, BPC-*Panx1*^{+/+} female mice seemed to display a more aggressive tumor progression than males. Other researchers have recently noted this outcome in a C57B/6J background, but the origin of this sex dimorphism has not been clarified yet [37]. It has been speculated that this may be due to the presence of alternative steroid receptors in melanoma cells or technical limitations with tamoxifen (an estrogen receptor modulator) differentially influencing the mouse sexes in this melanoma model [37]. Although there were no significant differences among genotypes, this sex-dependency was lost in BPC-*Panx1*^{-/-} mice, possibly indicating that *Panx1*-deletion may influence such a sex-driven phenotype. It is known that sexual dimorphism exists in the response of *Panx1*-deficient mice in ischemia [38] and epilepsy [39], and research on this is lacking in the melanoma and immune cell recruitment contexts. In contrast to our observation, recent evidence has shown that tumor progression and anti-tumoral T cell response are sex-dependent in a syngeneic melanoma mouse model, where females had less tumor growth rate and higher CD4⁺ and CD8⁺ T cell infiltrates compared to males [40]. Thus, sex-driven differences will require further attention, especially in the melanoma and PANX1 research context.

Of note, our previous *in vitro* and *ex vivo* work targeting PANX1 employed murine melanoma cell lines (B16-F0, -F1, -F10) and BRAF(V600E)-mutant human melanoma cell lines (A375-P and A375-M2) that do not entirely share the same genomic alterations of the BPC model [10, 41]. The deletion of *Pten* is known to have a synergistic effect and dramatically accelerate BRAFV600E-induced melanoma tumors in BPC mice [21, 22, 42].

Therefore, these oncogenic mutations may have overridden the anti-tumoral effect of *Panx1*-deletion. Also, the deletion of *Panx1* may not have the same effect seen with the use of PANX1 channel blockers (e.g., with carbenoxolone, probenecid, or spironolactone) due to possible compensation with other channels proteins (e.g., connexins or other paralogs), and PANX1 blockers are yet to be tested in melanoma using an *in vivo* model.

Despite the global PANX1 deficiency, micro-metastasis to draining inguinal lymph nodes did occur in our conditions, as reported elsewhere [21-23, 43]. Thus, we conclude that PANX1 does not control the early spread of melanoma. Since this is a highly penetrant mouse model, a syngeneic melanoma model may be more suitable to study the effect of *Panx1*-deletion in melanoma metastasis [44]. Furthermore, due to the ubiquitous expression of *Panx1*, its global deletion should have affected many cell types, including melanoma and immune cells. Therefore, we reason that this scenario may resemble the effect of a continuous, systemic, and irreversible depletion of PANX1 function in which adaptative or alternative molecular mechanisms are in play to sustain tumor growth.

To date, there are no reports of major abnormalities or immune-related diseases in the *Panx1*-deficient mice (reviewed at [13]). Here, we report for the first time that tumor-bearing BPC-*Panx1*^{-/-} female mice have significantly augmented spleen size compared to male counterparts. Although the tumor may have caused this condition, we found a lower cell proliferation (ki67 staining) in BPC-*Panx1*^{-/-} spleens than in the wildtype cohort with no evident signs of melanoma metastasis in any of the mice. Due to the short timeframe for tumor growth (up to 2 months) and the sexual dimorphism found only in BPC-*Panx1*^{-/-} spleens, we speculate that developmental differences may account for this phenotypic characteristic of *Panx1*^{-/-} mice. Further research is warranted to determine whether global *Panx1*-deletion exerts a sex-specific systemic immune dysregulation and whether this is reflected in the spleen size.

Tumor-infiltrating lymphocytes (TILs) have already been described in this BPC model [23]. However, others have highlighted that this model does not appear to induce a marked immune response due to the lack of additional tumoral somatic mutations/neoepitopes [44]. Notably, our results showed that increased TILs were detected in BPC-*Panx1*^{-/-} tumors.

Similar to previous reports [23], we found increased T-lymphocytes and macrophage markers in all the tumors. Interestingly, in those reports, myeloid-derived suppressor cells, along with high PD-1 expression on the T cells, have been attributed to causing a highly immunosuppressive environment in this melanoma model. However, we found no difference in the abundance of tumor-infiltrating T-reg cells between both mice cohorts but had a limited analysis of generic markers to determine exactly all the sources of possible immunosuppression. Therefore, it is unclear if other subsets of CD4⁺ T cells (Th1 or Th17), macrophages (M1 or M2), or myeloid-derived suppressor cells infiltrated the tumors and may have contributed to immune evasion and melanoma progression. Despite the significant increase of CD8⁺ T cells in *Panx1*-deficient melanoma tumors, we found no changes in the activation of TILs as judged by the expression of CD69 as this early T cell activation marker is expressed by several subsets of tissue-resident immune T cells [45, 46]. Indeed, the higher incidence of GzmB⁺ cells (could be CD8⁺ T cells or NK cells) found in the BPC-*Panx1*^{-/-} tumors supports an increased immune cell activation phenotype. However, as these primary tumors were so aggressive, a meaningful tumor reduction may only be observed if checkpoint inhibitors were applied at early tumor induction stages. Interestingly, BRAF(V600E), *Pten*-null melanomas, seem resistant to immune checkpoint inhibitory antibodies, where PTEN loss inhibits T cell-mediated killing and trafficking to the tumors [47]. This suggests that targeting PANX1 could be an alternative to overcome this type of immune resistance in tumors.

Based on the PANX1-mediated release of proinflammatory cytokine IL-1 β , PANX1 has been proposed as a potential target to regulate antitumor immunity in melanoma (reviewed in [48]). In the current study, we found no significant differences in IL-1 β mRNA expression among cohorts, but we cannot rule out that the secretion of IL-1 β , at the protein level, was not affected in *Panx1*-deficient tumors. However, earlier studies showed that marrow-derived macrophages of this *Panx1*^{-/-} mouse strain have no difference in the secretion of IL-1 β or the inflammasome activation [15]. Recently, Medina et al. demonstrated that thymocyte-specific *Panx1*-deletion attenuated metabolite release from apoptotic lymphocytes and the inflammation *in vivo* in mouse models of inflammatory arthritis and lung transplant rejection [8]. This underscores the need for research into the

crosstalk between immune- and melanoma cells and cell-specific PANX1 suppression/inhibition conditions to better understand the implications of PANX1 targeting in the context of melanoma.

4.5 Conclusions

In conclusion, our study demonstrates that although a *Panx1* deletion cannot overcome the aggressive tumorigenic effect of Braf(V600E)/Pten(del) driver mutations, it increases the tumor T cell infiltration with a preference in CD8⁺ cytotoxic T cells. This could be advantageous since a considerable therapeutic benefit is achieved in patients with a pre-existing CD8⁺ T cell infiltration within the melanoma microenvironment [49]. Although this transgenic melanoma mouse model was developed to harness two significant oncogenic alterations (BRAF^{V600E} and PTEN(loss), it is not representative of the larger patient population since only ~5.0 % of them had co-occurrence of both mutations (Supplemental Fig. S4-1A). Furthermore, since *PANX1* expression seems independent of genomic alterations of melanoma (Supplemental Fig. S1B) and is present at all stages of the disease [10], a large patient population may benefit from PANX1 targeted therapy. Future preclinical studies should include the combination strategies in which PANX1 inhibition could be used initially as neoadjuvant therapy to checkpoint inhibitors (e.g., anti-PD-1 or anti-CTLA4) and stimulate cytotoxic T cell tumor infiltration to improve the efficacy of immunotherapies.

4.6 Acknowledgments

We thank Dr. Saman Maleki-Vareki and Dr. Frank Beier for their input on the article. This study was supported by a Canadian Institutes of Health Research CIHR Project grant to Silvia Penuela and Lina Dagnino (FRN 153112).

4.7 References

1. Tas, F., *Metastatic behavior in melanoma: timing, pattern, survival, and influencing factors*. J Oncol, 2012. **2012**: p. 647684.
2. Havel, J.J., D. Chowell, and T.A. Chan, *The evolving landscape of biomarkers for checkpoint inhibitor immunotherapy*. Nat Rev Cancer, 2019. **19**(3): p. 133-150.

3. Dempke, W.C.M., et al., *Second- and third-generation drugs for immuno-oncology treatment-The more the better?* Eur J Cancer, 2017. **74**: p. 55-72.
4. Wolchok, J.D., et al., *Overall Survival with Combined Nivolumab and Ipilimumab in Advanced Melanoma.* N Engl J Med, 2017. **377**(14): p. 1345-1356.
5. Jerby-Arnon, L., et al., *A Cancer Cell Program Promotes T Cell Exclusion and Resistance to Checkpoint Blockade.* Cell, 2018. **175**(4): p. 984-997 e24.
6. Trujillo, J.A., et al., *Secondary resistance to immunotherapy associated with beta-catenin pathway activation or PTEN loss in metastatic melanoma.* J Immunother Cancer, 2019. **7**(1): p. 295.
7. Cabrita, R., et al., *The Role of PTEN Loss in Immune Escape, Melanoma Prognosis and Therapy Response.* Cancers (Basel), 2020. **12**(3).
8. Medina, C.B., et al., *Metabolites released from apoptotic cells act as tissue messengers.* Nature, 2020. **580**(7801): p. 130-135.
9. Penuela, S., et al., *Loss of pannexin 1 attenuates melanoma progression by reversion to a melanocytic phenotype.* J Biol Chem, 2012. **287**(34): p. 29184-93.
10. Freeman, T.J., et al., *Inhibition of Pannexin 1 Reduces the Tumorigenic Properties of Human Melanoma Cells.* Cancers (Basel), 2019. **11**(1).
11. Sayedyahosseini, S., et al., *Pannexin 1 binds beta-catenin to modulate melanoma cell growth and metabolism.* J Biol Chem, 2021: p. 100478.
12. Chekeni, F.B., et al., *Pannexin 1 channels mediate 'find-me' signal release and membrane permeability during apoptosis.* Nature, 2010. **467**(7317): p. 863-7.
13. Crespo Yanguas, S., et al., *Pannexin1 as mediator of inflammation and cell death.* Biochim Biophys Acta Mol Cell Res, 2017. **1864**(1): p. 51-61.
14. Douanne, T., et al., *Pannexin-1 limits the production of proinflammatory cytokines during necroptosis.* EMBO Rep, 2019. **20**(10): p. e47840.
15. Qu, Y., et al., *Pannexin-1 Is Required for ATP Release during Apoptosis but Not for Inflammasome Activation.* The Journal of Immunology, 2011. **186**(11): p. 6553-6561.
16. Woehrle, T., et al., *Pannexin-1 hemichannel-mediated ATP release together with P2X1 and P2X4 receptors regulate T-cell activation at the immune synapse.* Blood, 2010. **116**(18): p. 3475-84.
17. Woehrle, T., et al., *Hypertonic stress regulates T cell function via pannexin-1 hemichannels and P2X receptors.* J Leukoc Biol, 2010. **88**(6): p. 1181-9.
18. Chen, W., et al., *Enhanced Macrophage Pannexin 1 Expression and Hemichannel Activation Exacerbates Lethal Experimental Sepsis.* Sci Rep, 2019. **9**(1): p. 160.

19. Velasquez, S., et al., *Pannexin1 Channels Are Required for Chemokine-Mediated Migration of CD4+ T Lymphocytes: Role in Inflammation and Experimental Autoimmune Encephalomyelitis*. J Immunol, 2016. **196**(10): p. 4338-47.
20. Penuela, S., et al., *Panx1 regulates cellular properties of keratinocytes and dermal fibroblasts in skin development and wound healing*. J Invest Dermatol, 2014. **134**(7): p. 2026-2035.
21. Dankort, D., et al., *Braf(V600E) cooperates with Pten loss to induce metastatic melanoma*. Nat Genet, 2009. **41**(5): p. 544-52.
22. Damsky, W.E., et al., *beta-catenin signaling controls metastasis in Braf-activated Pten-deficient melanomas*. Cancer Cell, 2011. **20**(6): p. 741-54.
23. Hooijkaas, A.I., et al., *Targeting BRAFV600E in an inducible murine model of melanoma*. Am J Pathol, 2012. **181**(3): p. 785-94.
24. Lamprecht, M.R., D.M. Sabatini, and A.E. Carpenter, *CellProfiler: free, versatile software for automated biological image analysis*. Biotechniques, 2007. **42**(1): p. 71-5.
25. Faul, F., et al., *G*Power 3: a flexible statistical power analysis program for the social, behavioral, and biomedical sciences*. Behav Res Methods, 2007. **39**(2): p. 175-91.
26. Sviatoha, V., et al., *Immunohistochemical analysis of the S100A1, S100B, CD44 and Bcl-2 antigens and the rate of cell proliferation assessed by Ki-67 antibody in benign and malignant melanocytic tumours*. Melanoma Res, 2010. **20**(2): p. 118-25.
27. Xiong, T.F., F.Q. Pan, and D. Li, *Expression and clinical significance of S100 family genes in patients with melanoma*. Melanoma Res, 2019. **29**(1): p. 23-29.
28. Ubellacker, J.M., et al., *Lymph protects metastasizing melanoma cells from ferroptosis*. Nature, 2020. **585**(7823): p. 113-118.
29. Nguyen, A.V. and A.M. Soulika, *The Dynamics of the Skin's Immune System*. Int J Mol Sci, 2019. **20**(8).
30. Richmond, J.M. and J.E. Harris, *Immunology and skin in health and disease*. Cold Spring Harb Perspect Med, 2014. **4**(12): p. a015339.
31. Park, S.L., T. Gebhardt, and L.K. Mackay, *Tissue-Resident Memory T Cells in Cancer Immunosurveillance*. Trends Immunol, 2019. **40**(8): p. 735-747.
32. Zhang, Z., et al., *T Cell Dysfunction and Exhaustion in Cancer*. Front Cell Dev Biol, 2020. **8**: p. 17.
33. Freeman, G.J., et al., *Engagement of the PD-1 immunoinhibitory receptor by a novel B7 family member leads to negative regulation of lymphocyte activation*. J Exp Med, 2000. **192**(7): p. 1027-34.

34. Cerami, E., et al., *The cBio cancer genomics portal: an open platform for exploring multidimensional cancer genomics data*. *Cancer Discov*, 2012. **2**(5): p. 401-4.
35. Gao, J., et al., *Integrative analysis of complex cancer genomics and clinical profiles using the cBioPortal*. *Sci Signal*, 2013. **6**(269): p. p11.
36. Jiang, J.X. and S. Penuela, *Connexin and pannexin channels in cancer*. *BMC Cell Biol*, 2016. **17 Suppl 1**: p. 12.
37. Zhai, Y., et al., *Differences in tumor initiation and progression of melanoma in the *Braf*(CA) ;*Tyr-CreERT2*;*Pten*(*ff*) model between male and female mice*. *Pigment Cell Melanoma Res*, 2020. **33**(1): p. 119-121.
38. Freitas-Andrade, M., et al., *Pannexin1 knockout and blockade reduces ischemic stroke injury in female, but not in male mice*. *Oncotarget*, 2017. **8**(23): p. 36973-36983.
39. Aquilino, M.S., et al., *Pannexin-1 Deficiency Decreases Epileptic Activity in Mice*. *Int J Mol Sci*, 2020. **21**(20).
40. Dakup, P.P., et al., *Sex differences in the association between tumor growth and T cell response in a melanoma mouse model*. *Cancer Immunol Immunother*, 2020. **69**(10): p. 2157-2162.
41. Melnikova, V.O., et al., *Genomic alterations in spontaneous and carcinogen-induced murine melanoma cell lines*. *Oncogene*, 2004. **23**(13): p. 2347-56.
42. Karreth, F.A., et al., *In vivo identification of tumor- suppressive PTEN ceRNAs in an oncogenic BRAF-induced mouse model of melanoma*. *Cell*, 2011. **147**(2): p. 382-95.
43. Hooijkaas, A., et al., *Selective BRAF inhibition decreases tumor-resident lymphocyte frequencies in a mouse model of human melanoma*. *Oncoimmunology*, 2012. **1**(5): p. 609-617.
44. Meeth, K., et al., *The YUMM lines: a series of congenic mouse melanoma cell lines with defined genetic alterations*. *Pigment Cell Melanoma Res*, 2016. **29**(5): p. 590-7.
45. Cibrian, D. and F. Sanchez-Madrid, *CD69: from activation marker to metabolic gatekeeper*. *Eur J Immunol*, 2017. **47**(6): p. 946-953.
46. Edwards, J., et al., *CD103(+) Tumor-Resident CD8(+) T Cells Are Associated with Improved Survival in Immunotherapy-Naive Melanoma Patients and Expand Significantly During Anti-PD-1 Treatment*. *Clin Cancer Res*, 2018. **24**(13): p. 3036-3045.
47. Peng, W., et al., *Loss of PTEN Promotes Resistance to T Cell-Mediated Immunotherapy*. *Cancer Discov*, 2016. **6**(2): p. 202-16.
48. Varela-Vazquez, A., et al., *Emerging functions and clinical prospects of connexins and pannexins in melanoma*. *Biochim Biophys Acta Rev Cancer*, 2020. **1874**(1): p. 188380.

49. Massi, D., et al., *The density and spatial tissue distribution of CD8(+) and CD163(+) immune cells predict response and outcome in melanoma patients receiving MAPK inhibitors*. *J Immunother Cancer*, 2019. 7(1): p. 308.

Chapter 5

5 Discussion

5.1 Summary of main findings

Pannexins are channel-forming glycoproteins supporting ATP, Ca²⁺, and other ions/metabolites-dependent signaling [1, 2]. The wide-ranging expression of PANX1 in several tissues (brain, kidney, liver, and skin) [1], along with the discovery of PANX2's more widespread expression [3], makes it attractive in the pannexin field, to study them in the context of their co-expression and interaction, that was previously shown as a factor regulating their channel function and trafficking [4-6]. In addition, another essential aspect that has gained notoriety over the years is the regulation by post-translational modifications (PTMs) that control several pannexin properties, ranging from fine-tuning regulation of channel activation to determining where the protein will be sorted in the cells [7, 8]. More importantly, defining how pannexins behave in physiological and pathological conditions has become a goal in studying this protein family and a promising path for developing novel and enhanced therapies against a broad range of illnesses, including neurodegeneration, inflammation, and cancer [9-11]. The overall goal of this thesis was to fill the gap of knowledge on PANX1 and PANX2 roles in the health and disease states of the skin. A particular emphasis was given to the regulation of PANX2 by two types of PTMs (e.g., N-glycosylation and caspase cleavage) that were not addressed by previous research. As increasing evidence showed that PANX1 (but not PANX2) is heavily involved in the tumorigenesis of cutaneous melanoma skin cancer, we included an exploratory study to test PANX1 contribution to melanoma progression *in vivo* and related events of immune infiltration.

In Chapter 2, we showed how PANX2 expression in the skin (particularly in keratinocytes) is represented by an uncharacterized splice variant (Pax2-202) that seems dominant at the protein level and present throughout skin aging. Moreover, we uncovered the PANX2 cleavable sites in the C-terminus by executioner caspases-3/7 during UV-induced cell death and the pro-apoptotic role of PANX2 in keratinocytes, which may participate in the

maintenance of skin homeostasis. In Chapter 3, we delved into the regulation of PANX2 intracellular sorting by N-glycosylation and found that although it is not a prerequisite, it assists with PANX2 trafficking to the cell membrane, with the latter enhanced by the concurrent presence of PANX1 in the cell. Importantly, we confirmed that N-glycosylation was not required for the interaction between PANX2 and the lower glycosylated species of PANX1. Finally, in Chapter 4, we generated a global *Panx1*-knockout (KO) melanoma mouse model to study the outcome of *Panx1*-deletion on melanoma progression and immune cell infiltration. We showed that *Panx1* global deletion does not reduce the tumorigenic effect of two prominent oncogenes (*Braf* and *Pten*) as mice devoid of PANX1 still exhibited disease progression and had no improvement in survival. However, we discovered that the lack of PANX1 remarkably increased the spleen size in a sex-specific manner in this model (a phenotype previously overlooked in all reported *Panx1*-KO models to date) and augmented the infiltration of effector anti-tumor T-lymphocytes and Granzyme B (GzmB) + cells in the TME that could be useful to enhance immunotherapy against melanoma. To our knowledge, this is the first study to examine the role of PANX1 on immune infiltration in the cancer context. This chapter will further discuss the relevance and limitations of our findings and propose new directions to continue advancing our understanding of pannexins in skin health and disease.

5.1.1 PANX1 and PANX2 expression and implications for regulation of skin homeostasis

Previous studies have demonstrated that PANX1 and PANX3 expression in the skin have significance in modulating skin development, renewal, and repair upon injury [12-18]. Furthermore, PANX1 and PANX3 expression levels fluctuate dependent on age, with PANX1 higher in newborn skin and lower in adult and aged skin, while PANX3 seems to be unchanged [12, 16]. To the extent of our knowledge, there were only two previous reports of PANX2 in the skin [3, 19]. In these reports, PANX2 expression at the protein and mRNA levels were detected in the skin after screening tissues of either wildtype or *Panx1/Panx3* double knockout mice, but its regulation through aging was not addressed. In Chapter 2, we further characterized PANX2 expression in the mouse skin of different ages and at cellular levels. Although we found PANX2 expressed as a splice variant

(PANX2-202) differing from the canonical isoform, further studies will be required to investigate if this is also the case for other tissues. Indeed, studies of splice variants remain limited and poorly understood in the pannexin field, in which most of the work has focused on PANX1 [20, 21]. Early studies identified two PANX2 human splice variants (PANX2alt1 and PANX2alt2) differing in length and speculated that the expression of one might play regulatory roles on the other one [22]. My studies and those of Abitbol *et al.* [19] were the first to bring attention to this differential expression in murine skin. However, the functional implications of each splice variant need to be addressed further. Since the differences in amino acid sequence fall within the first extracellular loop and the C-terminus of PANX2, the alternative splice variants may differ in channel function and localization.

In terms of its temporal expression, it seems that PANX2 follows a similar pattern to PANX3 and remains expressed in newborn and adult skin, the opposite to PANX1, suggesting that PANX2 and PANX3 may be needed in skin maintenance instead of development or early tissue maturation. This pattern of pannexin expression may be shared among tissues, although with some differences since, for example, in the murine central nervous system, PANX1 and PANX2 display opposite trends. *Panx1* mRNA levels are higher in embryonic stages before postnatal day 15 (P15) and decreasing onwards [23, 24]. In contrast, *Panx2* transcript and protein levels rise during postnatal development and are sustained during adulthood [25, 26]. Interestingly, *Panx2* expression is downregulated in immature mouse neurons during neurogenesis but re-expressed after terminal differentiation. This selective and temporal expression is thought to modulate the timing of neuronal differentiation [26].

On the other hand, PANX1 and PANX3 overexpression restrain keratinocyte proliferation, whereas PANX3 promotes keratinocyte differentiation, and excessive PANX1 dysregulates this process affecting epidermal architecture [12, 17]. Moreover, PANX1 and PANX3 have also been reported to regulate keratinocyte proliferation and migration [12, 17, 18]. Although poorly understood, some of the molecular mechanisms governing these processes have been elucidated [17]. However, until the writing of this thesis, most of these

elements warrant further investigation in the PANX2 context. Following our results in Chapter 2, I propose that PANX2 may be relevant for keratinocyte differentiation and programmed cell death in the skin, thus supporting skin homeostasis. In agreement with this, we found PANX2 increased in a differentiating rat keratinocyte cell line and enriched intracellular immunofluorescence staining in the suprabasal layers of the epidermis, as has been reported with PANX1 and PANX3 subcellular localization [12, 13, 16, 18]. This finding highlights the possibility that PANX2 may be required during keratinocyte differentiation, perhaps as a Ca^{2+} /ion channel as previously suggested for paralogs PANX1 and PANX3 [17, 27, 28]. The calcium gradient in the epidermis is essential for regulating keratinocyte differentiation [29], and pannexins could have a redundant function to connexins, transient receptor potential (TRP), and other intracellular channels closely related to the regulation of Ca^{2+} abundance and its uptake by keratinocytes in the epidermis [30]. It has been speculated that PANX2 could function as a Ca^{2+} channel at the ER based on its localization in the ER-mitochondria contact sites [31]. However, there is a lack of supporting evidence and reliable methods for testing PANX2 Ca^{2+} channel function. Additionally, we also detected the PANX2-202 splice variant in primary dermal mouse fibroblasts, where its mRNA expression is downregulated after TGF- β -induced *in vitro* activation into myofibroblasts. As discussed in Chapter 2, this could point out a different role of PANX2 in these cells, where its expression may restrain fibroblast differentiation or is no longer required in myofibroblast activation, a subject that could be explored further.

The germline deletion of *Panx1* and *Panx3* has consequences for skin architecture as well as keratinocyte and fibroblast differentiation during wound healing [16-18]. Notably, no overt skin phenotype was reported in a previous *Panx2*-KO mouse model, but this mouse was not thoroughly characterized and is not publicly available [9]. In that case, we could argue that a closer inspection of the skin in the *Panx2*-KO model, especially under stress conditions or after an injury, has the potential to reveal differences compared to the wildtype counterpart [32]. However, a factor to consider is that any PANX2 deficiency due to the germline deletion may be ameliorated by compensation with other channels (such as connexins hemichannels) or other pannexin proteins as it has been suggested for

the skin and other tissues (e.g., neurons, arterial wall, and vomeronasal organ) using *Panx1*-KO and *Panx3*-KO models [19, 33]. Furthermore, given the known contribution of pannexin dysregulation to a myriad of pathophysiological processes [34, 35], the differential and temporal expression suggest that tight control of pannexin activity is required for proper cell differentiation and homeostasis in adult tissue. Nevertheless, more research on the significance of *Panx2* expression for skin development and maintenance is required.

5.1.2 Considerations on the importance of PANX2 N-glycosylation for its subcellular trafficking and interaction with PANX1

In Chapters 2 and 3, we uncovered the specific sites for caspase cleavage and N-glycosylation modifications previously predicted in [8]. Moreover, we demonstrated the implications of such PANX2 PTMs for subcellular trafficking, intermixing with PANX1 (Fig. 5-1), and contributions to the cellular homeostasis and programmed cell death mechanisms. In particular, N-glycosylation appeared crucial for PANX2 proper folding and intracellular compartmental distribution.

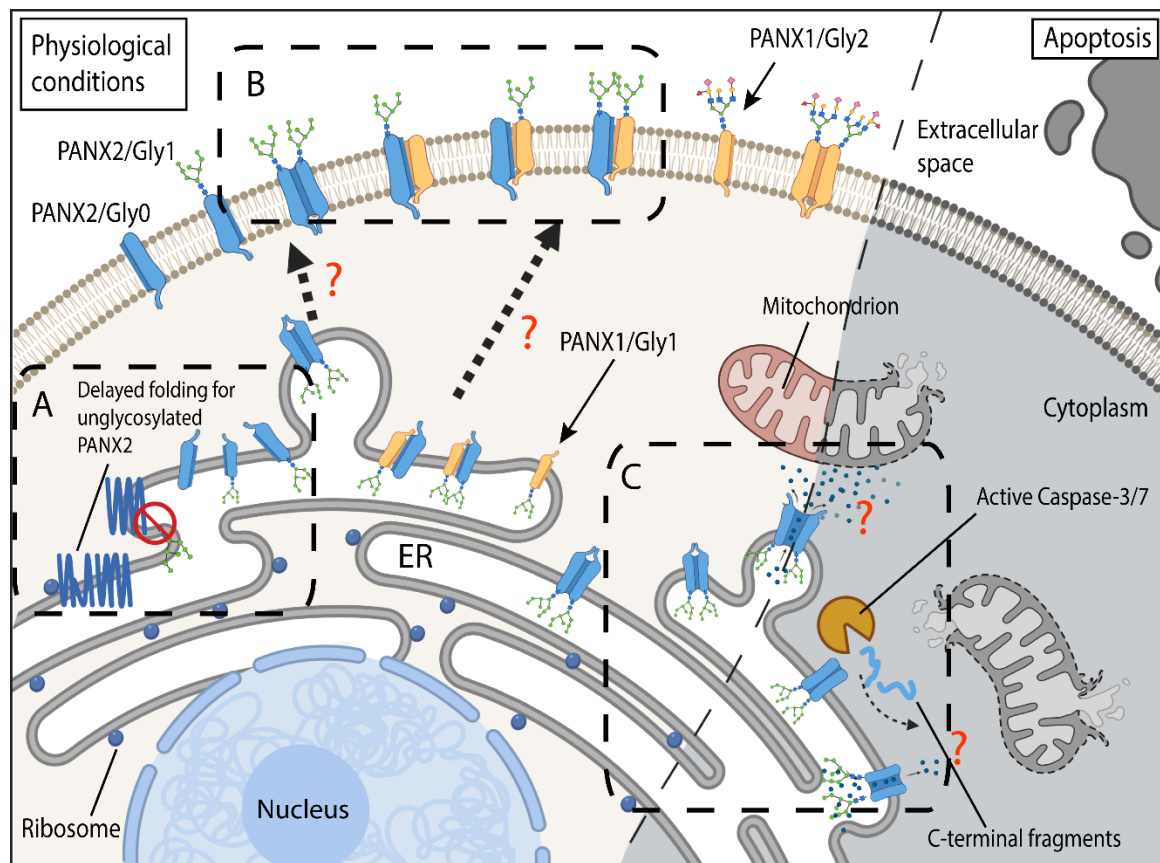
Figure 5-1.

Figure 5-1 Graphical representation of the proposed model of PANX2 regulation by N-glycosylation and caspase cleavage.

PANX2 is synthesized in the endoplasmic reticulum (ER) and post-translationally modified by N-glycosylation, aiding its folding (**inset A**) and further sorting within the cells during physiological conditions. PANX1 and PANX2 monomers can interact within the ER and be transported by an unknown pathway (dotted arrows) to the cell membrane. Lower glycosylated PANX1 species (Gly0 and Gly1) can interact with PANX2 regardless of its glycosylation status (**inset B**). The putative channel function of PANX2 in the ER may regulate the ER-mitochondrial crosstalk, especially during the activation of programmed cell death (apoptosis), where PANX2 accelerates the cascade of apoptotic events leading to caspase 3/7 activation. As the PANX2 C-terminus is targeted by caspase-3 cleavage, it is unclear whether this proteolytic cleavage influences its biological function during cell death (**inset C**). Figure created with BioRender.com.

Since all pannexins have consensus sites for N-glycosylation [8], this distinctive PTM may play a significant role in their regulation, considering that most glycoproteins synthesized in the ER must undergo glycosylation as the first step for quality control mechanism against protein misfolding. Furthermore, in the amino acid sequence of PANX2, there is a high degree of conservation of this site among species (Fig. 5-2), suggesting that from an evolutionary point of view, glycosylation may be a crucial step to guarantee the proper folding of PANX2, which at the same time is a larger protein compared to the other pannexins paralogs. Indeed, the protein quality control system (QC) in the ER is expected to retain misfolded proteins, where a retrograde export mechanism or ER-associated degradation (ERAD) pathway secures their degradation by the cytosolic-ubiquitin proteasome system [36]. Thus, although the intracellular aggregation of the unglycosylated PANX2^{N86Q} mutant was likely protein misfolding due to overexpression, it confirmed the N-glycosylation importance in PANX2 since the wildtype glycosylated canonical variant was subjected to similar conditions and never was found aggregated as the mutant. In that respect, the misfolded PANX2^{N86Q} mutant decreased colocalization with chaperones (e.g., PDI) and delocalization of Golgi elements (e.g., GM-130) and possibly triggered cellular stress. However, we did not measure unfolded protein response or oxidative stress indicators [37], but in our experience, cell death was common upon transfection of the *Panx2* constructs. This suggests that dysregulation of PANX2 expression or defects on its glycosylation may be deleterious for the cell, especially if it plays pro-apoptotic roles, as shown in Chapter 2 and proposed elsewhere [9, 31, 38].

Figure 5-2 N-glycosylation site in mouse PANX2 is highly conserved among species.

Red squares indicate the PANX2 N-glycosylation and the caspase cleavage sites identified in this thesis. Only N86 exhibited a high degree of conservation. Conservation analysis was performed in the ConSurf web server (<https://consurf.tau.ac.il/>) [37]. The Homologues sequences were collected from UNIREF90, and Multiple Sequence Alignment was built using MAFFT. The homolog search algorithm used was HMMER (E-value: 0.0001). Maximal sequence identity was 95%, and 150 sequences were sampled conforming to the list of homologs of a minimum 35% identity. Conservation scores were calculated using the Bayesian method.

It is generally accepted that glycoproteins exhibiting high-mannose species are more localized to the ER, whereas those that transit through Golgi are prone to turn into complex glycosylated proteins that end in the plasma membrane. Indeed, studies on PANX1 indicated that similar to what we observed with PANX2^{N86Q}, PANX1 glycosylation-defective mutant (N254Q) has a reduced surface expression, but it can still form dye uptake channels in the cell membrane [8]. Thus, glycosylation in pannexins assists with intracellular sorting but is not a requirement for cell membrane trafficking. In this respect, some authors have indicated that based on the characteristic intracellular location and glycosylation level (up to Gly1 only), PANX2 cell membrane localization may be an artifact of overexpression and follows an alternative sorting mechanism than the other pannexins [7, 31, 39]. In this respect, Bhalla-Gehi et al. (2009) showed that PANX1 and PANX3 follow the same ER-Golgi route through a secretion-associated and RAS related (Sar1) GTPase-dependent and coat protein II (COPII)-mediated pathway; thus explaining the resulting Gly2 species [39].

PANX2 does not transit through Golgi in our proposed model, but how it reaches the cell membrane independently of N-glycosylation remains elusive. Le Vasseur *et al.* (2019) showed ectopic EGFP-tagged PANX2 in C6 rat glioma cells and endogenous PANX2 in mouse brain localized to membranes of the ER-mitochondria contact sites but not in other organelles [31]. This evidence also suggested that PANX2 does not transit through Golgi compartments and is retained in the ER. In contrast, although under ectopic overexpression conditions, in Chapter 3, we detected untagged mouse PANX2 colocalizing with GM-130 (a cis-Golgi marker) and at the cell surface. Thus, we speculate the difference seen in localization is cell-type and condition-specific, as other authors have reported [8, 26, 31]. Nevertheless, we support the notion that PANX2 follows an alternative anterograde trafficking pathway that bypasses the Golgi apparatus, which will require further investigation.

It is important to note that besides glycosylation, there are other determinants of anterograde trafficking of pannexins. The C-terminus is the most highly heterogeneous domain varying in sequence homology and length in pannexins. Notably, the PANX1 C-

terminus has proven to be a potent regulator of its oligomerization and trafficking. There are examples of mutation or truncation of the PANX1 C-terminal domain enough to cause its retention in the ER and limit its glycosylation to Gly1 species [40, 41]. Furthermore, a previous study using a chimeric PANX2 containing the PANX1 C-terminus showed that the PANX1/2 chimera had a diffuse intracellular distribution different from the canonical mouse PANX2 and insufficient capacity to relocate to the cell surface [42]. In agreement with these authors, we can reason that determinants at the C-terminal domain do not control the mechanism for regulating PANX2 trafficking as in PANX1 [43].

Finally, although co-expression experiments with different pannexins have shown that the glycosylation state can modulate the level of interaction among paralogs [5], we found that for PANX2, glycosylation status was not a limiting factor, at least for interacting with PANX1. We also confirmed that PANX1 and PANX2 intermixing increases the trafficking of both pannexins to the cell membrane. Such interaction may occur preferentially at the ER level since we found it consistent that only high-mannose and un-glycosylated PANX1 species are co-immunoprecipitated with PANX2, regardless of PANX2 glycosylation status [6, 8]. Considering the relevant role of PANX1 in the skin, it would be interesting to determine if PANX1/PANX2-202 intermixing occurs naturally when both pannexins are expressed simultaneously in neonatal skin cells and whether it influences their function in those cells.

5.1.3 Possible pro-apoptotic roles and effects of caspase cleavage of PANX2 in skin cells

As we discussed before, one of the critical functions of the skin is to act as the first barrier against external pathogens and other environmental insults, including UV radiation. In Chapter 2, UVB light was used as a relevant biological model to induce lethal damage to keratinocytes to test whether PANX2 expression would influence their programmed cell death response. According to our data, PANX2 promotes keratinocyte death during UVB-induced apoptosis independently of its cleavage at the C-terminus. Thus, we can reason that the low but continuing PANX2 expression in the upper layers of the epidermis of adult skin tissue may help ensure opportune apoptosis after deadly insults like UVB, something

we discuss further in the following paragraphs. However, this hypothesis would need to be tested in an *in vivo* context. To evaluate PANX2 relevance for cell death and skin lesions after UVB skin exposure (sunburn), perhaps a mouse model with inducible and keratinocyte-specific *Panx2*-deletion would be better rather than germline-deletion to reduce any compensatory mechanisms by the expression of other paralogs or channel proteins.

In addition, due to previous reports on PANX2 participation in different types of cell death (e.g., cytokine-mediated, thapsigargin-, staurosporine-, ischemia-induced apoptosis and ferroptosis) [9, 31, 38, 44, 45] and the potential of caspase-3/7 to cleave PANX2 [8], here we aimed to define the site of this PTM and whether this proteolytic cleavage has any effect on the UVB-induced programmed cell death. In other contexts, PANX1 at the cell surface is cleaved by the same executioners caspases cleaving PANX2 [8], activating the channel constitutively to release ATP and other metabolites in dying cells [46-48]. Since PANX2 is more likely to form intracellular channels in the ER membranes and to be located in the ER-mitochondria contact sites [31], a plausible theory is that, as we mentioned before, PANX2 channels may serve as a conduit for ions (e.g., Ca^{2+}) (Fig. 5-1) in the ER as it has been proven for the intracellular PANX3 channels in keratinocytes [17]. However, further research will need to address how caspase cleavage would alter PANX2 channel permeability and the implications for the apoptotic process. In this sense, since we did not observe a substantial dysregulation of the apoptotic rate between cells expressing wildtype and caspase cleavage-resistant PANX2^{D416A}, we attempt to speculate that the PANX2 gating mechanism is different and may not be as significantly altered by caspase cleavage as it happens with PANX1 [46-50].

In physiological conditions during terminal differentiation, caspase-3 is not readily cleaved/activated [51]. We have observed that PANX2 levels (at least *in vitro* in REK cells) are increased during keratinocyte differentiation, implying that PANX2 makes differentiating keratinocytes more susceptible to cell death if UVB damage occurs. Thus, by fostering apoptosis of UVB-damaged cells in the skin, PANX2 could be part of a mechanism to eliminate populations of malignant keratinocytes and act as a tumor

suppressor as it has been proposed in other cell contexts like glioma [38, 52]. Interestingly, Cowan and colleagues (2012) showed that PANX1 and PANX3 levels are highly reduced in human keratinocyte tumors (basal and squamous cell carcinomas) compared to normal epidermis samples [13]. However, no evidence of dysregulation in PANX2 expression in these cancers has been shown to date. Therefore, it would be interesting to investigate whether PANX2 expression may play a protective role against the development of basal and squamous cell carcinomas that are the most common cutaneous malignancies, mainly due to sun-damaged skin [53, 54].

Notably, our data showed that the cleavage of PANX2 C-terminus in apoptotic keratinocytes does not significantly influence the apoptosis rate. However, we cannot rule out that this caspase-mediated PANX2 cleavage will have the same effect in other cells and different physiological and pathological circumstances. For example, it has been shown that caspase-3 activation occurring in the spinous layer of the epidermis (where differentiating keratinocytes are located) is related to pathologic events in atopic dermatitis but at the same time could also be occurring in physiological contexts like in basal (undifferentiated) keratinocytes during epidermal renewal [55]. Since PANX2 is targeted by caspase-3, we wonder if a link between PANX2 and any of those processes exists in keratinocytes.

5.1.4 Pannexin 1: a new regulator of tumor immune infiltration in melanoma

In the context of skin disease, it is known that PANX1 can be dysregulated with a high expression in malignant melanoma [56]. Since our group has reported that the genetic and pharmacological inhibition of PANX1 decreases melanoma cells' tumorigenic properties *in vitro* and *ex vivo* [56-58], in Chapter 4, we examined the effect of global deletion of *Panx1* on *in vivo* melanoma progression by crossing the Genentech *Panx1*-KO mice [59] with the inducible melanoma model: *Braf*^{CA}, *Pten*^{loxP}, *Tyr::CreER*^{T2} (BPC) [60]. Contrary to our expectations, *Panx1* germline deletion did not reduce the effect of *BRAF*(V600E) mutant and *Pten*(deletion) oncogenes in inducing primary tumor formation, invasion to lymph nodes, nor improved BPC mice survival (Figure 5-3). Although at first, this may

appear inconsistent, it is essential to note that there are significant differences between *in vitro* and *ex vivo* (melanoma cell cultures, tumors grown in Chick -CAM) [56-58] and *in vivo* (mouse model) (herein, Chapter 4) where PANX1 role has been tested. The increased complexity of the factors (e.g., hallmarks of cancer, driving mutations, TME, and tumor-immune cells interplay) [61, 62] leading to tumor formation and progression to metastatic disease in melanoma can explain why the simply global deletion of *Panx1* does not thwart melanoma tumorigenesis *in vivo*.

We also explored if the *Panx1* deletion could induce changes in the expression of *Panx2* in the non-melanoma skin and the tumors. However, real-time qPCR data indicated that *Panx2* mRNA expression does not significantly change when comparing BPC-*Panx1* genotypes (WT vs. KO) and non-melanoma skin versus melanoma tumors, ruling out any compensatory effect PANX2 may have. Previously, PANX2 was identified as a marker for prostate cancer cells [45], and it was associated with shorter survival of clear cell renal cell carcinoma patients [63]. Although not included in Chapter 4, we further analyzed TCGA patient data that showed no correlation between *PANX1* and *PANX2* expression or survival prediction in patients with melanoma (Fig. 5-4). Therefore, we concluded that PANX2 levels are not significantly altered in melanoma skin cancer which would agree with our data in Chapter 2, where *Panx2* expression seems more related to keratinocytes than melanocytes, the primary cell type dysregulated and causative of melanoma.

Figure 5-3

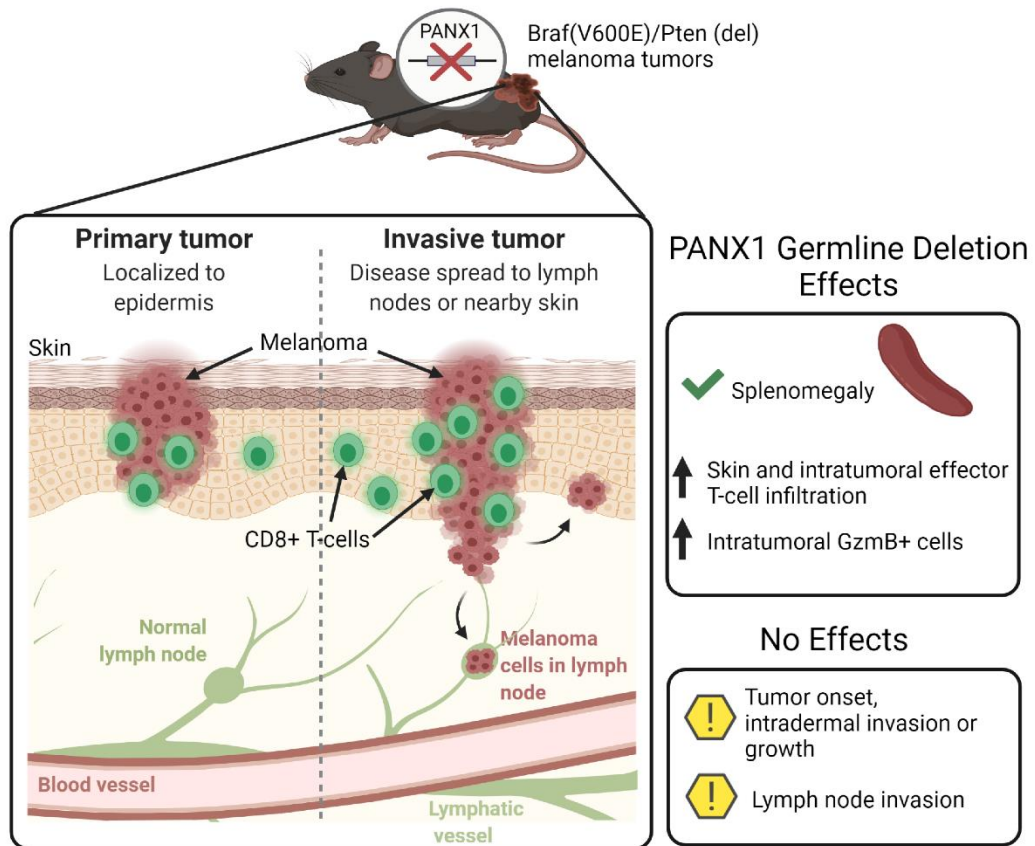


Figure 5-3 Graphical representation of main findings in the *Panx1*-deficient BPC mouse melanoma model.

Global deletion of *Panx1* did not influence tumor onset, invasion to draining lymph nodes, and melanoma progression in BPC mice. However, splenomegaly was a phenotypic characteristic of BPC-*Panx1*KO mice of unknown significance, and there was a significant increase of effector T-lymphocytes and Granzyme B+ cells (GzmB+) in the TME. Figure created with Biorender.com.

Figure 5-4.

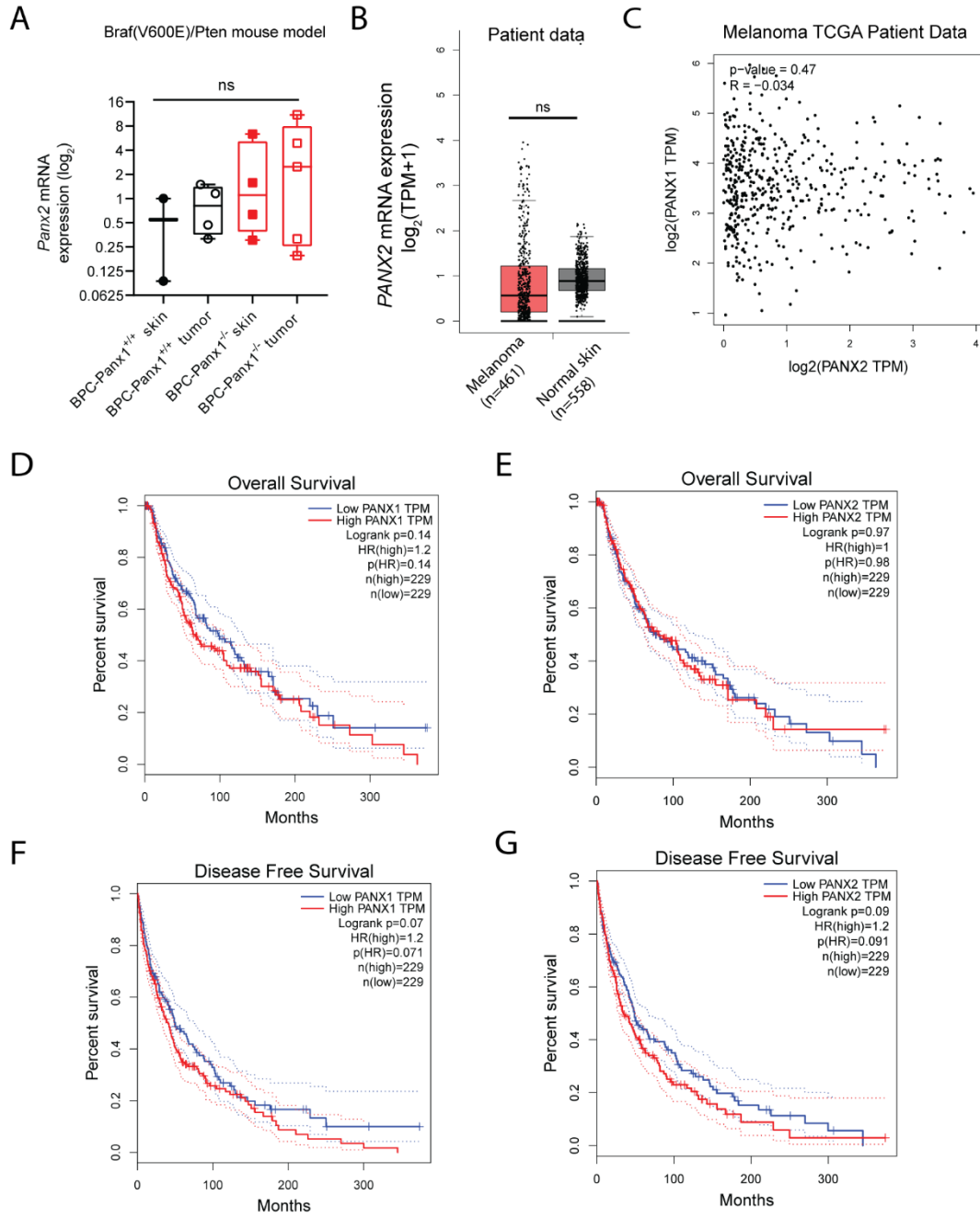


Figure 5-4 *PANX2* mRNA expression does not correlate with *PANX1* nor predict survival of patients with malignant melanoma.

(A) Analysis of *Panx2* transcript expression in the BPC mouse model (Chapter 4) revealed similar mRNA expression in tamoxifen-induced tumors compared to matched non-tamoxifen treated skin samples regardless of the BPC-Panx1 genotype. *Gapdh* was used as the housekeeping gene for normalization. At least N=5 paired samples were assayed by triplicate (n=3) for real-time-qPCR analysis. Statistical significance is shown as $p < 0.05$ (*).

(B) Matched normal skin (data from TCGA and GTEx) and melanoma tumor patient samples (from TCGA) display no significant differences in mRNA expression. (C) *PANX1* and *PANX2* mRNA expressions are not correlated and do not predict survival of cutaneous melanoma patients (D-G). Symbols display the individual expression data per mouse or patient. Box plots represent the 95% confidence interval (CI) and the median (inner line), with whiskers representing the maximum and minimum gene expression values. T-test (for B) or two-way ANOVA and Tukey's post hoc test (for A) were used to compare the means $\log_2(\text{Expression})$. Patient samples gene expression and survival analysis were done using the GEPIA web server [64].

Remarkably, the spleens of female tumor-induced BPC-*Panx1*-KO mice were significantly enlarged compared to male mice, a phenotype not previously reported for *Panx1*-KO mice. The spleen is a secondary immunological organ that controls hematopoiesis, red blood cell clearance, and immune response against blood-borne pathogens and foreign materials [65]. Spleen enlargement (splenomegaly) has been observed in tumor cell transplantable models [66, 67] where specific immune cells (e.g., T-lymphocytes, monocytes, and immunosuppressive myeloid cells) generated or in transit through the spleen can modulate cancer progression for the host [68]. Furthermore, in age-matched tumor-bearing mice littermates, the number of splenocytes (spleen cells) can increase progressively in proportion with the days of tumor growth in mice [69]. Although we did not measure the cell density or the relative cell size per spleen to rule that out, we do not consider that this was the cause of such sex-specific difference in spleen size since both cohorts of mice lived for a comparable length of time after tumor induction. In addition, our measurements of cell proliferation (assessed by Ki67 immunofluorescence) showed that tumor-bearing mice lacking PANX1 had a significantly lower number of proliferative spleen cells per field of view, ruling out any contribution of cell proliferation due to the tumor induction. It is important to consider that sexual dimorphisms already exist in the response of *Panx1*-deficient mice during pathological states such as ischemia [70] and epilepsy [71], so in this case the presence of the tumor could be a factor influencing this phenotypic difference in BPC-*Panx1*^{-/-} mice.

Furthermore, although malignant melanoma can metastasize to the spleen and cause splenomegaly, it is an infrequent occurrence in patients and is mainly found after autopsies [72, 73]. In our case, we did not find a conclusive indication of metastasis to the spleen (like black lesions seen under the skin and the lymph nodes); thus, further immunohistochemical analysis was not pursued. To the extent of our knowledge, only one report of increased spleen size exists for the BPC mouse melanoma model due to the treatment with an anti-CD40 agonist antibody used to evoke an anti-tumor response and restrict tumor growth and, as a side note, did not increase in intra-tumoral infiltration CD4+ and CD8+ T-cells [74]. Thus, the increased TILs in skin and tumor tissues of BPC-*Panx1*-KO mice may not be a direct consequence of the splenomegaly but an effect of the *Panx1*

germline deletion itself in this mouse strain that will need to be further studied. On the other hand, it is possible that prolonged pharmacological targeting of PANX1 through systemic application of PANX1 blockers (CBX, PBN, or spironolactone) could act in the spleen and cause similar effects on the size of this organ. Thus, future studies looking at pharmacological inhibition of PANX1 should consider this and evaluate the consequences for the inflammatory response.

In my opinion, the significant increase of CD4⁺, CD8⁺ T-lymphocytes, and GzmB⁺ cells in tumors of BPC-*Panx1*-KO mice needs to be explored further. Although it has been suggested that this melanoma model is poorly immunogenic [75-78], many authors continue using it to study factors regulating immune infiltration and to test new approaches for immunotherapy [74, 79-87]. This "so-called" low immunogenicity strengthens our results in showing that somehow the *Panx1* deletion elicits increased TILs in the context of this cancer. Indeed, more extensive evidence shows that BRAF-mutated melanomas exhibit immunologically 'cold' features (reviewed in [88]) where low T cell infiltration and increased immunosuppressive cells are unfavorable elements for immunotherapy (i.e., checkpoint inhibitors). In this respect, as we explained in Chapter 1, checkpoint inhibitors block the engagement of immune checkpoint molecules in immune (e.g., CTLA-4, PD-1, PD-L1) and tumor cells (e.g., PD-L1), preventing activation of effector T cells and further elimination of cancerous cells [89]. Indeed, checkpoint inhibitor therapy is currently the standard of care for patients with advanced metastatic melanoma [90] but has a limited patient response rate, in part due to limited tumoral immune cell infiltration. Based on our results, it is possible that targeting PANX1 before immune checkpoint inhibitor therapy could increase CD4⁺ and CD8⁺ T cell infiltration in TME, boosting the effect of this immunotherapy. Notably, this treatment could be expanded beyond BRAF-mutant patients with metastatic melanoma, including a larger cohort that may not qualify for kinase inhibitor therapy as PANX1 is also overexpressed in most patients regardless of the BRAF mutation status or the stage of the disease (Chapter 4, Fig S4-1 and [56]).

Of note, β -catenin signaling and PTEN loss have been revealed as a mechanism leading to a non-T cell-inflamed TME and resistance to therapy in patients [84, 91]. Previously,

Spranger et al. (2015) showed that the activation of the WNT/ β -catenin pathway, intrinsic of melanoma cells, correlates with the lack of T cells in metastatic melanoma, hindering the therapeutic effect of checkpoint blockade therapy that depends on the reactivation of tumor infiltrated CD8+ T cells [87]. Furthermore, the same group showed that activation of β -catenin in tumor cells causes immune evasion due to defective tumoral recruitment of CD103+ dendritic cells and defective T cell priming against tumor-associated antigens [87]. Interestingly, in keeping with our results, the BPC mice used in that study showed infiltration of CD4+ and CD8+ T-cells but also the expression of markers of T cell dysfunction (e.g., *PD-1* and *Lag3*), PD-L1, and defective production of IL-2 in the melanoma tumors, requiring a combination of anti-CTLA-4 and anti-PD-L1 monoclonal antibodies to delay tumor outgrowth [87]. Interestingly, recent evidence by our group confirmed that genetic or pharmacological inhibition of PANX1 in melanoma cells decreases expression and disrupts localization of β -catenin and transcription of downstream target genes like MITF [58]. Thus, it is conceivable that in our BPC-*Panx1*-KO model, the lack of PANX1 in melanoma cells enhanced T cell infiltration into the TME, yet checkpoint inhibitor therapy would still be required to ameliorate tumor progression. However, such models require further verification as we did not test for differences in β -catenin expression in the induced tumors nor used checkpoint inhibitors as a therapeutic resource.

5.2 Experimental Limitations

In Chapter 2, we proved by real-time qPCR that two *Panx2* transcripts could be detected in the skin at all ages assayed, and using three different affinity-purified polyclonal antibodies, we verified its expression at the protein level. However, immunoblots indicated various immunoreactive species that differed from the expected MW of canonical PANX2. As shown previously for pannexins [1, 8], such variation in the banding profile could indicate the presence of PTMs or gene-splicing events rendering different transcript and protein variants. In our case, our assessment of the PANX2-202 splice variant included verifying predicted isoforms shown in genomic databases. Thus, based on the MW and transcript sequence differences, we were able to identify which splice variant was most

likely to be in the skin. However, the use of polyclonal antibodies brings disadvantages to detecting specifically the protein of interest due to the recognition of multiples epitopes and increased cross-reaction with similar antigens (false positives) and heterogeneity within the sample [92]. Thus, the anti-PANX2 polyclonal antibodies may have recognized not only the PANX2-202 isoform but other unrelated proteins affecting the specificity and sensitivity of PANX2 detection and localization in the skin. Therefore, further work to verify PANX2 protein in the skin more accurately should be carried out using a *Panx2*-KO mouse model or preincubation with cognate peptides as controls as it has been done in the past to validate other anti-pannexins antibodies [1, 8, 15]. In addition, despite possibly low endogenous PANX2 expression in the skin, mass spectrometry would be ideal for peptide fingerprinting since previous reports indicate that transcription levels are a poor predictor of PANX2 protein abundance in different tissues [3].

Another aspect that had experimental limitations was the *in vitro* differentiation studies done in keratinocytes. As mentioned in Chapter 2, only significant changes in PANX2 expression after Ca^{2+} induction were detected using the immortalized REK cell line but not in primary mouse keratinocytes. In addition, some differentiation markers did not significantly change as were expected (e.g., *k5*, *k14*, *Ivl*) to indicate a proper transition to terminal differentiation of the primary keratinocytes. Therefore, we cannot rule out that our *in vitro* experimental conditions may not have been optimal for complete keratinocyte differentiation and show significant upregulation of mouse *Panx2-202* due to incomplete or abnormal differentiation, which is typical for *in vitro* models of keratinocyte differentiation [93].

On the other hand, to determine the effect of PANX2 cleavage during apoptosis, we used CRISPR-Cas9-mediated genetic deletion and transient overexpression of canonical mouse PANX2 and the PANX2^{D416A} mutant rather than using the rat ortholog and stable expression in the REK cell line. The drastic PANX2 deletion or overexpression could affect the intrinsic aspects of programmed cell death (e.g., cytosolic Ca^{2+} flux and mitochondrial overload [94]), especially considering that PANX2 has been found in the mitochondria-associated membranes interface that is critical for regulating Ca^{2+} homeostasis and

crosstalk between ER-mitochondria during apoptosis (reviewed in [95]). Furthermore, as we mentioned in Chapter 2, the rat *Panx2* has only one spliced form, which is canonical and has a different conservative substitution (D to E) at the 416 residue that renders this site uncleavable by caspases 3/7 but maintain the site D400 that is also conserved in human PANX2 and the mouse splice variant PANX2-202. However, we did not confirm whether the endogenous rat PANX2 ortholog can still be cleaved by apoptotic caspases or investigated why wildtype REK cells exhibited the highest rate of apoptosis that the wildtype mouse PANX2 overexpression could not entirely rescue.

In Chapter 3, we observed that overexpression of the un-glycosylated Panx2^{N86Q} mutant led to increased intracellular aggregation. Thus, N-glycosylation seems to avoid PANX2 aggregation in the ER and Golgi compartments, possibly due to misfolding of the Panx2^{N86Q} mutant [96]. However, these misfolding events were likely exacerbated by overexpression since cells expressing lower levels of the unglycosylated mutant did not exhibit such a degree of protein aggregation. For that purpose, it would have been beneficial to use stably expressing cells.

Moreover, as discussed in Chapter 4, the BPC mouse model displayed very aggressive melanoma tumors, as reported by [60, 97]. The fast tumor growth rate made it impossible to detect other visceral metastasis (e.g., lungs [60]) that would have been valuable for a more clinically translatable characterization of immune infiltration. Furthermore, despite our attempts in limiting the age group for analysis to avoid the known spontaneous formation of tumors (due to leaky Cre, in >3 months old mice reported by [60]), on some occasions, multiples spontaneous cutaneous tumors arose, prompting us to euthanize the mice very early in our protocol. The latter could have limited our ability to determine a more accurate survival analysis and extend our study to distant metastasis more clinically relevant to characterize the immune infiltration. In the same chapter, we detected increased spleen size of tumor-bearing mice; however similar comparison was not performed in non-tumor induced or non-BPC mice; thus, it is difficult to define whether this phenotype in *Panx1*-deficient mice is distinguished only under melanoma tumor conditions. Moreover, the tumor immune infiltration characterization was limited to markers for a selected

immune cell population and using real-time qPCR and immunofluorescence. However, we omitted other relevant immune cells like MSDCs and markers of other lineage-specific myeloid cells like M2-polarized tumor-associated macrophages essential in the melanoma immune evasion and exclusion mechanisms [62, 98]. Besides, using other more high-throughput techniques such as flow-cytometry with multiple and more extensive cell surface markers would have been beneficial to identify and quantify the immune cell subtypes in the tumors more accurately.

5.3 Future directions

Although our findings contribute to a better understanding of transcriptional and PTM regulation of pannexins, they also opened new questions that need to be addressed in further studies. Throughout the text in previous chapters, we did include some details about future research that could be done to investigate their role during health and disease in the skin. In the following paragraphs, we will summarize some of the work that needs to be addressed to complement the results showed by this thesis.

In Chapter 2, we showed that the PANX2-202 splice variant is the dominant isoform in the skin. Since most of the research elsewhere has only focused on the canonical variant of PANX2, further characterization of its expression in other organs, including the brain, would clarify if this is a tissue-specific variant or has regulatory roles, as was suggested early on with the other alternative human splice variants [22]. We also noted that PANX2 levels are likely to increase during keratinocyte differentiation in agreement with the high immunostaining of the suprabasal layer of the mouse epidermis (Chapter 2, Fig 2-2). Thus, it would be interesting to know whether PANX2 is important or influences the keratinocyte differentiation process by overexpression and gene silencing experiments, including organotypic epidermis *in vitro* models and the analysis of the dorsal skin of PANX2-deficient mice under normal and pathological stages (e.g., wound healing), as has been already done for PANX1 and PANX3 [12, 16-18].

Regarding the pro-apoptotic role of PANX2 in the skin, experiments encompassing the measurement of the intracellular PANX2 channel function in keratinocytes are desirable.

However, we recognize that no PANX2-specific channel blockers, inhibitors, or a straightforward way of stimulating the opening of PANX2 channels have been reported to date, making this task extremely difficult, on top of the various intracellular ion channels that may have a similar activity in the ER. Therefore, a combination of gene silencing and genetically engineered PANX2 channels, perhaps as done before with PANX1 with the introduction of Tobacco Etch Virus (TEV) protease sites [47] or photocleavage by optogenetics [99], would help elucidate the consequences of constitutive PANX2 channel opening. At the same time, it is puzzling how the caspase cleavage at the PANX2 C-terminus has no apparent effect on the cellular apoptotic rate. Now that we discovered the specific sites where this cleavage occurs, further work clarifying the role of such modifications can be undertaken using different cell lines.

Chapter 3 identified N-glycosylation as a regulator for PANX2 subcellular localization, but the remaining question is whether endogenous PANX2 and its splice variant are glycosylated and under what circumstances. Interestingly, S-palmitoylation is another PTM shown in PANX2 un-glycosylated species that likely prevents its localization to the cell membrane before terminal neuron differentiation [26]. Thus, a further exploratory study could determine the glycosylation status of PANX2 is influenced by the differentiation status in keratinocytes. On the other hand, due to the low endogenous protein levels in this tissue, we did not perform PANX2 de-glycosylation experiments as these are more amenable in overexpression systems than with lower endogenous protein amounts. Future experiments should consider cloning the PANX2-202 splice variant and test if glycosylation and caspase cleavage also regulate this isoform and determine the influence of co-expression with the canonical on keratinocyte differentiation and apoptosis.

Finally, in Chapter 4, due to the complex interplay of cells expressing PANX1 in the melanoma TME, using the BPC model, it was not possible to determine in what cell type (cancer or immune cell) PANX1 exerts a dominant role in aiding the disease progression. We previously knew that PANX1 contributes to the tumorigenic properties of melanoma cells and the inflammation in other contexts different from cancer. Our findings suggest that PANX1 regulates immune phenotypic characteristics like the spleen morphology and

recruitment of T-lymphocyte effector cells and other GzmB⁺ cells to the melanoma tumor. Future experiments should explore this and the molecular mechanisms (e.g., activation of signaling pathways, nucleotide, cytokine, or metabolite release) or cellular processes (e.g., phenotype switching and migration of immune cells) behind this enhanced immune cell recruitment into the tumor. Experiments involving a more controlled syngeneic melanoma model or adoptive immune cell transfer from *Panx1*-KO mice would help elucidate where and how targeting PANX1 can aid tumor regression. More importantly, exploratory studies using PANX1 blockers combined with checkpoint inhibitor therapy (anti-PD-1, anti-CTLA4 antibodies) could help determine how relevant targeting PANX1 is for immunotherapy and the clinical setting.

In addition, recent evidence has shown that tumor growth and T cell response is sex-dependent in a syngeneic melanoma mouse model where females had less tumor growth rate and higher populations of CD4⁺ and CD8⁺ cells compared to males [100]. Thus, it is interesting that we found that females had a more aggressive tumor growth compared to males of the BPC-*Panx1*^{+/+} cohort, but this was not the case for *Panx1*-KO mice. Therefore, the increased immune cell infiltration in skin and tumors and the sex-specific differences in spleen size of the *Panx1*-KO mice may have influenced this, and future work should include sex as an essential factor for evaluating the anti-tumoral response in *Panx1*-targeted experiments.

5.4 Overall conclusions

In summary, the work presented in this thesis complement the growing evidence of the diverse roles of pannexins contributing to critical cellular processes (e.g., differentiation and cell death) in health and disease states of the skin. Moreover, we demonstrated how regulation by PTMs like glycosylation and caspase cleavage define PANX1 and PANX2 localization, their interaction, and potentially their function within the same cellular context. This thesis further revealed the translational potential of PANX1 that needs to be studied along with immunotherapy to likely improve the clinical outcome of cutaneous melanoma.

5.5 References

1. Penuela, S., R. Gehi, and D.W. Laird, *The biochemistry and function of pannexin channels*. Biochim Biophys Acta, 2013. **1828**(1): p. 15-22.
2. Narahari, A.K., et al., *ATP and large signaling metabolites flux through caspase-activated Pannexin 1 channels*. Elife, 2021. **10**.
3. Le Vasseur, M., et al., *Pannexin 2 protein expression is not restricted to the CNS*. Front Cell Neurosci, 2014. **8**: p. 392.
4. Ambrosi, C., et al., *Pannexin1 and Pannexin2 channels show quaternary similarities to connexons and different oligomerization numbers from each other*. J Biol Chem, 2010. **285**(32): p. 24420-31.
5. Penuela, S., et al., *Glycosylation regulates pannexin intermixing and cellular localization*. Mol Biol Cell, 2009. **20**(20): p. 4313-23.
6. Sanchez-Pupo, R.E., D. Johnston, and S. Penuela, *N-Glycosylation Regulates Pannexin 2 Localization but Is Not Required for Interacting with Pannexin 1*. Int J Mol Sci, 2018. **19**(7).
7. Boyce, A.K.J., et al., *Transcriptional and post-translational regulation of pannexins*. Biochim Biophys Acta Biomembr, 2018. **1860**(1): p. 72-82.
8. Penuela, S., et al., *Diverse post-translational modifications of the pannexin family of channel-forming proteins*. Channels (Austin), 2014. **8**(2): p. 124-30.
9. Bargiotas, P., et al., *Pannexins in ischemia-induced neurodegeneration*. Proc Natl Acad Sci U S A, 2011. **108**(51): p. 20772-7.
10. Crespo Yanguas, S., et al., *Pannexin1 as mediator of inflammation and cell death*. Biochim Biophys Acta Mol Cell Res, 2017. **1864**(1): p. 51-61.
11. Jiang, J.X. and S. Penuela, *Connexin and pannexin channels in cancer*. BMC Cell Biol, 2016. **17 Suppl 1**: p. 12.
12. Celetti, S.J., et al., *Implications of pannexin 1 and pannexin 3 for keratinocyte differentiation*. J Cell Sci, 2010. **123**(Pt 8): p. 1363-72.
13. Cowan, K.N., et al., *Pannexin1 and Pannexin3 exhibit distinct localization patterns in human skin appendages and are regulated during keratinocyte differentiation and carcinogenesis*. Cell Commun Adhes, 2012. **19**(3-4): p. 45-53.
14. Flores-Munoz, C., et al., *Restraint of Human Skin Fibroblast Motility, Migration, and Cell Surface Actin Dynamics, by Pannexin 1 and P2X7 Receptor Signaling*. Int J Mol Sci, 2021. **22**(3).

15. Penuela, S., et al., *Pannexin 1 and pannexin 3 are glycoproteins that exhibit many distinct characteristics from the connexin family of gap junction proteins*. J Cell Sci, 2007. **120**(Pt 21): p. 3772-83.
16. Penuela, S., et al., *Panx1 regulates cellular properties of keratinocytes and dermal fibroblasts in skin development and wound healing*. J Invest Dermatol, 2014. **134**(7): p. 2026-2035.
17. Zhang, P., et al., *Pannexin 3 regulates skin development via Epiprofin*. Sci Rep, 2021. **11**(1): p. 1779.
18. Zhang, P., et al., *Pannexin-3 Deficiency Delays Skin Wound Healing in Mice due to Defects in Channel Functionality*. J Invest Dermatol, 2019. **139**(4): p. 909-918.
19. Abitbol, J.M., et al., *Double deletion of Panx1 and Panx3 affects skin and bone but not hearing*. J Mol Med (Berl), 2019. **97**(5): p. 723-736.
20. Ma, W., et al., *Pharmacological characterization of pannexin-1 currents expressed in mammalian cells*. J Pharmacol Exp Ther, 2009. **328**(2): p. 409-18.
21. Li, S., M. Tomic, and S.S. Stojilkovic, *Characterization of novel Pannexin 1 isoforms from rat pituitary cells and their association with ATP-gated P2X channels*. Gen Comp Endocrinol, 2011. **174**(2): p. 202-10.
22. Baranova, A., et al., *The mammalian pannexin family is homologous to the invertebrate innexin gap junction proteins*. Genomics, 2004. **83**(4): p. 706-16.
23. Ray, A., et al., *Site-specific and developmental expression of pannexin1 in the mouse nervous system*. Eur J Neurosci, 2005. **21**(12): p. 3277-90.
24. Sanchez-Arias, J.C., et al., *Pannexin 1 Regulates Network Ensembles and Dendritic Spine Development in Cortical Neurons*. eNeuro, 2019. **6**(3).
25. Vogt, A., S.G. Hormuzdi, and H. Monyer, *Pannexin1 and Pannexin2 expression in the developing and mature rat brain*. Brain Res Mol Brain Res, 2005. **141**(1): p. 113-20.
26. Swayne, L.A., C.D. Sorbara, and S.A. Bennett, *Pannexin 2 is expressed by postnatal hippocampal neural progenitors and modulates neuronal commitment*. J Biol Chem, 2010. **285**(32): p. 24977-86.
27. Ishikawa, M., et al., *Pannexin 3 functions as an ER Ca(2+) channel, hemichannel, and gap junction to promote osteoblast differentiation*. J Cell Biol, 2011. **193**(7): p. 1257-74.
28. Vanden Abeele, F., et al., *Functional implications of calcium permeability of the channel formed by pannexin 1*. J Cell Biol, 2006. **174**(4): p. 535-46.
29. Bikle, D.D., Z. Xie, and C.L. Tu, *Calcium regulation of keratinocyte differentiation*. Expert Rev Endocrinol Metab, 2012. **7**(4): p. 461-472.

30. Blaydon, D.C. and D.P. Kelsell, *Defective channels lead to an impaired skin barrier*. J Cell Sci, 2014. **127**(Pt 20): p. 4343-50.
31. Le Vasseur, M., et al., *Pannexin 2 Localizes at ER-Mitochondria Contact Sites*. Cancers (Basel), 2019. **11**(3).
32. Penuela, S. and D.W. Laird, *The cellular life of pannexins*. Wiley Interdisciplinary Reviews: Membrane Transport and Signaling, 2012. **1**(5): p. 621-632.
33. Whyte-Fagundes, P., et al., *A Potential Compensatory Role of Panx3 in the VNO of a Panx1 Knock Out Mouse Model*. Front Mol Neurosci, 2018. **11**: p. 135.
34. Yeung, A.K., C.S. Patil, and M.F. Jackson, *Pannexin-1 in the CNS: Emerging concepts in health and disease*. J Neurochem, 2020. **154**(5): p. 468-485.
35. Penuela, S., et al., *Pannexin channels and their links to human disease*. Biochem J, 2014. **461**(3): p. 371-81.
36. Krebs, M.P., et al., *Quality control of integral membrane proteins*. Trends Biochem Sci, 2004. **29**(12): p. 648-55.
37. Gregersen, N. and P. Bross, *Protein misfolding and cellular stress: an overview*. Methods Mol Biol, 2010. **648**: p. 3-23.
38. Lai, C.P., J.F. Bechberger, and C.C. Naus, *Pannexin2 as a novel growth regulator in C6 glioma cells*. Oncogene, 2009. **28**(49): p. 4402-8.
39. Bhalla-Gehi, R., et al., *Pannexin1 and pannexin3 delivery, cell surface dynamics, and cytoskeletal interactions*. J Biol Chem, 2010. **285**(12): p. 9147-60.
40. Gehi, R., Q. Shao, and D.W. Laird, *Pathways regulating the trafficking and turnover of pannexin1 protein and the role of the C-terminal domain*. J Biol Chem, 2011. **286**(31): p. 27639-53.
41. Sang, Q., et al., *A pannexin 1 channelopathy causes human oocyte death*. Sci Transl Med, 2019. **11**(485).
42. Wicki-Stordeur, L.E., A.K. Boyce, and L.A. Swayne, *Analysis of a pannexin 2-pannexin 1 chimeric protein supports divergent roles for pannexin C-termini in cellular localization*. Cell Commun Adhes, 2013. **20**(3-4): p. 73-9.
43. Epp, A.L., et al., *A novel motif in the proximal C-terminus of Pannexin 1 regulates cell surface localization*. Sci Rep, 2019. **9**(1): p. 9721.
44. Berchtold, L.A., et al., *Pannexin-2-deficiency sensitizes pancreatic beta-cells to cytokine-induced apoptosis in vitro and impairs glucose tolerance in vivo*. Mol Cell Endocrinol, 2017. **448**: p. 108-121.

45. Liao, D., et al., *Identification of Pannexin 2 as a Novel Marker Correlating with Ferroptosis and Malignant Phenotypes of Prostate Cancer Cells*. *Onco Targets Ther*, 2020. **13**: p. 4411-4421.
46. Chekeni, F.B., et al., *Pannexin 1 channels mediate 'find-me' signal release and membrane permeability during apoptosis*. *Nature*, 2010. **467**(7317): p. 863-7.
47. Sandilos, J.K., et al., *Pannexin 1, an ATP release channel, is activated by caspase cleavage of its pore-associated C-terminal autoinhibitory region*. *J Biol Chem*, 2012. **287**(14): p. 11303-11.
48. Medina, C.B., et al., *Metabolites released from apoptotic cells act as tissue messengers*. *Nature*, 2020. **580**(7801): p. 130-135.
49. Ruan, Z., et al., *Structures of human pannexin 1 reveal ion pathways and mechanism of gating*. *Nature*, 2020.
50. Wang, J., et al., *The membrane protein Pannexin1 forms two open-channel conformations depending on the mode of activation*. *Sci Signal*, 2014. **7**(335): p. ra69.
51. Lippens, S., et al., *Epidermal differentiation does not involve the pro-apoptotic executioner caspases, but is associated with caspase-14 induction and processing*. *Cell Death Differ*, 2000. **7**(12): p. 1218-24.
52. Xu, J., et al., *MicroRNA-423-3p promotes glioma growth by targeting PANX2*. *Oncol Lett*, 2018. **16**(1): p. 179-188.
53. Tanese, K., *Diagnosis and Management of Basal Cell Carcinoma*. *Curr Treat Options Oncol*, 2019. **20**(2): p. 13.
54. Combalia, A. and C. Carrera, *Squamous Cell Carcinoma: An Update on Diagnosis and Treatment*. *Dermatol Pract Concept*, 2020. **10**(3): p. e2020066.
55. Simon, D., et al., *Epidermal caspase-3 cleavage associated with interferon-gamma-expressing lymphocytes in acute atopic dermatitis lesions*. *Exp Dermatol*, 2006. **15**(6): p. 441-6.
56. Freeman, T.J., et al., *Inhibition of Pannexin 1 Reduces the Tumorigenic Properties of Human Melanoma Cells*. *Cancers (Basel)*, 2019. **11**(1).
57. Penuela, S., et al., *Loss of pannexin 1 attenuates melanoma progression by reversion to a melanocytic phenotype*. *J Biol Chem*, 2012. **287**(34): p. 29184-93.
58. Sayedyahosseini, S., et al., *Pannexin 1 binds beta-catenin to modulate melanoma cell growth and metabolism*. *J Biol Chem*, 2021: p. 100478.
59. Qu, Y., et al., *Pannexin-1 Is Required for ATP Release during Apoptosis but Not for Inflammasome Activation*. *The Journal of Immunology*, 2011. **186**(11): p. 6553-6561.

60. Dankort, D., et al., *Braf(V600E) cooperates with Pten loss to induce metastatic melanoma*. Nat Genet, 2009. **41**(5): p. 544-52.
61. Broertjes, J., *The Ten Hallmarks of Cancer in Cutaneous Malignant Melanoma*. UNAV Journal for Medical Students, 2015. **1**: p. 6-12.
62. Tucci, M., et al., *Immune System Evasion as Hallmark of Melanoma Progression: The Role of Dendritic Cells*. Front Oncol, 2019. **9**: p. 1148.
63. Kim, K.M., et al., *The Expression Patterns of FAM83H and PANX2 Are Associated With Shorter Survival of Clear Cell Renal Cell Carcinoma Patients*. Front Oncol, 2019. **9**: p. 14.
64. Tang, Z., et al., *GEPIA: a web server for cancer and normal gene expression profiling and interactive analyses*. Nucleic Acids Res, 2017. **45**(W1): p. W98-W102.
65. Lewis, S.M., A. Williams, and S.C. Eisenbarth, *Structure and function of the immune system in the spleen*. Sci Immunol, 2019. **4**(33).
66. Beheshti, A., et al., *Tumor-host signaling interaction reveals a systemic, age-dependent splenic immune influence on tumor development*. Oncotarget, 2015. **6**(34): p. 35419-32.
67. Fang, J.J., et al., *Effect of spleen lymphocytes on the splenomegaly in hepatocellular carcinoma-bearing mice*. Biomed Environ Sci, 2014. **27**(1): p. 17-26.
68. Bronte, V. and M.J. Pittet, *The spleen in local and systemic regulation of immunity*. Immunity, 2013. **39**(5): p. 806-18.
69. Radoja, S., et al., *Mice bearing late-stage tumors have normal functional systemic T cell responses in vitro and in vivo*. J Immunol, 2000. **164**(5): p. 2619-28.
70. Freitas-Andrade, M., et al., *Pannexin1 knockout and blockade reduces ischemic stroke injury in female, but not in male mice*. Oncotarget, 2017. **8**(23): p. 36973-36983.
71. Aquilino, M.S., et al., *Pannexin-1 Deficiency Decreases Epileptic Activity in Mice*. Int J Mol Sci, 2020. **21**(20).
72. Dusseau, B., et al., *Metastatic melanoma of the spleen without known primary*. J Surg Case Rep, 2020. **2020**(12): p. rjaa456.
73. Sen, C.A., et al., *Isolated and solitary splenic metastasis detected by positron emission tomography in a patient with malignant melanoma: case report and review of the literature*. Contemp Oncol (Pozn), 2013. **17**(2): p. 214-7.
74. Ho, P.C., et al., *Immune-based antitumor effects of BRAF inhibitors rely on signaling by CD40L and IFNgamma*. Cancer Res, 2014. **74**(12): p. 3205-17.
75. Leick, K.M., et al., *Patterns of immune-cell infiltration in murine models of melanoma: roles of antigen and tissue site in creating inflamed tumors*. Cancer Immunol Immunother, 2019. **68**(7): p. 1121-1132.

76. Homet Moreno, B., et al., *Response to Programmed Cell Death-1 Blockade in a Murine Melanoma Syngeneic Model Requires Costimulation, CD4, and CD8 T Cells*. *Cancer Immunol Res*, 2016. **4**(10): p. 845-857.
77. Wang, J., et al., *UV-induced somatic mutations elicit a functional T cell response in the YUMMER1.7 mouse melanoma model*. *Pigment Cell Melanoma Res*, 2017. **30**(4): p. 428-435.
78. Meeth, K., et al., *The YUMM lines: a series of congenic mouse melanoma cell lines with defined genetic alterations*. *Pigment Cell Melanoma Res*, 2016. **29**(5): p. 590-7.
79. Hooijkaas, A., et al., *Selective BRAF inhibition decreases tumor-resident lymphocyte frequencies in a mouse model of human melanoma*. *Oncoimmunology*, 2012. **1**(5): p. 609-617.
80. Hooijkaas, A.I., et al., *Targeting BRAFV600E in an inducible murine model of melanoma*. *Am J Pathol*, 2012. **181**(3): p. 785-94.
81. Kim, S.H., et al., *Phenformin Inhibits Myeloid-Derived Suppressor Cells and Enhances the Anti-Tumor Activity of PD-1 Blockade in Melanoma*. *J Invest Dermatol*, 2017. **137**(8): p. 1740-1748.
82. Lelliott, E.J., et al., *A novel immunogenic mouse model of melanoma for the preclinical assessment of combination targeted and immune-based therapy*. *Sci Rep*, 2019. **9**(1): p. 1225.
83. Momin, N., et al., *Anchoring of intratumorally administered cytokines to collagen safely potentiates systemic cancer immunotherapy*. *Sci Transl Med*, 2019. **11**(498).
84. Peng, W., et al., *Loss of PTEN Promotes Resistance to T Cell-Mediated Immunotherapy*. *Cancer Discov*, 2016. **6**(2): p. 202-16.
85. Zhang, Y., et al., *Dendritic cell-derived interleukin-15 is crucial for therapeutic cancer vaccine potency*. *Oncoimmunology*, 2014. **3**(10): p. e959321.
86. Deken, M.A., et al., *Targeting the MAPK and PI3K pathways in combination with PD1 blockade in melanoma*. *Oncoimmunology*, 2016. **5**(12): p. e1238557.
87. Spranger, S., R. Bao, and T.F. Gajewski, *Melanoma-intrinsic beta-catenin signalling prevents anti-tumour immunity*. *Nature*, 2015. **523**(7559): p. 231-5.
88. Pelster, M.S. and R.N. Amaria, *Combined targeted therapy and immunotherapy in melanoma: a review of the impact on the tumor microenvironment and outcomes of early clinical trials*. *Ther Adv Med Oncol*, 2019. **11**: p. 1758835919830826.
89. Havel, J.J., D. Chowell, and T.A. Chan, *The evolving landscape of biomarkers for checkpoint inhibitor immunotherapy*. *Nat Rev Cancer*, 2019. **19**(3): p. 133-150.
90. Marconcini, R., et al., *Current status and perspectives in immunotherapy for metastatic melanoma*. *Oncotarget*, 2018. **9**(15): p. 12452-12470.

91. Trujillo, J.A., et al., *Secondary resistance to immunotherapy associated with beta-catenin pathway activation or PTEN loss in metastatic melanoma*. *J Immunother Cancer*, 2019. **7**(1): p. 295.
92. Lipman, N.S., et al., *Monoclonal versus polyclonal antibodies: distinguishing characteristics, applications, and information resources*. *ILAR J*, 2005. **46**(3): p. 258-68.
93. Borowiec, A.S., et al., *Optimal differentiation of in vitro keratinocytes requires multifactorial external control*. *PLoS One*, 2013. **8**(10): p. e77507.
94. Danese, A., et al., *Calcium regulates cell death in cancer: Roles of the mitochondria and mitochondria-associated membranes (MAMs)*. *Biochim Biophys Acta Bioenerg*, 2017. **1858**(8): p. 615-627.
95. Wang, N., et al., *The MAMs Structure and Its Role in Cell Death*. *Cells*, 2021. **10**(3).
96. Ferris, S.P., V.K. Kodali, and R.J. Kaufman, *Glycoprotein folding and quality-control mechanisms in protein-folding diseases*. *Dis Model Mech*, 2014. **7**(3): p. 331-41.
97. Damsky, W.E., et al., *beta-catenin signaling controls metastasis in Braf-activated Pten-deficient melanomas*. *Cancer Cell*, 2011. **20**(6): p. 741-54.
98. Ceci, C., et al., *Targeting Tumor-Associated Macrophages to Increase the Efficacy of Immune Checkpoint Inhibitors: A Glimpse into Novel Therapeutic Approaches for Metastatic Melanoma*. *Cancers (Basel)*, 2020. **12**(11).
99. Zhang, W., et al., *Optogenetic control with a photocleavable protein, PhoCl*. *Nat Methods*, 2017. **14**(4): p. 391-394.
100. Dakup, P.P., et al., *Sex differences in the association between tumor growth and T cell response in a melanoma mouse model*. *Cancer Immunol Immunother*, 2020. **69**(10): p. 2157-2162.

Appendix

Letter of approval for animal care protocol-Chapter 4



2019-070:1:

AUP Number: 2019-070

AUP Title: The role of pannexins in malignant melanoma

Yearly Renewal Date: 11/01/2021

The YEARLY RENEWAL to Animal Use Protocol (AUP) 2019-070 has been approved by the Animal Care Committee (ACC), and will be approved through to the above review date.

Please at this time review your AUP with your research team to ensure full understanding by everyone listed within this AUP.

As per your declaration within this approved AUP, you are obligated to ensure that:

- 1) Animals used in this research project will be cared for in alignment with:
 - a) Western's Senate MAPPs 7.12, 7.10, and 7.15
http://www.uwo.ca/univsec/policies_procedures/research.html
 - b) University Council on Animal Care Policies and related Animal Care

Committee procedures

http://uwo.ca/research/services/animalethics/animal_care_and_use_policies.html

- 2) As per UCAC's Animal Use Protocols Policy,
 - a) this AUP accurately represents intended animal use;
 - b) external approvals associated with this AUP, including permits and scientific/departmental peer approvals, are complete and accurate;
 - c) any divergence from this AUP will not be undertaken until the related Protocol Modification is approved by the ACC; and
 - d) AUP form submissions - Annual Protocol Renewals and Full AUP Renewals - will be submitted and attended to within timeframes outlined by the ACC.

http://uwo.ca/research/services/animalethics/animal_use_protocols.html

- 3) As per MAPP 7.10 all individuals listed within this AUP as having any hands-on animal contact will
 - a) be made familiar with and have direct access to this AUP;
 - b) complete all required CCAC mandatory training (training@uwo.ca); and
 - c) be overseen by me to ensure appropriate care and use of animals.

- 4) As per MAPP 7.15,
 - a) Practice will align with approved AUP elements;
 - b) Unrestricted access to all animal areas will be given to ACVS Veterinarians

and ACC Leaders;

- limited to:
- c) UCAC policies and related ACC procedures will be followed, including but not
 - i) Research Animal Procurement
 - ii) Animal Care and Use Records

iii) Sick Animal Response

iv) Continuing Care Visits

5) As per institutional OH&S policies, all individuals listed within this AUP who will be using or potentially

exposed to hazardous materials will have completed in advance the appropriate institutional OH&S training, facility-level training, and reviewed related (M)SDS Sheets, <http://www.uwo.ca/hr/learning/required/index.html>

Submitted by: Copeman, Laura
on behalf of the Animal Care Committee
University Council on Animal Care

Copyright information – Chapter 2



International Journal of
Molecular Sciences



Open Access Article

N-Glycosylation Regulates Pannexin 2 Localization but Is Not Required for Interacting with Pannexin 1

by Rafael E. Sanchez-Pupo , Danielle Johnston and Silvia Penuela *

Department of Anatomy and Cell Biology, Schulich School of Medicine & Dentistry, University of Western Ontario, London, ON N6A5C1, Canada

* Author to whom correspondence should be addressed.

Int. J. Mol. Sci. **2018**, *19*(7), 1837; <https://doi.org/10.3390/ijms19071837>

Received: 27 April 2018 / Revised: 16 June 2018 / Accepted: 20 June 2018 / Published: 22 June 2018

(This article belongs to the Special Issue *Interplay of Connexins and Pannexins in Tissue Function and Disease*)

This is an open access article distributed under the **Creative Commons Attribution License** which permits unrestricted use, distribution, and reproduction in any medium, provided the original work is properly cited

MDPI Open Access Information and Policy

All articles published by MDPI are made immediately available worldwide under an open access license. This means:

- everyone has free and unlimited access to the full-text of *all* articles published in MDPI journals;
- everyone is free to re-use the published material if proper accreditation/citation of the original publication is given;
- open access publication is supported by the authors' institutes or research funding agencies by payment of a comparatively low **Article Processing Charge (APC)** for accepted articles.

Permissions

No special permission is required to reuse all or part of article published by MDPI, including figures and tables. For articles published under an open access Creative Common CC BY license, any part of the article may be reused without permission provided that the original article is clearly cited. Reuse of an article does not imply endorsement by the authors or MDPI.

Copyright information – Figures created with BioRender



639 Queen St. W Suite 401
Toronto ON M5V 2B7 Canada
www.biorender.com

Confirmation of Publication and Licensing Rights

June 20th, 2021
Science Suite Inc.

Subscription: *Student Plan*

To whom this may concern,

This document is to confirm that **Rafael Sanchez** has been granted a license to use the BioRender content, including icons, templates and other original artwork, appearing in the attached completed graphic pursuant to BioRender's [Academic License Terms](#). This license permits BioRender content to be sublicensed for use in journal publications.

All rights and ownership of BioRender content are reserved by BioRender. All completed graphics must be accompanied by the following citation: "Created with BioRender.com".

BioRender content included in the completed graphic is not licensed for any commercial uses beyond publication in a journal. For any commercial use of this figure, users may, if allowed, recreate it in BioRender under an Industry BioRender Plan.

Licensing was granted to this thesis' author Rafael Sanchez on June 20, 2021, by Science Suite Inc. with the following agreement numbers listed per figure:

Fig. 1-2: *FO22M2KN5R, XU22M2FCA7, PB22M2F4LK, RJ22M2HME0* for Panels A, B, C, Legend, respectively.

Fig. 1-4: *QD22M2G3KF, IC22M2G00V* for Panels A and B, respectively.

Fig. 1-5: *RO22M2FUV2*

Fig. 1-6: *QU22M2DRAG*

Fig. 5-1: *JX22M2ENAZ*

Fig. 5-3: *XZ22M2E6J0*

BioRender Publication Guide assessed on June 20, 2021: "*BioRender content that was exported for use in a publication while a premium plan is active can be used in the relevant publication after the plan terminates and Completed Graphics containing BioRender content may be cropped, reshaped or resized for such purpose.*"

Curriculum Vitae

Name: Rafael Enrique Sánchez Pupo

Post-secondary Education and Degrees: The University of Western Ontario
London, Ontario, Canada
Ph.D. Anatomy and Cell Biology
(*Transferred from master's on Jan 27th, 2017*)
2015-2021

University of Havana
La Habana, Cuba
BSc. Biochemistry and Molecular Biology
2007-2012

Honors and Awards: CaRTT Strategic Training Program - Ph.D. Fellowship Award.
2017-2018

Western Graduate Research Scholarship
2015-2020

IGJC Travel Award
2017

ACB Graduate Travel Prize. The University of Western Ontario
2016, 2020

Related Work Experience Teaching Assistant
The University of Western Ontario
Anatcell 4461B- Translational Models of Cancer
2017-2020

Publications:

- **Sanchez-Pupo R.E.**, O'Donnell B., Johnston D., Gyenis L., Litchfield D.W., Penuela S. Pannexin 2 is expressed in the murine skin and promotes UVB-induced apoptosis of keratinocytes. (*Submitted for publication-2021*)
- **Sanchez-Pupo R.E.**, Finch G., Johnston D., Abdo R., Barr K., Kerfoot S., Dagnino L. Penuela S. Global Pannexin 1-deletion increases tumor-infiltrating lymphocytes in the BRAF/Pten mouse melanoma model. (*Submitted for publication-2021*)
- **Sanchez-Pupo R.E.**, Johnston D., Penuela S. N-Glycosylation Regulates Pannexin 2 Localization but Is Not Required for Interacting with Pannexin 1. *Int. J. Mol. Sci.* **2018**, 19, 1837.
- Wakefield C., Lee V., Johnston D., Boroumand P., Pillon N., Sayedyahosseini S., **Sanchez-Pupo R.**, Barr K., Gros R., Borradaile N., Klip A., Beier F., and Penuela S. Pannexin 3 deletion reduces fat accumulation and inflammation in a sex-specific manner. (In Revision at *Int. J. Obes.* – 2021.)
- Nouri-Nejad D., O'Donnell B. L., Patil C. S., **Sanchez-Pupo R.E.**, Johnston D., Sayedyahosseini S., Jurcic K., Lau R., Gyenis L., Litchfield D. W., Jackson M.F., Gloor G.B., and Penuela S. Pannexin 1 mutation found in melanoma tumor reduces phosphorylation, glycosylation, and trafficking of the channel-forming protein. *MBoC*, **2021**, 32(5), 376-390 (*Contributed with Cell Surface Biotinylation, Immunoprecipitation, Silver staining and Data Analysis*)
- Freeman, T.J.; Sayedyahosseini, S.; Johnston, D.; **Sanchez-Pupo, R.E.**; O'Donnell, B.; Huang, K.; Lakhani, Z.; Nouri-Nejad, D.; Barr, K.J.; Harland, L.; Latosinsky, S.; Grant, A.; Dagnino, L.; Penuela, S. Inhibition of Pannexin 1 Reduces the Tumorigenic Properties of Human Melanoma Cells. *Cancers*, **2019**, 11(102). (*Contributed with Cell Surface Biotinylation and ATP release assays*).
- González L., **Sánchez R. E.**, Rojas L., Pascual I., García-Fernández R., Chávez M. A., Betzel C. Screening of Protease Inhibitory Activity in Aqueous Extracts of Marine Invertebrates from Cuban Coast. *AJAC*, **2016**, 7(4): 319-331.
- Pedrera, L., Gomide, A., **Sánchez, R.E.**, Ros, U., Wilke, N., Maggio, B., Lanio, M.E., Itri, R., Fanani, M.L., Alvarez, C. (2015) The presence of sterols favours St

I-membrane association and pore formation regardless of its ability to form laterally segregated domains. *Langmuir*, **2015**, 31(36): 9911-23.

Conference Oral presentations:

- **Sanchez-Pupo Rafael** (Feb **2021**). Pannexin-1 deletion in an inducible mouse model of melanoma and the effects on intratumoral immune infiltration. IGJC 2022. Webinar series (**Oral/Zoom presentation**).
- **Sanchez Pupo RE**, Johnston D, Penuela S (**2017**). Absence of N-glycosylation affects Panx2 subcellular localization and its interaction with the mitochondrial protein ATAD3A. Proceedings of the International Gap Junction Conference. Glasgow, Scotland. July 29th-August 2nd, 2017. *Platform presentation*

Conference Poster Presentations:

- **Sanchez-Pupo R.**, Freeman T, Johnston D, Sayedyahosseini S, Nouri Nejad D, O'Donnell B, Barr K, Latosinsky S, Grant A, and Penuela S. Pannexin 1 channels modulate tumorigenic properties of melanoma. (**2019**). The Terry Fox Research Institute Ontario Node Research Symposium. Toronto, ON, Canada. Date: December 12th, 2019. (Poster)
- **Sanchez-Pupo RE**, Freeman TJ, Johnston D, Sayedyahosseini S, Nouri Nejad D, O'Donnell B, Kelly J, Barr KJ, Herrera C, Deweyert A, Hu Xu, Matthew Hebb, Harland L1, Latosinsky S, Grant A, Ronald J and Penuela S. Pannexin 1 channels promote the tumorigenic properties of melanoma and glioblastoma multiforme. Tumour Biology. The Canadian Cancer Research Conference (CCRA) **2019**, Ottawa, ON, Canada. Date: November 3 -5, 2019. (Poster # 94)
- **Sanchez-Pupo R.E.**, Johnston D, Nouri-Nejad D, Freeman T, and Penuela S. (**2018**). The role of Pannexin 1 and its post-translational modifications in melanoma. 15th ANNUAL ONCOLOGY RESEARCH & EDUCATION DAY. London, ON, Canada. Date: June 8th, 2018 (Poster)
- **Sanchez-Pupo R.E.**, Johnston D, Huang K, Penuela S. (**2018**). Effect of N-glycosylation on Pannexin 2 subcellular localization and its interaction with Pannexin 1. London Health Research Day, London, ON. May 10th, 2018. Poster.

- **Sanchez Pupo RE**, Johnston D, Penuela S (2016). Lack of N- glycosylation of Panx2 triggers aggregation in the endoplasmic reticulum without ablating its capacity to traffic to the cell surface. London Health Research Day, London, ON. March 28th, 2017. Poster.
- **Sanchez Pupo RE**, Johnston D, Penuela S (2016). Lack of N- glycosylation of Panx2 triggers aggregation in the endoplasmic reticulum without ablating its capacity to traffic to the cell surface. Proceedings of the American Society of Cell Biology Annual Meeting. San Francisco, CA. December 3-7th, 2016. Abstract program number P430.
- **Sanchez Pupo RE**, Johnston D, Penuela S (2016). The effect of post-translational modifications on the localization and function of Pannexin 2 channels. London Health Research Day, London, ON. March 29th, 2016. Poster number 109 (selected for Top 100 posters).

Co-authored peer-reviewed conference proceedings (abstracts):

- O'Donnell B, **Sanchez-Pupo R**, Johnston D, Zhang C, Kelly J, Barr K and Penuela S (2021). Pannexin 3 channels regulate architecture, keratinocyte adhesion, and barrier function in skin. London Health Research Day. May 11, 2021. Online Virtual Booth and Poster Presentation.
- Sayedyahosseini S, Johnston D, Huang K, Lakhani Z, Nouri-Nejad D, **Sanchez-Pupo RE**, Penuela S. (2019). Pannexin 1 is a novel regulator of the Wnt signaling pathway in melanoma. Proceedings of the International Gap Junction Conference. Victoria, BC. July 27th- 31st, 2019. *Platform presentation by S. Sayedyahosseini*.
- O'Donnell B, Wakefield CB, Abitbol J, Kelly JJ, **Sanchez RE**, Johnston D, Barr KJ, Penuela S. (2019). The characterization of Panx1 and Panx3 in skin using two knockout mouse models. Proceedings of the International Gap Junction Conference. Victoria, BC. July 27th- 31st, 2019. *Platform presentation by B. O'Donnell*.
- Johnston D, Kelly JJ, **Sanchez-Pupo RE**, O'Donnell B, Herrera C, Deweyert A, Xu H, Hebb M, Ronald J, Penuela S. (2019). Pannexin 1 is upregulated in patient-derived glioblastoma multiforme cells and its inhibition can impair cancer cell

- viability and tumor formation. Proceedings of the International Gap Junction Conference. Victoria, BC. July 27th- 31st, 2019. Poster P-A-15.
- Nouri-Nejad D, O'Donnell B, Patil C, **Sanchez-Pupo RE**, Johnston D, Jurcic K, Litchfield D, Jackson M, Gloor G, Penuela S. (2019). A novel phosphorylation site present in ancestral and derived Pannexin 1 variants regulates glycosylation, trafficking and cell viability. Proceedings of the International Gap Junction Conference. Victoria, BC. July 27th- 31st, 2019. Poster P-C-47.
 - Sayedyahosseini S, Johnston D, Huang K, Lakhani Z, Nouri-Nejad D, **Sanchez-Pupo RE**, Penuela S. (2019). Pannexin 1 is a novel regulator of the Wnt signaling pathway in melanoma. Oncology Research and Education Day, London, ON, June 14th, 2019. *Platform presentation by S. Sayedyahosseini*.
 - Nouri-Nejad D, Freeman TJ, Sayedyahosseini S, Johnston D, **Sanchez-Pupo RE**, O'Donnell B, Huang K, Lakhani Z, Barr KJ, Harland L, Latosinsky S, Grant A, Penuela S. (2019). Inhibition of Pannexin 1 channels reduces tumorigenic properties of melanoma. Oncology Research and Education Day, London, ON, June 14th, 2019. Poster.
 - Nouri-Nejad D, O'Donnell B, Patil C, **Sanchez-Pupo RE**, Johnston D, Jurcic K, Litchfield D, Jackson M, Gloor G, Penuela S. (2019). Identification of a prevalent ancestral *PANX1* variant and a novel tyrosine phosphorylation site that affects glycosylation and trafficking of PANX1. Oncology Research and Education Day, London, ON, June 14th, 2019. Poster.
 - O'Donnell B, Wakefield CB, **Sanchez RE**, Johnston D, Penuela S. (2019). The characterization of Panx1 and Panx3 in skin using two knockout mouse models. London Health Research Day, London, ON. April 30th, 2019. Poster.
 - Nouri-Nejad D, Freeman TJ, Sayedyahosseini S, Johnston D, **Sanchez-Pupo RE**, O'Donnell B, Huang K, Lakhani Z, Barr KJ, Harland L, Latosinsky S, Grant A, Penuela S. (2019). Inhibition of Pannexin 1 channels reduces tumorigenic properties of melanoma. London Health Research Day, London, ON. April 30th, 2019. Poster.

- Nouri-Nejad D, Freeman TJ, Sayedyahosseini S, Johnston D, **Sanchez-Pupo RE**, O'Donnell B, Huang K, Lakhani Z, Barr KJ, Harland L, Latosinsky S, Grant A, Penuela S. (2019). Inhibition of Pannexin 1 channels reduces tumorigenic properties of melanoma. Experimental Biology, Orlando, Florida USA. April 6-9th, 2019. Poster B162 674.15.
- Nouri-Nejad D, O'Donnell B, Johnston D, Barr KJ, Sanchez-Pupo R, Penuela S. (2018) Pannexin and its mutant isoforms in the crosstalk between melanoma and immune cells. Oncology Research and Education Day, London, ON, June 8th, 2018. Poster.
- Nouri-Nejad D, O'Donnell B, Johnston D, **Sanchez-Pupo R**, Penuela S. (2018) Characterization of PANX1 mutations from patient-derived melanoma tumours. London Health Research Day, London, ON. May 10th, 2018. Poster.
- Freeman T, **Sanchez-Pupo R**, Johnston D, Barr KJ, Nouri-Nejad D, O'Donnell B, Harland, Penuela S (2018). Targeting PANX1 channels can reduce the malignant properties of human melanomas. Proceedings of the 11th Conference on Signalling in Normal and Cancer Cells, Banff, Alberta. April 15-19, 2018. Poster abstract #51
- Nouri-Nejad D, O'Donnell B, Johnston D, Barr KJ, **Sanchez-Pupo R**, Penuela S. (2018) Pannexin and its mutant isoforms in the crosstalk between melanoma and immune cells. Proceedings of the 11th Conference on Signalling in Normal and Cancer Cells, Banff, Alberta. April 15-19, 2018. Poster abstract #48.
- Freeman T, Harland L, Nouri-Nejad D, O'Donnell B, Johnston D, **Sanchez-Pupo R**, Barr KJ, Penuela S (2017). Inhibition of Pannexin 1 channels reduces tumorigenic properties of melanoma. Proceedings of the Canadian Cancer Research Conference, Vancouver, BC. November 4-7th, 2017. Abstract ID 12433.
- Freeman T, Harland L, Nouri-Nejad D, O'Donnell B, Johnston D, **Sanchez-Pupo R**, Barr KJ, Penuela S (2017). Pannexin 1 channels as novel regulators of malignant melanoma. Proceedings of the International Gap Junction Conference. Glasgow, Scotland. July 29th-August 2nd, 2017. *Keynote presentation by S Penuela.*